

**A subcellular compartmental modeling approach to pulmonary  
drug development**

**by**

**Jingyu Yu**

A dissertation submitted in partial fulfillment  
of the requirements for the degree of  
Doctor of Philosophy  
(Medicinal Chemistry)  
in The University of Michigan  
2011

Doctoral Committee:

Associate Professor Gustavo Rosania, Chair  
Associate Professor George A. Garcia  
Associate Professor Kathleen A. Stringer  
Assistant Professor Oleg V. Tsodikov

*To my parents and my wife*

*With all my love and thanks*

## Acknowledgements

The first person I would like to thank is my Ph.D. advisor, Dr. Gus R. Rosania, for his tremendous effort to make me a better person, a better team player, and a better scientist. What he gave me is beyond the knowledge, skills, and publications listed in my resume. What's most valuable thing I learned is the attitude toward science, being curious, being critical, being innovative, being open, and being brave, which he taught me in deeds not words. I am also grateful for his continuous support to my future career development, including pursuing a dual M.A. in Statistics, doing 3 months internship in industry, and attending various conferences.

I would also thank Dr. Kathleen A. Stringer, for her support on the *in vivo* lung studies, which is critical for my research. I also appreciate the hands-on help from Gerta Mane, Jennifer Racz, and Dr. Zachary Walls.

I would like to thank my dissertation committee members, Drs. George A. Garcia, Oleg V. Tsodikov, and Kathleen A. Stringer (again) for their valuable time, and inputs. The questions, challenges, and suggestions inspired me to think more deeply and critically about my work.

I also thank Dr. Rose Feng and Dr. Gordon M. Crippen for training me in the area of the Pharmacometrics and Cheminformatics, respectively.

I would especially like to thank other lab members, Dr. Xinyuan Zhang, Nan Zheng, Kyoung-Ah Min, and Jason Baik for their help. I am indebted to the staff of the College of Pharmacy for all their help, with special thanks to Maria Herbal, Jeanne Getty, Pat Greeley and L.D. Hieber.

Lastly, I want to thank my wife, Shanshan Liang, for her full support.

## TABLE OF CONTENTS

DEDICATION.....	ii
ACKNOWLEDGEMENTS .....	iii
LIST OF TABLES.....	vii
LIST OF FIGURES.....	viii
LIST OF APPENDICES.....	xi
CHAPTER 1.....	1
<b>Introduction.....</b>	<b>1</b>
1.1 Physiology and Histology of Lung.....	1
1.2 Difference between Airways and Alveoli.....	2
1.3 Pharmacokinetics (PK) and Pharmacodynamics (PD).....	4
1.4 The Systemic and Local Pharmacokinetics (PK) of Inhaled Drugs.....	5
1.5 Existing Models.....	6
1.6 The Rational Design of Inhaled Drugs Products.....	10
1.7 References.....	14
CHAPTER 2.....	18
<b>Cell-based multiscale computational modeling of small molecule     absorption and retention in the lungs</b>	
2.1 Introduction.....	18
2.2 Methods.....	20
2.3 Results.....	30
2.4 Discussion.....	35
2.5 References.....	50
CHAPTER 3.....	54
<b>The in silico studies of differential exposure of airways and alveoli     with injection vs. intratracheal instillation.....</b>	<b>54</b>

3.1 Introduction.....	54
3.2 Methods.....	56
3.3 Results.....	63
3.4 Discussion.....	67
3.5 References.....	80
<b>CHAPTER 4 .....</b>	<b>82</b>
<b>Study of the effect of acidic phospholipids binding on the     pharmacokinetics with a hybrid Lung PBPK Model.....</b>	<b>82</b>
4.1 Introduction.....	82
4.2 Methods.....	84
4.3 Results.....	89
4.4 Discussion.....	90
4.5 References.....	99
<b>CHAPTER 5.....</b>	<b>100</b>
<b>A mathematical model coupling dissolution and absorption in lungs     to explore the chemical space for rational design of inhalation     products.....</b>	<b>100</b>
5.1 Introduction.....	100
5.2 Methods.....	105
5.3 Results.....	112
5.4 Discussion.....	113
5.5 References.....	122
<b>CHAPTER 6.....</b>	<b>124</b>
<b>Device Invention.....</b>	<b>124</b>
6.1 Introduction.....	124
6.2 Description of Device.....	129
6.3 Discussions.....	135
6.4 References.....	139
<b>CHAPTER 7.....</b>	<b>140</b>
<b>Conclusions.....</b>	<b>140</b>
7.1 Summary.....	140
7.2 Future Directions.....	142
7.3 References.....	151
<b>APPENDICES.....</b>	<b>152</b>

## LIST OF TABLES

Table 2.1. Parameters for the tracheaobronchial airways and alveolar region in the rats.....	40
Table 2.2. Structures, physicochemical properties, observed $absT_{50}$ , $K_a$ , and predicted absorption profile of nine monocharged molecules.....	41
Table 3.1. Sensitivity Analysis via exchanging the values of airways and alveoli.....	73
Table 4.1. Physiological parameters for tissue volumes and blood flow rates in rats.....	93
Table 4.2. Physicochemical properties and PK parameters for atenolol, and propranolol .....	94
Table 5.1. Summary of analysis of simulation results.....	116
Table 7.1. Geometric parameter values for human airways.....	147
Table 7.2. Histological parameter values for human airways and alveoli.....	148

## LIST OF FIGURES

Figure. 2.1. Diagram representing the general route of drug transport from the airways to the blood, across the histological architecture of lung tissue.....	42
Figure 2.2. The relationship between the physicochemical properties and the absorption or tissue retention in the airways.....	43
Figure 2.3. The relationship between the physicochemical properties and the absorption or tissue retention in the alveolar region.....	44
Figure 2.4. The relationship between the physicochemical properties and the absorption in the whole lung with a dosage deposition of 70% in airways and 30% in alveolar region.....	45
Figure 2.5. Observed $K_a$ and predicted $K_a$ are related, for small drug-like molecules of intermediate size range.....	46
Figure 2.6. The correlation between the observed and predicted $\log K_a$ , obtained by partial least square (PLS) regression using the predicted $\log K_a$ and Petitjean radius as variables.....	47
Figure 2.7. The effect of an apical airway efflux transporter with $K_m = 423 \mu\text{M}$ .....	48
Figure 2.8. The simulated effect of organelle sequestration on lung pharmacokinetics of small molecules of varying physicochemical properties.....	49



Figure 3.1. General methodology of hybrid PBPK model.....	74
Figure 3.2. The relationship between the physicochemical properties of monobasic compounds and the tissue exposure (i.e., AUC) in the airways, alveoli, and the exposure contrast of airways to alveoli.....	75
Figure 3.3. The relationship between the physicochemical properties of monobasic compounds and the mass deposition pattern in the airways, alveoli relative to the whole lung.....	76
Figure 3.4. The relationship between the physicochemical properties of monobasic compounds and $T_{ss}$ (the time to reach steady state) in the airways and alveoli.....	77
Figure 3.5. The simulated tissue concentration in airways (dash line) and alveoli (solid line).....	78
Figure 3.6. Microscopic fluorescence distribution of Hoechst 33342 (blue), Mitotracker Red (red) in the lung.....	80
Figure 4.1. General methodology of hybrid PBPK model.....	95
Figure 4.2. Comparison between the simulated tissue concentration profiles of propranolol with experimental data.....	96
Figure 4.3. Comparison between the simulated tissue concentration profiles of atenolol with experimental data.....	97
Figure 4.4. Comparison between the simulated tissue concentration curve in airways and alveoli for inhaled and IV injected atenolol and propranolol with AP binding.....	98

Figure 5.1. A schematic representation of mathematical model coupling dissolution and absorption.....	117
Figure 5.2. Illustration of simulated time-course of mass in different compartments with the dissolution-absorption model.....	118
Figure 5.3. The effect of formulation (Particle radius) and device (At) on the pharmacokinetics of inhaled drugs with high permeability ( $10^{-4}$ cm/s).....	119
Figure 5.4. The effect of formulation(Particle radius) and device (At) on the pharmacokinetics of inhaled drugs with medium permeability ( $10^{-6}$ cm/s).....	120
Figure 5.5. The effect of formulation(Particle radius) and device (At) on the pharmacokinetics of inhaled drugs with low permeability ( $10^{-8}$ cm/s).....	121
Figure 6.1. Schematic diagram of the device.....	136
Figure 6.2. Schematic diagram for mathematical simultaneous modeling of dissolution and absorption.....	138
Figure 7.1. Relationship between physicochemical properties and Peff of human lung.....	149
Figure 7.2. Synergistic paradigm of drug discovery and development .....	150

## LIST OF APPENDICES

APPENDIX A.....	153
Equations and Parameters in Chapter 2.....	153
APPENDIX B.....	171
Parameter and Sensitivity Analysis in Chapter 3.....	171
APPENDIX A.....	185
Matlab Code.....	185

## CHAPTER 1

### Introduction

#### 1.1 Physiology and Histology of Lung

Inhaled drugs are mainly designed for the treatment of local lung diseases, such as COPD, asthma, pneumonia, etc. The therapeutic advantages of inhalation over the systemic delivery include the fast on-set due to the direct deposition of drug in lung, high local concentration and reduced systemic side effect with low dosage.<sup>1</sup> In the past decades the development of inhaled medications for the treatment of systemic disease has also attracted increasing attention. Inhalation can offer some therapeutic benefits for systemically acting drugs. <sup>1, 2</sup>First, the lung has large surface area available for the absorption of drug into the blood stream. Second, the transport and metabolic activity in the lung is limited compared to that in gastrointestinal (GI) tract and liver.<sup>1, 3-5</sup> Third, there is little first-pass metabolism involved for drugs absorbed from the lung. Therefore, the inhaled drugs often possess fast absorption and high bioavailability. <sup>6</sup> And tremendous effort has been made to deliver the biologics by inhalation for treating systemic disease. <sup>2, 6</sup>

Lung has a sophisticated self-defense system to remove the foreign substances and pathogens by various mechanisms, including mechanical (e.g.,

cough, sneezing and mucociliary clearance), chemical (antioxidants, protease, surfactant lipids) and immunological defense mechanisms.<sup>7, 8</sup> For the drug discovery and development, this host defense system in the lung is the barriers to be overcome in order to achieve efficient drug deposition, retention and absorption for the inhaled medications.

Most of the metabolic enzymes in the liver are also expressed in the lung, however the expression level in lung is much lower than that in liver.<sup>9</sup> For example, as the major cytochrome P450 (CYP) in human liver, the expression level of CYP3A4 in the lung is only 20% of that in liver. In addition, the lung has much lower proteolytic activity than most of the other organs,<sup>10</sup> but this may be affected by the pathophysiological changes in the lung.

Pathophysiological conditions in the lung may be caused by inflammation in the lung, including COPD, asthma, and mucosal injury by viruses or chemical toxicants. The resultant chronic structural changes in airways (i.e., airways remodeling) may include the hyperplasia of smooth muscle, hyper-secretion of mucus, sub-epithelial fibrosis, and epithelial disruption.<sup>11</sup> These pathophysiological changes may significantly alter the deposition pattern of inhaled drugs in the lung as well as the integrity of the epithelium barriers.<sup>12</sup>

## **1.2 Difference between Airways and Alveoli**

As the absorption site and/or site of action, the lung can be divided into two functional regions: the conducting airways and the respiratory alveolar region. Airways start with trachea and continuously branch dichotomously into smaller children branches.<sup>13</sup> Two functional regions are supplied with two

different circulatory systems. The bronchial and the pulmonary circulation supply the airways and alveolar region respectively.<sup>14, 15</sup> The bronchial circulation is a part of the systemic circulation and receives about 1% of cardiac output. The pulmonary circulation has an extensive vascular bed and receives the 100% of cardiac output, which perfuse the alveolar region to achieve an efficient gas exchange.

On the top of the lung mucosa there is a thin layer of surface lining fluid, which covers nearly 100% all surface area and generates a high humidity in the lung<sup>1, 16</sup>. The thickness of the surface lining fluid is estimated to be 5–10 um and gradually decreases with the airway generations. The surface lining liquid is composed of various types of surfactants mainly secreted by the alveolar type II cells. And it usually comprise a mixture of phospholipids, surfactant, and proteins.<sup>15</sup> Previous studies suggest that interaction between the phospholipids in the surface lining liquid and drugs may alter the solubility, absorption, retention and clearance of drugs in the lung.<sup>17-19</sup>

The cellular composition of the lung epithelium varies among different airway branches of the lung. Smooth muscle is only present in airways not alveoli. And various cell types, including basal cells, ciliated cells, brush cells, goblet cells, and Clara cells, are present in the airways.<sup>20</sup> Epithelial type I and II cells, alveolar brush cells (type III) and macrophages can be found in the alveolar region.<sup>20, 21</sup> The squamous type I cell in alveoli covers approximately 96% of the surface area, the rest 3% of the surface is covered by the cuboidal type II cells. The endothelial surface of the lung is the largest among all the organs in the

body to optimize the efficiency of gas exchange <sup>1</sup>. The interstitium of the lung, the extracellular and extravascular space, contain a variety of cells (e.g. fibroblasts, monocytes, and lymphocytes), collagen, and interstitial fluid, etc.<sup>20</sup> The heterogeneous cellular composition across different regions of the lung is expected to result in the difference in drug transport behavior between airways and alveoli.<sup>22</sup>

Other than the aforementioned difference between airways and alveoli, regional deposition pattern of drug particles across the lung is also important factor for the drug absorption and disposition in pulmonary system. The regional deposition pattern depends on many factors, including the formulation properties (e.g., size, shape, density and charge), device, respiratory tract morphology and breathing pattern (e.g., inflow rate and tidal volume).<sup>23</sup>

### **1.3 Pharmacokinetics (PK) and Pharmacodynamics (PD)**

The concept of 'pharmacokinetics' in the English was first introduced in 1961 in Nelson's publication.<sup>24</sup> The rapid growing period for pharmacokinetics was from 1961 to 1972, <sup>25, 26</sup> pioneered by the works done by Wagner and Nelson.<sup>24</sup> Based on the assumption that there is causal relationship between exposure and response, the pharmacokinetics serve as a portal to link to pharmacodynamic and subsequent clinical outcomes. Pharmacodynamics is a division of pharmacology dealing with the drug effects in subjects.<sup>27-32</sup> In a more vivid way, pharmacokinetics is what the body does to the drug; pharmacodynamics is what the drug does to the body. PK/PD profile of a compound is often studied in a format of mathematical models, which link drug

concentration in certain body fluid (serum, blood, urine) to a physiologic response (blood pressure, liver function tests) or clinical outcome (survival, adverse effect). Based on the mathematical expression, the pharmacodynamic models can be categorized as some types, including fixed, linear,  $E_{max}$ , sigmoid  $E_{max}$ , and indirect response.<sup>33-35</sup> PK/PD modeling and simulations are very important in the drug discovery and development as they bridge the gap between the basic sciences and the clinical application of drugs.

#### **1.4 The Systemic and Local Pharmacokinetics (PK) of Inhaled Drugs**

The PK studies are often focused on the process of the absorption, distribution, metabolism, and excretion (ADME) of an administered drug. In most of case, PK profiles provide a quantitative measure about the drug exposure, such as area under the concentration curve (AUC), which eventually determines the pharmacological effect at the site of action. The PK data are often time-course drug concentration collected from biofluid in systemic circulation, such as blood, plasma. The rational of using blood or plasma concentration as representative of drug exposure at the site of action is that the drug concentration in blood (i.e., systemic circulation) is approximately in equilibrium with that in the targeted organs or tissues, and it is often referred to as systemic PK. Therefore, systemic PK can be used for evaluation of the systemic therapeutic or side effect for inhaled drugs. However, systemic PK is not applicable for the evaluation of the local lung exposure of the inhaled drugs. The inhaled drug exposure for lung diseases is reflected by local drug concentration in lung tissue (i.e., local PK), which is dominantly determined by the drug mass deposited in lung rather than



drug in systemic circulation. Furthermore, it's difficult to make direct measurement of drug concentration in lung due to the limitation of current technology and ethic issues in clinical studies. This poses a challenge for reliable evaluation of the local PK and exposure and establishment of bioequivalence for the inhaled drug products.<sup>36</sup>

## **1.5 Existing Models**

### **1.5.1 *In silico* and *in vivo* Lung Models**

The structures of the animal or human lung have been analyzed quantitatively over the past decades, either by mathematical model based on *in vitro* morphological measurements of the airways,<sup>37-39</sup> or by analyzing them based on *in vivo* images, such as CT scans.<sup>40</sup> Two different number systems have been developed to describe the hierarchy of the branching system in the lung: (1). Weibel's generation,<sup>13</sup> which numbers from tracheal down to the alveoli; (2) Horsfield order,<sup>39</sup> which numbers in the opposite way from the alveoli toward the tracheal. We use the Weibel's generations throughout this thesis. In the Weibel's generation system, the trachea is generation 0. The generation number increase by 1 at each bifurcation node. Each bronchi was considered as a cylinder tube in this thesis. The lengths, diameters and number of the branches within each generation have a typical range [54]. The size of the bronchi decreases continuously with the increase of generations. At the end of airways trees, there are three generations (on average) of respiratory bronchioles and alveoli, where gas exchange takes place.

Various models describing the particle transport in a pulmonary system in a stochastic manner have been extensively reported in literature.<sup>41-43</sup> The other relevant parameters to describe the lung morphology include the lung density (g/cm<sup>3</sup>, the mean bulk density of the lung). T/D Ratio (the wall thickness (T) divided by the total diameter of the bronchus (D) and bronchoarterial ratio (the diameter of the bronchial lumen (D-2T) divided by its accompanying pulmonary artery). Many experimental and mathematical models have been developed to address the particle clearance in lungs.<sup>44, 45</sup> These mathematical transport models incorporated the mucociliary transport rates of particles as a function of lung morphology, the clearance fraction as an empirical function of particle diameter, and considered the slower mucus clearance at bifurcation sites.<sup>45</sup> Furthermore, mechanisms were proposed to explain the relationship between the delayed mucus clearance and particle size.

Several biological and *in silico* models have been developed for investigation of the behavior of inhaled drugs in lung, such as the permeability screening transwell system using lung cell culture, lung on a chip, *in vivo* pharmacokinetic studies in animals or human and *in silico* permeability predictions from physicochemical descriptors. The most popular permeability screening method is using pulmonary epithelial cell lines, such as the Calu-3 cells. A microfluidics system on a 2 cm polymer chip was developed to reproduce the lung's alveolar-capillary interface and mimic the mechanical effects of breathing on that interface.<sup>46</sup> This lung-on-a-chip technology is more reliable than other *in vitro* systems for the studies of toxicity and efficacy of inhaled drug

candidates. Schanker and coworkers studied the absorption profiles of a series of small molecules with diverse structure delivered by inhalation, and the disappearance kinetics of compounds in the rat lung was evaluated.<sup>47, 48</sup> Furthermore, some *in vivo* studies of the absorption profile of inhaled drugs from the lung lumen to the blood stream have been reported.<sup>16</sup> However, the absorption process from *in vivo* pharmacokinetic study is convoluted with the other organs in the body. The noise can include the systemic distribution, metabolism and excretion of the compound in other organs of the body, making it difficult to elucidate the lung specific event.

The most commonly used experiment is the isolated perfused lung (IPL) experiment, which is an *ex in vivo* experimental procedure and can capture the lung specific absorption process, meanwhile keep the structural and cellular integrity of the lung tissue, the permeability of barriers, and the interaction of various cell types in the lung.<sup>1, 49, 50</sup> The limitation is that this experiment is labor-intensive and technique demanding, hence they are not suitable for high throughput screening. These models are also not able to yield predictions in terms of the most desirable physicochemical properties of drug molecules for local lung delivery. In the analogous case of drug absorption in the gut, there are many drugs that are orally bioavailable. The existence of such drugs allowed Chris Lipinski to devise the famous “Rule of 5” for oral drugs.<sup>51</sup> In the case of local delivery to the lung, the number of locally acting medications is very few. Thus, coming up with a heuristic like the “Rule of 5” in the case of pulmonary drug delivery will be very difficult.

### 1.5.2 Physiologically-based Pharmacokinetics (PBPK) Model

The theoretical framework of PBPK models was first introduced by Teorell.<sup>52</sup> An overview of the PBPK modeling studies for a variety of chemicals is given by Reddy et al, including volatile organics, aromatics, pesticides, dioxins, metals, and chemical mixtures.<sup>53</sup> Recently, PBPK modeling has gained increasing popularity in academia and pharmaceutical industry.<sup>54</sup> In the whole body PBPK modeling, tissues and organs are connected via the vascular system, mimicking the anatomical structure of the species studied. Generally, tissue distribution of xenobiotics can be modeled as the perfusion rate limited (well stirred) model, or the permeability limited model. The well stirred model assumes that the drug instantaneously achieve homogeneous distribution inside the tissue, however, the permeability limited model represents the tissue as two or three compartments separated by capillary and/or cell membrane, where a permeability rate limited transport occurs. In addition, the influx and efflux activity mediated by the active transporter can also be included in some PBPK models to capture the active diffusion mechanism.

Compared to empirical “compartmental” PK models, PBPK model is more descriptive in terms of the transport mechanism with its physiologically-based nature. And the structure of an empirical PK model is typically based on the drug concentration data collected from certain body fluid (e.g., blood, urea) without focus on the underlying mechanism. The major difference in functionality between empirical PK and PBPK models is that the PBPK models can predict time-course of drug concentration in specific tissues of interest, but the empirical

compartmental PK model are often limited to describe the observed drug concentration in easily accessible compartment (e.g., blood, urea). The PBPK models have great potential for a variety of mechanism-based extrapolation beyond the experimental data, including cross-compounds, and across-dose, cross-species, and cross-population extrapolations. The successful application of the PBPK models at the early stage of drug development can facilitate the *in silico* screen of candidate drugs.<sup>54</sup> However, in the PBPK model the lung is often included as single homogeneous perfusion-limited compartment without differentiating between the airways and alveoli. And the PBPK model failed to predict lung PK when the drug is delivered by inhalation.

### **1.5.3 1Cell PK**

The *in silico* cell-based pharmacokinetic model (1Cell PK) has been successfully applied to the prediction of the permeability in Caco-2 cell monolayer for a serial of monobasic drugs.<sup>55, 56</sup> In this model, transcellular passive diffusion of small molecules was described by a set of coupled mass balanced differential equation based on a compartmental model of a cell with three subcellular compartments. Other statistical computational models for the prediction of permeability are also widely studied.<sup>57</sup> However, the validity of using cell monolayer for prediction of the *in vivo* absorption of pulmonary drug had not been studied and need further evaluation.

## **1.6 The Rational Design of Inhaled Drugs Products**

The development of combinatorial chemistry and high-throughput screening has accelerated the findings of experimental and computational models to predict the absorption, distribution, metabolism, and excretion (ADME) based on physicochemical property. In the biopharmaceutical classification system (BCS) adopted by FDA,<sup>58</sup> the permeability and solubility are two important factors in determining the class of a drug. However, most research done so far has focused on the experimental and *in silico* model of the drug transport across the intestinal and blood-brain barriers,<sup>57, 59</sup> only a few investigators have focused on the PK profiles in the pulmonary system.<sup>16, 49, 50, 60</sup> The investigation of the relation between the lung PK and systemic PK with the drugs' molecular properties is valuable for medicinal chemists to design inhaled drugs for lung disease and systemic diseases. More importantly, the identification of optimal chemical space that can lead to airways or alveoli targeting will facilitate the understanding the transport mechanism of small molecules and improve the efficacy and safety profiles for lung-targeting drugs.

Unlike the oral drugs which dissolve in a bulk liquid in gastrointestinal lumen, the dissolution of inhaled drugs in pulmonary system takes place on a very thin (10  $\mu\text{m}$  or less) surface lining liquid layer on top of airway epithelial cell. This special physiological environment of the lung will interact with the physical characteristics of inhaled formulations (e.g. size, density), deposition pattern of particles (e.g. device) and physiochemical properties of molecules (permeability, pKa), thereby determining the local and systemic PK profiles of inhaled therapeutics. Therefore, the efficacy and safety of inhaled drug product suffers

from a large variability. Therefore a variety of factors have to be taken into account in order to achieve the optimal drug design. However, no *in vitro* and *in silico* systems has been developed to quantitatively analyze the systemic and local PK by coupling dissolution and absorption under physiologically relevant conditions. Development of such model will offer a quantitative insight about the design of inhaled drugs in a systematical manner by integrating various factors, such as formulation, device, and chemical structure

Lacking a large dataset of inhaled drugs locally acting that could be used for developing a QSAR model, we propose an alternative approach to rational design of lung targeted small molecules: to develop a biophysically-based mechanistic model of drug transport in the different regions of lung, specifically airways and alveoli. This is a radical, innovative approach, in terms offering a way to tackle this difficult drug targeting problem without having a large database of known, lung-targeted chemotherapeutic medications with which to build a QSAR model.

Accordingly, the primary purpose of this project is to construct a cell based mechanistic PK model for the airways and alveoli. The usage of the model includes: (1) Relate the physiochemical properties to lung PK to optimize the drug exposure (2) Formulate hypothesis about the region-specific targeting mechanism in lungs which can be tested in experiments. The innovative aspect of this work is its nature of cell-based mechanistic PK model, which predicts the *in vivo* absorption and distribution profile of compound with their membrane transport properties of small molecules in airways and alveoli, respectively.

The cell based computational PK model appears very promising due to the success of the 1Cell PK model in predicting cell monolayer permeability.<sup>55</sup> However 1Cell PK had not been applied to predict the *in vivo* absorption and distribution of small molecules at tissue and organ level. The strategy adopted in this thesis is to integrate the drug specific characteristics with a detailed structural lung where the cell layers in airways and alveoli tissue are modeled as basic compartments. The mechanistic computational pharmacokinetic model of lung herein will minimize recourse to data fitting and exploits the physiological, anatomical and histological information as exists in the biomedical literature. The predictions and hypothesis generated from the model will be tested via *in vivo* experiments, in which the fluorescent probes are used as model compounds to study the disposition behavior in different regions of lung.

Another goal in this thesis is to construct a mathematical model for coupling the dissolution and absorption for the evaluation of the interaction between physiochemical properties of compounds, formulation, and device in terms of local and systemic PK. This theoretical framework will lead us to optimal physiochemical properties for small molecules in terms of minimization of variability of local and systemic PK by taking into account the factors of formulation and device. In addition, an experimental device was proposed to mimic the dissolution-absorption process in lungs, thereby facilitating the construction and validation of the mathematical model.



## 1.7 References

1. Ehrhardt, C.; Kim, K.-J., *Drug absorption studies: in situ, in vitro and in silico models*. Springer: Arlington, VA, 2008.
2. Brewis, R. L.; Corrin, B.; Geddes, D. M.; Gibson, G. J., *Respiratory Medicine*. second ed.; WB Saunders Company Ltd: London, 1995.
3. Anttila, S.; Hukkanen, J.; Hakkola, J.; Stjernvall, T.; Beaune, P.; Edwards, R. J.; Boobis, A. R.; Pelkonen, O.; Raunio, H., Expression and localization of CYP3A4 and CYP3A5 in human lung. *American Journal of Respiratory Cell and Molecular Biology* **1997**, *16* (3), 242-249.
4. Doppenschmitt, S.; Spahn-Langguth, H.; Regardh, C. G.; Langguth, P., Role of P-glycoprotein-mediated secretion in absorptive drug permeability: An approach using passive membrane permeability and affinity to P-glycoprotein. *J Pharm Sci* **1999**, *88* (10), 1067-72.
5. Hamilton, K. O.; Backstrom, G.; Yazdanian, M. A.; Audus, K. L., P-glycoprotein efflux pump expression and activity in Calu-3 cells. *J Pharm Sci* **2001**, *90* (5), 647-58.
6. Gumbleton, M.; Taylor, G., Challenges and innovations in effective pulmonary systemic and macromolecular drug delivery. *Adv Drug Deliv Rev* **2006**, *58* (9-10), 993-5.
7. Nicod, L. P., Pulmonary Defence Mechanisms. *Respiration* **1999**, *66* (1), 2-11.
8. DeLong, P. A.; Kotloff, R. M., An overview of pulmonary host defense. *Seminars in Roentgenology* **2000**, *35* (2), 118-123.
9. Upton, R.; Doolette, D., KINETIC ASPECTS OF DRUG DISPOSITION IN THE LUNGS. *Clinical and Experimental Pharmacology and Physiology* **1999**, *26* (5-6), 381-391.
10. Wall, D. A., Pulmonary Absorption of Peptides and Proteins. *Drug Delivery* **1995**, *2* (1), 1-20.
11. Jeffery, P. K., Remodeling and Inflammation of Bronchi in Asthma and Chronic Obstructive Pulmonary Disease. *Proc Am Thorac Soc* **2004**, *1* (3), 176-183.
12. O'Byrne, P. M.; Dolovich, M.; Dirks, R.; Roberts, R. S.; Newhouse, M. T., Lung epithelial permeability: relation to nonspecific airway responsiveness. *Journal of Applied Physiology* **1984**, *57* (1), 77-84.
13. Weibel, E. R., *Morphometry of the Human Lung*. Springer: Heidelberg, 1963.
14. Staub, N. C., *The Pulmonary intravascular macrophage*. Futura Pub. Co.: Bedford Hills, N.Y., 1989; p ix, 180 p.
15. Staub, N. C., *Basic respiratory physiology*. Churchill Livingstone: New York, 1991; p ix, 242 p.
16. Tronde, A. Pulmonary drug absorption: in vitro and in vivo investigations of drug absorption across the lung barrier and its relation to drug physicochemical properties. Uppsala University, 2002.

17. Gonda, I., The ascent of pulmonary drug delivery. *Journal of Pharmaceutical Sciences* **2000**, 89 (7), 940-945.
18. Van 't Veen, A.; Gommers, D.; Verbrugge, S. J. C.; Wollmer, P.; Mouton, J. W.; Kooij, P. P. M.; Lachmann, B., Lung clearance of intratracheally instilled <sup>99m</sup>Tc-tobramycin using pulmonary surfactant as vehicle. *British Journal of Pharmacology* **1999**, 126 (5), 1091-1096.
19. Liao, X.; Wiedmann, T. S., Solubilization of Cationic Drugs in Lung Surfactant. *Pharmaceutical Research* **2003**, 20 (11), 1858-1863.
20. Harding, R.; Pinkerton, K., *The Lung : development, aging and the environment*. Academic: San Diego, Calif. London, 2004; p xiv, 403 p.
21. Rojanasakul, Y.; Wu-Pong, S.; SpringerLink (Online service), *Biopharmaceutical drug design and development*. 2nd ed.; Humana Press, Springer: Totowa, N.J., 2008; p x, 375 p.
22. Godfrey, R. W. A., Human airway epithelial tight junctions. *Microscopy Research and Technique* **1997**, 38 (5), 488-499.
23. Gehr, P.; Heyder, J., *Particle-lung interactions*. M. Dekker: New York, 2000; p xxi, 802 p.
24. Wagner, J. G.; Nelson, E., Per cent absorbed time plots derived from blood level and/or urinary excretion data. *Journal of Pharmaceutical Sciences* **1963**, 52 (6), 610-611.
25. Gibaldi, M., *Biopharmaceutics and clinical pharmacokinetics*. 2d ed.; Lea & Febiger: Philadelphia, 1977; p ix, 181 p.
26. Evans, W. E.; Schentag, J. J.; Jusko, W. J., *Applied pharmacokinetics : principles of therapeutic drug monitoring*. Applied Therapeutics: San Francisco, 1980; p xii, 708 p.
27. Hughes, R., *A manual of pharmacodynamics*. Fifth edition, a reprint with a supplement. ed.; Leath and Ross,: London,, 1886.
28. Francis, F.; Fortescue-Brickdale, J. M., *Chemical basis of pharmacology; an introduction to pharmacodynamics based on the study of the carbon compounds*. Arnold: London,, 1908; p 372 p.
29. McGuigan, H., *An introduction to chemical pharmacology; pharmacodynamics in relation to chemistry*. P. Blakiston's son & co.: Philadelphia,, 1921; p xii, 418 p.
30. Johns, M. P., *Pharmacodynamics and patient care*. Mosby: Saint Louis, 1974; p x, 337 p.
31. Stoicescu, C.; Munteanu, L., *Natural curative factors of the main, balneoclimateric resorts in Romania : pharmacodynamics and their use with therapeutical purposes*. Sport-Turism: Bucharest, 1977; p 188 p., [20] leaves of plates.
32. Barnett, G.; Chiang, C. N., *Pharmacokinetics and pharmacodynamics of psychoactive drugs : a research monograph*. Biomedical Publications: Foster City, Calif., 1985; p 24 cm.
33. Tozer, T. N.; Rowland, M., *Introduction to pharmacokinetics and pharmacodynamics : the quantitative basis of drug therapy*. Lippincott Williams & Wilkins: Philadelphia, 2006; p x, 326 p.

34. Burton, M. E., *Applied pharmacokinetics and pharmacodynamics : principles of therapeutic drug monitoring*. 4th ed.; Lippincott Williams & Wilkins: Baltimore, 2006.
35. Kwon, Y.; NetLibrary Inc., Handbook of essential pharmacokinetics, pharmacodynamics and drug metabolism for industrial scientists. Kluwer Academic Publishers: New York, 2002; pp. xix, 291.
36. Lee, S. L.; Adams, W. P.; Li, B. V.; Conner, D. P.; Chowdhury, B. A.; Yu, L. X., In vitro considerations to support bioequivalence of locally acting drugs in dry powder inhalers for lung diseases. *AAPS J* **2009**, *11* (3), 414-23.
37. Leeming, A.; Schroter, R., A model morphology of the pulmonary acinus. *Proceedings of the Institution of Mechanical Engineers, Part H: Journal of Engineering in Medicine* **2008**, *222* (4), 429-437.
38. Florens, M.; Sapoval, B.; Filoche, M., An anatomical and functional model of the human tracheobronchial tree. *Journal of Applied Physiology* *110* (3), 756-763.
39. Parker, H.; Horsfield, K.; Cumming, G., Morphology of distal airways in the human lung. *Journal of Applied Physiology* **1971**, *31* (3), 386-391.
40. Tawhai, M. H.; Hunter, P.; Tschirren, J.; Reinhardt, J.; McLennan, G.; Hoffman, E. A., CT-based geometry analysis and finite element models of the human and ovine bronchial tree. *Journal of Applied Physiology* **2004**, *97* (6), 2310-2321.
41. USMANI; #160; S., O.; BIDDISCOMBE; F., M.; BARNES; J., P., *Regional lung deposition and bronchodilator response as a function of Beta2-agonist particle size*. American Lung Association: New York, NY, ETATS-UNIS, 2005; Vol. 172, p 8.
42. Shoyele, S. A.; Cawthorne, S., Particle engineering techniques for inhaled biopharmaceuticals. *Adv Drug Deliv Rev* **2006**, *58* (9-10), 1009-29.
43. Liang, L.; University of Michigan., Development and application of a random lung model for dose calculations in radiotherapy. 2007.
44. King, M., Experimental models for studying mucociliary clearance. *European Respiratory Journal* **1998**, *11* (1), 222-228.
45. Sturm, R.; Hofmann, W.; Scheuch, G.; Sommerer, K.; Camner, P.; Svartengren, M., Particle Clearance in Human Bronchial Airways: Comparison of Stochastic Model Predictions with Experimental Data. *Annals of Occupational Hygiene* **2002**, *46* (suppl 1), 329-333.
46. Huh, D.; Matthews, B. D.; Mammoto, A.; Montoya-Zavala, M.; Hsin, H. Y.; Ingber, D. E., Reconstituting Organ-Level Lung Functions on a Chip. *Science* *328* (5986), 1662-1668.
47. Schanker, L. S.; Hemberger, J. A., Relation between Molecular-Weight and Pulmonary Absorption Rate of Lipid-Insoluble Compounds in Neonatal and Adult-Rats. *Biochemical Pharmacology* **1983**, *32* (17), 2599-2601.
48. Schanker, L. S.; Mitchell, E. W.; Brown, R. A., Species Comparison of Drug Absorption from the Lung after Aerosol Inhalation or Intratracheal Injection. *Drug Metabolism and Disposition* **1986**, *14* (1), 79-88.

49. Tronde, A.; Norden, B.; Jeppsson, A. B.; Brunmark, P.; Nilsson, E.; Lennernas, H.; Bengtsson, U. H., Drug absorption from the isolated perfused rat lung--correlations with drug physicochemical properties and epithelial permeability. *J Drug Target* **2003**, *11* (1), 61-74.
50. Tronde, A.; Norden, B.; Marchner, H.; Wendel, A. K.; Lennernas, H.; Bengtsson, U. H., Pulmonary absorption rate and bioavailability of drugs in vivo in rats: structure-absorption relationships and physicochemical profiling of inhaled drugs. *J Pharm Sci* **2003**, *92* (6), 1216-33.
51. Lipinski, C. A.; Lombardo, F.; Dominy, B. W.; Feeney, P. J., Experimental and computational approaches to estimate solubility and permeability in drug discovery and development settings. *Adv Drug Deliv Rev* **2001**, *46* (1-3), 3-26.
52. Teorell, T., Kinetics of distribution of substances administered to the body. II: The intra-vascular mode of administration. *Arch Int Pharmacodyn* **1937**, *57*.
53. Reddy, M. B., *Physiologically based pharmacokinetic modeling : science and applications*. Wiley-Interscience: Hoboken, N.J., 2005; p xix, 420 p.
54. Rowland, M.; Balant, L.; Peck, C., Physiologically based pharmacokinetics in Drug Development and Regulatory Science: A workshop report (Georgetown University, Washington, DC, May 29–30, 2002). *The AAPS Journal* **2004**, *6* (1), 56-67.
55. Zhang, X.; Shedden, K.; Rosania, G. R., A cell-based molecular transport simulator for pharmacokinetic prediction and cheminformatic exploration. *Molecular Pharmaceutics* **2006**, *3* (6), 704-716.
56. Zhang, X.; Zheng, N.; Rosania, G. R., Simulation-based cheminformatic analysis of organelle-targeted molecules: lysosomotropic monobasic amines. *J Comput Aided Mol Des* **2008**, *22* (9), 629-45.
57. Oprea, T. I., Chemical space navigation in lead discovery. *Current Opinion in Chemical Biology* **2002**, *6* (3), 384-389.
58. Amidon, G. L.; Lennernas, H.; Shah, V. P.; Crison, J. R., A Theoretical Basis for a Biopharmaceutic Drug Classification - the Correlation of in-Vitro Drug Product Dissolution and in-Vivo Bioavailability. *Pharmaceutical Research* **1995**, *12* (3), 413-420.
59. Norinder, U.; Haeberlein, M., Computational approaches to the prediction of the blood-brain distribution. *Advanced Drug Delivery Reviews* **2002**, *54* (3), 291-313.
60. Yu, J. Y.; Rosania, G. R., Cell-based multiscale computational modeling of small molecule absorption and retention in the lungs. *Pharm Res* **2010**, *27* (3), 457-67.

## CHAPTER 2

### Cell-based multiscale computational modeling of small molecule absorption and retention in the lungs

#### 2.1. Introduction

The therapeutic benefits of inhaled drugs for treating pulmonary diseases (e.g. asthma, chronic obstructive pulmonary disease (COPD) and pulmonary hypertension) have been appreciated for several decades <sup>1, 2</sup>. These benefits include the rapid onset of drug action, low systemic exposure and resultant reduction in side effects <sup>3</sup>. In addition, the large absorptive surface area, limited metabolic enzyme activity and active transporters in the pulmonary system make inhalation a favorable delivery strategy for systemic drugs with low bioavailability <sup>4-6</sup>. Inhaled formulations of locally- and systemically-active drugs have been used for quite some time, including formulations of biological agents that are poorly bioavailable such as peptides, proteins, and oligonucleotides <sup>7-11</sup>.

Although inhalation is an established delivery strategy, the relationship between drug physicochemical properties and drug absorption kinetics in the lung has not been extensively investigated. In fact, most of the attention in terms

of optimizing drug delivery to the lung has focused on engineering of aerosol particles and of devices to deliver these particles deep into the lower airways to take advantage of the large absorptive surface area of the alveolar region for systemic drug delivery <sup>12, 13</sup>. Yet, investigation of the absorption kinetics in the lung tissues in relation to the drugs' molecular properties is also critical to the design of locally-acting medications for treating lung disease. Although oral drug absorption is an important area of pharmaceutical research <sup>14-16</sup>, comparatively little attention has been devoted to the question of how to optimize local drug absorption and retention in the lung.

There are various models applicable to investigate inhaled drug absorption and retention, ranging from *in vitro* permeability screening experiments in cell culture to *ex vivo* and *in vivo* pharmacokinetic analyses in animals or human. Schanker and coworkers studied the absorption profile of a series of compounds delivered to the lung of anesthetized rats, in which the disappearance rate of compounds in the rat lung was assessed <sup>17-19</sup>. Effros and coworkers investigated the transport and composition of fluid and electrolytes in the lung using the exhaled breath condensate (EBC) approach <sup>20,21</sup>. In addition, Tronde and coworkers performed a serial of *in vitro*, *in vivo* and *ex vivo* investigations of the absorption profile of drugs from the lung to the systemic circulation and related it to the physicochemical descriptors empirically <sup>22-25</sup>. However, these cellular, tissue or *in vivo* models are labor-intensive and technique demanding, hence they are not readily applicable to screening large numbers of compounds at early stage. Many computational models are available

for the prediction of cell permeability and oral absorption<sup>14, 15, 26</sup>, but they are not necessarily applicable to inhaled drugs due to the difference in the anatomy and physiology between the lung and GI tract and the complexity of lung delivery. In addition, construction of an *in silico* statistical prediction model requires a large amount of experimental data, which is not readily available for inhaled medications.

Recently, an *in silico* cell based pharmacokinetic model (1CellPK) has been successfully applied to the prediction of the permeability of monobasic drugs across cell monolayers<sup>27, 28</sup>. In 1CellPK, the transcellular passive diffusion of small molecules is described by a set of coupled mass balanced differential equation based on a compartmental model of a cell with three subcellular compartments. Most importantly, 1CellPK not only allowed calculation of the rate of transcellular mass transport, but also the mass of intracellular drug, in the presence of a transcellular concentration gradient. Here, we used 1CellPK as the basis for constructing a cell-based, multiscale, mechanistic drug transport model to analyze drug absorption kinetics and retention in the cells and tissues of rat lung.

## **2.2. Methods**

### **2.2.1. Overall Modeling Strategy**

As proposed in this study, each compartment in the lung model represents a cell type delimited by a phospholipid bilayer (Figure 2.1.). For simulation, the passage of small molecules across the air-blood barrier is captured by a set of

differential equations that describe mass transport across a series of cellular compartments bounded by lipid bilayers (Supporting Information, eq 1). Since the primary force driving drug transport is the concentration gradient of drug molecules between adjacent compartments, the Nernst-Planck and Fick equations can be used to describe the rate of mass transport of charged and neutral species of a molecule across each of the lipid bilayers. In turn, the time course change of compound concentration in each compartment can be obtained by numerically solving the differential equation system, according to the known physiological and histological structure of the rat lung (Table 2.1.). For a monoprotic weak acid or weak base, the concentration of molecule in each subcellular compartment is divided into two components: neutral and ionized. Accordingly, three physicochemical properties are used as input to calculate the rate of mass transport across each lipid bilayer: the logarithms of the lipid:water partition coefficient of the neutral and ionized form of the molecule, and the  $pK_a$  of the molecule. Different compartments have different pHs and lipid fractions, so the free active fraction of neutral form and ionized form of molecules is calculated according to the molecule's  $pK_a$ ,  $\log P_n$ ,  $\log P_d$ . Based on values previously used as input parameters for a generic epithelial cell <sup>27, 28</sup>, we estimated the electrical potential and permeability of each lipid bilayer (Figure 2.1B.) and the pHs of the subcellular compartments.

### **2.2.2. Modeling of Passive Diffusion across Lipid Bilayers**

According to the Fick's First law, the net flux of passive diffusion of neutral form of molecules is:



$$J_{o,i,n} = \mathbf{P}_n(a_{o,n} - a_{i,n}) \quad (1)$$

$\mathbf{P}_n$  is the permeability of the neutral form of molecules across membranes,  $a_n$  is the activity of the molecules, subscripts  $o$  and  $i$  indicate the direction of flux  $J$  is from outside (positive) to inside (negative),  $n$  indicates the neutral form of molecules.

For electrolytes the driving force of passive diffusion are not only chemical potential but also electrical potential, which is described by the Nernst-Plank equation (eq2).

$$J_{o,i,d} = \mathbf{P}_d \frac{N}{e^N - 1} (a_{o,d} - a_{i,d} e^N) \quad (2)$$

$$N = zEF / RT \quad (3)$$

Subscript  $d$  is for ionized/dissociated form of molecules.  $\mathbf{P}_d$  is the permeability of the ionized form of molecules across biomembranes.  $a_d$  is the activity of the ionized form of molecules. In eq3,  $z$  is the electronic charge,  $E$  is the membrane potential,  $F$  is the Faraday constant,  $R$  is the universal gas constant,  $T$  is the absolute temperature. To calculate the overall net fluxes ( $J_{o,i}$ ) for a compound across the membrane, the net fluxes of the neutral ( $J_{o,i,n}$ ) and ionized ( $J_{o,i,d}$ ) are summed as :

$$J_{o,i} = \mathbf{P}_n(a_{o,n} - a_{i,n}) + \mathbf{P}_d \frac{N}{e^N - 1} (a_{o,d} - a_{i,d} e^N) \quad (4)$$

Based on Henderson-Hasselbalch equation, eq 5 is derived to describe the relation between the activity of neutral form ( $a_n$ ) and ionized form ( $a_d$ ) of molecules in each compartment.

$$a_d = a_n \times 10^{i(\text{pH}-\text{pK}_a)} \quad (5)$$

Therefore, the fraction of the activities ( $a_n$  and  $a_d$ ) in the total concentrations ( $C_t$ ) of molecules can be described by eq 6 and eq 7.

$$f_n = a_n / C_t = \frac{1}{W/\gamma_n + K_n/\gamma_n + W \times 10^{i(\text{pH}-\text{pK}_a)} / \gamma_d + K_d \times 10^{i(\text{pH}-\text{pK}_a)} / \gamma_d}$$

(6)

$$f_d = a_d / C_t = f_n 10^{i(\text{pH}-\text{pK}_a)} \quad (7)$$

$$K_{n/d} = L \times 1.22 \times K_{ow,n/d} \quad (8)$$

$f_{n/d}$  is the fraction of free active neutral or ionized form in the total molecular concentration.  $W$  is the volumetric water fraction in each compartment,  $\gamma$  is the activity coefficient in each compartment. The activity coefficient of all neutral molecules ( $\gamma_n$ ) is calculated based on the ionic strength  $I$  (moles). Using the Setchenov equation,  $\gamma_n$  is 1.23 at  $I = 0.3$  mol. The activity of ions ( $\gamma_d$ ) is estimated as 0.74 at  $I = 0.3$  with the Davies approximation of the modified Debye-Hückel equation (29). For noncellular compartments no corrections for the ionic strength are made ( $\gamma_{n/d} = 1$ ).  $K_{n/d}$  is the sorption coefficient of the neutral or ionized form of molecules, which are estimated by eq 8.  $L$  is the lipid fraction in each compartment,  $K_{ow,n/d}$  is the liposomal partition coefficient described by eq 9.

$$K_{ow,n/d} = 10^{\log P_{n/d,lip}} \quad (9)$$

Empirical equations 10-13 is used to calculate the liposomal partition coefficient ( $\log P_{n/d,lip}$ ) for neutral and ionized form of bases and acids<sup>29</sup>.

$$\log P_{n,lip} = 0.33 \log P_n + 2.2 \quad (\text{Neutral forms of bases}) \quad (10)$$

$$(\text{Neutral forms of acids}) \quad \log P_{n,lip} = 0.37 \log P_n + 2.2 \quad (11)$$

$$\log P_{d,lip} = 0.37 \log P_d + 2 \quad (\text{Cationic forms of bases}) \quad (12)$$

$$\log P_{d,lip} = 0.33 \log P_d + 2.6 \quad (\text{Anionic forms of acids}) \quad (13)$$

Eq 14 was used to estimate the partition coefficients ( $\log P_d$ ) of ionized form of the molecules from  $\log P_n$ .

$$\log P_d = \log P_n - 3.7 \quad (14)$$

The membrane permeability  $P_n$  and  $P_d$  were estimated by eq 15<sup>30</sup>.

$$P_{n/d} = DK / \Delta x \quad (15)$$

D is the diffusion coefficient, which is estimated as  $10^{-14}$  m<sup>2</sup>/s for organic molecules in lipids. K is the partition coefficient and approximates the liposomal partition coefficient  $K_{ow,n/d}$ ,  $\Delta x$  is the membrane thickness (approximately 50 nm for a phospholipid bilayer).

The expanded coupled ordinary differential equations (ODEs) can be derived based on the forementioned equations (Supporting information, eq 2). Each equation describes the rate of concentration change for a corresponding compartment. The time course of concentration change for each compartment was obtained by numerically solving the differential equation system using Matlab<sup>®</sup> (Version R2007b, The Mathworks Inc, Natick, MA). The ODE15S solver was used to address the issue of the stiffness in the differential equations system, and the relative and absolute error tolerance was set as  $10^{-12}$  to achieve good accuracy for the numerical solutions.

### **2.2.3. Parameters of the Compartmental Model**

Lung tissue varies in histological and anatomical properties from the trachea, to the bronchi, to the lower airways, and all the way down to the alveolar region, as a function of the branching generation. For the sake of simplicity, the lung was divided into two components: (1) the upper airways encompassing trachea and bronchi, with its blood supply provided by the bronchial circulation; and, (2) the lung parenchyma mainly composed of alveoli, with its blood supply provided by the pulmonary circulation. Several cell types are present in the upper airways epithelium, including basal cells, goblet cells, ciliated cells, brush cells, and mast cells etc. Also for the sake of simplicity, three major cell types were considered; (1) apical epithelial cells; (2) endothelial cells; and (3) interstitial cells including smooth muscle and immune cells. In the alveolar region of the lung, the major cell types are epithelial, endothelial and macrophages. Unlike in the trachea-bronchial airways, there is no substantial smooth muscle or other interstitial cells in the alveolar region.

Most of the histological parameters (cell thickness, surface area) of the airways and the alveolar region were obtained from the scientific literature (Table 2.1.)<sup>31-35</sup>. The volume of each cell layer in each branching generation was estimated as the product of surface area and cell thickness. The parameters of the immune cells in the interstitium were estimated based on 10 percent of interstitial cells being macrophages. Nevertheless, the cell thickness and surface area of epithelium and smooth muscle in tracheaobronchial airways varies, as reported in the literature<sup>31, 34, 36</sup>. We adopted the Yeh model to estimate the

thickness, surface area of epithelium and smooth muscle cells in airways<sup>37</sup>. Yeh model describes a “typical” pathway from trachea to terminal bronchioles with 16 generations of branches, in which the number of airways, diameter, and length at each generation is pre-established. Airways at each generation are considered as cylindrical tubes, so that the total surface area of basement membrane beneath the epithelium at each generation of airways can be calculated based on the respective diameter, length, and the number of airways at each generation. Assuming that the epithelium and smooth muscle form around the airway as cylinder tubes with same perimeter as the basement membrane, and that their cell thickness decreases by 1  $\mu\text{m}$  with each generation beginning with the trachea, one can estimate the volume of epithelium and smooth muscle for each branching generation of airways. The volume and surface area of cells at each generation is then added up as geometric parameters describing the corresponding compartment (Appendix, Table I). The average interstitial thickness in airway (excluding the interstitial cells) was estimated to be 1  $\mu\text{m}$  and the surface area and volume of immune cells was estimated as 1 percent of interstitium<sup>38, 39</sup>. The surface area of endothelium was estimated as one fifth of the airway surface area<sup>40</sup>. The lipid fraction for surface lining liquid in airway and alveoli is estimated to be 0.2 and 0.95, respectively<sup>41, 42</sup>. The physiological parameters for an epithelial cell were extracted from literature<sup>27</sup>. The membrane potential for other cell types was set as -60 mv. To perform sensitivity analysis, each parameter in the model was randomly sampled 1000 times from a uniform distributed variable within 1/100 and 100 times of the default value or a realistic

span based on prior knowledge. All default parameter values and the sensitivity analysis are given in the Appendix, Table II, III and IV. The logP and pK<sub>a</sub> of propranolol were used as input parameters to evaluate the robustness of the model.

#### **2.2.4. Simulations of the Transcellular Absorption of Small Molecules in Tracheobronchial Airways and Alveolar Region**

For simulation, a standard initial dose of 50 nmol was delivered to the surface liquid (drug donor compartment) based on drug absorption experiments in rats<sup>23, 24</sup>. For simulation, the pK<sub>a</sub> (5 to 14 with interval of 0.2 units) and logP (-2 to 4 with interval of 0.1 units, corresponding to logP<sub>n</sub>) of mono-basic compounds were varied independently and used as input. For each logP and pK<sub>a</sub> combination, the time course change of amount of compounds in each compartment in airways or alveolar region was obtained by numerically solving the coupled differential equations at a predetermined time point, and then multiplying the calculated local concentrations by the volume of the corresponding compartment. For each time point, the amount of compound in each cellular compartment (macrophage, epithelium, smooth muscle, etc) was summed up as the total amount of compound in lung tissue. The absorption rate constant (K<sub>a</sub>, min<sup>-1</sup>) was defined as follows:

$$K_a = \frac{\ln 2}{\text{abs}T_{50}} \quad (16)$$

The absorption half life (absT<sub>50</sub>, minutes) refers to the time when a half of dosage appears in the drug receiver compartment (the plasma). P<sub>max</sub> refers to the

maximal percentage of amount of compounds retained by the lung tissue as well as other cell types during the absorption process, and  $T_{\max, \text{lung}}$  is the time when the peak of amount of compounds in the lung tissue is reached.

### **2.2.5. Simulations of the Transcellular Absorption of Small Molecules in Whole Rat Lung**

For simulating drug absorption in whole rat lung, the regional distribution of dose in the rat lung was used as input parameter, to mimic the drug deposition pattern achieved by aerosol devices. Based on published experimental findings, simulation was performed using 50 nmol as total dose with regional distribution of 70% total dosage deposited in the tracheaobronchial airways and 30% deposited in alveoli<sup>23, 24</sup>. After solving the differential equations system for airways and alveoli separately, we generalized all compartments in airways and alveoli area as three compartments, including drug donor compartment (the surface liquid), lung tissue (the sum of all cellular compartments in airway and alveolar region), and drug receiver compartment (the plasma). The  $\text{abs}T_{50}$  is defined as the time when a half of the total dose (25 nmol) enters the generalized drug receiver compartment.

### **2.2.6. Simulations of Efflux Transporters and Organelle Sequestration**

Efflux transporters were included at the apical membrane of epithelial cells in both airway and alveolar region. The Michaelis-Menten equation was used to describe this saturable drug efflux component. The  $K_m$  value (432  $\mu\text{M}$ ) used for modeling was extracted from the *in vitro* measurement of talinolol as substrate of

P-glycoprotein (P-gp)<sup>43-45</sup>. Lacking quantitative information of kinetic parameters of P-gp or other transporters in rat lung, we performed simulations by gradually increasing the  $V_{\max,area}$  from  $1 \times 10^{-15}$  mol/sec/cm<sup>2</sup> (the  $V_{\max}$  of the P-gp inhibitor verapamil in normal Caco-2 cell line) up to  $1 \times 10^{-6}$  mol/sec/cm<sup>2</sup>, thereby making the simulation conditions cover a physiologically-relevant range of values based on experiments in other systems<sup>46</sup>. In the simulation, the density of transporters was considered as a constant throughout the lung epithelium. Due to the squamous character of alveolar epithelium, the  $V_{\max,area}$  was divided by 50 to get the normalized  $V_{\max,area}$  for alveolar region (because the average surface area of alveolar and intestinal epithelium is 5000  $\mu\text{m}^2$ <sup>31</sup>, and 100  $\mu\text{m}^2$ , respectively). We assumed  $V_{\max,area}$  for airway is the same as the  $V_{\max,area}$  in cell lines. The  $V_{\max}$  (unit: mol/sec) for airways and alveoli was computed by multiplying the corresponding surface area of apical membrane of epithelial cells with the  $V_{\max,area}$ .

Two organelle compartments (mitochondria and lysosome) were incorporated in the epithelial cell types at the airway and alveolar region. The volume ( $\text{m}^3$ ) of mitochondria and lysosome were estimated as 5% each of corresponding cytoplasm of epithelial cells. The surface area ( $\text{m}^2$ ) of mitochondria and lysosome were calculated by multiplying  $5.99 \times 10^6$  with their corresponding volume. Membrane potential for mitochondria and lysosome was set as -160 mv and +10 mv, respectively<sup>27, 28</sup>. pH in mitochondria and lysosome was set as 8 and 5, respectively.



## 2.3. Results

### 2.3.1. Absorption and Retention of Small Molecules in Tracheobronchial Airways

Combinations of  $\log P$  (corresponding to  $\log P_n$ , ranging from -2 to 4) and  $pK_a$  (ranging from 5 to 14) were used as input to calculate  $absT_{50}$ ,  $T_{max}$ , and  $P_{max}$  (Figure 2.2.). In airways, compounds with higher lipophilicity were absorbed more rapidly, but this trend was less pronounced when  $\log P > 1$  (Figure 2.2A.). The absorption rate of compounds with basic  $pK_a < 7.5$  was fastest and less influenced by lipophilicity and  $pK_a$ . For hydrophilic compounds with  $\log P < 0$  and  $7.5 < pK_a < 9$ , the  $abs T_{50}$  was most sensitive to the change of  $pK_a$  and  $\log P$ . Over this range, a one unit change in  $pK_a$  or  $\log P$  increased or decreased  $absT_{50}$  by 3 minutes. For compounds with  $pK_a > 9$ , the  $pK_a$  had little effect on  $abs T_{50}$ , and only  $\log P$  affected the  $abs T_{50}$  in this range.

The rate limiting step for the transport across the airway epithelium was the diffusion across the apical membrane (Appendix, Figure 3). The amount of drug retained by airway tissue ranged from 20 to 60 % of total dosage during the absorption process (Figure 2.2B.). For molecules with  $pK_a$  greater than 9, the maximal percentage of compounds retained by the lung tissue during the absorption process was 40 to 60% (Figure 2.2B.) and  $t_{max, lung}$  of 0.8 to 5 minutes (Figure 2.2C.), which could provide a sufficient exposure and fast onset of action for compounds acting locally. Smooth muscle retained up to 50% of the total dose administered to the airway (Figure 2.2D.). Molecules with lower  $\log P$  and

higher  $pK_a$  had a greater tendency to be distributed into the airway tissues, with airway tissue retention being most sensitive to changes of drug physicochemical properties when  $7 < pK_a < 9$  (Figure 2.2C., 2.2D.).

For compounds with high  $pK_a$  and low  $\log P$ , the efflux rate from the airway tissue to the plasma was slower than the rate of absorption from the surface layer into the airway, explaining their high tissue accumulation. Lower  $\log P$  and higher  $pK_a$  slowed down the plasma efflux rate of compounds from the airway more than it slowed the influx rate into the airway tissue, which in turn led to more drug retention and exposure in the airway tissue. Thus, for optimizing locally acting drugs targeting the upper airway, a strategy for prolonging the therapeutic effect can exploit the factors determining the compound's leaving kinetics from lung tissue (e.g. smooth muscle retention, organelle sequestration, and protein binding), and not just solubility, dissolution, and permeability properties affecting absorption into the lung tissue.

### **2.3.2. Absorption and Retention of Small Molecules in Alveolar Region**

The absorption rate in the alveolar region was very fast: even the longest  $absT_{50}$  of monobasic compounds in alveolar region was less than one and half minutes (Figure 2.3A.). The rate limiting step for the transport across the alveolar epithelium was the diffusion across the apical membrane (Appendix, Figure 3). For monobasic compounds, only those with  $pK_a < 7.5$  possessed  $absT_{50} > one$  minute. The physicochemical properties of compounds had a minor effect on the absorption in the alveolar region, over the range tested. The maximal percentage of compounds retained in alveolar tissue ranged from 1 to 16% of total dose. The

major cell type of tissue retention was the epithelium with maximal 5% accumulation (Figure 2.3B., 2.3D.). More importantly,  $t_{max}$  in alveolar tissue was less than 0.3 minutes (Figure 2.3C.), with the influx and efflux rate of monobasic small molecules into and out of the alveolar tissue being very fast.

### **2.3.3. Absorption in the Lung as a Function of Regional Deposition Pattern**

Regional drug deposition patterns can affect absorption and bioavailability in the lung<sup>17, 19, 47</sup>. To mimic the deposition pattern of *in vivo* and *ex vivo* drug inhalation experiments<sup>22-24</sup> simulation was performed to calculate the  $absT_{50}$  for the whole lung under the condition that 70% of the starting dose was deposited in the airway and 30% dosage was deposited in the alveolar region.. The  $absT_{50}$  for the whole lung ranged from 1 to 9 minutes depending on the physicochemical properties of the drug (Figure 2.4.). The general trend of how  $absT_{50}$  changed in the whole lung was similar to the trend observed in the airways.

### **2.3.4. Model Validation and Parameter Sensitivity Analysis**

Based on published measurements<sup>17-19, 22-24</sup>, nine compounds with single ionized species under physiological pH conditions were used to test the model (Table 2.2.). These compounds included monovalent weak bases and acids with diverse structures and very different physicochemical properties (Table 2.2). The predicted  $absT_{50}$  for all these compounds in alveolar region was less than 1.5 minutes (Table 2.2). If the radius of the compounds was not taken into account, simulation results using  $\log P$  and  $pK_a$  alone as inputs yielded poor predictions of relative absorption half-life compared to the experimental data ( $R^2$  less than 0.1,

data not shown). Nevertheless, for compounds with moderate Petitjean radius from 5 to 8, the experimental and predicted  $K_a$  were significantly correlated ( $R^2 = 0.86$ ,  $P = 0.004$  (one tail)) (Figure 2.5.). By incorporating size as a factor in the predictions, the predicted  $K_a$  for all nine compounds yielded a good correlation ( $R^2 = 0.87$ ,  $P = 0.0001$  (one tail)) with the measured  $K_a$  values (Figure 2.6.).

Because of variation and uncertainty in the parameters used in the model, we analyzed the sensitivity of the predicted  $absT_{50}$  in the lung to variations of all the input parameters values (Appendix, Table III, IV). The prediction of the absorption half-life of applicable compounds had a maximal deviation of 0.38 minutes in the lung (Appendix, table III, IV). Although the relative deviation from the corresponding predicted value was about 30% in the lung, the  $absT_{50}$  and  $K_a$  calculated with the simulations were within range of the experimentally measured values.

### **2.3.5. Additional Factors Affecting the Absorption Kinetics of Small Molecules in the Lung**

We assessed the theoretical effect of P-gp on the apical epithelial cell membrane on the lung pharmacokinetics of talinolol. The  $K_m$  (423  $\mu\text{M}$ ) of talinolol served as input, with  $V_{\text{max,area}}$  ( $\text{mol}/\text{sec}/\text{cm}^2$ ) ranging from  $1 \times 10^{-15}$   $\text{mol}/\text{sec}/\text{cm}^2$  (the  $V_{\text{max,area}}$  of P-gp inhibitor verapamil in Caco-2 cells<sup>46</sup>) to a value that was nine orders of magnitude higher, scanning a physiologically realistic range of  $V_{\text{max,area}}$ . The transporter effect was most significant when the initial dose was deposited only in the airways ( $R = 100\%$ ; Figure 2.7.). In the alveolar region, the transporter effect was reduced. Based on simulation results the  $absT_{50}$  of talinolol

fell into the observed range of 12-22 minutes (Figure 2.7.) if 70% of 50 nmol dose was deposited in the airways and the predicted  $V_{\max,area}$  for talinolol was from  $2 \times 10^{-9}$  mol/sec/cm<sup>2</sup> to  $6 \times 10^{-9}$  mol/sec/cm<sup>2</sup> (Figure 2.7.).

Lastly, we assessed the effect of intracellular organelles on lung pharmacokinetics. Including mitochondria and lysosomes in the simulations increased the predicted  $absT_{50}$  for monobasic compounds only slightly for most  $pK_a$  and  $\log P$  conditions (Figure 2.8.). The most pronounced effect of organelles was observed for monobasic compounds with  $pK_a > 10$  with lung  $absT_{50}$  increasing by a factor of 10 or more (Figure 2.8A.). The organelle sequestration effect was quite pronounced in the airway (Figure 2.8B.) and comparatively insignificant in the alveoli (Figure 2.8C.).

## 2.4. Discussions

In this study, a multiscale, cell-based compartmental model was developed to analyze the transport of cell-permeant, weakly basic or acidic, monoprotic small molecules in the lung. To predict drug absorption, the transcellular diffusion of small molecules across the phospholipid bilayer was modeled with Fick's and Plank-Nernst's equations. The ionization state and lipid partitioning of neutral and ionized forms of the molecules was used to compute the free aqueous fraction of concentration for both neutral and ionized form in each subcellular compartment. Based on the concentration gradient of neutral and ionized, free aqueous species, the concentration and amount at different compartments within the lung could be calculated through time, in accordance with the histological and morphological architecture of the airways and alveolar region.

For development of locally-targeted small molecule drugs, a cell-based biophysical model is able to capture how the behavior of small molecules in airways and alveolar region are different. Our results illustrate how such a model can provide quantitative insights about the relationship between the physicochemical properties and absorption and tissue retention in the upper airways vs. alveolar region. The simulations suggest that a molecule is absorbed at a slower rate in the upper airway, and has more tissue retention than in alveolar region. Organelle sequestration also has a far more significant effect on upper airway pharmacokinetics. Therefore, the upper airway appears as the preferred drug targeting site for local (inhaled) drug therapy with monoprotic

weakly basic small molecules. Conversely, the alveolar region is a far more challenging site to target with locally-active inhaled, cell-permeant, monoprotic weakly basic molecules, while it would be the preferred site for facilitating their absorption into the systemic circulation.

The predicted absorption kinetics in lung are very rapid compared with that of the GI tract, and were all consistent in time scale with respect to experimentally-measured absorption kinetics in rat lungs. For model validation, the correlation between predicted and reported values for small lipophilic, monobasic or monoacid molecules within the size range of most drugs (i.e.  $4 < \text{Petitjean radius} < 9$ ) was found to be significant ( $R^2 = 0.86$ ). For molecules of larger or smaller size, the molecular radius is far more important than logP and  $pK_a$  in determining absorption kinetics. Only by accounting for radius with a semi-empirical formula, the correlation between predicted and reported values for compounds that included molecules with extreme size range was significant ( $R^2 = 0.87$ ). As a caveat, the correlation ( $R^2$ ) was 0.60 ( $P = 0.06$  (one tail)) if losartan was removed, which points to the need of acquiring more experimental data for furthering model refinement and validation.

Compared to the other organ systems, the effect of active transporters on drug absorption in the lung have not been extensively studied, although there are suggestions that bioavailability of inhaled medications is minimally affected by such transporters<sup>24</sup>. We used talinolol as a model P-gp substrate in simulations to quantify the potential role of transporters on the  $absT_{50}$  using the *in vitro* kinetic parameters (i.e.  $V_{max}$  and  $K_m$ ). P-gp expression in lung cell lines and *in vivo* is

lower than in Caco-2 cells with measured  $V_{\max}$  only around  $2 \times 10^{-12}$  mol/sec/cm<sup>2</sup>.<sup>46,48-50</sup> Therefore, the predicted much larger  $V_{\max}$  values ( $2 \times 10^{-9}$  to  $6 \times 10^{-9}$  mol/sec/cm<sup>2</sup>) suggests that efflux by P-gp at the apical side of lung epithelial cells cannot account for talinolol's slower-than-expected absorption. As an alternative explanation, the absorption of talinolol could be mostly limited by its larger size and low solubility<sup>24, 48</sup>.

By running simulations with and without mitochondria and lysosomes, the effect of organelle sequestration on small molecule retention and absorption in airways vs. alveoli was also analyzed. The results indicate that organelle sequestration slows down of absorption of monobasic small molecules in the upper airways when  $pK_a > 10.5$ . This effect is largely due to the membrane potential-dependent uptake of positively-charged, protonated species in the mitochondria. The organelle sequestration effect in alveoli is minimal, due to the larger apical and basolateral membrane surface areas in relation to the mitochondrial surface area of alveolar epithelial and endothelial cells, as well as the absence of interstitial cells. For molecules with  $pK_a < 10.5$  the passive diffusion of the neutral species of the molecule does not allow for prolonged retention in mitochondria or lysosomes, with minimal effect on  $absT_{50}$  in both airways and alveoli.

While helping formulate quantitative hypothesis, these results illustrate how a cell-based computational model can help us interpret experimental data on the absorption and retention of small compounds in the lung in the context of the branching structure of the airways, and the cellular organization of the walls of



the airways. Presently, the scope of the model is constrained to basic or acidic, monoprotic compounds which are cell permeant, of a limited size range for which the transcellular route is the primary absorption pathway. Admittedly, the uncertainty and inter-individual variability in the estimated or measured parameters for cell types are factors that can affect the accuracy of the model<sup>31</sup>,<sup>34</sup>. Nevertheless, the parameter sensitivity (error propagation) analysis indicates that the predictions are robust and error-tolerant within the aforementioned constraints and the range of uncertainty of the estimated model parameters.

While this cell-based, mechanistic model can be further elaborated and improved, one of its important applications may reside in its ability to help design inhaled compounds with optimal physiochemical properties at early stage of drug design, thereby improving drug targeting and delivery in the lung. It can also help make predictions about the bioaccumulation and biodistribution properties of inhaled chemical agents, for toxicity risk assessment. More importantly, because the model incorporates quantitative species-specific information about the anatomy, physiology and histology of the lung, it can be scaled to predict human lung absorption. Its potential to bridge the gap between animal species and humans may be particularly valuable when clinical lung absorption data is scarce.

To summarize, a cell-based biophysical model of drug absorption in the lungs is a computational tool that can provide mechanistic insights about a relatively unexplored site of drug targeting and delivery. As additional small molecule absorption experiments are performed, the model can be further validated, refined and elaborated, to increase its accuracy and extend its domain

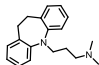
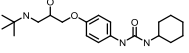
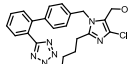
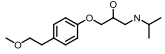
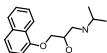
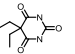
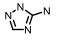
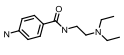
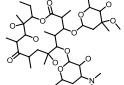
of applicability. Planned experiments and future development effort will aim at exploring the size dependency of transport behavior, modeling paracellular transport routes of more hydrophilic compounds and macromolecules, probing active transport effects, as well as extending the model to zwitterionic and multivalent molecules.

**Table 2.1.** Parameters for the tracheobronchial airways and alveolar region in the rat <sup>a</sup>

Compartments	Tracheobronchial Airways			Alveolar Region		
	Average thickness (μm)	Surface area (cm <sup>2</sup> )	Volume (cm <sup>3</sup> )	Average thickness (μm)	Surface area (cm <sup>2</sup> )	Volume (cm <sup>3</sup> )
Surface lining liquid	15 <sup>b</sup>	108	0.162	5	3870	1.935
Macrophage	-	-	-	-	42	0.0282
Epithelium	24-9 <sup>c</sup>	108	0.072 <sup>d</sup>	0.384	3870	0.148
Interstitial	1 <sup>d</sup>	108	0.0108 <sup>d</sup>	0.693	3870	0.268
Immune cells	-	1.08 <sup>d</sup>	0.000108 <sup>d</sup>	-	4.2 <sup>d</sup>	0.00282 <sup>d</sup>
Smooth muscle	19.3-4.3 <sup>e</sup>	216 <sup>d</sup>	0.047 <sup>d</sup>	-	-	-
Endothelium	0.4 <sup>f</sup>	21.6 <sup>d</sup>	0.000864 <sup>d</sup>	0.358	4520	0.162

a. All parameters were extracted from <sup>31</sup> unless otherwise specified  
b. <sup>32</sup> c. <sup>34</sup> d. Calculated or estimated (See methods) e. <sup>33</sup> f. <sup>35</sup>

**Table 2.2.** Structures, physicochemical properties, observed  $\text{absT}_{50}$ ,  $K_a$ , and predicted absorption profile of nine monocharged molecules <sup>a</sup>

Drug name	Structure	$\text{pK}_a$	logP	Petitjean radius	obs $\text{T}_{50}$ observed (min)	$K_a$ observed ( $\text{min}^{-1}$ )	Predicted			
							obs $\text{T}_{50}$ (min)	$K_a$ ( $\text{min}^{-1}$ )	obs $\text{T}_{50}$ in airway (min)	obs $\text{T}_{50}$ in alveolar (min)
Imipramine		9.2	4.01	5	1	0.69	1.12	0.62	1.41	0.62
Talinolol		9.76	2.46	9	17	0.041	1.26	0.55	1.69	0.59
Losartan		8.15 <sup>b</sup>	4.18	8	26	0.027	2.27	0.30	2.97	1.27
Metoprolol		9.67	1.49	7	2.5	0.28	1.48	0.47	2.10	0.60
Propranolol		9.67	2.5	6	2	0.35	1.25	0.55	1.66	0.59
Barbital		7.58 <sup>b</sup>	0.74	3	0.93	0.75	2.42	0.29	3.20	1.32
Amitrole		8.59 <sup>b</sup>	0.31	2	1.3	0.53	2.30	0.30	3.03	1.26
Procainamide		9.04	0.83	6	2.3	0.30	1.63	0.42	2.31	0.68
Erythromycin		8.38	1.22	8	6.3	0.11	1.58	0.44	2.05	0.85

a. Observed  $\text{absT}_{50}$  is from <sup>17, 23, 24</sup>. logP and  $\text{pK}_a$  was calculated by Chemaxon <sup>49</sup>. The Petitjean descriptor was calculated by MOE <sup>50, 51</sup>.  
b. acid  $\text{pK}_a$

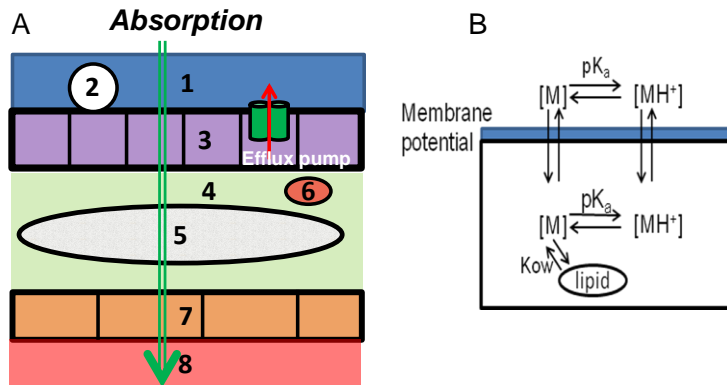


**Figure 2.1. A.** Diagram representing the general route of drug transport from the airways to the blood, across the histological architecture of lung tissue. 1: Surface lining (liquid) layer (Drug donor compartment); 2: Macrophage (in alveolar region only) 3: Airway epithelial cells 4: Extracellular fluid (interstitium) 5: Smooth muscle (in airways only) 6. Immune cells 7: Endothelium cells 8: Systemic circulation (Drug receiver compartment). **B.** Diagram representing the path of a monobasic compound across adjacent compartments separated by a phospholipid bilayer, as captured by the model. The neutral form of the molecule is indicated as [M], and the protonated, cationic form of the molecule is indicated as [MH<sup>+</sup>].

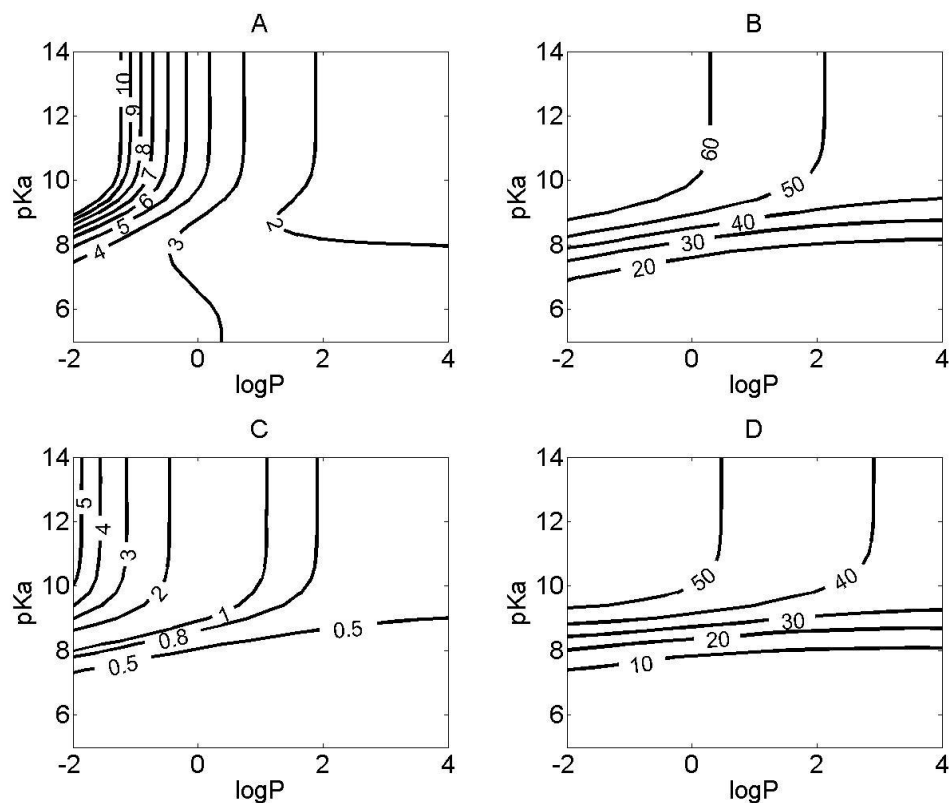


**Figure 2.2.** The relationship between the physicochemical properties and the absorption or tissue retention in the airways. For simulations, the initial dose was set to 50 nmol, and the  $\log P$  (corresponding to  $\log P_n$ ) and  $pK_a$  were varied independently. X axis represents the  $\log P$ , Y axis represents  $pK_a$ . Contour line indicates: **A.** The  $\text{absT}_{50}$  (unit: minutes) of molecules in airway; **B.** The maximal amount of compounds (%) retained by airway tissue during the absorption process. **C.** The time (minutes) when the maximal percentage of the total amount of compounds was reached in airway tissue. **D.** The maximal amount of compounds (%) retained by smooth muscle during the absorption process.

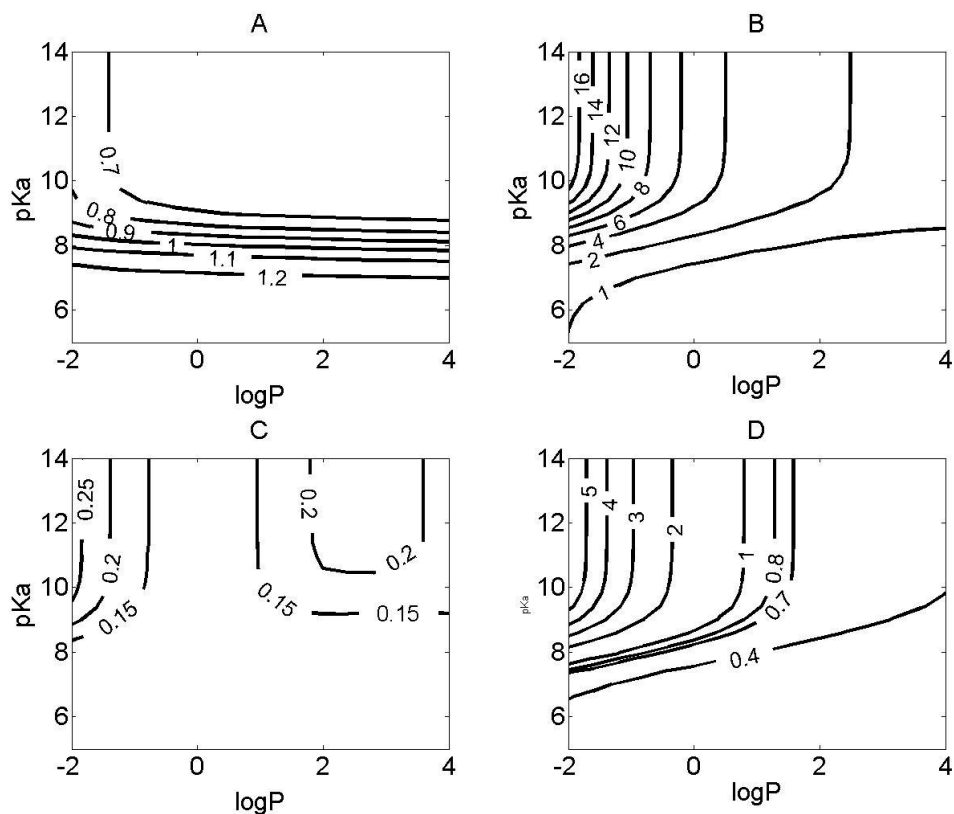


**Figure 2.3.** The relationship between the physicochemical properties and the absorption or tissue retention in the alveolar region. For simulations, the initial dose was set to 50 nmol, and  $\log P$  (corresponding to  $\log P_n$ ) and  $pK_a$  were varied independently. X axis represents the  $\log P$ . Y axis represents  $pK_a$ . Contour line indicates: **A.** The  $abst_{50}$  (unit: minutes) of molecules in alveolar region; **B.** The maximal amount of compounds (%) retained by alveolar tissue during the absorption process. **C.** The time (minutes) when the maximal percentage of amount of compounds was reached in alveolar tissue. **D.** The amount of compound (%) retained by alveolar epithelium during the absorption process.

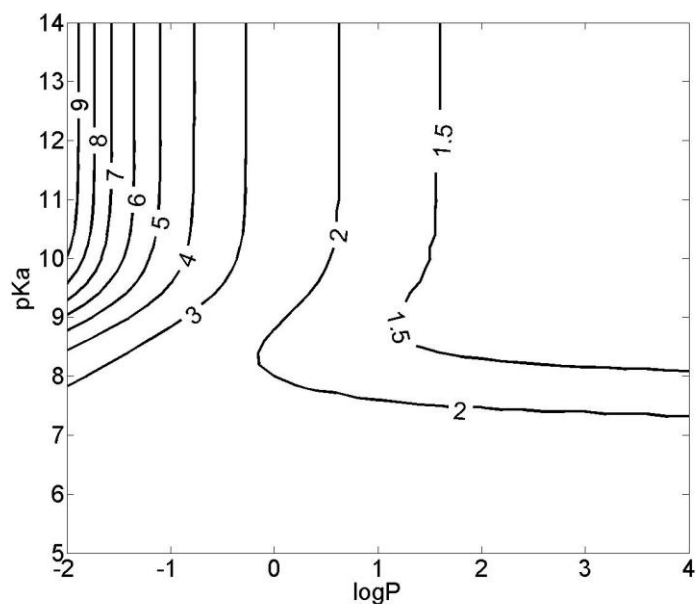


**Figure 2.4.** The relationship between the physicochemical properties and the absorption in the whole lung with a dosage deposition of 70% in airways and 30% in alveolar region. For simulations, the initial dose was set to 50 nmol, and  $\log P$  (corresponding to  $\log P_n$ ) and  $pK_a$  were varied independently. X axis represents the  $\log P$ . Y axis represents the  $pK_a$ . Contour line indicates the  $absT_{50}$  (minutes) of molecules in whole lung.



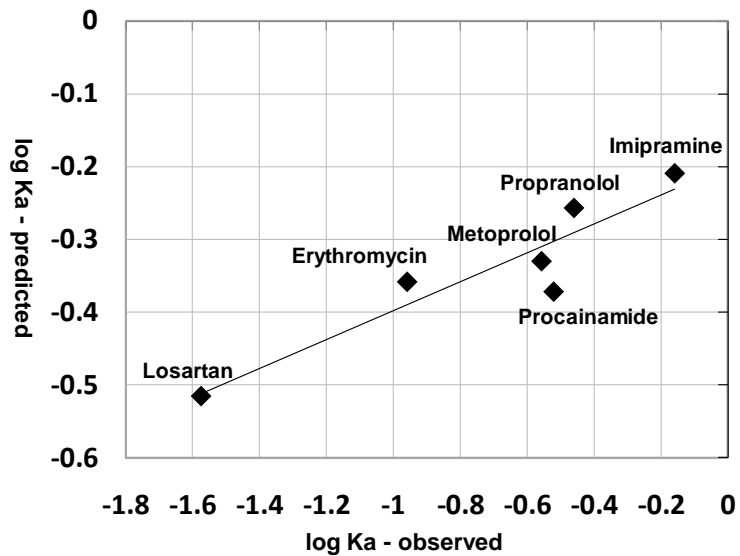


**Figure 2.5.** Observed  $K_a$  and predicted  $K_a$  are related, for small drug-like molecules of intermediate size range (Petitjean radius 5 to 8). Regression equation:  $\log K_a$  (predicted) = 0.198  $\log K_a$  (observed) – 0.199;  $R^2=0.86$ .

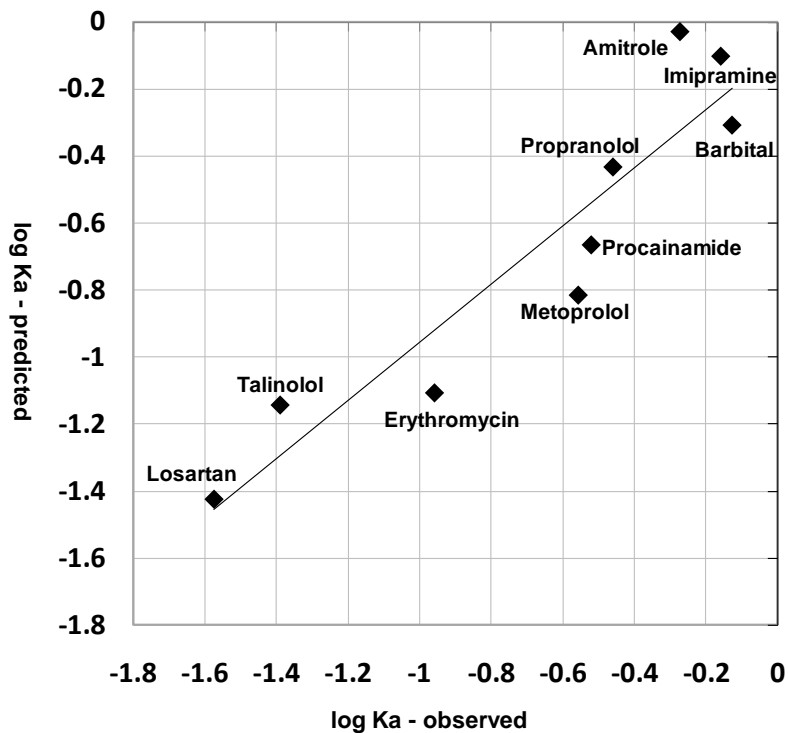


**Figure 2.6.** The correlation between the observed and predicted  $\log K_a$ , obtained by partial least square (PLS) regression using the predicted  $\log K_a$  and Petitjean radius as variables. The regression relationship was described by the following equation:  $\log K_a$  (observed) = 1.48 – 0.23 radius + 2.01  $\log K_a$  (predicted);  $R^2=0.87$ .

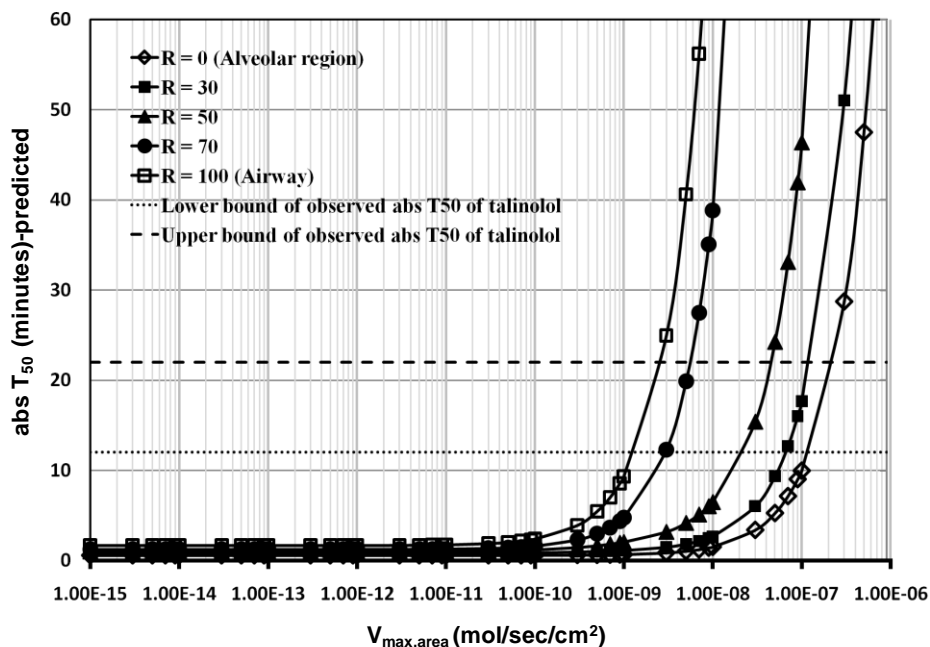


**Figure 2.7.** The effect of an apical airway efflux transporter with  $K_m = 423 \mu\text{M}$ . For simulations,  $V_{\text{max,area}}$  was varied from  $1 \times 10^{-15}$  to  $1 \times 10^{-6}$  ( $\text{mol}/\text{sec}/\text{cm}^2$ ).  $R$  is the percentage of total dose (50 nmol) deposited in the airways.

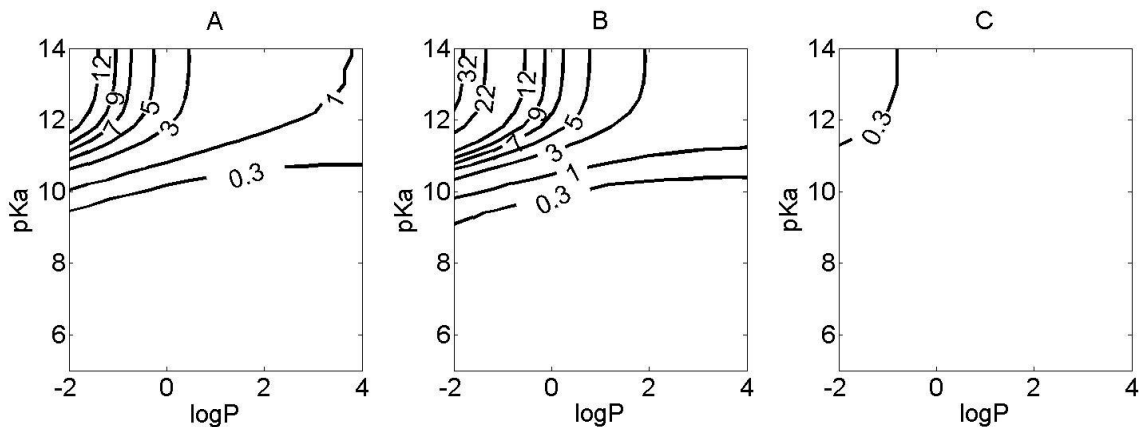


**Figure 2.8.** The simulated effect of organelle sequestration on lung pharmacokinetics of small molecules of varying physicochemical properties. For the simulations, the initial dose was 50 nmol.  $\log P$  (corresponding to  $\log P_n$ ) and  $pK_a$  were varied independently. X axis represents the  $\log P$ . Y axis represents  $pK_a$ . Contour line indicates: A. the difference in the  $\text{abs}T_{50}$  (minutes) between simulations carried out with and without organelles for the lung, with 70% of the dose in airways and 30% in alveolar region. B. the difference in the  $\text{abs}T_{50}$  (minutes) between simulations carried out with and without organelles for the airway. C. the difference in the  $\text{abs}T_{50}$  (minutes) between simulations carried out with and without organelles for the alveolar region.

## 2.5. References

1. Brewis, R. L.; Corrin, B.; Geddes, D. M.; Gibson, G. J., *Respiratory Medicine*. second ed.; WB Saunders Company Ltd: London, 1995.
2. Ehrhardt, C.; Kim, K.-J., *Drug absorption studies: in situ, in vitro and in silico models*. Springer: Arlington, VA, 2008.
3. Lipworth, B. J., Pharmacokinetics of inhaled drugs. *Br J Clin Pharmacol* **1996**, *42* (6), 697-705.
4. Wall, D. A.; Lanutti, A. T., High-Levels of Exopeptidase Activity Are Present in Rat and Canine Bronchoalveolar Lavage Fluid. *International Journal of Pharmaceutics* **1993**, *97* (1-3), 171-181.
5. Patton, J. S., Mechanisms of macromolecule absorption by the lungs. *Advanced Drug Delivery Reviews* **1996**, *19* (1), 3-36.
6. Anttila, S.; Hukkanen, J.; Hakkola, J.; Stjernvall, T.; Beaune, P.; Edwards, R. J.; Boobis, A. R.; Pelkonen, O.; Raunio, H., Expression and localization of CYP3A4 and CYP3A5 in human lung. *American Journal of Respiratory Cell and Molecular Biology* **1997**, *16* (3), 242-249.
7. Niven, R. W., Delivery of Biotherapeutics by Inhalation Aerosol. *Critical Reviews in Therapeutic Drug Carrier Systems* **1995**, *12* (2-3), 151-231.
8. LiCalsi, C.; Christensen, T.; Bennett, J. V.; Phillips, E.; Witham, C., Dry powder inhalation as a potential delivery method for vaccines. *Vaccine* **1999**, *17* (13-14), 1796-1803.
9. Russell, K. E.; Read, M. S.; Bellinger, D. A.; Leitermann, K.; Rup, B. J.; McCarthy, K. P.; Keith, J. C., Jr.; Khor, S. P.; Schaub, R. G.; Nichols, T. C., Intratracheal administration of recombinant human factor IX (BeneFix) achieves therapeutic levels in hemophilia B dogs. *Thromb Haemost* **2001**, *85* (3), 445-9.
10. Skyler, J. S.; Cefalu, W. T.; Kourides, I. A.; Landschulz, W. H.; Balagtas, C. C.; Cheng, S. L.; Gelfand, R. A.; Grp, I. I. P. I. S., Efficacy of inhaled human insulin in type 1 diabetes mellitus: a randomised proof-of-concept study. *Lancet* **2001**, *357* (9253), 331-335.
11. Patton, J. S.; Byron, P. R., Inhaling medicines: delivering drugs to the body through the lungs. *Nature Reviews Drug Discovery* **2007**, *6* (1), 67-74.
12. Gumbleton, M.; Taylor, G., Challenges and innovations in effective pulmonary systemic and macromolecular drug delivery. *Adv Drug Deliv Rev* **2006**, *58* (9-10), 993-5.
13. Shoyele, S. A.; Cawthorne, S., Particle engineering techniques for inhaled biopharmaceuticals. *Adv Drug Deliv Rev* **2006**, *58* (9-10), 1009-29.
14. Yu, L. X.; Lipka, E.; Crison, J. R.; Amidon, G. L., Transport approaches to the biopharmaceutical design of oral drug delivery systems: Prediction of intestinal absorption. *Adv Drug Deliver Rev* **1996**, *19* (3), 359-376.
15. Egan, W. J.; Lauri, G., Prediction of intestinal permeability. *Advanced Drug Delivery Reviews* **2002**, *54* (3), 273-289.
16. Norinder, U.; Haeberlein, M., Computational approaches to the prediction of the blood-brain distribution. *Advanced Drug Delivery Reviews* **2002**, *54* (3), 291-313.

17. Brown, R. A.; Schanker, L. S., Absorption of Aerosolized Drugs from the Rat Lung. *Drug Metabolism and Disposition* **1983**, 11 (4), 355-360.
18. Schanker, L. S.; Hemberger, J. A., Relation between Molecular-Weight and Pulmonary Absorption Rate of Lipid-Insoluble Compounds in Neonatal and Adult-Rats. *Biochemical Pharmacology* **1983**, 32 (17), 2599-2601.
19. Schanker, L. S.; Mitchell, E. W.; Brown, R. A., Species Comparison of Drug Absorption from the Lung after Aerosol Inhalation or Intratracheal Injection. *Drug Metabolism and Disposition* **1986**, 14 (1), 79-88.
20. Effros, R. M.; Pornsuriyasak, P.; Porszasz, J.; Casaburi, R., Indicator dilution measurements of extravascular lung water: basic assumptions and observations. *Am J Physiol Lung Cell Mol Physiol* **2008**, 294 (6), L1023-31.
21. Effros, R. M., Exhaled breath condensates and COPD. *Eur Respir J* **2009**, 33 (5), 1238.
22. Tronde, A. Pulmonary drug absorption: in vitro and in vivo investigations of drug absorption across the lung barrier and its relation to drug physicochemical properties. Uppsala University, 2002.
23. Tronde, A.; Norden, B.; Jeppsson, A. B.; Brunmark, P.; Nilsson, E.; Lennernas, H.; Bengtsson, U. H., Drug absorption from the isolated perfused rat lung--correlations with drug physicochemical properties and epithelial permeability. *J Drug Target* **2003**, 11 (1), 61-74.
24. Tronde, A.; Norden, B.; Marchner, H.; Wendel, A. K.; Lennernas, H.; Bengtsson, U. H., Pulmonary absorption rate and bioavailability of drugs in vivo in rats: structure-absorption relationships and physicochemical profiling of inhaled drugs. *J Pharm Sci* **2003**, 92 (6), 1216-33.
25. Manford, F.; Tronde, A.; Jeppsson, A. B.; Patel, N.; Johansson, F.; Forbes, B., Drug permeability in 16HBE14o- airway cell layers correlates with absorption from the isolated perfused rat lung. *European Journal of Pharmaceutical Sciences* **2005**, 26 (5), 414-20.
26. Oprea, T. I., Chemical space navigation in lead discovery. *Current Opinion in Chemical Biology* **2002**, 6 (3), 384-389.
27. Zhang, X.; Shedden, K.; Rosania, G. R., A cell-based molecular transport simulator for pharmacokinetic prediction and cheminformatic exploration. *Molecular Pharmaceutics* **2006**, 3 (6), 704-716.
28. Zhang, X.; Zheng, N.; Rosania, G. R., Simulation-based cheminformatic analysis of organelle-targeted molecules: lysosomotropic monobasic amines. *J Comput Aided Mol Des* **2008**, 22 (9), 629-45.
29. Balon, K.; Riebesehl, B. U.; Muller, B. W., Drug liposome partitioning as a tool for the prediction of human passive intestinal absorption. *Pharm Res* **1999**, 16 (6), 882-8.
30. Trapp, S.; Horobin, R. W., A predictive model for the selective accumulation of chemicals in tumor cells. *Eur Biophys J* **2005**, 34 (7), 959-66.
31. Parent, R. A., *Treatise on Pulmonary Toxicology: Comparative biology of the normal lung*. CRC Press: Boca Raton, 1992.
32. Widdicombe, J. G., Airway liquid: a barrier to drug diffusion? *Eur Respir J* **1997**, 10 (10), 2194-7.

33. Salmon, M.; Walsh, D. A.; Huang, T. J.; Barnes, P. J.; Leonard, T. B.; Hay, D. W.; Chung, K. F., Involvement of cysteinyl leukotrienes in airway smooth muscle cell DNA synthesis after repeated allergen exposure in sensitized Brown Norway rats. *Br J Pharmacol* **1999**, *127* (5), 1151-8.
34. Cohen, M. D.; Zelikoff, J. T.; Schlesinger, R. B., *Pulmonary Immunotoxicology*. Springer: 2000.
35. Crane, G. J.; Kotecha, N.; Luff, S. E.; Neil, T. O., Electrical coupling between smooth muscle and endothelium in arterioles of the guinea-pig small intestine. *Phys Med Biol* **2001**, *46* (9), 2421-34.
36. James, A. L.; Bai, T. R.; Mauad, T.; Abramson, M. J.; Dolhnikoff, M.; McKay, K. O.; Maxwell, P. S.; Elliot, J. G.; Green, F. H., Airway smooth muscle thickness in asthma is related to severity but not duration of asthma. *Eur Respir J* **2009**.
37. Yeh, H. C.; Schum, G. M.; Duggan, M. T., Anatomic models of the tracheobronchial and pulmonary regions of the rat. *Anat Rec* **1979**, *195* (3), 483-92.
38. Miller, L. A.; Hurst, S. D.; Coffman, R. L.; Tyler, N. K.; Stovall, M. Y.; Chou, D. L.; Putney, L. F.; Gershwin, L. J.; Schelegle, E. S.; Plopper, C. G.; Hyde, D. M., Airway generation-specific differences in the spatial distribution of immune cells and cytokines in allergen-challenged rhesus monkeys. *Clin Exp Allergy* **2005**, *35* (7), 894-906.
39. Ross, M. H.; Pawlina, W., *Histology: A Text and Atlas: With Correlated Cell and Molecular Biology*. 5th ed.; Lippincott Williams & Wilkins: 2006.
40. Kroll, F.; Karlsson, J. A.; Persson, C. G., Tracheobronchial microvessels perfused via the pulmonary artery in guinea-pig isolated lungs. *Acta Physiol Scand* **1987**, *129* (3), 445-6.
41. Sims, D. E.; Horne, M. M., Heterogeneity of the composition and thickness of tracheal mucus in rats. *Am J Physiol* **1997**, *273* (5 Pt 1), L1036-41.
42. Veldhuizen, R.; Nag, K.; Orgeig, S.; Possmayer, F., The role of lipids in pulmonary surfactant. *Biochim Biophys Acta* **1998**, *1408* (2-3), 90-108.
43. Doppenschmitt, S.; Spahn-Langguth, H.; Regardh, C. G.; Langguth, P., Role of P-glycoprotein-mediated secretion in absorptive drug permeability: An approach using passive membrane permeability and affinity to P-glycoprotein. *J Pharm Sci* **1999**, *88* (10), 1067-72.
44. Troutman, M. D.; Thakker, D. R., Efflux ratio cannot assess P-glycoprotein-mediated attenuation of absorptive transport: asymmetric effect of P-glycoprotein on absorptive and secretory transport across Caco-2 cell monolayers. *Pharm Res* **2003**, *20* (8), 1200-9.
45. Tubic, M.; Wagner, D.; Spahn-Langguth, H.; Bolger, M. B.; Langguth, P., In silico modeling of non-linear drug absorption for the P-gp substrate talinolol and of consequences for the resulting pharmacodynamic effect. *Pharm Res* **2006**, *23* (8), 1712-20.
46. Shirasaka, Y.; Sakane, T.; Yamashita, S., Effect of P-glycoprotein expression levels on the concentration-dependent permeability of drugs to the cell membrane. *Journal of Pharmaceutical Sciences* **2008**, *97* (1), 553-565.

47. French, M. C.; Wishart, G. N., Isolated Perfused Rabbit Lung as a Model to Study the Absorption of Organic Aerosols. *Journal of Pharmacological Methods* **1985**, 13 (3), 241-248.
48. Wagner, D.; Glube, N.; Berntsen, N.; Tremel, W.; Langguth, P., Different dissolution media lead to different crystal structures of talinolol with impact on its dissolution and solubility. *Drug Dev Ind Pharm* **2003**, 29 (8), 891-902.
49. *Marvin and Calculator*, 4.1.11; ChemAxon: Budapest, Hungary, 2007.
50. Petitjean, M., Applications of the Radius Diameter Diagram to the Classification of Topological and Geometrical Shapes of Chemical-Compounds. *J Chem Inf Comp Sci* **1992**, 32 (4), 331-337.
51. *MOE: Molecular Operating Environment*, Chemical Computing Group: Montreal, Quebec, Canada, 2007.



## CHAPTER 3

### **The *in silico* studies of differential exposure of airways and alveoli with injection vs. intratracheal instillation**

#### **3.1 Introduction**

Geometrically, the anatomy of the lungs can be mathematically modeled as a tree-like branching system of cylinders of narrowing diameter. Starting with the trachea as the trunk of the tree and ending in the alveoli as the leaves, each branching segment corresponds to an airway 'generation' that can be characterized by its surface area, blood flow, and cellular organization.<sup>1, 2</sup> Histologically, the wall of the airway or alveoli can be mathematically modeled as a sequence of membrane-bound compartments (epithelial, interstitial and endothelial cell layers) separating the air from the blood. Several pronounced structural and functional differences between the airways and alveoli are noteworthy: 1. Cartilage and smooth muscle are present only in the interstitium of the airways. 2. The surface area in alveoli is 2 orders of magnitude larger than airways. 3. Airways and alveoli are supplied with different blood circulation.<sup>3, 4</sup>

Previously, we elaborated this *in silico* cell-based multiscale PK modeling approach, to predict the pharmacokinetics of monobasic, passively diffusing small monobasic molecules in an isolated perfused lung.<sup>2</sup> The model is based on the kinetic, passive diffusive transport properties of small molecules across cellular membranes, as well as the local partitioning of molecules into lipid in different subcellular compartments. The model considers that different molecules can exist in neutral or ionized forms depending on the  $pK_a$  of the functional groups of the molecules, and the pH of the microenvironment of the molecule is in. Based on the lipophilicity of the different neutral and charged species, differential equations are used to compute the flux of molecules across membranes bounding the cell and subcellular compartment.

Here, this multiscale, cell-based model was linked to a systemic PK model, to facilitate estimations of the regional concentration profiles of monobasic compounds in airways vs. alveoli, after inhalation or systemic administration. In doing so, we were able to simulate drug transport in the context of the entire living organism, which revealed how the transport, biodistribution and retention of molecules in different regions of the lung depends on drug route of administration as well as physicochemical characteristics determining organelle accumulation. Traditionally, physiologically-based pharmacokinetic models usually consider lungs as a homogeneous and well-stirred compartment<sup>5</sup>,<sup>6</sup>. In contrast, our approach provides unique insights in terms of how the histological organization, circulatory parameters and route of administration determines the differential transport of small molecules in airways and alveoli, in

a manner that can be exploited for bioimaging probe development or for optimizing the local concentration of pulmonary medications.<sup>7, 8</sup>

## 3.2 Methods

### 3.2.1 General Methodology

The multiscale framework of rat lungs was described in our previous work.<sup>2</sup> Briefly, a cellular or subcellular compartment (e.g. mitochondria) delimited by a biomembrane in respective tissue was described as a compartment, where the compounds undergo diffusion, ionization and partition/binding simultaneously (Figure 3.1A.). The passage of small molecules from the airway/blood to the blood/airway (Figure 3.1B.) is captured by a set of ordinary differential equations (ODEs), which describe mass transport across a series of cellular compartments bounded by lipid bilayers (Appendix, eq 1). For a monoprotic base, the concentration of molecule in each subcellular compartment is divided into two components: neutral and ionized. The drug specific properties are used as input to simulate the transport process across each lipid bilayer: the logarithms of the octanol:water partition coefficient of the neutral and ionized form of the molecule (i.e.,  $\log P_n$ ,  $\log P_d$ ), the  $pK_a$  of the molecule. For different compartments with different pHs and lipid fractions, the free fraction of neutral form and ionized form of molecules is calculated according to the molecule's  $pK_a$ ,  $\log P_n$ ,  $\log P_d$ . All of the default values of relevant parameters for rat lungs were from previously published model<sup>2</sup> and provided in Appendix (Table I-VII).

The lung model mathematically expressed in ODEs was then connected with the empirical one compartment PK model, which takes into account the impact from rest of body. The ODEs of hybrid Lung PK model was solved numerically in Matlab<sup>®</sup> simulation environment (Version R2009b, The Mathworks Inc, Natick, MA). The ODE15S solver was used to address the issue of the stiffness in ODEs, and the relative and absolute error tolerance was set as  $10^{-12}$  to minimize the numerical errors.

### 3.2.2 Multiscale Biophysical Model of Airway and Alveoli

According to the Nernst-Planck and Fick equations, the overall net fluxes ( $J_{o,i}$ ) for a weakly basic lipophilic small molecule across the membrane can be described as a sum of the net fluxes of the neutral and ionized species as eq 1 and 2<sup>9-13</sup>

$$J_{o,i} = \mathbf{P}_n(a_{o,n} - a_{i,n}) + \mathbf{P}_d \frac{N}{e^N - 1} (a_{o,d} - a_{i,d}e^N) \quad (1)$$

$$N = zEF / RT \quad (2)$$

Subscript n/d is for neutral/ionized form of molecules, subscripts o/i indicate the outside/inside  $\mathbf{P}_{n/d}$  is the permeability of the neutral/ionized form of molecules across biomembranes.  $a_{o/i,n/d}$  is the activity of the neutral/ionized form of molecules outside/inside,. In eq 2, z is the electronic charge, E is the membrane potential, F is the Faraday constant, R is the universal gas constant, T is the absolute temperature

The membrane permeability  $\mathbf{P}_n$  and  $\mathbf{P}_d$  were estimated by eq 3.<sup>14</sup>

$$\mathbf{P}_{n/d} = DK / \Delta x \quad (3)$$

D is the diffusion coefficient, which is estimated as  $10^{-14}$  m<sup>2</sup>/s for organic molecules in lipids.  $K$  is the partition coefficient and approximates the liposomal partition coefficient  $K_{ow,n/d}$ ,  $\Delta x$  is the membrane thickness (approximately 50 nm for a phospholipid bilayer).

The fraction of the activities ( $a_n$  and  $a_d$ ) in the total concentrations ( $C_t$ ) of molecules can be described by eq 4 and eq 5.<sup>9, 10, 12</sup>

$$f_n = a_n / C_t = \frac{1}{W/\gamma_n + K_n/\gamma_n + W \times 10^{i(pH-pK_a)}/\gamma_d + K_d \times 10^{i(pH-pK_a)}/\gamma_d} \quad (4)$$

$$f_d = a_d / C_t = f_n 10^{i(pH-pK_a)} \quad (5)$$

$f_{n/d}$  represents the free fraction of neutral or ionized form in the total concentration.  $W$  is the volumetric water fraction in each compartment.  $\gamma$  is the activity coefficient in each compartment, which is calculated based on the ionic strength  $I$  (moles). Using the Setchenov equation,  $\gamma_n$  is 1.23 at  $I = 0.3$  mol, and  $\gamma_d$  is 0.74 at  $I = 0.3$  mol with the Davies approximation of the modified Debye-Hückel equation.<sup>10</sup> No corrections for the ionic strength were made for the extracellular compartment ( $\gamma_{n/d} = 1$ ).  $K_{n/d}$  is the sorption coefficient of the neutral/ionized form of molecules, which are calculated by eq 6.  $L$  is the lipid fraction in each compartment.  $K_{ow,n/d}$  is the liposomal partition coefficient estimated by eq 7.<sup>9, 10, 12</sup>

$$K_{n/d} = L \times 1.22 \times K_{ow,n/d} \quad (6)$$

$$K_{ow,n/d} = 10^{\log P_{n/d,lip}} \quad (7)$$

Empirical regression relationship was used to calculate the logarithms of liposomal partition coefficient  $\log P_{n/d, lip}$  from  $\log P_{n/d}$ .<sup>9, 10</sup> Eq 8 was used to estimate  $\log P_d$  (ionized form of the molecules) from  $\log P_n$  calculated by ChemAxon.

$$\log P_d = \log P_n - 3.7 \quad (8)$$

### 3.2.3 Integration of lungs with the one compartment PK model

Both the airway and alveoli compartmental model were linked to systemic circulation via the respective tissue blood compartment and systemic circulation using the empirical PK model as described by eq 9.<sup>5</sup>

$$V_b \frac{dC_b}{dt} = -C_b CL \quad (9)$$

*In vivo* plasma clearance was set at zero to eliminate the confounding effect from systemic PK.<sup>5, 6</sup> The volume of venous and artery blood is estimated to be 13.6 and 6.8 ml, respectively.<sup>5, 15</sup> For i.v. bolus injection, initial concentration in venous blood was calculated by eq 10.

$$C_{0, vb} = Dose / V_{vb}, \quad (10)$$

### 3.2.4 Simulations of PK Profile of Small Monobasic Molecules in Airways and Alveoli via Systemically Delivery

To investigate the PK features of small molecules in airway and alveoli via systemic delivery (e.g IV bolus), the concentration in blood concentration was fixed as 1  $\mu$ M to mimic the steady state, assuming no significant protein binding in plasma, and B:P (drug concentration ratio of blood to plasma) = 1.  $\log P_n$  (-2 to

4 with interval of 0.1 units) and the  $pK_a$  (5 to 14 with interval of 0.2 units) of monobasic compounds were varied independently and used as input. For each set of physicochemical property, two important PK relevant indexes were calculated at steady state: 1. the regional mass distribution pattern was described as percentage of mass deposited in airways and alveoli normalized by total mass in whole lung. 2.  $T_{ss}$  (unit: minutes) was defined as time for airway or alveoli to reach the 95% of steady state concentration.

### **3.2.5 Simulations of PK of Small Monobasic Molecules in Airways and Alveoli via Inhalation**

The same initial dose (1 mg/kg) was used as input parameter to simulate intratracheal instillation experiments in airway and alveoli, respectively. The clearance in systemic circulation was fixed at zero to eliminate the impact from systemic clearance. The tissue was defined as space including surface lining liquid, interstitium, and cellular compartments. The tissue concentration was defined as total tissue mass divided by total tissue volume. By independently varying the  $\log P_n$  (-2 to 4 with interval of 0.1 units) and  $pK_a$  (5 to 14 with interval of 0.2 units) of monobasic compounds, the AUC (area under the tissue concentration curve) was calculated with trapezoidal rules for airway and alveoli. The AUC ratio of airways to alveoli after inhalation was evaluated for all possible combinations of physicochemical properties.

### **3.2.6 Simulations of Distribution of Fluorescent Probes in Airways and Alveoli via Intratracheal Instillation and IV bolus Injection.**

For intratracheal injection same initial concentration (1mM) of Mitotracker Red and Hoechst was assumed as initial condition in airways and alveoli. For IV injection, same dosage (mass) as used in IT injection as was used in initial bolus dose in venous blood circulation. The clearance was fixed as 0. The physiochemical properties of fluorescent probes Mitotracker Red (MitoRed) and Hoechst33342 were used as inputs to the hybrid lung PK model to simulate time-course change of concentration in the airways and alveoli, respectively. MitoRed is an organic cation with  $\log P_d = 0.16$ . Hoechst33342 is a lipophilic monobasic molecules with  $pK_a=7.8$ ,  $\log P=4.49$  calculated with Chemaxon.



### **3.2.7 Experiments of Intratracheal Instillation and IV bolus Injection**

The C57BL/6 mice (BW: 20-30 g) were used. 50 ug MitoRed in 10 ul DMSO and 90 ul Hoechst solution (10 mg/ml) was mixed to make 100 ul of mixture of fluorescent dye. The final concentration of MitoRed and Hoechst is 0.94 and 14.61 mM, respectively. 50 ul of mixture of dye or 50 saline (control) was administered through IV tail vein injection or intratracheal instillation. The intratracheal instillation experiments were performed with anesthetized mice. In order to study the differential regional distribution of fluorescent dyes in the lung, 40 minutes after the treatment, the whole mice lung (total weight: ~ 120 mg) was cross cut and fluorescent probe distributions across the lung were observed under fluorescent microscopy.

### **3.2.8 Parameter Sensitivity Analysis**

To interrogate the underlying mechanism that leads to the difference in exposure or distribution of small molecules between airways and alveoli, we examined the sensitivity of the predicted exposure to variation in the nominal parameter values, and evaluated the robustness and stability of our model. We match the parameters values in airways with corresponding ones in alveoli, or in an opposite match direction, namely match the parameters values in alveoli with corresponding ones in airways. The change in airways or alveoli exposure for MitoRed made by the match of parameter values were analyzed and listed in Table 3.1.

### 3.3 Results

#### 3.3.1 Tissue Exposure in Airway and Alveoli via Inhalation

The relationship between the physicochemical properties with tissue exposure (AUC) in airway and alveoli via inhalation was explored by varying the  $\log P_n$  and  $pK_a$  independently (Figure 3.2A., and 3.2B.). In general, for both airway and alveoli the compounds with low  $\log P_n$  and high  $pK_a$  possess high tissue exposure. The effect of change of physicochemical properties on the alveoli tissue exposure is less pronounced in comparison with that on airway tissue exposure. The contrast ratio of exposure of airway to alveoli was also related to physicochemical properties (Figure 3.2C.). The contrast ratio in exposure between the airway and alveoli is range from 100 to 700 and increases with higher  $\log P_n$  and  $pK_a$ . For compounds with  $9 < pK_a < 11$ , the contrast ratio of exposure of airway to alveoli is less sensitive to the change of  $\log P_n$  than  $pK_a$ .

#### 3.3.2 Mass Distribution of Small Molecules in Airway and Alveoli via IV

Simulations were performed with independently varying  $\log P_n$  and  $pK_a$  to calculate the mass deposition pattern in airway and alveoli under steady state via IV, thereby establishing the relationship between the physicochemical properties of small molecules with their absolute and relative mass distribution in airway and alveoli. As shown in Figure 3.3., under steady state using IV the majority of mass deposited in lungs lies in alveoli region, where the percentage normalized by total mass is greater than 80%. On the other hand, airways only hold less than 20% of total lung mass. In airways and alveoli, the mass distribution for compounds with

$8 < pK_a < 10$  is largely dependent on  $pK_a$ , the change in  $\log P_n$  has much less effect on mass distribution. For compounds with  $pK_a < 8$  or  $pK_a > 10$ , both  $pK_a$  and  $\log P_n$  has minor effect on mass distribution in airway and alveoli. The contrast ratio of mass in alveoli to airway is range from 5 to 40. Compounds with high  $\log P_n$  and low  $pK_a$  tend to have large contrast ratio of mass of alveoli to airway. The contrast ratio of mass in alveoli to airway for compounds with  $pK_a > 10$  are all below 5, and much less dependent on their physicochemical properties than other regions.

### 3.3.3 $T_{ss}$ of Small Molecules in Airways and Alveoli via IV

$T_{ss}$  (time to reach steady state) of tissue concentration with constant concentration at respective tissue blood compartment can provide quantitative insights about how accurate the well-stirred (perfusion limited) model can approximate the real tissue disposition kinetics given the corresponding permeability barrier. As shown in Figure 3.4., in general lower  $\log P_n$  and higher  $pK_a$  make compounds need longer time to reach steady state in both alveoli and airway. In alveoli the range of  $T_{ss}$  is from 4 to 30 minutes, however, the effect of physicochemical properties on  $T_{ss}$  is significant only for compounds with  $pK_a > 11$  and  $\log P_n < 0.5$ . On the other hand, in airways the range of  $T_{ss}$  is from 12 up to 3000 minutes, which is a much longer and wider span than that in alveoli. More importantly,  $T_{ss}$  longer than 60 minutes implies the inaccuracy of modeling airway with the well-stirred (perfusion limited) model for monobasic molecules with  $pK_a > 9$  and  $\log P_n < 0.5$ . The effect of physicochemical properties on  $T_{ss}$  in airway is particularly significant for compounds with  $pK_a > 9$ .

### 3.3.4 The Simulation and Experimental Results of Distribution of Fluorescent Probes

In order to validate the model predictions about the distribution of small molecules in airways and alveoli, two fluorescent molecules were chosen as test compounds, including Mitotracker Red, an organic cation with  $\log P_d = 0.16$  and Hoechst, a lipophilic monobasic molecules with  $pK_a=7.5$ ,  $\log P=4.49$ . As shown in Figure 3.5., the predicted concentration of these two fluorescent molecules in airways and alveoli given by the hybrid lung PK model demonstrated different pattern between IT and IV injection. When given IT injection, the predicted concentration of MitoRed in airways is 10 fold higher than that in alveoli, but the predicted concentration of Hoechst in airways is comparable (only 2 fold lower) with that in alveoli. When given IV injection, the predicted concentration of MitoRed in airways is almost same with that in alveoli, the predicted concentration of Hoechst in alveoli is only 3 fold higher than that in airways.

The microscopic images generated from lung cross-section of mice via IV tail injection and IT injection are shown in Figure 3.6. In general, after IV injection there is no significant difference between airways and alveolar regions of lung for both MitoRed and Hoechst, which is comparable with the simulation results. After IT injection, the accumulation of MitoRed in airways is much 10 fold higher than that in alveoli. However, Hoechst did not show different distribution between airways and alveoli.

### 3.3.5 Parametric Analysis

To gain quantitative insight about the mechanism that makes the airways and alveoli demonstrate different transport profile, we performed the parameter sensitivity analysis. Parameter values describing airways was made equal to their counterpart in alveoli, or in a reverse direction, which is to make parameters values in alveoli equal to their counterpart in airways. As shown in table 3.1., the influential parameters on airways or alveoli exposure are airway smooth muscle, interstitium volume, and mitochondria volume.

If the value of parameters describing airways (e.g., volume of smooth muscle) was replaced with those in alveoli, namely, the volume of smooth muscle in airways is set as 0, the exposure of the MitoRed in airways decreases by 5-8 folds. If the value of parameters describing interstitium in airways was replaced with those in alveoli, the exposure of the MitoRed or Hoechst in airways decreases by 1.5-5 fold. If the value of parameters describing mitochondrial volume in airways was replaced with those in alveoli, the exposure of the MitoRed or Hoechst in airways decreases by 1.5-5 fold. If the value of parameters describing alveoli (e.g., volume of smooth muscle = 0) was replaced with those in airways, the exposure of the MitoRed in alveoli increases by 1.5-5 folds. If the value of parameters describing interstitium in alveoli was replaced with those in airways, the exposure of the MitoRed in alveoli decreases by 1-1.5 fold. If the value of parameters describing mitochondrial volume in alveoli was replaced with those in airways, the exposure of the MitoRed in alveoli decreases

by 1-1.5 fold. The comprehensive results of parameter sensitivity analysis are listed as Appendix.

### **3.4 Discussion**

PK modeling has been used extensively to study the ADME profile of compounds in animals and human. In the present study, a hybrid PK model was developed by incorporating the multiscale, cell-based compartmental models of rat lungs into the empirical PK model. The model of lungs includes two components: airways and alveoli, composed of membrane delimited cellular or extracellular compartments, which are organized according to their histology, physiology, and anatomy (Figure 3.1.). After integrating the airways and alveoli into the empirical PK model, the hybrid lung PK model described as ODEs was solved numerically to generate the time-course concentration curve for each of the compartments.

The main advantage of our hybrid lung PK model over the generic PBPK model is that it can simulate the lung tissue concentration profile of small molecules delivered via inhalation (from air to blood) and elucidate the difference in PK behavior between airway and alveoli using inhalation or systemic delivery as routes of administration.

For orally inhalation medication, extensive studies have demonstrated that the regional lung deposition of drugs is largely dependent on the aerodynamic particle size generated by delivery devices.<sup>16-19</sup> Yet little was known about the regional lung deposition of drugs delivered by systemic circulation (e.g., IV) and its relationship with the physicochemical properties of compounds. So

simulations were performed with systemic delivered monobasic small molecules, suggesting that the majority of drug mass (>80% of total mass in lungs) is deposited in the alveoli majorly because of its larger volume and higher lipid content, and the compounds with high lipophilicity and low  $pK_a$  tend to deposit in alveoli more than airway. These results are of great value for rational design of systemic delivered drugs targeting at specific regions of lungs.

In generic PBPK model most of the included organs including lungs is viewed as a well-stirred (perfusion limited) compartment, and the concentration equilibrium between the tissue and its corresponding drug donor side (i.e., blood circulation) is achieved instantaneously. Such approximation was able to give good prediction for tissue concentration profile of systemic delivered drugs in many cases given the well-estimated  $K_p$  or  $K_{pu}$  values.<sup>5, 6</sup> However, one should keep in mind that there exist theoretical scenarios of permeability limited kinetics due to the poor permeability of drug in certain tissues. Instead of taking lungs as one well-stirred compartment, we calculated  $T_{ss}$  in airway and alveoli separately for monobasic compounds with all kinds of possible physicochemical properties. The results indicated that alveoli are fast-equilibrium tissue with  $T_{ss}$  shorter than a half hour even for monobase molecules with extreme physicochemical properties, approximation as perfusion limited model won't lead to significant errors, especially when the time of prediction exceeds a half hour. On the other hand, there may be a pitfall of modeling airway as perfusion-limited tissue when the properties of molecules fall into the range of  $pK_a > 9$  and  $\log P_n < 0.5$ , making the  $T_{ss}$  from 1 up to 50 hours. From the perspective of modeling, a perfusion-

limited model may suffice to capture the kinetics well as a whole lung, since alveoli receive most of lung mass and is a fast-equilibrium tissue. However, this approach may lead to large deviation from real kinetics for compounds with aforementioned properties when the airways are specifically focused in the model.

It is critical to identify the key factors that differentiate the transport profile of small molecules in airways and in alveoli. Hypothesis generated from the model about two well-studied fluorescent compounds, MitoRed or Hoechst, is that there is a difference in distribution pattern between airways and alveoli given different routes of administration. As what the model predicts in Figure 3.5., when the IT instillation is used, the organic cation, MitoRed tends to accumulate more (10 fold higher) in airways than that in alveoli, but Hoechst nearly even distributed across airways and alveoli. This prediction is partly confirmed with the experimental results with intratracheal instillation of mixture of fluorescent probes (right panel in Figure 3.6.). However, this distribution pattern is very different when the IV injection is used. Based on the simulation results in Figure 3.5., concentration of Hoechst in alveoli is marginally higher than that in airways, but MitoRed achieves nearly even distribution across airways and alveoli. This hypothesis was partly confirmed in the *in vivo* experiments with IV injection (left panel in Figure.3.6.).

To account for the simulated and observed different pattern in distribution of fluorescent probes between airways and alveoli, we performed the parametric analysis to elucidate the key mechanism. As shown in table 3.1., the smooth muscle is a critical compartment for high exposure of MitoRed when given IT



instillation. One possible explanation is that the cation MitoRed is pushed into the smooth muscle when MTR passing through the airways tissue, leading to a high accumulation or retention in airways. And the alveoli does not have smooth muscle, therefore there is no accumulation or retention in alveoli for MitoRed. Hoechst is lipophilic basic compounds with  $pK_a = 7.5$ , therefore half of the species will exist as neutral whose diffusion is much faster than that of cation. So there is no significant accumulation or retention for Hoechst in both airways and alveoli.

When IV injection is used as routes of administration, the direction of distribution is from blood to the tissue. The distribution between blood and tissue at steady state or pseudo steady state is dependent on partition or binding of molecules to the tissue. In alveoli, there is a large amount of lipid-rich surfactant covering the epithelium. Thus, Hoechst, a compound with  $\log P > 4$ , has more tendency to partition into the alveoli than airways. MitoRed will has much less partition in both airways and alveoli, and the difference between airways and alveoli is not obvious. Our arguments here can't rule out the other possible factors that might cause this regional difference in distribution.

Admittedly, this hybrid lung PK model with a biophysical multiscale lung can be further elaborated and refined with more relevant experimental data and measurements. With the regard to the scope of applicable molecules, the current model was only proved to be able to predict the transport process of neutral and cationic species. However, as an *in silico* model, it can facilitate the early-stage rational design of inhaled or systemically delivered compounds specifically

targeting airway or alveoli with the optimal physiochemical properties. More importantly, it allows us to formulate hypothesis to prioritize the experiments. Furthermore, it is relevant if we intend to design an inhalation dose regimen based on the dose-exposure profile of the systemically delivered drugs. For example, this hybrid lung PK model will be of great value to make predictions about the proper inhaled dosage that should be deposited in airways to achieve same tissue exposure as other systemically administered dose, thereby guiding the drug targeting and delivery in the airway. In addition, since the hybrid lung PK model incorporates quantitative species-specific information about the anatomy, physiology and histology of the lung and physiology of other organs, it can be scaled to predict human PK profile and detailed lung tissue exposure of small molecules using inhalation or systemic delivery, which is particularly valuable when clinical lung PK data are scarce due to various practical reasons. Details in this regard are discussed in the Chapter 6.

To summarize, a hybrid lung PK model with lungs composed of airway and alveoli is a computational tool that can provide mechanistic and quantitative insights about airway and alveoli. As more *in vivo* experiments are performed with various molecules, the model can be further validated, refined and expanded, to increase its accuracy and extend its domain of applicability. Due to the compartmental nature of the multiscale lung model, it can be linked with models of upstream process, such as pulmonary particle deposition, dissolution and mucus clearance, as well as of downstream process, such as pharmacodynamic (PD) model,<sup>20-22</sup> thereby facilitating the discovery and

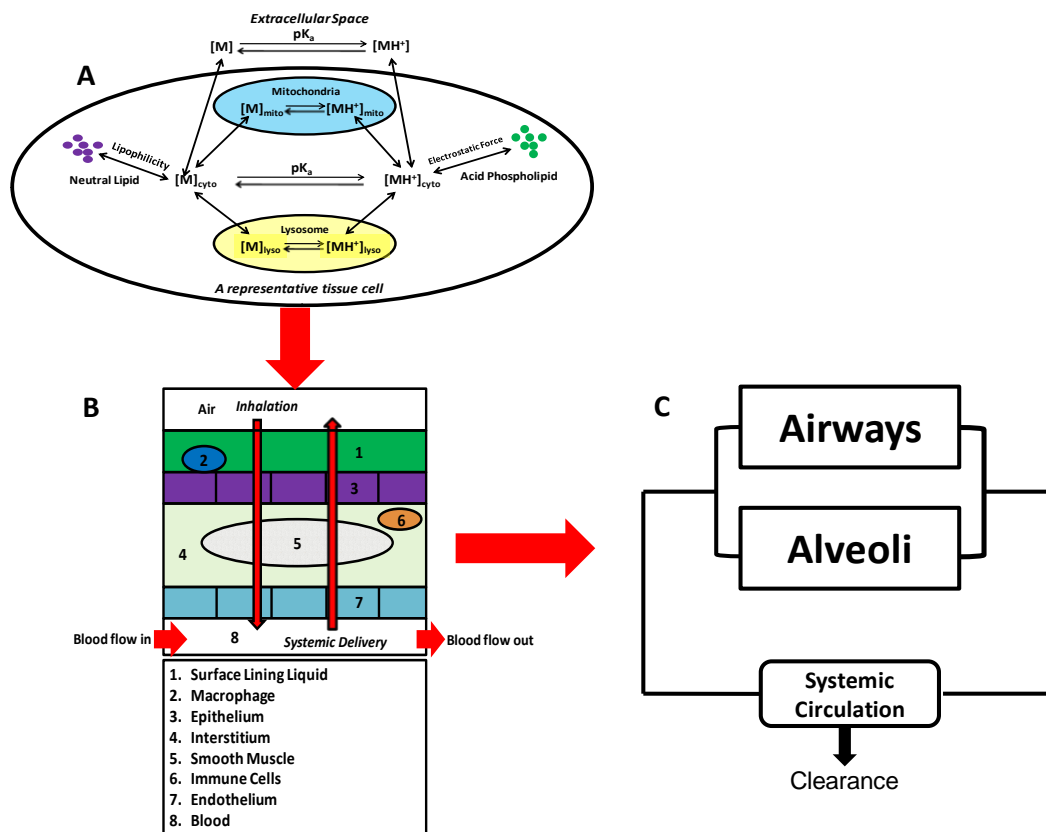
development of inhalation medication. Future development effort will focus on modeling paracellular transport routes of more hydrophilic compounds and macromolecules, probing mucus clearance and active transport effects,<sup>23, 24</sup> exploring the effect of pathological conditions on lung PK, as well as extending the model to zwitterionic and multivalent molecules.

Table 3.1. Sensitivity Analysis via exchanging the values of airways and alveoli

	Airways	Alveoli
Epithelium Surface Area	↑	↓
Smooth Muscle Volume	↓ ↓ ↓	↑ ↑
Endothelium Area	↓	↑
Macrophage Volume	—	—
Immune Cells Volume	—	—
Interstitial Volume	↓ ↓	↓
Mitochondria Volume	↓ ↓	↑
Blood Flow Rate	—	—
Clearance <sup>a</sup>	—	↓

One arrow: 1~ 1.5 fold  
 Two arrows: 1.5~2 fold  
 Three arrows: 5~ 8 fold  
 — :less than 1.1 fold

a. Increase Clearance by 10 fold



**Figure 3.1.** General methodology of hybrid PBPK model **A.** Cellular level: A representative cell in airway or alveoli with organelles. Monobasic compound diffuses across a phospholipid bilayer and undergoes ionization and partition/binding in each compartment. The neutral form of the monobasic molecule is indicated as  $[M]$ , and the protonated, cationic form of the molecule is indicated as  $[MH^+]$ . **B.** Histological level: The general route of drug transport from the lung lumen/blood to the blood/lumen via inhalation/systemic delivery, across the histological architecture of lung tissue. **C.** Systemic PK level: Integration of airway and alveoli tissue model with the systemic circulation.

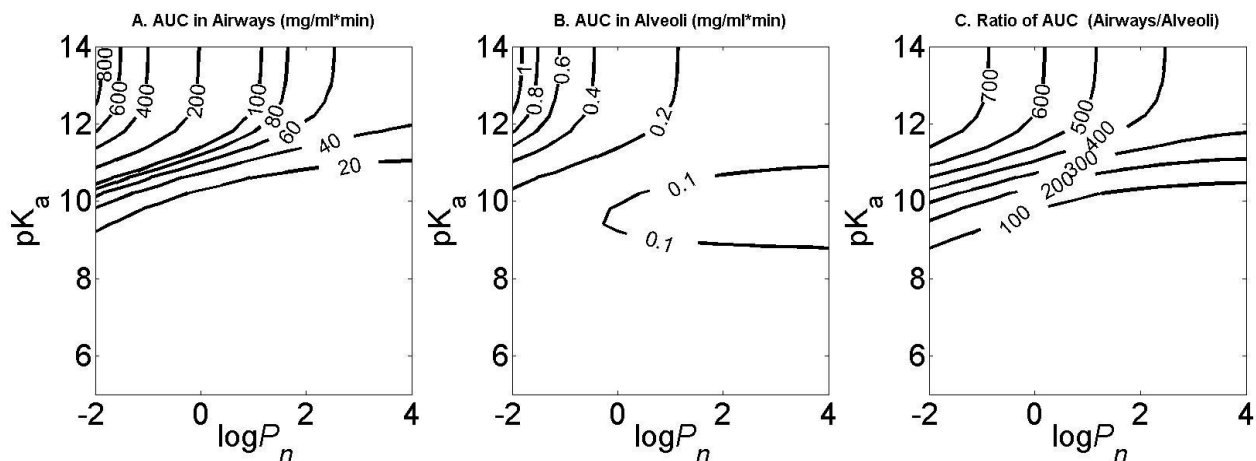


**Figure 3.2.** The relationship between the physicochemical properties of monobasic compounds and the tissue exposure (i.e., AUC) in the airways, alveoli, and the exposure contrast of airways to alveoli. For simulations, same dose was set to 1mg/kg for airways and alveoli, and the  $\log P_n$  and  $pK_a$  were varied independently. X axis represents the  $\log P_n$ , Y axis represents  $pK_a$ . Contour line indicates: **A.** The AUC (unit: mg/ml\*min) in airways; **B.** The AUC (unit: mg/ml\*min) in alveoli; **C.** The AUC contrast ratio of airways to alveoli

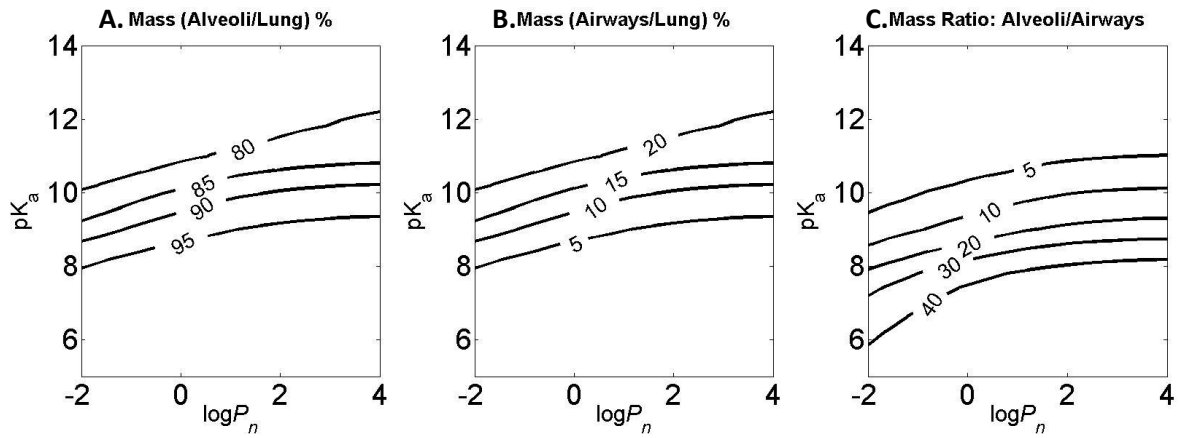


**Figure 3.3.** The relationship between the physicochemical properties of monobasic compounds and the mass deposition pattern in the airways, alveoli relative to the whole lung. For simulations, the concentration in corresponding tissue blood was fixed as 1ug/ml for airways and alveoli, and the  $\log P_n$  and  $pK_a$  were varied independently. X axis represents the  $\log P_n$ , Y axis represents  $pK_a$ . Contour line indicates: **A.** The mass percentage (%) of alveoli normalized by total lung mass; **B.** The mass percentage (%) of airways normalized by total lung mass; **C.** The mass contrast ratio of alveoli to airways.

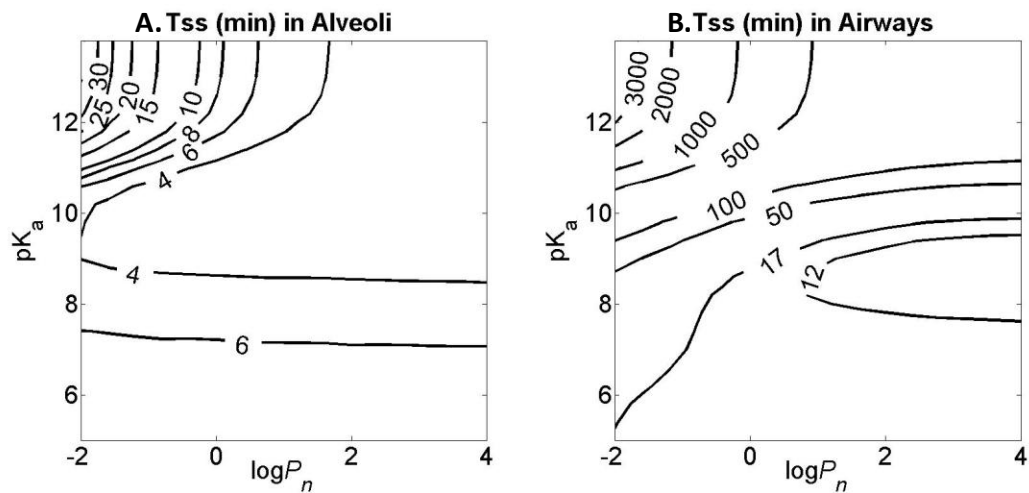


**Figure 3.4.** The relationship between the physicochemical properties of monobasic compounds and  $T_{ss}$  (the time to reach steady state) in the airways and alveoli. For simulations, the concentration in corresponding tissue blood was fixed as 1ug/ml for airways and alveoli, and the  $\log P_n$  and  $pK_a$  were varied independently. X axis represents the  $\log P_n$ , Y axis represents  $pK_a$ . Contour line indicates: **A.**  $T_{ss}$  in alveoli (unit: minutes); **B.**  $T_{ss}$  in airways (unit: minutes).



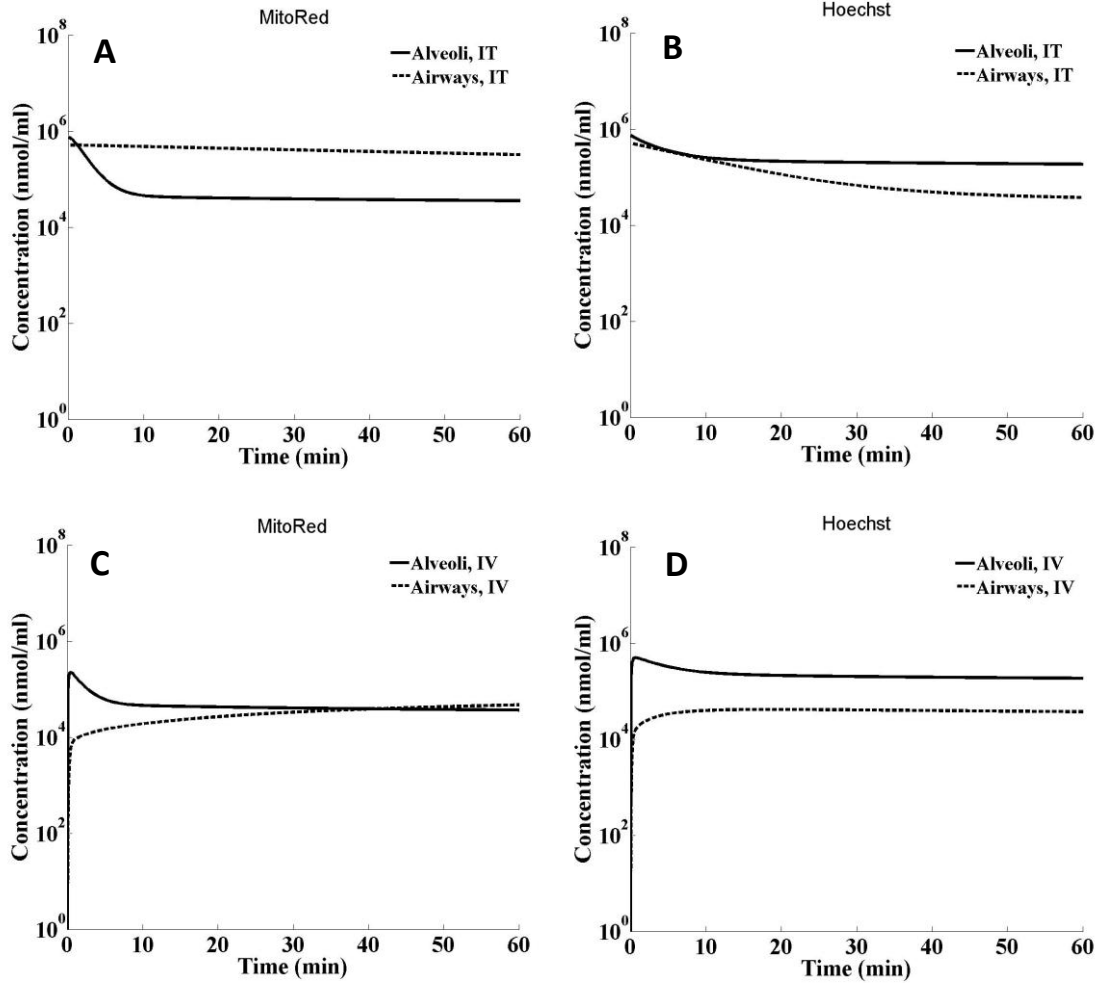


**Figure 3.5.** The simulated tissue concentration in airways (dash line) and alveoli (solid line). **A.** MitoRed given by IT instillation; **B.** Hoechst given by IT instillation; **C.** MitoRed given by IV injection; **D.** Hoechst given by IV injection;

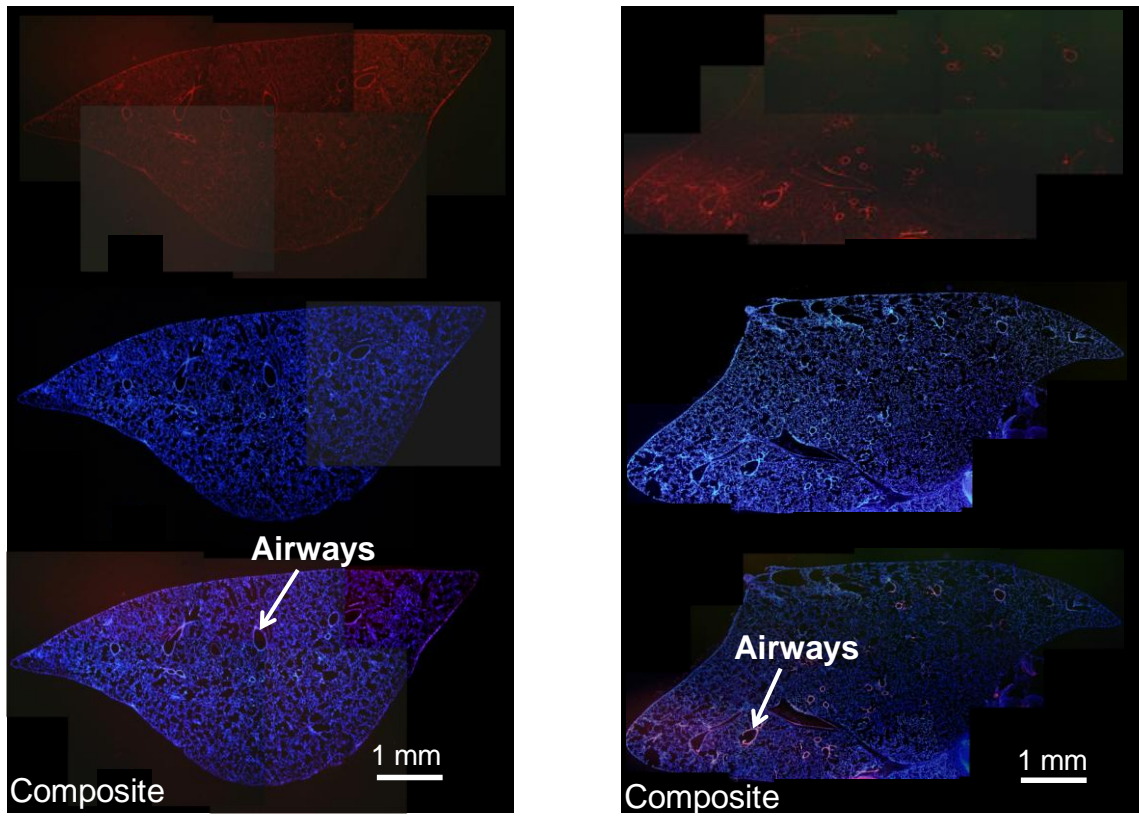


**Figure 3.6.** Microscopic fluorescence distribution of Hoechst 33342 (blue) and Mitotracker Red (red) in the lung. Left panel are the images by IV injection. Right panel are the images by intratracheal injection.

### 3.5. References

1. Yeh, H. C.; Schum, G. M.; Duggan, M. T., Anatomic models of the tracheobronchial and pulmonary regions of the rat. *Anat Rec* **1979**, *195* (3), 483-92.
2. Yu, J. Y.; Rosania, G. R., Cell-based multiscale computational modeling of small molecule absorption and retention in the lungs. *Pharm Res* **2010**, *27* (3), 457-67.
3. Parent, R. A., *Treatise on Pulmonary Toxicology: Comparative biology of the normal lung*. CRC Press: Boca Raton, 1992.
4. Ross, M. H.; Pawlina, W., *Histology: A Text and Atlas: With Correlated Cell and Molecular Biology*. 5th ed.; Lippincott Williams & Wilkins: 2006.
5. Poulin, P.; Theil, F. P., Prediction of pharmacokinetics prior to in vivo studies. II. Generic physiologically based pharmacokinetic models of drug disposition. *J Pharm Sci* **2002**, *91* (5), 1358-70.
6. Rodgers, T.; Leahy, D.; Rowland, M., Physiologically based pharmacokinetic modeling 1: predicting the tissue distribution of moderate-to-strong bases. *J Pharm Sci* **2005**, *94* (6), 1259-76.
7. Krondahl, E.; Tronde, A.; Eirefelt, S.; Forsmo-Bruce, H.; Ekstrom, G.; Bengtsson, U. H.; Lennernas, H., Regional differences in bioavailability of an opioid tetrapeptide in vivo in rats after administration to the respiratory tract. *Peptides* **2002**, *23* (3), 479-88.
8. Miller, L. A.; Hurst, S. D.; Coffman, R. L.; Tyler, N. K.; Stovall, M. Y.; Chou, D. L.; Putney, L. F.; Gershwin, L. J.; Schelegle, E. S.; Plopper, C. G.; Hyde, D. M., Airway generation-specific differences in the spatial distribution of immune cells and cytokines in allergen-challenged rhesus monkeys. *Clin Exp Allergy* **2005**, *35* (7), 894-906.
9. Trapp, S., Plant uptake and transport models for neutral and ionic chemicals. *Environ Sci Pollut Res Int* **2004**, *11* (1), 33-9.
10. Trapp, S.; Horobin, R. W., A predictive model for the selective accumulation of chemicals in tumor cells. *Eur Biophys J* **2005**, *34* (7), 959-66.
11. Zhang, X. *From Cell to Organism: A Predictive Multiscale Model of Drug Transport*. University of Michigan, Ann Arbor, 2009.
12. Zhang, X.; Shedden, K.; Rosania, G. R., A cell-based molecular transport simulator for pharmacokinetic prediction and cheminformatic exploration. *Molecular Pharmaceutics* **2006**, *3* (6), 704-716.
13. Zhang, X.; Zheng, N.; Rosania, G. R., Simulation-based cheminformatic analysis of organelle-targeted molecules: lysosomotropic monobasic amines. *J Comput Aided Mol Des* **2008**, *22* (9), 629-45.
14. Balon, K.; Riebesehl, B. U.; Muller, B. W., Drug liposome partitioning as a tool for the prediction of human passive intestinal absorption. *Pharm Res* **1999**, *16* (6), 882-8.
15. Lee, H. B.; Blaufox, M. D., Blood Volume in the Rat. *J Nucl Med* **1985**, *26* (1), 72-76.

16. Brewis, R. L.; Corrin, B.; Geddes, D. M.; Gibson, G. J., *Respiratory Medicine*. second ed.; WB Saunders Company Ltd: London, 1995.
17. Gumbleton, M.; Taylor, G., Challenges and innovations in effective pulmonary systemic and macromolecular drug delivery. *Adv Drug Deliv Rev* **2006**, *58* (9-10), 993-5.
18. Usmani; Omar, S.; Biddiscombe; Martyn, F.; Barnes; Peter, J. G. X., Regional lung deposition and bronchodilator response as a function of beta2-agonist particle size. American Lung Association: New York, NY, ETATS-UNIS, 2005; Vol. 172, p 8.
19. Shoyele, S. A.; Cawthorne, S., Particle engineering techniques for inhaled biopharmaceuticals. *Adv Drug Deliv Rev* **2006**, *58* (9-10), 1009-29.
20. Macheras, P.; Iliadis, A.; SpringerLink (Online service), *Modeling in biopharmaceutics, pharmacokinetics, and pharmacodynamics : homogeneous and heterogeneous approaches*. Springer: New York, 2006; p xx, 442 p.
21. Derendorf, H.; Lesko, L.; Chaikin, P.; Colburn, W.; Lee, P.; Miller, R.; Powell, R.; Rhodes, G.; Stanski, D.; Venitz, J., Pharmacokinetic/pharmacodynamic modeling in drug research and development. *The Journal of Clinical Pharmacology* **2000**, *40* (12), 1399-1418.
22. Burton, M. E., *Applied pharmacokinetics and pharmacodynamics : principles of therapeutic drug monitoring*. 4th ed.; Lippincott Williams & Wilkins: Baltimore, 2006.
23. Van 't Veen, A.; Gommers, D.; Verbrugge, S. J. C.; Wollmer, P.; Mouton, J. W.; Kooij, P. P. M.; Lachmann, B., Lung clearance of intratracheally instilled <sup>99m</sup>Tc-tobramycin using pulmonary surfactant as vehicle. *British Journal of Pharmacology* **1999**, *126* (5), 1091-1096.
24. Sakagami, M.; Omid, Y.; Campbell, L.; Kandalaf, L. E.; Morris, C. J.; Barar, J.; Gumbleton, M., Expression and transport functionality of FcRn within rat alveolar epithelium: A study in primary cell culture and in the isolated perfused lung. *Pharmaceutical Research* **2006**, *23* (2), 270-279.

## CHAPTER 4

### Study of the effect of acidic phospholipids binding on the pharmacokinetics with a hybrid Lung PBPK Model

#### 4.1 Introduction

Undesirable pharmacokinetics profiles of drug candidates are a common reason for the late stage attrition of many drug development programs.<sup>1</sup> Early prediction of the pharmacokinetics of drug candidates is a challenging task in the discovery and development of drugs. To facilitate the generation of pharmacokinetic profiles, aid the rational selection of compounds in early stage of drug development and eventually reduce the attrition rate at late stage, a comprehensive understanding about the pharmacokinetics behavior of drug candidates is required. Prediction across compounds and species can be enhanced by relating the pharmacokinetic profiles of a compound to its physicochemical properties and physiology of species. Conventionally, pharmacokinetics studies are often descriptive because the observed *in vivo* pharmacokinetics data of a compound is described by empirical models, such as exponentials or compartmental models. These empirically models are often used

to describe the observed pharmacokinetics profiles, but they have very limited power to predict the compounds out of the range of compounds and species in existing studies.

Therefore transition from empirical pharmacokinetics models towards more mechanistic models is gaining more popularity, since a mechanistic model can be applied to different compounds and animal species. Physiological based pharmacokinetic (PBPK) models have been widely used in pharmaceutical industry and academia. Here we integrated the PBPK model with the multiscale cell-based lung model to simulate the pharmacokinetics in the airways and alveoli tissues. A challenge in the development of this type of hybrid lung PBPK model is to predict incorporate the binding affinities between lipids and species of monobasic molecules. We adopted equations developed by Poulin, Rowland, and their colleagues. Such mechanistic equations were derived based on mechanistic understanding of the underlying physiology and the transport behavior of drugs within a tissue. They have been extensively applied to predict the  $K_p$  (drug concentration ratio of tissue to blood) values of a structurally diverse basic and neutral compounds in academia and industry.<sup>1-3</sup> Their work suggested that the acidic phospholipid (AP), such as phosphatidylserine (PS), mono- and diphosphatidylglycerol (PG), phosphatidylinositol (PI) and phosphatidic acid (PA)) in tissue cells dominantly control the distribution of the basic compounds. The interaction between basic compounds ( $pK_a = 9.5$ ) and AP is electrostatic as both exist mostly as ionised species at physiological pH. Other than electrostatic interactions with AP, unionized form of basic compounds can also partition into

neutral lipids and neutral phospholipids. Yata and colleagues 5 found that propranolol ( $pK_a > 9$ ) have a very strong binding affinity with PS, PG and PI. Therefore, the binding of ionized species with AP needs to be considered to capture the underlying transport mechanism in the tissues.

## **4.2 Methods**

### **4.2.1 General Methodology**

Both the airway and alveoli model mathematically expressed in ODEs were then integrated accordingly via systemic circulation (tissue blood) compartment with the ODEs-based generic PBPK model, which also contains the rest of organs, such as liver, kidney, brain, and heart (Figure 4.1C.). Using the obtained hybrid Lung-PBPK model, the pharmacokinetics of included organs of small molecules via the inhalation or systemic delivery was simulated with corresponding inputs. The ODEs of hybrid Lung-PBPK model was solved numerically in Matlab<sup>®</sup> simulation environment (Version R2009b, The Mathworks Inc, Natick, MA). The ODE15S solver was used to address the issue of the stiffness in ODEs, and the relative and absolute error tolerance was set as  $10^{-12}$  to minimize the numerical errors.

### **4.2.2 Multiscale biophysical Model of Airway and Alveoli**

Since the experimental  $K_{pu_{BC}}$  values are available for propranolol (45.1) and atenolol (1.2), we adapted mechanistic equation developed by Rowland and his colleagues to better estimate the partition/binding between the ionized form of monobasic compounds (i.e., positive species) and the negatively charged acid

phospholipids (AP).<sup>2</sup> For all cellular compartments, the  $K_d$  was given by eq 1-2.

$$K_d = \frac{[AP^- \cdot MH^+]}{[MH^+]} = [AP^-]_{Lung} \cdot K_{aBC} \quad (1)$$

$$K_d = [AP^-]_{Lung} \cdot \left[ K_{puBC} - \frac{1+10^{pK_a - pH_{BC}}}{1+10^{pK_a - pH_p}} \cdot f_{IW,BC} - \frac{K_{ow,n} \cdot f_{NL,BC} + (0.3P + 0.7) \cdot f_{NP,BC}}{1+10^{pK_a - pH_p}} \right] \cdot \frac{1+10^{pK_a - pH_p}}{[AP^-]_{BC} \cdot 10^{pK_a - pH_{BC}}} \quad (2)$$

Subscript *Lung*, *BC*, and *p* refer to lung, blood cell, and plasma, respectively.  $[AP^- \cdot MH^+]$  represents the ionized acid phospholipid-base complex concentration.  $[MH^+]$  is the free aqueous ionized monobase concentration.  $[AP^-]$  is the concentration of the charged acidic phospholipid.  $K_{aBC}$  indicates the binding affinity between  $[MH^+]$  and  $[AP^-]$  in blood cell, and serves as a representative in all tissues. Assuming total ionization under physiological condition and non-saturating condition,  $[AP^-]$  was approximated as the total AP concentration, including phosphatidylserine (PS), phosphatidylglycerol (PG), phosphatidylinositol (PI), and phosphatidic acid (PA).  $[AP^-]_{BC}$  and  $[AP^-]_{Lung}$  were 0.5 mg/g and 3.91 mg/g, respectively.  $f_{IW,BC}$ ,  $f_{NL,BC}$ , and  $f_{NP,BC}$  represent the fractional tissue volume of intracellular water, neutral lipid, and neutral phospholipids in blood cells, whose values are obtained from literature.<sup>2</sup>  $pH_{BC}$  and  $pH_p$  were taken to be 7.22 and 7.4.  $K_{puBC}$  values for propranolol and atenolol are 45.1 and 1.2, respectively.

#### 4.2.3 Hybrid model: Integration of lungs with the other organs in PBPK model

Both the airway and alveoli compartmental model were coupled via the respective tissue blood compartment with the generic PBPK model.<sup>3</sup> Physiological data of tissues and drug specific inputs for other organs in PBPK



modeling were obtained from literature and summarized in Table 4.1., and 4.2. As shown in Figure 4.1C., the blood supply for airway and alveoli are the bronchial circulation (1% total blood flow from artery) and pulmonary circulation (almost 100% blood flow from vein). Due to the limited data of experimentally measured  $K_p$  values for all the organs, not all the organs illustrated in Figure 4.1C. were included in the hybrid PBPK modeling. For atenolol, the hybrid PBPK model included the lung, arterial blood, venous blood, brain, liver, and the rest of body. For propranolol, the hybrid PBPK included the lung, arterial blood, venous blood, adipose, bone, brain, gut, heart, kidney, liver, muscle, skin, spleen, and the rest of body. All other organs except for the lung were assumed to be well-stirred perfusion-limited compartments. For a non-elimination organ/tissue, the mass change within that organ/tissue can be expressed by eq 3.

$$V_{ts} \frac{dC_{ts}}{dt} = Q_{ts} C_{ab} - Q_{ts} C_{v,ts} \quad (3)$$

Subscript  $ts$  stands for a non-elimination tissue/organ, such as heart ( $ca$ ), bone ( $bo$ ), muscle ( $mu$ ), fat ( $fa$ ), skin ( $sk$ ), brain ( $br$ ), spleen ( $sp$ ), rest of body ( $rob$ ), etc.  $V$  stands for volume of the tissue;  $C_{ts}$  stands for total tissue concentration;  $Q_{ts}$  stands for blood flow rate of that tissue/organ;  $C_{ab}$  stands for arterial blood concentration; and  $C_{v,ts}$  is venous tissue concentration, which can be converted to total tissue concentration  $C_{ts}$  by eq 4.

$$C_{v,ts} = \frac{C_{ts}}{K_{p,t} / B:P} \quad (4)$$

Where  $K_{p,t}$  is tissue : plasma partition coefficient, and B:P is blood : plasma partition coefficient. For arterial blood and venous blood, mass balance can be expressed by eq 5 and 6, respectively.

$$V_{ab} \frac{dC_{ab}}{dt} = Q_{al} C_{v,al} - Q_{al} C_{ab} \quad (5)$$

$$V_{vb} \frac{dC_{vb}}{dt} = \sum_i Q_i C_{v,i} - Q_{al} C_{vb} \quad (6)$$

$Q_{al}$  is the blood flow of pulmonary circulation into alveoli, which is 100% of cardiac output.  $C_{vb}$  and  $C_{ab}$  is venous and artery blood concentration, respectively.  $Q_i C_{v,i}$  refers to the product of each of venous tissue concentration and its corresponding blood flow, which is a input mass flow into the vein.

*In vivo* plasma clearance of atenolol was obtained from published literature<sup>4</sup> and converted to blood clearance using equation 7.

$$CL_b = \frac{CL_p}{B:P} \quad (7)$$

where  $CL_b$  and  $CL_p$  are blood and plasma clearance, respectively. Clearance was allocated to venous blood compartment.

For propranolol, the liver was modeled using eq 8<sup>3</sup>.

$$V_{hv} \frac{dC_{hv}}{dt} = Q_{ha} C_{ab} + Q_{sp} C_{v,sp} + Q_{gu} C_{v,gu} - Q_{hv} C_{hv} - (Q_{ha} C_{ab} + Q_{gu} C_{v,gu} + Q_{sp} C_{v,sp}) E_h \quad (8)$$

Where subscripts *hv* and *ha* refer to liver and liver artery, respectively.  $E_h$  is the hepatic extraction ratio and was calculated by eq 9 and the intrinsic clearance  $CL_{int}$  was obtained from Poulin et al.<sup>3</sup>.

$$E_h = CL_{int} / (CL_{int} + Q_{hv}), \quad (9)$$

For i.v. bolus injection, initial concentration in venous blood was calculated by eq 10.

$$C_{0,vb} = Dose / V_{vb}, \quad (10)$$

#### **4.2.4 Simulations of Propranolol and Atenolol PK Profile via IV Bolus and Inhalation**

To simulate the concentration time-course profile for airway, alveoli, and other organs via inhalation or IV bolus, a 250 mg rat was given 1 mg/kg (atenolol) and 1.5 mg/kg (propranolol) as literature reported.<sup>4</sup> Both i.v. bolus injection and inhalation as route of administration were used. For inhalation the dose reaching the lungs is assumed to be same with IV bolus, and with 70% of dosage deposited in airway, 30% of dosage deposited in alveoli to mimic the commonly used experimental condition,<sup>5, 6</sup> assuming instantaneous dissolution in surface lining liquid. By numerically solving the ODEs, the time-course concentration profile can be simulated for each compartment in hybrid model. The lung tissue is composed of airways and alveoli. The mass in all cellular and extracellular compartments (except for tissue blood) in airways, alveoli were lumped together

as apparent mass for respective tissue, whose apparent concentration was then obtained via dividing the apparent mass by respective lumped tissue volume. The AUC (area under the concentration curve) was calculated as integrated area until time reaches to 20 hours, when less than 1% of amount of drugs remains in the body.

## 4.3 Results

### 4.3.1 Model Validation

Experimental tissue concentration profile of two well-studied compounds, propranolol and atenolol,<sup>4</sup> were used to validate the hybrid model. As shown in Figure 4.2., for propranolol, the model using an empirical relationship expressed as eq 8 (chapter 2) to estimate  $K_d$  value underpredicted the lung tissue concentration by around one order of magnitude. After incorporating the specific binding affinity  $K_{aBC}$  between the positively charged propranolol and  $AP^-$  described by eq 1-2, the prediction of lung tissue concentration profile is comparable with observed *in vivo* data. For concentration profile of other tissues (e.g., liver, brain, and kidney, etc), model using two different equations for lipid binding gave similar predictions, which are consistent with experimental results. In addition, no significant difference in predicted concentration profile of other tissues was observed between the model using two different equations for lipid binding. For atenolol, models using two different equations for lipid binding gave a consistent prediction with observed data for concentration profile for lungs as well as other included tissues (Figure 4.3.).

### **4.3.2 Comparison of Tissue Exposure in Airway and Alveoli using IV bolus and Inhalation**

For propranolol and atenolol with IV bolus and inhalation as administration routes, the simulated time-course tissue concentration curve in airway and alveoli were shown in Figure 4.4.. Generally, propranolol has one order of magnitude higher tissue exposure in both airway and alveoli than atenolol in terms of AUC regardless of the administration route. When drugs are administered via IV injection, there is no significant difference in tissue exposure between airway and alveoli for each of two compounds. However, the inhalation gives 2 orders of magnitude higher tissue exposure (i.e., AUC) for airway than alveoli for propranolol and atenolol. For alveoli, both IV bolus and inhalation generates similar tissue exposure for propranolol and atenolol. However, for airways, inhalation enhances significantly the airway tissue exposure for both compounds, which is 50 fold higher than that given by IV bolus.

### **4.4 Discussion**

PBPK has been used extensively to study the ADME profile of compounds in animals and human. In the present study, a hybrid PBPK model was developed by incorporating the multiscale, cell-based compartmental models of rat lungs into the generic PBPK model. The model of lungs includes two components: airways and alveoli, composed of membrane delimited cellular or extracellular compartments, which are organized according to their histology, physiology, and anatomy (Figure 4.1.). After integrating the airways and alveoli into the conventional PBPK model, the hybrid PBPK model described as ODEs

was solved numerically to generate the time-course concentration curve for each of the compartments.

For propranolol and atenolol, the simulated lung tissue concentration profile via IV bolus is comparable with the experimental data. When the  $K_{pu_{BC}}$  value is available for a compound (e.g., propranolol, atenolol), the mechanistic equation developed by Rowland was used to estimate its partition into  $AP^-$  as described by eq 1-2. The simulation results suggest that the accurate estimation of binding of positively charged monobase with  $AP^-$  via electrostatic interaction is crucial for prediction of lung tissue concentration, since the monobase with  $pK_a > 8$  exists mainly as positively charged species under physiological pH. If empirical equation (eq 8 in chapter 2) instead of eq 1-2 was used to estimate the  $K_d$  without  $AP^-$  binding, model underpredicted lung tissue concentration of propranolol by 5-10 folds. Similarly, in previous works by Poulin and Rowland,<sup>2, 3</sup> severe underprediction for lung tissue partition coefficient ( $K_p$  or  $K_{pu}$ ) was also observed for propranolol. If propranolol's  $K_{pu_{BC}}$  value was used to estimate the partition of charged species into lipids using eq 1-2 with  $AP^-$  binding, the prediction of lung tissue concentration profile given by our model is consistent with experimental results. Because propranolol has an uncommonly high  $K_{pu_{BC}}$  value of around 45, indicating a strong binding affinity of its charged form with  $AP^-$  based on the Rowland's mechanistic equation. However, for atenolol, a compound with moderate  $K_{pu_{BC}}$  value around 1, an empirical estimation of partition of charged species into  $AP^-$  from lipophilicity (i.e.,  $\log P_d$ ) with eq 1-2 generated as good prediction of the lung tissue concentration profile as the one

using empirical equation without AP binding (eq 8 in chapter 2). So if the protonated specie of a monobasic compound has no significant binding or partition into  $AP^-$  (e.g.,  $K_{pu_{BC}} < 5$ ), the empirical relationship without AP binding described by eq 8 in chapter 2 will be able to generate reasonably good prediction.

**Table 4.1.** Physiological parameters for tissue volumes and blood flow rates in rats

Tissues		Volumes (V)		Blood Flow Rates (Q)	
		Fraction of total volume	of body volume (ml)	Fraction of cardiac output	Blood flow rate (ml/min)
Arterial blood		0.0272	6.8	---	---
Venous blood		0.0544	13.6	---	---
Adipose		0.076	19	0.07	5.82
Bone		0.04148	10.37	0.122	10.14
Brain		0.0057	1.425	0.02	1.66
Gut		0.027	6.75	0.131	10.88
Heart		0.0033	0.825	0.049	4.07
Kidney		0.0073	1.825	0.141	11.72
Liver		0.0366	9.15	0.175 <sup>b</sup>	14.54
Lung	airways	0.005 <sup>a</sup>	0.292	0.01	0.831
	alveoli		2.544	1	83.09 <sup>c</sup>
Muscle		0.404	101	0.278	23.1
Skin		0.19	47.5	0.058	4.82
Spleen		0.002	0.5	0.02	1.66
Rest of body		0.12002	30.005	0.077	6.3979

<sup>a</sup>. calculated by summing the cellular and extracellular volume in the airways and alveoli tissue<sup>7</sup>

<sup>b</sup>. The blood flow rate for the liver corresponds to the summation of portal vein and hepatic artery. The portal vein represents 15.1%, where 13.1% for gut and other and 2% for spleen.

<sup>c</sup>. Total cardiac output was calculated with an allometric equation ( $0.235 \cdot \text{body weight}^{0.75} \cdot 1000$ ) in ml/min<sup>3</sup>.



**Table 4.2.** Physicochemical properties and PK parameters for atenolol, and propranolol<sup>a</sup>

Properties		Atenolol	Propranolol
MW		266.3	259.4
logP <sub>n</sub>		0.16 <sup>b</sup>	3.2 <sup>b</sup>
logP <sub>d</sub>		-3.54	-0.5
pK <sub>a</sub>		9.6 <sup>b</sup>	9.5 <sup>b</sup>
f <sub>up</sub>		0.96 <sup>c</sup>	0.13
B:P		1.11 <sup>c</sup>	0.80
K <sub>p</sub>	Adipose	---	0.18
	Bone	---	6.90
	Brain	0.11	9.20
	Gut	---	8.22
	Heart	---	4.97
	Kidney	---	3.80
	Liver	3.21	5.67
	Muscle	---	2.20
	Skin	---	7.22
	Spleen	---	2.98
	Rest of body	1.00	1.25
Elimination		CL=38.9 ml/min/kg	E <sub>h</sub> = 0.985

<sup>a</sup>. All parameters from literature<sup>8</sup> unless otherwise specified

<sup>b</sup>. Calculated by Chemaxon<sup>9</sup>

<sup>c</sup>. *In vitro* data measured in humans were used as surrogate for rats<sup>4</sup>

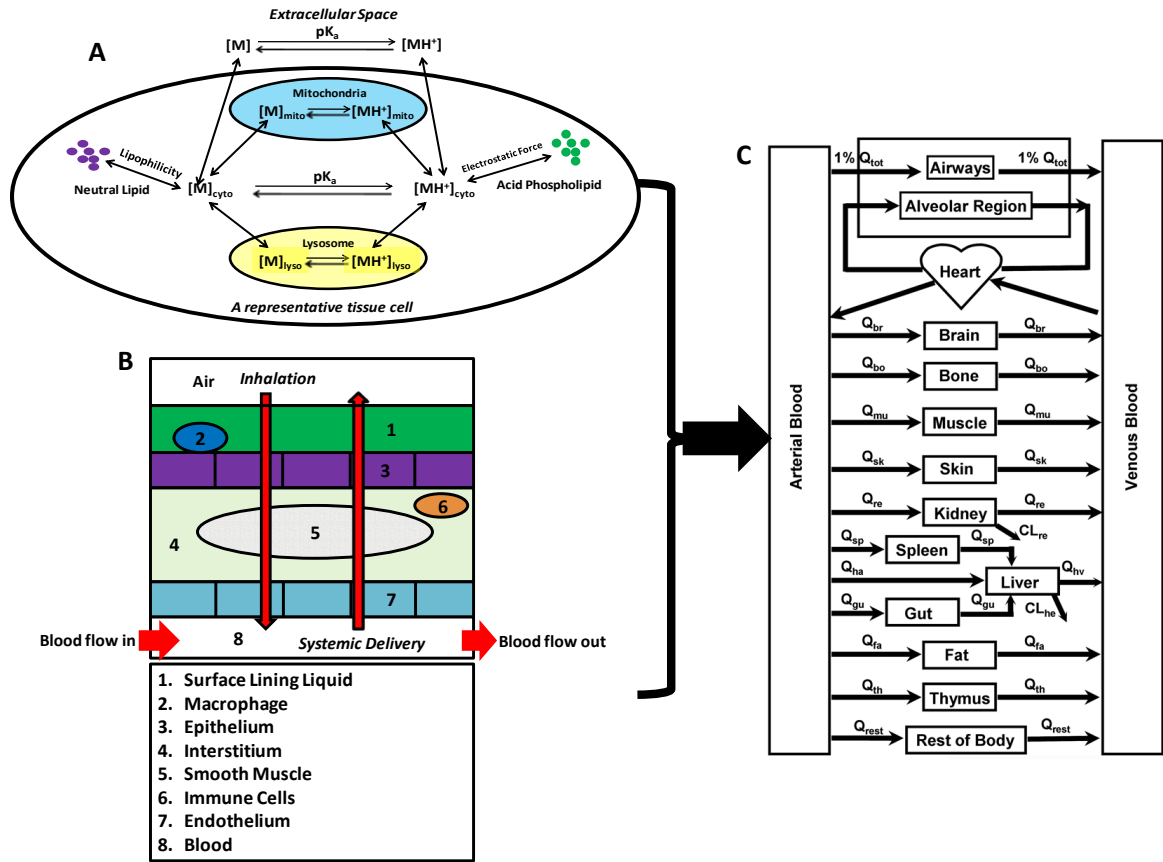


**Figure 4.1.** General methodology of hybrid PBPK model **A.** Cellular level: A representative cell in airway or alveoli with organelles. Monobasic compound diffuses across a phospholipid bilayer and undergoes ionization and partition/binding in each compartment. The neutral form of the monobasic molecule is indicated as  $[M]$ , and the protonated, cationic form of the molecule is indicated as  $[MH^+]$ . **B.** Histological level: The general route of drug transport from the lung lumen/blood to the blood/lumen via inhalation/systemic delivery, across the histological architecture of lung tissue. **C.** Physiological and anatomical level: Integration of airway and alveoli tissue model with whole body PBPK model.

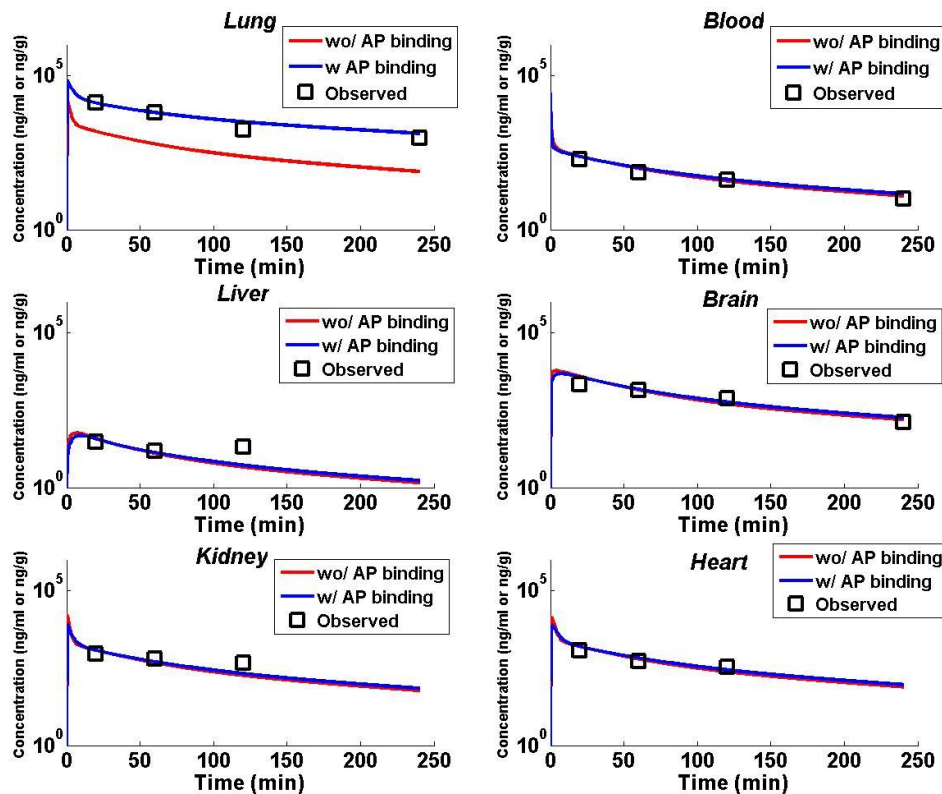


**Figure 4.2.** Comparison between the simulated tissue concentration profiles of propranolol with experimental data. The red line is the simulated concentration profile of propranolol given by the model with using an empirical relationship expressed by eq 8 in chapter 2 to estimate  $K_d$  value without AP binding. The blue line is the simulated concentration profile of propranolol given by the model incorporating the specific binding affinity  $K_{aBC}$  between the positively charged propranolol and  $AP^-$  described by eq 1-2.

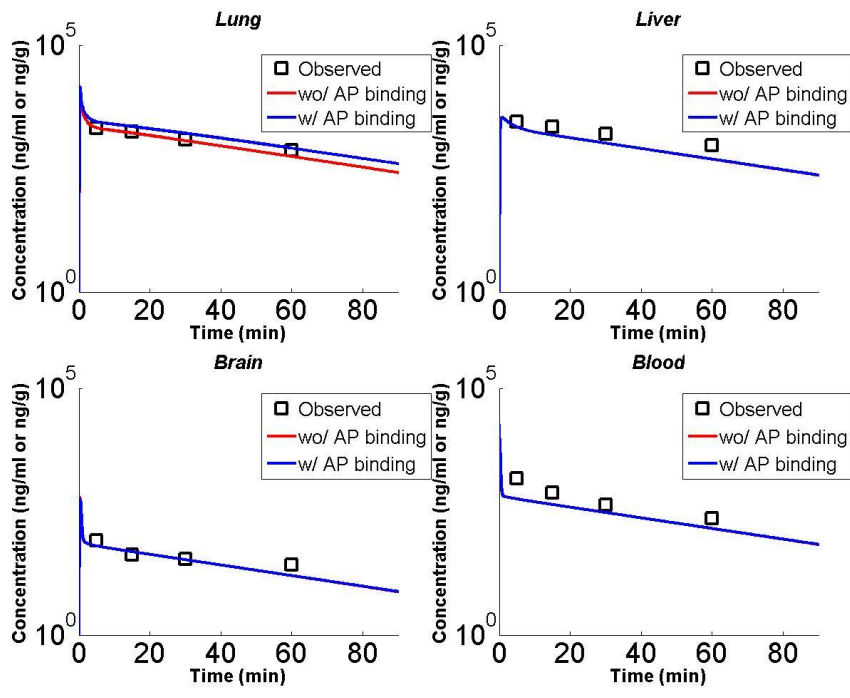


**Figure 4.3.** Comparison between the simulated tissue concentration profiles of atenolol with experimental data. The red line is the simulated concentration profile of atenolol given by the model with using an empirical relationship expressed by empirical equation to estimate  $K_d$  value without AP binding. The blue line is the simulated concentration profile of atenolol given by the model incorporating the specific binding affinity  $K_{aBC}$  between the positively charged propranolol and AP described by eq 1-2.

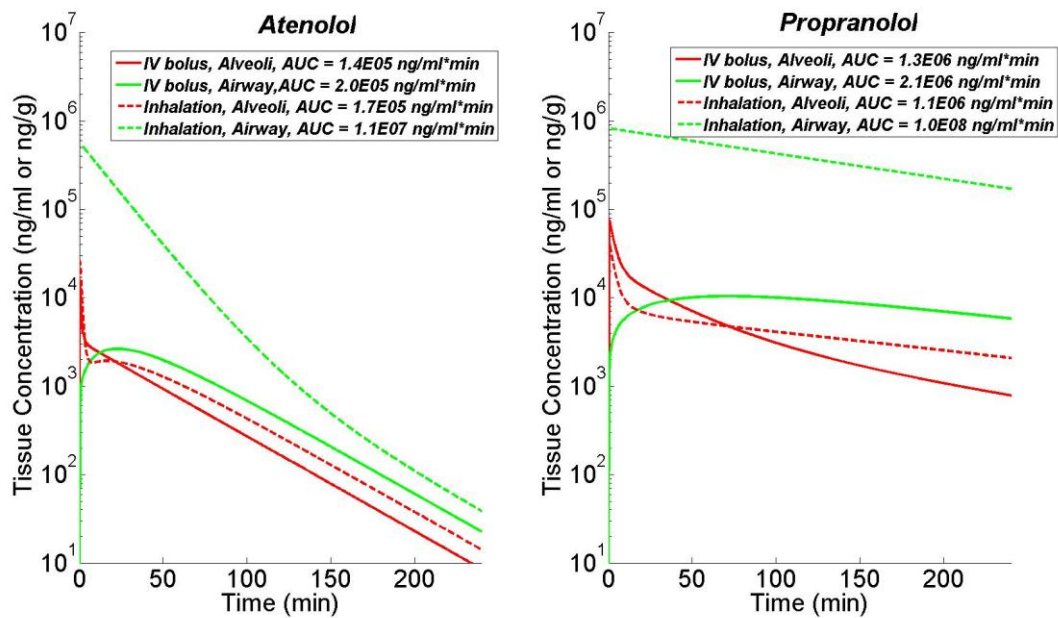


**Figure 4.4.** Comparison between the simulated tissue concentration curve in airways and alveoli for inhaled and IV injected atenolol and propranolol with AP binding. Red line: in alveoli; Green line: in airways; Solid line: IV bolus; Dash line: Inhalation.

## 4.5 References

1. Derendorf, H.; Lesko, L.; Chaikin, P.; Colburn, W.; Lee, P.; Miller, R.; Powell, R.; Rhodes, G.; Stanski, D.; Venitz, J., Pharmacokinetic/pharmacodynamic modeling in drug research and development. *The Journal of Clinical Pharmacology* **2000**, *40* (12), 1399-1418.
2. Rodgers, T.; Leahy, D.; Rowland, M., Physiologically based pharmacokinetic modeling 1: predicting the tissue distribution of moderate-to-strong bases. *J Pharm Sci* **2005**, *94* (6), 1259-76.
3. Poulin, P.; Theil, F. P., Prediction of pharmacokinetics prior to in vivo studies. II. Generic physiologically based pharmacokinetic models of drug disposition. *J Pharm Sci* **2002**, *91* (5), 1358-70.
4. Belpaire, F. M.; de Smet, F.; Vynckier, L. J.; Vermeulen, A. M.; Rosseel, M. T.; Bogaert, M. G.; Chauvelot-Moachon, L., Effect of aging on the pharmacokinetics of atenolol, metoprolol and propranolol in the rat. *J Pharmacol Exp Ther* **1990**, *254* (1), 116-22.
5. Tronde, A.; Norden, B.; Jeppsson, A. B.; Brunmark, P.; Nilsson, E.; Lennernas, H.; Bengtsson, U. H., Drug absorption from the isolated perfused rat lung--correlations with drug physicochemical properties and epithelial permeability. *J Drug Target* **2003**, *11* (1), 61-74.
6. Tronde, A.; Norden, B.; Marchner, H.; Wendel, A. K.; Lennernas, H.; Bengtsson, U. H., Pulmonary absorption rate and bioavailability of drugs in vivo in rats: structure-absorption relationships and physicochemical profiling of inhaled drugs. *J Pharm Sci* **2003**, *92* (6), 1216-33.
7. Yu, J. Y.; Rosania, G. R., Cell-based multiscale computational modeling of small molecule absorption and retention in the lungs. *Pharm Res* **2010**, *27* (3), 457-67.
8. Zhang, X. From Cell to Organism: A Predictive Multiscale Model of Drug Transport. University of Michigan, Ann Arbor, 2009.
9. *Marvin and Calculator*, ChemAxon, Budapest, Hungary, 2009.

## CHAPTER 5

### **A mathematical model coupling dissolution and absorption in lungs to explore the chemical space for rational design of inhalation products**

#### **5.1 Introduction**

##### **5.1.1 Physicochemical Properties and Formulations**

Design of inhaled drug poses particular challenges during the drug development as opposed to oral drugs. Such challenges include design of optimal new chemical entity (NCE), proper crystalline of active pharmaceutical ingredient (API), the formulation and reliable inhaler device for administration of inhaled drugs to the lungs.<sup>1</sup> Our focus was placed on drug design for the treatment of lung diseases, particularly establishment of design principles for inhaled drugs from the perspective of medicinal chemistry (i.e., physicochemical and structural properties). For oral drugs Lipinski's "the rule of 5" defines the most plausible range of physicochemical properties for oral drugs,<sup>2</sup> based on which there are extensive studies exploring the physicochemical properties of oral drugs. As a result, the Lipinski's rule has been widely used as guidance for

the development of oral drugs. However, only a few reported studies have been devoted to the guidance of rational design of inhaled drugs from mechanistic point of view.<sup>3-5</sup> There is a significant lack of knowledge about the rational design principles for inhaled drugs. In general, inhaled drugs are more lipophilic and possess a higher molecular weight compared to oral drugs. There is very limited research focused on physicochemical properties of inhaled molecules. Patton and Byron's work is centered on delivering drugs via inhalation to the lung.<sup>3, 6, 7</sup> A statistical analysis of inhaled drugs by Tronde and colleagues with the aid of elegant isolated perfused lung experiments, where the absorption profiles of small molecules in rat lungs were related to physicochemical properties, such as logD, PSA, molecular weight.<sup>5, 8, 9</sup> However, this is only empirical perception based on statistical data analysis on marketed inhaled drugs rather than mechanism-based rational.

The indispensable properties of marketable inhaled drugs are that they can achieve stable and predictable therapeutical effects in lungs.<sup>1, 10, 11</sup> This requires a consistent control over the variability of formulation and delivery by various devices, it is also important to minimize the risk of systemic side effect, for example, the potential safety concern for beta-adrenergic agonist to contribute to undesirable increased heart rate.

Formulation development involves a serial of steps in which an API ingredient is incorporated into a drug product to be applicable to patients. Pharmacological activity is a necessary element for a successful drug, but not the only one.<sup>1, 12</sup> Factors such as stability and cost of delivery device, and



bioavailability to the site of action are critical for the quality of a pharmaceutical product. Design of inhaled drug product with ideal properties in every aspect of these factors is often not feasible.<sup>13</sup> For example, compounds with good pharmacologic activity *in vitro* may display poor physicochemical properties or PK/PD profiles *in vivo*. Consequently, the final drug product on market is often a result of compromise between theoretically ideal one and realistic one. The development of inhaled drugs has its own particular challenges as both formulation and device design can affect the quality of inhaled drugs. In addition, between-subject variability of inhalation pattern and respiratory-tract anatomy and physiology introduce extra variability in the drug effects. Reliable, reproducible, and convenient inhalation device is required to achieve optimal drug effect. A comprehensive strategy of rational design incorporating formulation and corresponding device design can lead to a high quality inhaled drug product. The technical aspects of inhaler design and development have been extensively reviewed in other literature.<sup>1, 10</sup>

### **5.1.2 Inhalation Device**

Device for inhalation drugs can be categorized into 3 major types, including pressurized metered-dose inhalers (pMDIs), DPIs, and nebulizers. <sup>1</sup>Each type of inhalation device has its own strengths and weaknesses. The categorization of inhalation device is based on the choice of dispersion medium and means of delivery. Further classification within each type is based on technology of metering and dispersion of the device. pMDIs and DPIs generally contain solid drugs suspended or dissolved in a nonpolar medium. DPIs are

easier to use, more stable and efficient than pMDI because pMDI is pressurized to emit the dose at high velocity, resulting in high chance of undesirable deposition of drugs in the pharynx. Nebulizers are unique and different from pMDIs and DPIs for the drug is dissolved or suspended in a polar liquid (e.g., water). Nebulizers are mainly used in hospital and ambulatory settings, but rarely used for treating chronic lung disease as they are typically bulky, hence inconvenient for continuous use over a long period of time. The performances of the various inhalation devices have been extensively evaluated in many clinical trials as reported in a review.<sup>14</sup> Inhalation devices are comparable with each other in terms of clinical performance. Therefore, the device selection for each patient should take into account various factors, such as disease progression, convenience, cost of device, and patient personal preference.<sup>14, 15</sup>

### **5.1.3 Particle Size and Distribution**

Particle size and distribution are the important parameters for formulation design of inhaled drugs.<sup>16</sup> Aerodynamic diameter is the most relevant to inhalation delivery and its subsequent therapeutic effect. A tremendous effort has been made to relate the aerodynamic diameter and size distribution to the particle deposition pattern in specific regions of lung.<sup>17</sup> To reach the peripheral region of lung, the optimal particles should have 1-5  $\mu\text{m}$  aerodynamic diameter range. Particles larger than 10  $\mu\text{m}$  typically deposit in the oral cavity or pharynx, then they will be quickly cleared from the respiratory system. Particles smaller than 1  $\mu\text{m}$  may not be able to deposit into the lung at all for they may be exhaled out of lung due to the lack of gravity deposition. Dynamic shape factors are as

important as particle size, and can be obtained either experimentally or mathematical models.<sup>18</sup> Other than the theoretical optimization of size, shape, and number of particles according to breathing mode, the design and production of appropriate devices is also pivotal for the success of final drug product. The other concerns with the clinical effect of inhaled drugs are the patient's compliance and their skills with the inhalation device.<sup>14</sup>

#### **5.1.4 Objective**

In contrast to oral drug formulations, for inhaled drug formulations or for other particulate drug formulations that dissolve while the particles are in direct contact to a biological surface or interface, there are no in vitro assay systems that can be used to quantitatively analyze dissolution and permeability under physiologically relevant conditions. When a dissolving particle is in close proximity to a biological surface or membrane, dissolution and absorption are happening simultaneously. For inhaled drug formulations, dissolution and absorption are directly coupled to each other. Unlike oral drugs which require a glass of water or fluid to be taken and therefore dissolve in aqueous environment, the dissolution of inhaled drugs in respiratory system takes place on a very thin (10  $\mu\text{m}$  or less) surface lining liquid layer on top of airway epithelial cell. For inhaled drugs, the absorption barrier is formed by the apical cell membranes of the nasal or pulmonary epithelial cells which are in direct contact with the surface lining liquid layer on which drug particle dissolution is taking place. Under these conditions, the special physiological environment of the surface lining liquid interact with the physical characteristics of inhaled particles

(e.g. size, density), physiochemical properties of molecules (permeability, pKa), as well as the permeability and transport properties of the underlying lung epithelial cells to determine the pharmacokinetic profile of inhaled therapeutics. This will ultimately impact the pharmacodynamic behavior of the drug and affect drug efficacy and safety. In this work, a mechanistic model coupling the dissolution and permeation of small molecules across the lung barrier was developed to explore the effect of physiochemical properties and formulation on local and systemic pharmacokinetics of inhaled compounds. Our research does not address the issue of detailed optimization of inhalation and devices to produce the desired therapeutic effect. Instead, we focus on the exploration of chemical space of small molecules to minimize the variability of clinical outcomes caused by aforementioned factors, thereby reducing the uncertainty involved at the different stages of drug discovery and development.

## **5.2 Methods**

The mechanistic, theoretical underpinning of which is elaborated in figure 5.1.. Essentially as drug particles dissolve in a confined volume and in close proximity to a membrane, the concentration of drug is very different in the vicinity of the particle than at a distance from the particle. Around each particle, the concentration of drug is at the solubility limit of the drug. Then the concentration of soluble drug falls off over a certain distance to a bulk volume region between the particles where the concentration is at its lowest. Accordingly, there is an effective boundary layer surrounding each particle where the average drug concentration is halfway between the drug concentration in the bulk volume

regions that are most distant to the particle surface and the drug concentration in the regions that are immediately on the surface of the particle. In other words, an effective boundary region around each particle is defined as the volume where the concentration of freely soluble drug is half the value between the drug concentration at the particle surface and the “bulk volume” drug concentration at a distance from the particle. Within this boundary layer region the transport of drug molecule from the donor compartment to the acceptor compartment is governed by the permeability of the membrane or interface separating donor and receiver compartments, by the membrane area covered by the region encompassing this boundary layer, and by the average concentration of drug in this boundary layer (as defined). Similarly, outside the boundary layer region around each particle the transport of drug molecule from the donor compartment to the acceptor compartment is equally governed by the permeability of the membrane or interface separating donor and receiver compartments. Under these conditions, the number, size/area and density of drug in the particles will determine the boundary layer area and thickness, and the area over this boundary layer region exists in relation to the surface of the particles will become a key determinant of the transport behavior of the dissolved drug molecules from the donor compartment to the receiver compartment.

The rate of dissolution of a particle formulation coupled to the transport of dissolved drug molecules across the bounding membrane or diffusion layer interface can be computationally analyzed with the help of a mathematical dissolution-absorption models comprised of differential equations linking changes

in drug concentration in the donor compartment over time to the appearance of drug mass in the receiver compartment as well as the shrinking of the particles in the donor compartment. Such mathematical model based on ordinal differential equation (ODE) is used to describe the mass dissolution of drug from the particles in the donor compartment in a slab of liquid, coupled to the transport of drug from donor to receiver compartment across an interphase or membrane, perpendicular to the dissolution plane. Differentiation of a variable with respect to time simply describes the rate of the change of this variable with time. By coupling a set of ODEs given corresponding parameters, a mass-balanced ODE system can be used to simulate mass transport phenomenon. Solving the ODEs numerically can generate the time-course profile for each set of parameters included.

The area for absorption can be divided into two sections, one is the area ( $A_e$ ) covered by the particles coupled with corresponding diffusion layer, another is the rest of area in dissolution bulk ( $A_d$ ). The area covered by particles is governed by the number of particles, particle size, and diffusion layer thickness as indicated by eq 1.

$$A_e = N \cdot \pi \cdot (r + h)^2 \quad (1)$$

$N$  is the number of particles,  $r$  is the radius of a particle,  $h$  is the thickness of diffusion layer thickness surrounding each particle.

The area of dissolution bulk  $A_d$  is derived by subtracting  $A_e$  from  $A_t$  (total area) as eq 2. The dissolution bulk volume  $V_d$  is calculated by multiplying the  $A_d$  with the height of dissolution chamber  $L$  as eq 3.

$$A_d = A_t - A_e \quad (2)$$

$$V_d = A_d \cdot L \quad (3)$$

$$\frac{dm}{dt} = - \left[ \frac{N \cdot D \cdot 4 \cdot \pi \cdot r^2}{h} \cdot (C_s - C_d) + A_e \cdot P \cdot \left( \frac{C_s + C_d}{2} - C_r \right) \right] \quad m(0) = \text{Dose} \quad (4)$$

Eq 4 describes the rate of loss of drug mass from particles,<sup>19</sup> including first term describing the dissolution rate of a sphere particle with radius  $r$  using Nernst-Brunner equation and the second term describing the absorption rate across the  $A_e$  inside the diffusion layer. The concentration inside the diffusion layer is calculated as half of sum of  $C_s$  and  $C_d$ .  $m(0)$  is the initial condition at time 0, for example,  $m(0)$  equals to total amount of particles or dose placed in the dissolution chamber.

Based on eq 5 describing the relationship between mass, volume and radius ( $4\pi r^2$  is the surface area of a sphere with  $r$  as radius), the rate of change of radius  $r$  during the dissolution is expressed as eq 6.  $r(0)$  is the radius at time 0, for example, it can be known number by measuring the particle size.

$$\frac{dm}{dt} = \frac{N \cdot \text{Density} \cdot 4 \cdot \pi \cdot r^2 \cdot dr}{dt} \quad (5)$$

$$\frac{dr}{dt} = - \frac{\left[ \frac{N \cdot D \cdot 4 \cdot \pi \cdot r^2}{h} \cdot (C_s - C_d) + A_e \cdot P \cdot \left( \frac{C_s + C_d}{2} - C_r \right) \right]}{N \cdot 4 \cdot \pi \cdot r^2 \cdot \text{Density}} \quad r(0) = r_0 \quad (6)$$

Eq 7 describes the change of concentration in donor chamber, including first term describing the mass input from dissolution of particle, and mass output into receiver chamber via diffusion across membrane with area ( $A_d$ ). Then, dividing the rate of change of mass (numerator) by the volume of dissolution chamber  $V_d$  (denominator), the rate of change of donor concentration can be derived as eq 6. The  $C_d(0)$  at time 0 can be 0 when simulations start at the time when the particle is placed at dissolution chamber, or  $C_s$  when simulations start at time when the dissolution chamber is saturated at concentration  $C_s$  (namely, steady state between particles and dissolution buffer).

$$\frac{dC_d}{dt} = \frac{\frac{N \cdot D \cdot 4 \cdot \pi \cdot r^2}{h} \cdot (C_s - C_d) - A_d \cdot P \cdot (C_d - C_r)}{V_d} \quad C_d(0) = 0 \text{ or } C_s \quad (7)$$

Eq 8 describes the concentration change at receiver chamber, including two inputs as diffusion from two different associated areas,  $A_e$  and  $A_d$  with respective concentration gradient.  $V_r$  is a known constant describing the receiver chamber.  $C_r(0)$  represents the receiver concentration at time 0.

$$\frac{dC_r}{dt} = \frac{A_e \cdot P \cdot \left( \frac{C_s + C_d}{2} - C_r \right) + A_d \cdot P \cdot (C_d - C_r)}{V_r} \quad C_r(0) = 0 \quad (8)$$



When a fresh media input is constantly applied at the receiver chamber (i.e., concentration is extremely low), the  $C_r$  will be considered as 0, and  $V_r$  is a time-variant variable. Therefore, instead of describing concentration change in receiver chamber, eq 9 is used to describe the mass change in receiver chamber based on Fick's law.  $m_r(0)$  is the mass in receiver chamber at time 0.

$$\frac{dm_r}{dt} = A_e \cdot P \cdot \left( \frac{C_s + C_d}{2} - C_r \right) + A_d \cdot P \cdot (C_d - C_r) \quad m_r(0) = 0 \quad (9)$$

Notations of parameters and variables:

N: Number of particles

m: Particle mass (mg)

r: Particle radius ( $\mu\text{m}$ )

$A_e$ : Area covered by particles

$A_d$ : Area covered by dissolution bulk

$A_t$ : Total membrane area

$C_d$ : Concentration in donor chamber

$C_r$ : Concentration in receiver chamber

$m_r$ : Mass in receiver chamber

D: Diffusivity ( $\text{cm}^2/\text{s}$ )

Density: Particle density (g/ml)

Cs: Solubility (mg/ml)

h: Diffusion layer thickness (um)

P: Membrane Permeability (cm/s)

Based on the simulation results given by the ODE-based model, the metrics describing the systemic and local pharmacokinetics behavior can be obtained, including AbsT50 (time when 50% of drugs is absorbed into the drug receiver chamber), Cbmax (The concentration peak at bulk chamber), Tbmax (time when the peak concentration at bulk chamber is reached). We used compounds with low ( $10^{-8}$  cm/s), medium ( $10^{-6}$  cm/s), high permeability ( $10^{-4}$  cm/s) and low (0.01 mg/ml), high solubility (10 mg/ml) as physicochemical space inputs to the model, therefore there are 6 possible combinations of physicochemical properties in total. We use the particle size(r) (1 and 10 um) and number of particles (given the specific density and dose) as the formulation inputs. The area covered by particles ( $A_t$ ) was used as inputs to characterize the device property. With independently varying the parameters describing the physicochemical properties, formulation, devices as the inputs to the model, the outputs of the model can be analyzed based on AbsT50 (time when a half of drug is absorbed), Cbmax (the maximal concentration in dissolution bulk or drug donor), Tbmax (time when the maximal concentration is reached).

### 5.3 Results

An illustrative figure for the simulation results given by the ODE-based mechanistic model was given in Figure 5.2., from which AbsT50, Cbmax, T<sub>bmax</sub> can be derived for every set of parameters interested to explore the outcomes under different scenarios. The AbsT50 reflects the systemic pharmacokinetics behavior, and the Cbmax and T<sub>bmax</sub> reflect the local pharmacokinetics behavior. Relationship between these output of pharmacokinetics parameters and input parameters describing the physicochemical properties, formulation and device properties can elucidate the optimal chemical space for inhaled drugs. The key question we intend to address here is to locate what's the optimal chemical space for an inhaled drug designed for treating lung disease. We defined that the difference in T50 or T<sub>bmax</sub> greater than 5 minutes (300 seconds) and the relative change of Cbmax greater than 10 fold as observable effect. As shown in Figure 5.3., for compound with high permeability and low or high solubility, the deposition pattern ( $A_t$ ) and particle size ( $r$ ) has no observable effect on the T<sub>bmax</sub>, although there is 10 fold differences between T<sub>bmax</sub> with high solubility, the absolute difference is less than 100 seconds (i.e., difference between 1 and 100 seconds). As shown in right panel of Figure 5.3., for compound with high permeability and low solubility, the deposition pattern ( $A_t$ ) and particle size ( $r$ ) has is negatively related to the Cbmax. But for compound with high permeability and high solubility, only the deposition pattern ( $A_t$ ) is negatively related to the Cbmax, the particle size ( $r$ ) has no effect on Cbmax. For compound with high permeability and low solubility, the particle size ( $r$ ) is positively related to the AbsT50, but

deposition pattern ( $A_t$ ) has no observable effect on  $AbsT_{50}$ . But for compound with high permeability and high solubility, neither the deposition pattern ( $A_t$ ) nor particle size ( $r$ ) has observable effect on the  $AbsT_{50}$  despite that the particle size ( $r$ ) is negatively related to  $AbsT_{50}$ , but this effect is not observable based on the threshold (300 seconds). As shown in Figure 5.4. and 5.5., similar simulations and subsequent analysis was performed for other possible scenarios of physicochemical space, particle size, and deposition pattern, including medium and low permeability coupled with low and high solubility. The analysis results for all possible combination of parameters were summarized in table 5.1. In terms of local ( $C_{bmax}, T_{bmax}$ ) and systemic pharmacokinetics ( $AbsT_{50}$ ) profiles, the compound with medium permeability is least affected by particle size and deposition pattern compared to compounds with high and low permeability.

#### **5.4 Discussion**

The mechanistic model can describe the local and systemic pharmacokinetics of inhaled drugs by coupling the particle dissolution and subsequent permeation. The time-course change of mass and concentration at dissolution buffer and the drug receiver compartment was generated from numerical solution of the couple ODEs. Further analysis was performed based on the model outputs given various input parameters describing drug, formulation and devices.

The design of oral drugs has been studied extensively. Based on the BCS system, the optimal class I drug should have high permeability and high solubility to achieve high rate and extent of absorption. Class I Oral drug often possesses

high bioavailability and reduced variability in drug exposure. However, for inhaled drugs the barrier for efficacy and safety is the uncertainty in local and systemic exposure induced by variability in formulation and device instead of the bioavailability. The results from the table 5.1. suggest that the medium permeability is the optimal for locally acting inhaled drugs, because the effect of formulation (particle size) and devices (deposition pattern) on local and systemic pharmacokinetics was minimized. In addition, for compound with medium permeability, the solubility is not a key factor for controlling the uncertainty in pharmacokinetics caused by variability in formulation and devices. The systemic and local pharmacokinetics of compound with high and low permeability is comparable in terms of the vulnerability towards the variability in formulation and devices.

The underlying mechanism can be elaborated with the controlling or limiting factor for the local and systemic pharmacokinetics. It can be either dissolution or permeation exerting effect over the local and systemic pharmacokinetics, when one is much faster than another. In the case of inhaled drugs, the dissolution step is controlled by the particle size and solubility. Formulation with smaller particle and drugs with higher solubility will have faster rate of dissolution. The absorption is mainly controlled by permeability of drugs. When the permeability is high, hence the permeation is fast, the local and systemic pharmacokinetics will be mainly controlled by dissolution step determined by particle size. The  $C_{bmax}$  given a fixed dose is negatively related

to the dissolution bulk volume, which is determined by the area covered by the particles (i.e., deposition pattern,  $A_t$ ).

To conclude, a mechanistic model coupling the dissolution and permeation of small molecules in the lung was developed to explore the interaction of drug properties, formulation, and devices. Based on the analysis of the simulations results, the inhaled compounds with medium permeability will generate less uncertainty in local and systemic pharmacokinetics than compounds with high and low permeability given the variability in formulation and devices. The dissolution and permeation components included in the current version of the model can be further studied and improved independently. More importantly experimental data will be needed to validate and refine this model. The experimental device and design will be discussed in detail in chapter 6 of this thesis.

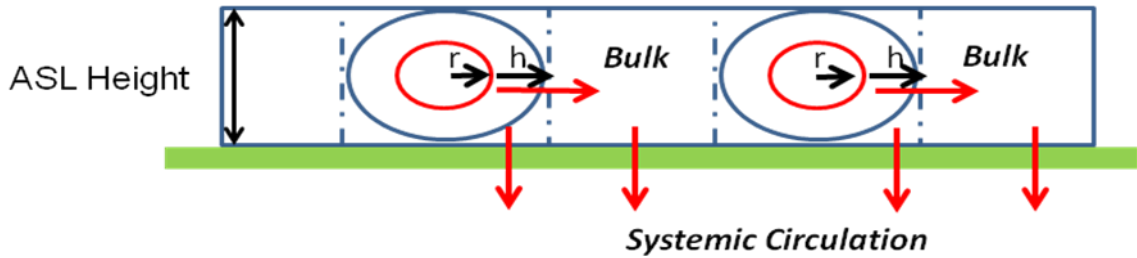
Table 5.1. Summary of analysis of simulation results.

a. Summary of analysis results for compounds with high solubility ( $C_s = 10$  mg/ml) based on right panels of figure 5.3., 5.4., and 5.5

	Low Permeability		Medium Permeability		High Permeability	
	Deposition(At)	Particle Size(R0)	Deposition(At)	Particle Size(R0)	Deposition(At)	Particle Size(R0)
AbsT50	0	+1	0	0	0	0
Cbmax	-1	0	0	0	-1	0
Tbmax	0	0	0	0	0	0

b. Summary of analysis results for compounds with low solubility ( $C_s = 0.01$  mg/ml) based on left panels of figure 5.3, 5.4, and 5.5

	Low Permeability		Medium Permeability		High Permeability	
	Deposition(At)	Particle Size(R0)	Deposition(At)	Particle Size(R0)	Deposition(At)	Particle Size(R0)
AbsT50	-1	0	-1	+1	0	+1
Cbmax	0	0	0	0	-1	-1
Tbmax	+1	+1	0	0	0	0



### Nernst-Brunner for dissolution

$$\frac{dm}{dt} = - \left[ \frac{D \cdot 4 \cdot \pi \cdot r^2}{h} \cdot (C_s - C_b) + A \cdot P \cdot \left( \frac{C_s + C_b}{2} - C_{sys} \right) \right]$$

$$A = 4 \cdot \pi \cdot (r + h)^2$$

$$A_b = A_t - A$$

$$V_b = A_b \cdot ASLHeight$$

$$\frac{dm}{dt} = \frac{Density \cdot 4 \cdot \pi \cdot r^2 \cdot dr}{dt}$$

$$\frac{dr}{dt} = - \frac{\left[ \frac{D \cdot 4 \cdot \pi \cdot r^2}{h} \cdot (C_s - C_b) + A \cdot P \cdot \left( \frac{C_s + C_b}{2} - C_{sys} \right) \right]}{4 \cdot \pi \cdot r^2 \cdot Density}$$

$$\frac{dC_b}{dt} = \frac{\frac{D \cdot 4 \cdot \pi \cdot r^2}{h} \cdot (C_s - C_b) - A_b \cdot P \cdot (C_b - C_{sys})}{V_b}$$

$$\frac{dC_{sys}}{dt} = \frac{A \cdot P \cdot \left( \frac{C_s + C_b}{2} - C_{sys} \right) + A \cdot P \cdot (C_b - C_{sys})}{V_{sys}}$$

Formulation/Device specific parameters

- r: particle radius
- h: Diffusion layer thickness
- Density: Particle Density
- A<sub>t</sub>: Total area covered( Deposition pattern)

API specific parameters

- D: Diffusivity of molecules
- C<sub>s</sub>: Solubility
- P: Permeability

Figure 5.1. A schematic representation of mathematical model coupling dissolution and absorption



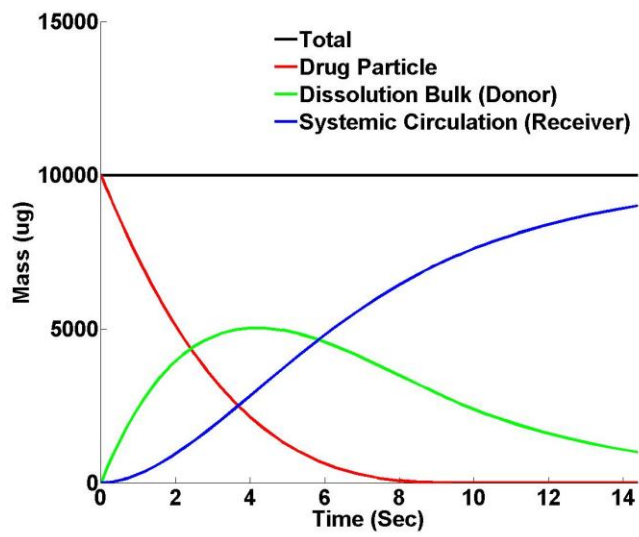


Figure 5.2. Illustration of simulated time-course of mass in different compartments with the dissolution-absorption model

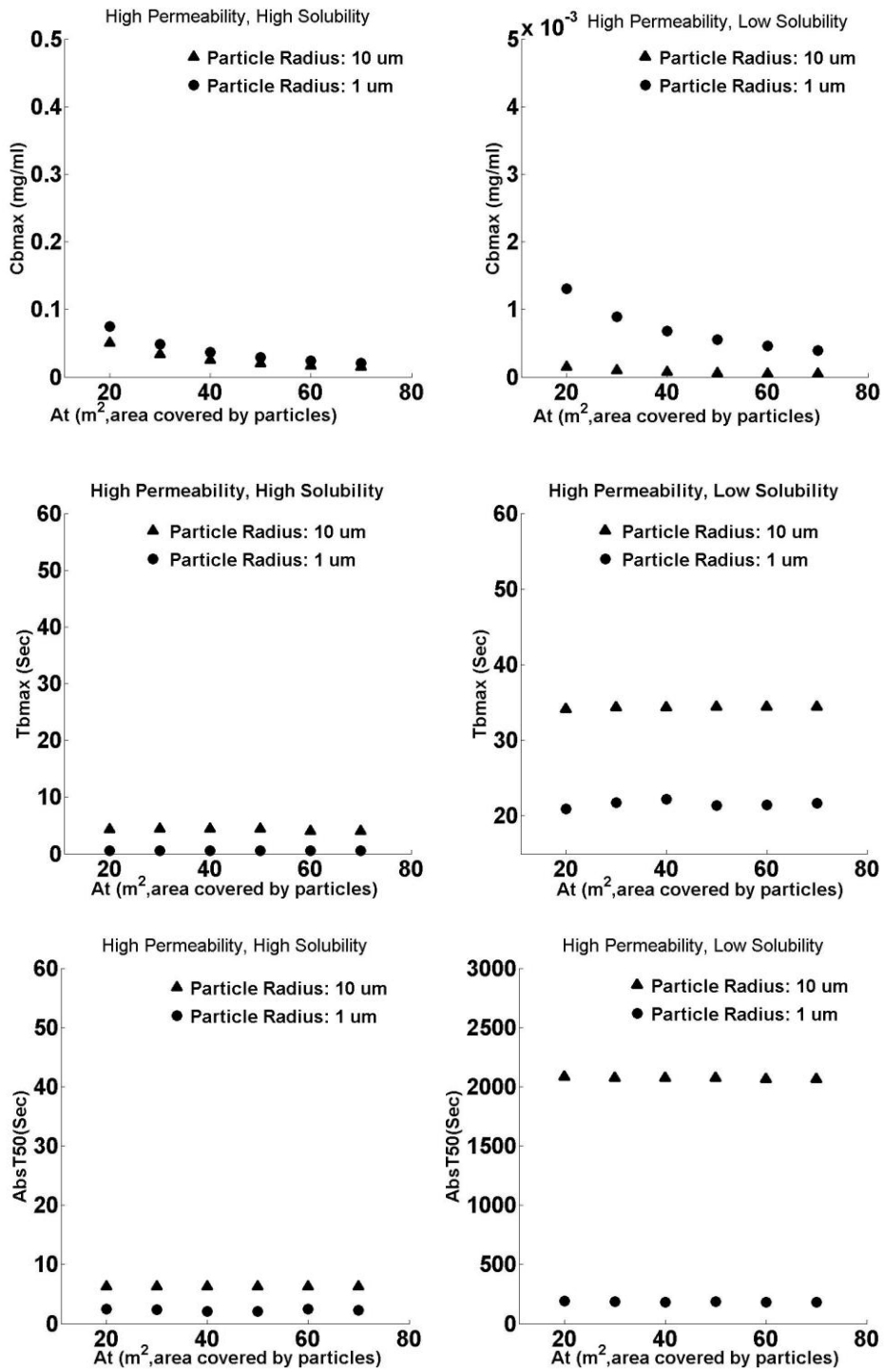


Figure 5.3. The effect of formulation (Particle radius) and device (At) on the pharmacokinetics of inhaled drugs with high permeability ( $10^{-4}$  cm/s)

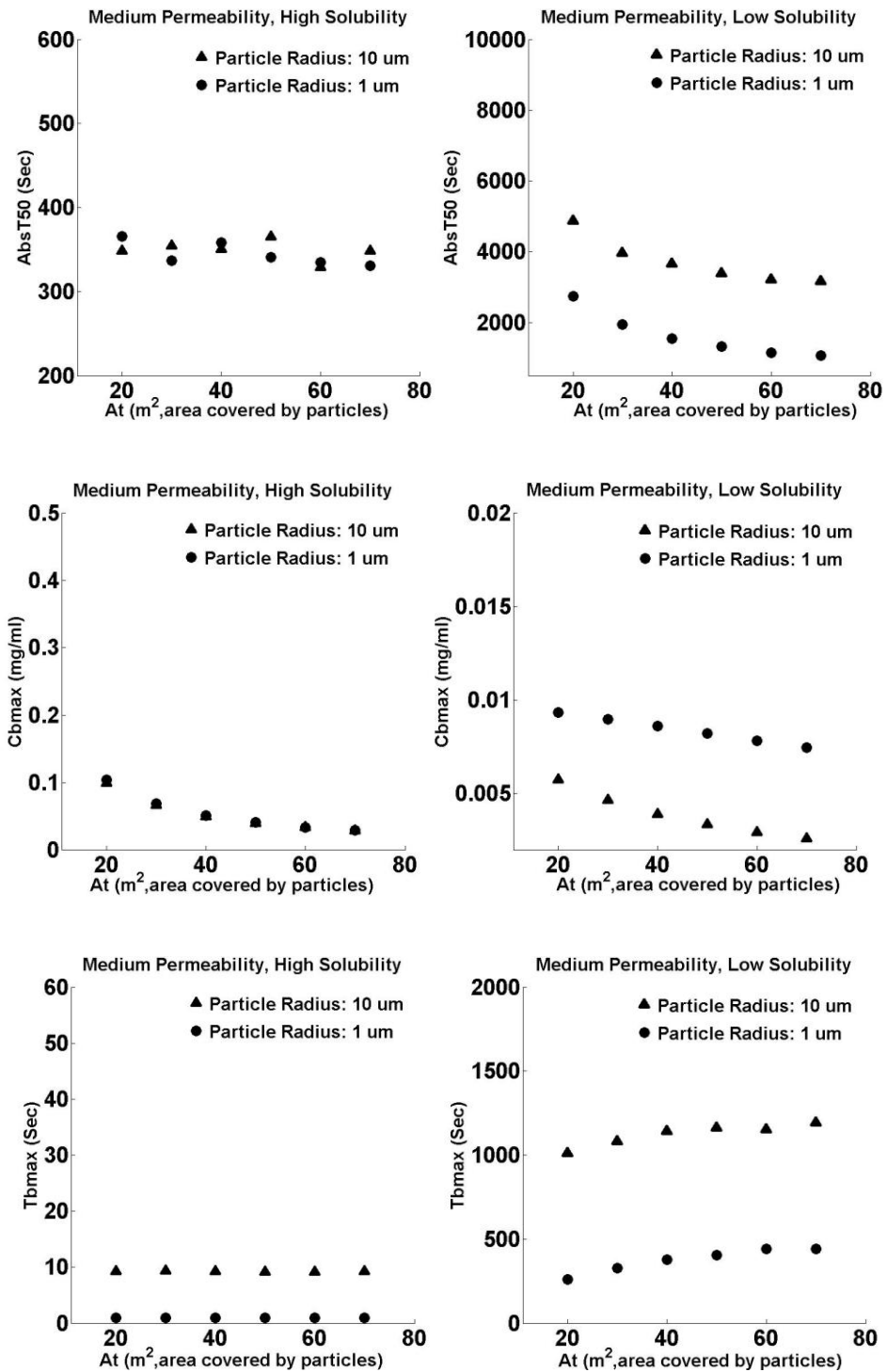


Figure 5.4. The effect of formulation(Particle radius) and device (At) on the pharmacokinetics of inhaled drugs with medium permeability ( $10^{-6}$  cm/s)

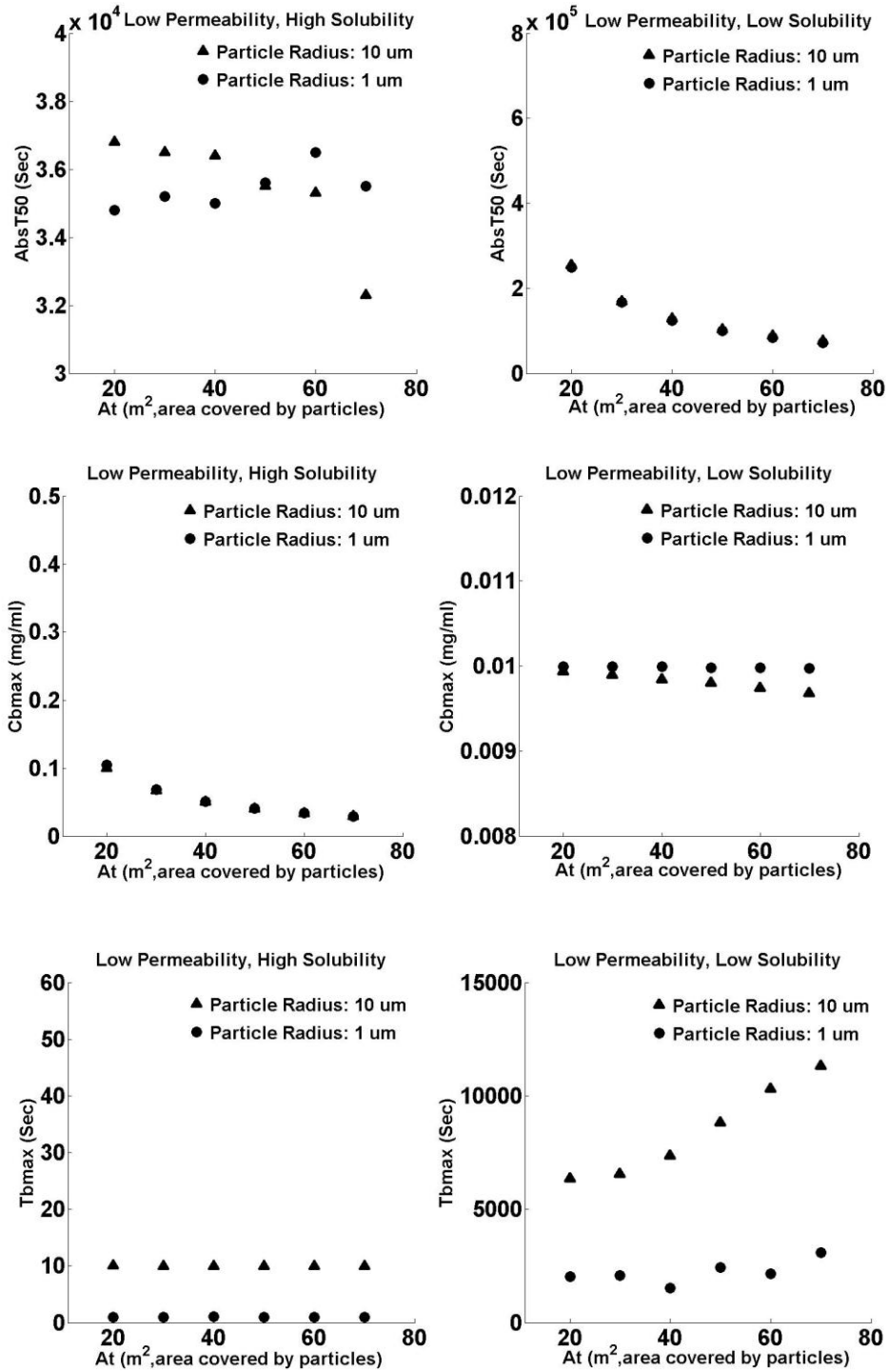


Figure 5.5. The effect of formulation(Particle radius) and device (At) on the pharmacokinetics of inhaled drugs with low permeability ( $10^{-8}$  cm/s)

## 5.5 References

1. Newman, S. P.; Busse, W. W., Evolution of dry powder inhaler design, formulation, and performance. *Respiratory medicine* 2002, 96 (5), 293-304.
2. Lipinski, C. A.; Lombardo, F.; Dominy, B. W.; Feeney, P. J., Experimental and computational approaches to estimate solubility and permeability in drug discovery and development settings. *Adv Drug Deliv Rev* 2001, 46 (1-3), 3-26.
3. Patton, J. S., Mechanisms of macromolecule absorption by the lungs. *Advanced Drug Delivery Reviews* 1996, 19 (1), 3-36.
4. Schanker, L. S.; Hemberger, J. A., Relation between Molecular-Weight and Pulmonary Absorption Rate of Lipid-Insoluble Compounds in Neonatal and Adult-Rats. *Biochemical Pharmacology* 1983, 32 (17), 2599-2601.
5. Tronde, A.; Norden, B.; Jeppsson, A. B.; Brunmark, P.; Nilsson, E.; Lennernas, H.; Bengtsson, U. H., Drug absorption from the isolated perfused rat lung--correlations with drug physicochemical properties and epithelial permeability. *J Drug Target* 2003, 11 (1), 61-74.
6. Byron, P. R.; Roberts, N. S. R.; Clark, R., An Isolated Perfused Rat Lung Preparation for the Study of Aerosolized Drug Deposition and Absorption. *Journal of Pharmaceutical Sciences* 1986, 75 (2), 168-171.
7. Patton, J. S.; Byron, P. R., Inhaling medicines: delivering drugs to the body through the lungs. *Nature Reviews Drug Discovery* 2007, 6 (1), 67-74.
8. Tronde, A. Pulmonary drug absorption: in vitro and in vivo investigations of drug absorption across the lung barrier and its relation to drug physicochemical properties. Uppsala University, 2002.
9. Tronde, A.; Norden, B.; Marchner, H.; Wendel, A. K.; Lennernas, H.; Bengtsson, U. H., Pulmonary absorption rate and bioavailability of drugs in vivo in rats: structure-absorption relationships and physicochemical profiling of inhaled drugs. *J Pharm Sci* 2003, 92 (6), 1216-33.
10. Biggadike, K.; Uings, I.; Farrow, S. N., Designing Corticosteroid Drugs for Pulmonary Selectivity. *Proc Am Thorac Soc* 2004, 1 (4), 352-355.
11. Baptist, A. P.; Reddy, R. C., Inhaled corticosteroids for asthma: are they all the same? *Journal of Clinical Pharmacy and Therapeutics* 2009, 34 (1), 1-12.
12. Rohatagi, S.; Shah, B.; Zhang, J.; Zeng, Z.; Kirkesseli, S.; Jensen, B. K., Estimating Mass Balance for Inhaled Drugs in Humans: An Example with a VLA-4 Antagonist, IVL745. *The Journal of Clinical Pharmacology* 2004, 44 (4), 348-358.
13. Aerosol Drug Delivery Optimization by Computational Methods for the Characterization of Total and Regional Deposition of Therapeutic Aerosols in the Respiratory System. *Current Computer - Aided Drug Design* 2007, 3, 13-32.
14. Dolovich, M. B.; Dhand, R., Aerosol drug delivery: developments in device design and clinical use. *The Lancet* 377 (9770), 1032-1045.
15. Scheuch, G.; Bennett, W.; Borgström, L.; Clark, A.; Dalby, R.; Dolovich, M.; Fleming, J.; Gehr, P.; Gonda, I.; O'Callaghan, C.; Taylor, G.; Newman, S., Deposition, Imaging, and Clearance: What Remains to be Done? *Journal of Aerosol Medicine and Pulmonary Drug Delivery* 23 (S2), S-39-S-57.

16. Carvalho, T. C.; Peters, J. I.; Williams lii, R. O., Influence of particle size on regional lung deposition - What evidence is there? *International Journal of Pharmaceutics* 406 (1-2), 1-10.
17. Shoyele, S. A.; Cawthorne, S., Particle engineering techniques for inhaled biopharmaceuticals. *Adv Drug Deliv Rev* 2006, 58 (9-10), 1009-29.
18. Hinds, W. C., *Aerosol technology : properties, behavior, and measurement of airborne particles*. 2nd ed.; Wiley: New York, 1999; p xx, 483 p.
19. Niebergall, P. J.; Milosovich, G.; Goyan, J. E., Dissolution rate studies II. Dissolution of particles under conditions of rapid agitation. *Journal of Pharmaceutical Sciences* 1963, 52 (3), 236-241.

## CHAPTER 6

### Device Invention

#### 6.1 Introduction

In vitro assay systems for quantitative analysis of drug dissolution and drug absorption are important scientific tools for developing of solid oral drug formulations. Drug formulations involves controlling particle size, shape, porosity and excipients composition and fractional drug mass to achieve desirable temporal release characteristics of the active drug product. <sup>1</sup>All these component characteristics interact with the physicochemical properties of the active drug ingredient to determine the rate at which the active drug ingredient is released into the surrounding environment. Because drug molecules are only able to exert their biological effects on their cellular receptors and target molecules when they are present in solution, the ability to control the release of soluble drug molecules from a particle is an important field of study in pharmaceutical engineering, with its own scientific journals and society. <sup>2, 3</sup> In the case of oral drug formulations, controlled release has been a fundamental advance for tailoring the rate at which drugs are absorbed from the gut into the body, and

therefore controlling the systemic pharmacokinetic and pharmacodynamic of the active drug ingredient.

To develop controlled release formulations to precise specifications, special apparatus have been invented to allow measurement of the rate of drug dissolution from a tablet, pill, capsule or powder into a physiologically-relevant media mimicking the contents of the stomach or intestine. Such apparatus enable precise measurements of drug dissolution in a physiologically relevant manner. Such apparatus are now widely accepted as surrogates for actual human experiments,<sup>4, 5</sup> hence regulatory standards can be implemented to ensure that a drug product on the market are able to dissolve in the stomach to stipulated specifications, so that the dissolved drug can be absorbed by the body to yield the expected concentrations and pharmacokinetics profiles in the blood. With in vitro dissolution apparatus in the laboratory, in vitro assays for assessing the performance of solid drug formulation have become a routine and essential component of quality assurance of oral pharmaceutical products. In vitro dissolution measurements are performed routinely, not only as part of the formulation development and testing, but also after drug products are manufactured and on the shelf, to insure that drug products are stable after manufacture and storage, and for many general quality control and assurance purposes. In terms of regulating drug safety and efficacy, with appropriate in vitro dissolution apparatus and standards, expensive clinical trials can be avoided because in vitro dissolution apparatus can allow excellent assessment of drug product quality, effectively capturing the actual dissolution behavior of drugs



in the human body (measuring the latter is often very cumbersome, with physiological measurements of drug concentrations in the blood being less reliable than the in vitro measurements of dissolved drug) . In the case of generic medications, in vitro assays for analyzing drug dissolution and absorption have been a crucial advance in terms of offering an inexpensive way for establishing that generic drug products are “bioequivalent” to the innovator products originally tested and approved in clinical trials. The adoption of an industry-wide standards related to the performance of in vitro dissolution apparatus has been a key advance facilitating a multibillion dollar market of generic drugs, as well as the tight FDA oversight and regulatory standards that presently governs the performance of oral generic drugs. <sup>6,7</sup>

For measuring dissolution of oral drug formulations in vitro, a number of instruments have been patented and are sold commercially.<sup>4-6</sup> These apparatus are all comprised of a large container in which the pill, tablet or capsule is placed, surrounded by a large volume of water or aqueous buffer, a stirring mechanism, and a sampling mechanism for determining the amount of drug that is dissolved. In the case of oral drugs, all existing in vitro assay systems for quantitative analysis oral dosage forms are designed to measure drug particle dissolution separately from drug permeability properties. This is because solid forms of oral drugs dissolve in the lumen of the stomach or the intestine before they are absorbed into the body across the mucosal lining of the intestines. Therefore, for oral dosage forms, dissolution and absorption are physiologically separable events. Thus dissolution of the drug tablet, pill or capsule can be assayed

separately the absorption of the dissolved drug. There are many examples of startup companies that currently focus on oral drug dissolution and absorption analysis systems.

The lack of a precise, quantitative in vitro dissolution apparatus to analyze the simultaneous dissolution and absorption of inhaled drug particles under physiologically relevant conditions makes the formulation of inhaled drugs a very expensive, risky, empirical, error-prone process. Ultimately, finding the ideal combination of drug solubility, permeability, excipients combinations and particle size properties for inhaled drugs must be done with expensive and cumbersome clinical trials because even animal models that are used to study inhaled drug absorption are not able to mimic the way humans inhale drugs, and more importantly, because precise quantitative delivery and dosing of particle drug formulations into the lungs of animals is extremely difficult to achieve. Not surprisingly, establishment of bioequivalence of inhaled formulations is so challenging that it has precluded development of generic versions of inhaled medications currently on the market.<sup>8</sup> Characterization of the dissolution and absorption kinetics of inhaled drug particles under conditions in which both dissolution and absorption occur simultaneously would be extremely valuable for establishing bioequivalence for inhaled generics, a relatively unexplored market whose market potential value is around 20 billion USD. To the extent that the ability to measure dissolution coupled to absorption in vitro could be used to predict the dissolution and absorption of drugs in vivo, an in vitro system to

measure the dissolution properties of inhaled drug formulations would be a major scientific advance of major commercial potential.<sup>8</sup>

The invention herein pertains to the field of pharmaceutical sciences, nanoparticle engineering, formulation development, drug dissolution and absorption. It is an apparatus for measuring the dissolution rates of a micrometer to nanometer-sized, solid drug particle formulation, when dissolution is simultaneously coupled to transport of the dissolved drug molecules across an adjacent biological surface. More generally, the scope of the present invention may extend to any device for measuring the dissolution of micrometer to nanometer-size particles simultaneously coupled to transport of the dissolved molecules across an adjacent surface or interface at the boundary of a confined dissolution volume. This device is relevant to any nanotechnology particle-based drug delivery device aimed at achieving controlled drug release in close proximity to a cell surface, mucosal surface or other body surface, a specific embodiment of this invention is a device for mimicking the dissolution of inhaled solid drug particles within the very thin layer of liquid lining the surface of airway epithelial cells(Figure 6.1. and 6.2.). Applications of this invention include facilitating the development of inhaled drug formulation with optimal dissolution and absorption characteristics, analyzing the bioequivalence properties between generic inhaled drug products and innovator drug products currently on the market, and discovering engineering principles for the rational design of controlled release systems for inhaled drug formulations to be used for treating local lung (as well as systemic) disease.

## 6.2 Description of the Device

Figure 6.1. depicts conceptually the arrangement of the apparatus. The apparatus is comprised of two adjoining chambers separated by a semipermeable membrane or diffusion boundary interface: a donor chamber (dissolution chamber) and receiver chamber (sink chamber). As depicted in the figure 6.1., the bottom surface of the donor chamber can be provided by a solid, flat chemically inert, unreactive surface that does not bind or interact with the drug molecules. A small, precise volume of drug particle suspension dissolved in aqueous buffer, airway surface lining liquid (or sputum) equivalent, or other physiologically relevant dissolution medium or bodily fluid is placed on this surface. This small volume is separated by a diffusion boundary layer interface or by a semipermeable porous membrane from the receiver chamber, such that the liquid volume and particle suspended in the volume of the donor chamber remain in the donor chamber during the course of the measurements, separate from the liquid in the receiver chamber. Nevertheless, dissolved drug molecules should be able to pass from the donor chamber to the receiver chamber by crossing the bounding semipermeable membrane or diffusion boundary layer interface, simultaneously with drug particle dissolution taking place in donor compartment.

An important aspect of this invention is that the height of the donor chamber is kept constant, such that the donor volume chamber effectively forms a “slab” (a plane of a constant thickness), and that the bottom surface of the donor compartment forms a plane parallel to the plane of the membrane or diffusion layer interphase separating it from the receiver compartment . The

volume of the donor compartment can therefore be calculated by multiplying the total surface area of the diffusion layer interface or membrane separating the receiver compartment from the donor compartment times the thickness (height) of the donor chamber. In the case of the lung, the aqueous surface layer lining the epithelial cells are generally less than 100 microns in thickness, and while it varies in different locations in the airways, it is generally in the order of 10 micron to 1 micron in thickness, from the bronchi to the alveoli. To mimic the thickness and volume of the aqueous surface layer lining of the airways, a micrometer sized, physical spacer element can be introduced into the donor chamber to keep the bottom surface of the donor chamber at a certain distance from the diffusion layer interface or membrane separating it from the receiver compartment. This physical spacer can be monodisperse, solid, rigid, polystyrene, latex, silica or other spherical particles in the donor chamber, or it can be a different physical spacer element that is micromachined, glued or otherwise fixed to the bottom surface of the apparatus. To prevent the liquid in the donor compartment from evaporating or oozing out the sides of the donor compartment a chemical sealant is used to prevent any donor liquid from escaping across the sides of the donor chamber.

In terms of the actual liquid in the donor compartment, different specific embodiments include physiological aqueous buffer as well as actual bodily fluids. Physiological aqueous buffer can include such commonly used buffers as Ringer's saline, Hanks Balanced Salt Solution, or phosphate buffered saline. To increase the physiological relevance, the physiological aqueous buffer can

incorporate natural or artificial additives, such as surfactants, lipids, amino acids, carbohydrate, nucleic acids and proteins. To further increase the physiological relevance the physiological aqueous buffer can include additives that alter the viscosity and diffusion coefficient of the dissolving drug, including glycerol, polyethylene glycol, mucus proteins, or other drug binding hydrophobic components (like detergent micelles). The liquid in the donor compartment can also be actual airway surface lining liquid or mucus secretion obtained from sputum of human volunteers, or from patients in a clinical trial. A different embodiment may include combinations of natural mucus with artificial physiological buffers. A different embodiment may include any of the aforementioned embodiments with variations in ion content, pH, or other components to study the effect of any one of said components on formulation dissolution and absorption performance.

Another important component of this invention is a diffusion layer interface separating the donor compartment from the receiver compartment. In its simplest embodiment, the diffusion layer interface can be formed by a semipermeable membrane: a very thin, porous, high permeability, chemically inert film made from polyester, polycarbonate, or other artificial or natural polymeric material. The membrane can be seeded with cells to better mimic the permeability properties of the cells that mediate drug absorption in the body. The membrane can actually be comprised by an alveolar epithelial cell or some other cell monolayer that is grown and differentiated onto a porous, polyester, polycarbonate, collagenous or other porous membrane support, so as to provide

an artificial membrane-supported cell monolayer that mimics the physiological properties of the cells that form the lining of the airways (or other biological surface on which drug dissolution is happening and across which absorption is taking place). A specific embodiment for the kind of membrane separating donor and receiver compartments would be the hydrophobic membrane commonly used in parallel artificial membrane permeability (PAMPA) assays for measuring drug permeability properties. The hydrophobic membrane used for PAMPA assays captures the physiochemical properties of the phospholipid bilayer of cells, and therefore can serve as a model for assessing the passive permeability of drugs across cellular membranes. Alternatively, cells can be grown as monolayers on polycarbonate or polyester membranes packed with pores, and these membrane-supported cell monolayer systems can provide a suitable biological interface across which freely soluble drug is transported. Yet in a different embodiment, the membrane can be a simple stagnant diffusion boundary layer interface separating an aqueous fluid in the donor compartment from a hydrophobic liquid in the receiver compartment. For this purpose, the receiver compartment can be filled with a liquid that forms a separate phase and therefore does not mix with the aqueous liquid in the donor compartment. Examples of such hydrophobic liquids include octanol, hexane, etc.

Another important component of the present invention is the receiver compartment. This compartment can be a large volume so as to keep the free drug concentration at the receiver drug concentration at a relatively low value compared to the drug concentration in the donor compartment. Or it can be as

small volume that is under a continuous flow. Most importantly, the receiver compartment should possess a mechanism so as to keep the drug concentration in the receiver compartment low and homogeneous. Such a mechanism can be provided by a stirring paddle in a closed system, by a solvent circulation mechanism in a closed system, or by an open solvent perfusion mechanism as would need to be the case if the receiver chamber is made very small, as in a microfluidic device.

Indeed, with an open perfusion system, the actual volume of the receiver compartment can be small, and the system could be miniaturized as in a microfluidic device. The liquid in the receiver compartment can be octanol, dodecane, or some other hydrophobic liquid, that phase separates from the liquid in the donor compartment. Alternatively, the receiver compartment can be filled with an aqueous, physiological buffer to mimic the blood or the interstitial fluid, the plasma, or the intracellular environment. Such a liquid can be kept separate from the liquid in the donor chamber if the membrane that separates the donor compartment from the receiver compartment is a water impermeant membrane, as in a PAMPA assay membrane or a membrane supported cell monolayer.

An optional component of this invention is incorporation of a measurement system to monitor changes in free drug concentration or changes in particle size occurring upon drug dissolution. In terms of measuring the dissolution of the particles, two general methods can be envisioned: 1) bulk chemical analysis methods for measuring the concentration of freely soluble drug



in the receiver compartment; 2) microscopic particle size analysis methods for measuring the change in particle size in the donor chamber. For bulk chemical analysis, a given volume of receiver compartment liquid can be removed at various time points during the course of an experiment. The mass of drug in these samples can be determined using absorbance, fluorescence, chromatography (HPLC), mass spectrometry, LC/MS, or some other standard chemical analysis method. Based on the volume of the receiver liquid removed, the total mass of drug in the receiver compartment can be calculated by multiplying the concentration of drug in the sample analyzed times the total volume of liquid in the receiver compartment. For microscopic analysis, the dissolving drug particles in the device could be directly monitored with a microscopic imaging system. Optical methods for microscopic analysis include but are not limited to fluorescence, absorbance, phase contrast, dark field, Nomarski, Raman confocal, brightfield, polarization, light scattering, or any other suitable optical microscopic method that can be used to reveal the size of the particle. Alternative non imaging methods to monitor drug particle size changes including dynamic light scattering in the case of particles that move by Brownian motion. As long as drug particles can be directly imaged or otherwise detected and their size monitored, and if the density of drug in the particle is known, the changes in drug particle radius can be translated to the amount of drug mass dissolved.

By using any one of a variety of mathematical algorithms to fit the time-course dissolution data obtained from chemical analysis and imaging systems

together with the initial conditions of the system to the ODEs and other known or measured parameter values (such as the interphase membrane permeability), one can estimate the parameter values of the variables governing the behavior of the system.

### **6.3 Discussions**

The present invention is a device for measuring the dissolution properties of particulate drug formulations, under conditions in which dissolution is simultaneously coupled to drug absorption across a bounding membrane or diffusion layer interface. The invention mimics the coupled dissolution-absorption process as it occurs in physiological conditions on the surface of airway epithelial cells, and therefore constitutes an in vitro dissolution system that mimics the in vivo dissolution properties of inhaled drug particle formulations. One envisioned commercial applications of this invention is to facilitate the engineering an inhaled drug formulation with optimal controlled release characteristics for achieving a desired pharmacokinetic or pharmacodynamic profile in the lung. Another envisioned commercialization application of this invention lies in providing a means for analyzing the performance of a formulation of inhaled generic drugs in terms of how dissolution and absorption behavior compares to that of the innovator drugs. Such an invention could be used to establish precise quantitative standards for assuring inhaled drug particles of a generic drug product is bioequivalent with an inhaled drug product that has already been approved by the FDA and on the market.

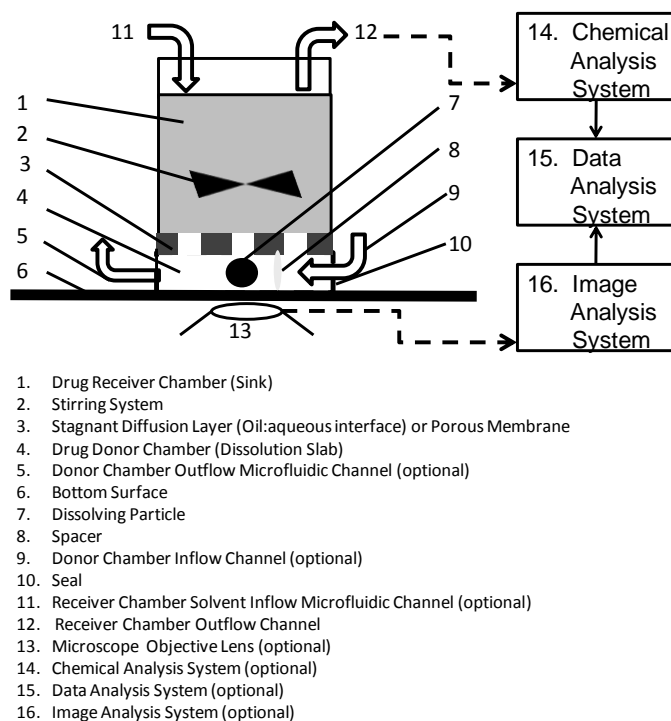


Figure 6.1. Schematic diagram of the device. The receiver chamber **1** encloses a volume of liquid and serves as a sink for dissolved drug molecules. The walls of the receiver chamber are made of some chemically inert, unreactive, solid material. A stirring system **2** in the receiver chamber is used to keep the contents of this compartment well mixed and in continuous agitation. A membrane or boundary layer interphase **3** forms the bottom of the receiver chamber. This membrane can be made from different materials, including hydrophobic, hydrophilic membrane, or porous membrane with pores filled with oil phase, or a biocompatible membrane on which cells can form a monolayer. The drug donor chamber **4** is a confined plane of constant height, bounded above by the semipermeable membrane interphase. For experiments, the volume of the donor chamber is held constant, but an outflow channel **5** can be used to withdraw air or liquid. The bottom surface of the donor chamber **6** is parallel to the membrane that separates it from the receiver chamber. Drug particles whose dissolution properties **7** need to be studied sit in the donor chamber. A spacer **8** can be included in the donor chamber, to maintain the separation between the membrane interphase and the bottom surface at a constant height. An inflow channel into the donor chamber **9** can serve to add particles or exchange liquid contents of the donor chamber. A seal **10** is used to keep the liquid in the donor chamber from oozing out the sides, and to prevent it from evaporating. To keep the liquid in the receiver chamber at low concentration, an inflow **11** and an outflow **12** channels can be applied at the receiver chamber to keep the concentration low and constant and facilitate the stirring. A microscopic imaging system **13** can be used to visualize changes in particle size and using Raman

imaging, changes in drug concentration in the donor compartment. Drug concentration in the receiver compartment can be analyzed with a chemical analysis system **14**. **A data analysis system 15** can be used to integrate information from chemical analysis and image analysis, with computational models of drug particle dissolution, to identify key parameters affecting dissolution behavior.

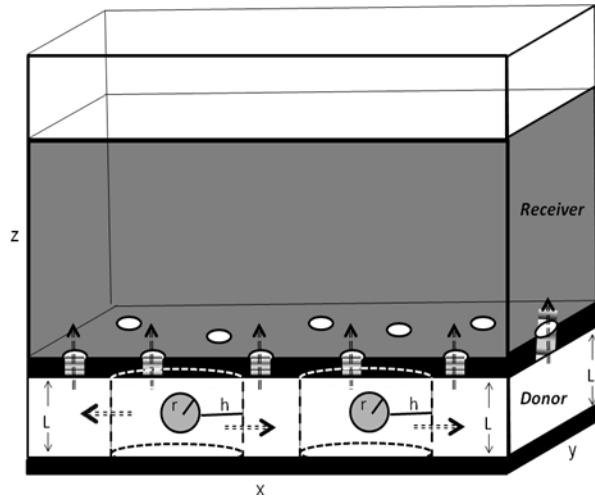


Figure 6.2. Schematic diagram for mathematical simultaneous modeling of dissolution and absorption. In the device donor chamber, dissolution of drug particles (of radius  $r$ ) happens in a non-stirred, aqueous slab volume, such that diffusion of freely soluble drug molecules into the aqueous medium happens along a horizontal plane  $x, y$  (indicated by horizontal broken arrows). According to the Nernst-Brunner equation, a diffusion boundary layer of thickness ( $h$ ) is present around each particle, with the diffusion layer forming a cylinder around each particle. Drug concentration at the surface of the particle corresponds to the solubility limit of the solid particle ( $C_s$ ). Dissolution of drug molecules from the particles into the donor compartment is coupled to transport of freely soluble drug from donor compartment into a well stirred, receiver compartment. This transport occurs perpendicularly to the dissolution plane in the  $z$  direction, across a physical membrane surface or receiver-donor interphase layer (indicated by upward pointing broken arrows), which can be created if the liquids in receiver and donor compartments form separate phases

## 6.4 References

1. Dolovich, M. B.; Dhand, R., Aerosol drug delivery: developments in device design and clinical use. *The Lancet* 377 (9770), 1032-1045.
2. Rathbone, M. J.; ebrary Inc., Modified-release drug delivery technology Volume 2. 2nd ed.; Informa Healthcare: New York, 2008.
3. Rathbone, M. J., *Modified-release drug delivery technology*. 2nd ed.; Informa Healthcare: New York, 2008.
4. Gray, V.; Kelly, G.; Xia, M.; Butler, C.; Thomas, S.; Mayock, S., The Science of USP 1 and 2 Dissolution: Present Challenges and Future Relevance. *Pharmaceutical Research* 2009, 26 (6), 1289-1302.
5. Azarmi, S.; Roa, W.; Lenberg, R., Current perspectives in dissolution testing of conventional and novel dosage forms. *International Journal of Pharmaceutics* 2007, 328 (1), 12-21.
6. Cohen, J. L.; Hubert, B. B.; Leeson, L. J.; Rhodes, C. T.; Robinson, J. R.; Roseman, T. J.; Shefter, E., The Development of USP Dissolution and Drug Release Standards. *Pharmaceutical Research* 1990, 7 (10), 983-987.
7. Qiu, Y.; Chen, Y.; Zhang, G. G. Z.; ScienceDirect (Online service), Developing solid oral dosage forms pharmaceutical theory and practice. 1st ed.; Academic: Amsterdam ; Boston ; London, 2009.
8. Lee, S. L.; Adams, W. P.; Li, B. V.; Conner, D. P.; Chowdhury, B. A.; Yu, L. X., In vitro considerations to support bioequivalence of locally acting drugs in dry powder inhalers for lung diseases. *AAPS J* 2009, 11 (3), 414-23.
9. Cohen, M. D.; Zelikoff, J. T.; Schlesinger, R. B., *Pulmonary Immunotoxicology*. Springer: 2000.
10. Parent, R. A., *Treatise on Pulmonary Toxicology: Comparative biology of the normal lung*. CRC Press: Boca Raton, 1992.
11. Ross, M. H.; Pawlina, W., *Histology: A Text and Atlas: With Correlated Cell and Molecular Biology*. 5th ed.; Lippincott Williams & Wilkins: 2006.
12. Staub, N. C., *Basic Respiratory Physiology*. Churchill Livingstone Inc: New York, 1991.
13. Weibel, E. R., *Morphometry of the Human Lung*. Springer: Heidelberg, 1963.

## CHAPTER 7

### Conclusions

#### 7.1 Summary

The primary goal of this thesis is to elucidate the relationship between the properties of inhaled drugs (e.g., formulation, device, physicochemical properties) and systemic and local PK of inhaled drugs at different regions of lung by building and utilizing a mechanistic cell-based lung model. We designed *in vivo* experiments based on the hypothesis generated from the simulations. This thesis will be a valuable guide for the rational design of inhaled drugs to optimize drug properties to achieve desirable local and systemic PK profiles.

A modular, multiscale, cell-based PK model of the lung was developed to simulate the time-course concentration of inhaled and systemically-injected compounds. The model captured the transport and distribution of drug in airways and alveoli, from the subcellular level to the whole organ level. Mathematically Fick's law and the Nernst-Planck equation were used to capture the mass transport of lipophilic drug molecules across cellular membranes. Henderson-Hasselbalch equation was used to capture the different ionization states of a molecule at a given pH, the fundamental transport properties of monobasic

compounds across a series of cellular compartments were described by sets of coupled ordinary differential equations (ODEs). The physicochemical properties of the compounds (i.e.,  $pK_a$  and  $\log P$ ) were used as input parameters. To model the structure and function of the lung, anatomical and physiological input parameters were incorporated, including the extracellular and intracellular pH values, lipid composition, cell thickness, membrane areas, cell volume, and membrane potential of the various different cell types that form the airways and alveoli. Values of input parameters were varied to capture the uncertainty associated with normal and pathological conditions.

The predictions given by model about the absorption profiles of some small monobasic molecules in the lung were found comparable with the observed data reported in literature. We further differentiated the PK between airways and alveoli, and formulated a hypothesis that the monobasic compounds with higher  $pK_a$  delivered via IT injection can accumulate more in the airways than in alveoli, suggesting that the organic cations will selectively target the airways. The underlying mechanism is that the cations may be retained by smooth muscle that can only be found in airways. However, simulations demonstrated the probes delivered through the IV showed only a marginal difference in distribution between airways and alveoli. This hypothesis was confirmed with microscopic images acquired from *in vivo* experiments in mice by delivering a mixture of two fluorescent probes through the IT and IV injection. In addition, the model facilitated the discovery of an airways fluorescent labeling agent, MitoRed.



Lastly, to advance practical applications, a model was built as a starting point to develop a rational approach to optimize the pharmaceutical properties of inhaled drug in terms of the variability of systemic and local PK. The interaction between the dissolution and absorption in the physiological environment of lung was explicitly incorporated. In this manner, mathematical PK model can overcome limitations associated with existing preclinical models used in pulmonary drug development, providing a rational basis for medicinal chemists to guide the design of inhaled medications for both systemic and local disease. The simulations result suggests that the compounds with medium permeability possess less variability of systemic and local PK caused by formulation and device. This serves as a theoretical guidance for medicinal chemists at very early stage of lead optimization. The physicochemical properties of drug candidates can be tailored to reduce the variability of PK profiles at later stage of drug development, when the formulation and device begin to impact the performance of a compound.

## **7.2 Future Directions**

The lung PK model and dissolution-absorption model are compartmental ODE-based models. The current models were limited to monobasic compounds and only include the passive diffusion of soluble drugs in lungs. In the future, it will be possible to expand the scope of current model to incorporate other mechanisms. In general we can further elaborate our current models toward the following directions: (1) Adapt lung models for other species, such as mice, human, etc. The parameter values may be obtained from literature or derived

based on inter-species allometry. (2) Link the current lung PK model with PD models to predict the pharmacological effect of specific compound. Empirical PD models<sup>1-3</sup> or complex signal transduction models<sup>4-6</sup> can be utilized to link the concentration at specific target site to its action, such as the virus in the surface lining liquid. (3) Develop and integrate a mucus clearance model<sup>7,8</sup> with current lung PK model and dissolution-absorption model to capture the transport kinetics of undissolved particles in lungs. To achieve these goals, various approaches of modeling and simulations can be adopted according to the availability of data, prior knowledge and experiment support. We'll not cover all the possible ways to achieve these goals. Instead, we would like to discuss some general guidance using system biology or 'bottom-up' approach to elaborate our model.

### **7.2.1 General Guidance for Refining and Expanding Current Models**

A useful mathematical model can represent a system in a physically and biologically realistic manner, incorporate a wide range of mechanisms, and formulate hypotheses. More importantly, it is critical to construct a robust model that can be subsequently validated with well designed experiments. The power of modern computer allowed us to construct a complex model for the dynamic systems to understand the underlying mechanism in an integrative manner.<sup>9</sup> However it is very challenging to develop an appropriate model that can simulate a system simultaneously involving a large number of components and mechanisms, for example mucus clearance, particle dissolution, absorption, and the downstream biochemical cascade.

Usually, we expect the variables and parameters in models to possess physical or biochemical meanings, such as pH, lipophilicity, ion strength, lipid content, etc. The challenge in the development of ODE-based models is how to specify the level of detail.<sup>6</sup> ODEs-based models can incorporate a large number of ODEs without much numerical difficulty due to the high efficiency and accuracy of various ODE solvers. However, a complex model can easily lead to the numerical instability and large uncertainty in predictions. On the other hand, if a simple model is chosen to proceed, the chance of missing the key mechanism will be high. Thus, sufficient prior information and exploratory data analysis are required to determine which components or mechanism should be included or excluded in the model and how detailed they should be if included. From a pragmatic point of view, the thumb of rule is that the better model is the simpler one in terms of components and parameters, and can generate an acceptable goodness of fit to the observed data. In other words, we should manage to achieve a balance between the complexity and prediction errors of the model.

### **7.2.2 Modeling lungs of other species**

One of the advantages of the cell-based lung model is that it can be scaled up to simulate the pharmacokinetics in other species. For clinical application of the model, the human parameters in the lung model can be obtained from literature or derived based on allometry.<sup>10-14</sup> Model the human lung will offer a quantitative tool for the rational design of inhaled drugs, and aid the prioritization of experiments. The parameter values for human lung were listed in the table 7.1. and table 7.2. This will enable us to simulate the transport profiles

of small molecules in human lung. For example, the apparent alveoli permeability can be calculated for various combinations of physiochemical properties of small molecules (Figure 7.1.). The absorption half life was obtained from simulation results, from which the apparent permeability was calculated using eq 1 ( $h$  is the thickness of surface lining liquid,  $AbsT50$  is the absorption half life). More importantly, it can be linked to the dissolution model as a comprehensive computational tool for design of inhaled medications.

$$P_{eff} = \frac{\ln 2}{AbsT50} \times h \quad (1)$$

### **7.2.3 Transforming the drug development “pipeline” into a drug development “engine”**

In a traditional paradigm of drug discovery and development, knowledge and information at each stage of drug development was mainly used to filter out candidate compounds in an empirical manner, especially during clinical trials. In addition, drug candidates progressed through each stage in a “pipeline” manner without incorporating feedback from the later stages of drug development. Up until today, this drug development “pipeline” has been inextricably linked to the high attrition rates that are commonplace in the pharmaceutical industry. As an alternative paradigm, computational modeling and simulation can serve as the basis for a drug development “engine” that can be integrated into the different stages of inhaled drug development, from the early stage of lead optimization to design of clinical trials, thereby facilitating the “learn and confirm” cycle<sup>15</sup>. Within a drug development “engine”, each stage of the development process will

synergize with each other, with models and experiments becoming highly interconnected components from beginning to the end (Figure. 7.2.). QSAR, 1CellPK, cell-based lung model, and dissolution-absorption model can provide an abstract and quantitative framework, to relate the chemical, physicochemical, formulation, and device properties to the resulting local and systemic PK/PD properties of the final drug product. By facilitating the design of preclinical and clinical studies, we envision that computational models will increasingly play a pivotal role in the development of inhaled drug products.

Table 7.1. Geometric parameter values for human airways<sup>9-13</sup>

## Geometry Human Airways

Generation	Number of AW	Diameter(mm)	Length(mm)	Surface	Sum_Surface
1	1	20.1	100	6311.4	6311.4
2	2	15.6	43.6	2135.702	4271.4048
3	4	11.3	17.8	631.5796	2526.3184
4	8	8.27	9.65	250.5893	2004.71416
5	16	6.51	9.95	203.3919	3254.27088
6	32	5.74	10.1	182.0384	5825.22752
7	64	4.35	8.9	121.5651	7780.1664
8	128	3.73	9.62	112.6714	14421.93459
9	256	3.22	8.67	87.66064	22441.12282
10	512	2.57	6.67	53.82557	27558.68979
11	1024	1.98	5.56	34.56763	35397.25517
12	2048	1.56	4.46	21.84686	44742.37747
13	4096	1.18	3.59	13.30167	54483.63213
14	8192	0.92	2.75	7.9442	65078.8864
15	16384	0.73	2.12	4.859464	79617.45818
16	32768	0.6	1.68	3.16512	103714.6522
					total (mm2)
					479429.5109
					total (m2)
					0.479429511

Table 7.2. Histological parameter values for human airways and alveoli<sup>9-13</sup>

Compartments	Tracheobronchial Airways			Alveolar Region		
	Average thickness (μm)	Surface area (m <sup>2</sup> )	Volume (cm <sup>3</sup> )	Average thickness (μm)	Surface area (m <sup>2</sup> )	Volume (cm <sup>3</sup> )
Surface lining liquid	15	0.48	7.2	5	89	445
Macrophage	-	-	-	-	-	54.7
Epithelium	50	0.48	24	0.36	89	32.5
Interstitialium	3.5	0.48	1.68	1.634	89	145.42
Immune cells	-	-	-	-	-	-
Smooth muscle	48	0.96	23.04		-	-
Endothelium	0.4	0.1	0.04	0.474	91	42.6

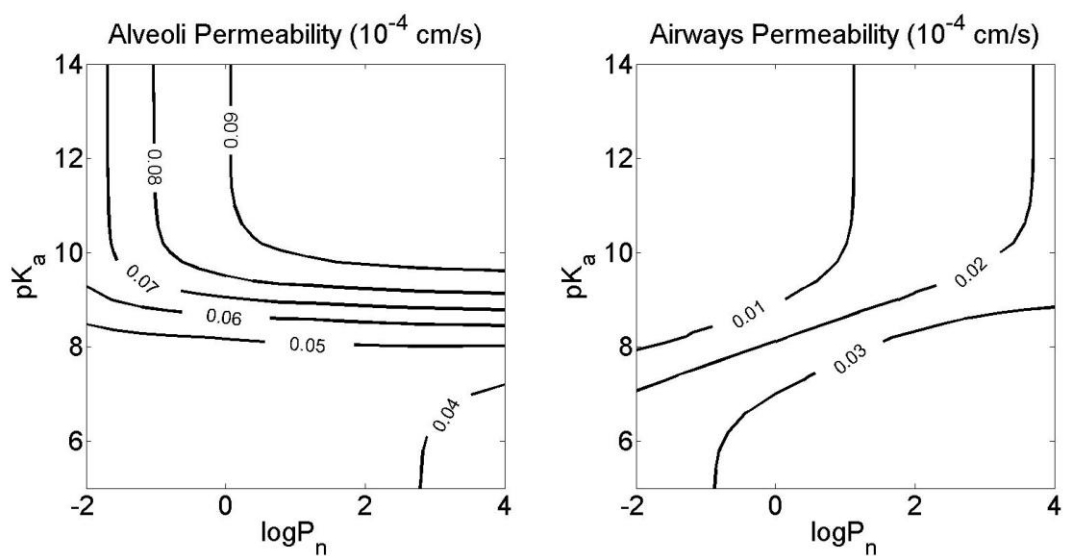


Figure 7.1. Relationship between physicochemical properties and  $P_{eff}$  of human lung



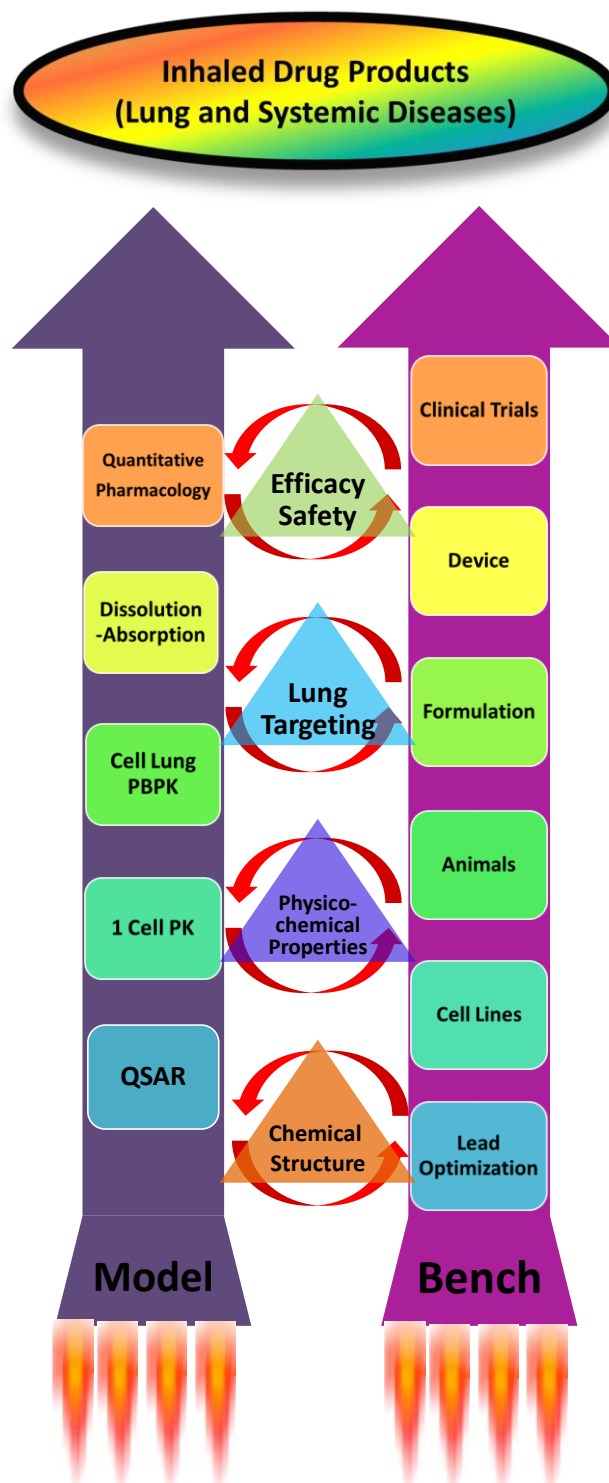


Figure 7.2. Synergistic paradigm of drug discovery and development

### 7.3 References

1. Macheras, P.; Iliadis, A.; SpringerLink (Online service), *Modeling in biopharmaceutics, pharmacokinetics, and pharmacodynamics : homogeneous and heterogeneous approaches*. Springer: New York, 2006; p xx, 442 p.
2. Kwon, Y.; NetLibrary Inc., *Handbook of essential pharmacokinetics, pharmacodynamics and drug metabolism for industrial scientists*. Kluwer Academic Publishers: New York, 2002; pp. xix, 291 p.
3. Burton, M. E., *Applied pharmacokinetics and pharmacodynamics : principles of therapeutic drug monitoring*. 4th ed.; Lippincott Williams & Wilkins: Baltimore, 2006.
4. Dada, J. O.; Mendes, P., Multi-scale modelling and simulation in systems biology. *Integrative Biology* 3 (2), 86-96.
5. Kitano, H., Computational systems biology. *Nature* **2002**, 420 (6912), 206-210.
6. Aldridge, B. B.; Burke, J. M.; Lauffenburger, D. A.; Sorger, P. K., Physicochemical modelling of cell signalling pathways. *Nat Cell Biol* **2006**, 8 (11), 1195-1203.
7. King, M., Experimental models for studying mucociliary clearance. *European Respiratory Journal* **1998**, 11 (1), 222-228.
8. Sturm, R.; Hofmann, W.; Scheuch, G.; Sommerer, K.; Camner, P.; Svartengren, M., Particle Clearance in Human Bronchial Airways: Comparison of Stochastic Model Predictions with Experimental Data. *Annals of Occupational Hygiene* **2002**, 46 (suppl 1), 329-333.
9. Germain, R. N.; Meier-Schellersheim, M.; Nita-Lazar, A.; Fraser, I. D. C., Systems Biology in Immunology: A Computational Modeling Perspective\*. *Annual Review of Immunology* 29 (1), 527-585.
10. Cohen, M. D.; Zelikoff, J. T.; Schlesinger, R. B., *Pulmonary Immunotoxicology*. Springer: 2000.
11. Parent, R. A., *Treatise on Pulmonary Toxicology: Comparative biology of the normal lung*. CRC Press: Boca Raton, 1992.
12. Ross, M. H.; Pawlina, W., *Histology: A Text and Atlas: With Correlated Cell and Molecular Biology*. 5th ed.; Lippincott Williams & Wilkins: 2006.
13. Staub, N. C., *Basic Respiratory Physiology*. Churchill Livingstone Inc: New York, 1991.
14. Weibel, E. R., *Morphometry of the Human Lung*. Springer: Heidelberg, 1963.
15. Sheiner, L. B., Learning versus confirming in clinical drug development. *Clin Pharmacol Ther* **1997**, 61 (3), 275-291.

## **APPENDICES**

## Appendix A

### Equations and Parameters Analysis in Chapter 2

#### 1. Equations to describe the transcellular transport process in lung

##### 1.1 Differential equation set 1:

$$\begin{aligned}\frac{dM_{aEp}}{dt} &= -A_{aEp}J_{aEp,cEp} - A_{imEp}J_{aEp,imEp} + \text{efflux}_{cEp,aEp} \\ \frac{dM_{imEp}}{dt} &= A_{imEp}J_{aEp,imEp} \\ \frac{dM_{cEp}}{dt} &= A_{aEp}J_{aEp,cEp} - A_{bEp}J_{bEp,int} - \text{efflux}_{cEp,aEp} \\ \frac{dM_{int}}{dt} &= A_{bEp}J_{bEp,int} - A_{sm}J_{int,sm} - A_{imInt}J_{int,imInt} - A_{bEd}J_{int,cEd} \\ \frac{dM_{sm}}{dt} &= A_{sm}J_{int,sm} \\ \frac{dM_{imInt}}{dt} &= A_{imInt}J_{int,imInt} \\ \frac{dM_{cEd}}{dt} &= A_{bEd}J_{int,cEd} - A_{aEd}J_{cEd,p} \\ \frac{dM_p}{dt} &= A_{aEd}J_{cEd,p} \\ \text{efflux} &= \frac{V_{\max} C_{cEp}}{K_m + C_{cEp}}\end{aligned}$$

## 1.2 Differential equation set 2:

$$\begin{aligned}
\frac{dC_{aEp}}{dt} &= -\frac{A_{aEp}}{V_{aEp}} [P_n (f_{aEpN} C_{aEp} - f_{cEpN} C_{cEp}) + P_d \frac{N_{aEp}}{e^{N_{aEp}} - 1} (f_{aEpD} C_{aEp} - f_{cEpD} C_{cEp} e^{N_{aEp}})] \\
&\quad - \frac{A_{imEp}}{V_{aEp}} [P_n (f_{aEpN} C_{aEp} - f_{imEpN} C_{imEp}) + P_d \frac{N_{imEp}}{e^{N_{imEp}} - 1} (f_{aEpD} C_{aEp} - f_{imEpD} C_{imEp} e^{N_{imEp}})] \\
&\quad + \frac{efflux_{cEp,aEp}}{V_{aEp}} \\
\frac{dC_{imEp}}{dt} &= \frac{A_{imEp}}{V_{imEp}} [P_n (f_{aEpN} C_{aEp} - f_{imEpN} C_{imEp}) + P_d \frac{N_{imEp}}{e^{N_{imEp}} - 1} (f_{aEpD} C_{aEp} - f_{imEpD} C_{imEp} e^{N_{imEp}})] \\
\frac{dC_{cEp}}{dt} &= \frac{A_{aEp}}{V_{cEp}} [P_n (f_{aEpN} C_{aEp} - f_{cEpN} C_{cEp}) + P_d \frac{N_{aEp}}{e^{N_{aEp}} - 1} (f_{aEpD} C_{aEp} - f_{cEpD} C_{cEp} e^{N_{aEp}})] \\
&\quad - \frac{A_{bEp}}{V_{cEp}} [P_n (f_{cEpN} C_{cEp} - f_{intN} C_{int}) + P_d \frac{N_{bEp}}{e^{N_{bEp}} - 1} (f_{cEpD} C_{cEp} - f_{intD} C_{cEp} e^{N_{bEp}})] - \frac{efflux_{cEp,aEp}}{V_{cEp}} \\
\frac{dC_{int}}{dt} &= \frac{A_{bEp}}{V_{int}} [P_n (f_{cEpN} C_{cEp} - f_{intN} C_{int}) + P_d \frac{N_{bEp}}{e^{N_{bEp}} - 1} (f_{cEpD} C_{cEp} - f_{intD} C_{cEp} e^{N_{bEp}})] \\
&\quad - \frac{A_{sm}}{V_{int}} [P_n (f_{intN} C_{int} - f_{smN} C_{sm}) + P_d \frac{N_{sm}}{e^{N_{sm}} - 1} (f_{intD} C_{int} - f_{smD} C_{sm} e^{N_{sm}})] \\
&\quad - \frac{A_{imInt}}{V_{int}} [P_n (f_{intN} C_{int} - f_{imIntN} C_{imInt}) + P_d \frac{N_{imInt}}{e^{N_{imInt}} - 1} (f_{intD} C_{int} - f_{imIntD} C_{imInt} e^{N_{imInt}})] \\
&\quad - \frac{A_{bEd}}{V_{int}} [P_n (f_{intN} C_{int} - f_{cEdN} C_{cEd}) + P_d \frac{N_{bEd}}{e^{N_{bEd}} - 1} (f_{intD} C_{int} - f_{cEdD} C_{cEd} e^{N_{bEd}})] \\
\frac{dC_{sm}}{dt} &= \frac{A_{sm}}{V_{sm}} [P_n (f_{intN} C_{int} - f_{smN} C_{sm}) + P_d \frac{N_{sm}}{e^{N_{sm}} - 1} (f_{intD} C_{int} - f_{smD} C_{sm} e^{N_{sm}})] \\
\frac{dC_{imInt}}{dt} &= \frac{A_{imInt}}{V_{imInt}} [P_n (f_{intN} C_{int} - f_{imIntN} C_{imInt}) + P_d \frac{N_{imInt}}{e^{N_{imInt}} - 1} (f_{intD} C_{int} - f_{imIntD} C_{imInt} e^{N_{imInt}})] \\
\frac{dC_{cEd}}{dt} &= \frac{A_{bEd}}{V_{cEd}} [P_n (f_{intN} C_{int} - f_{cEdN} C_{cEd}) + P_d \frac{N_{bEd}}{e^{N_{bEd}} - 1} (f_{intD} C_{int} - f_{cEdD} C_{cEd} e^{N_{bEd}})] \\
&\quad - \frac{A_{aEd}}{V_{cEd}} [P_n (f_{cEdN} C_{cEd} - f_{pN} C_p) + P_d \frac{N_{aEd}}{e^{N_{aEd}} - 1} (f_{cEdD} C_{cEd} - f_{pD} C_p e^{N_{aEd}})] \\
\frac{dC_p}{dt} &= \frac{A_{aEd}}{V_p} [P_n (f_{cEdN} C_{cEd} - f_{pN} C_p) + P_d \frac{N_{aEd}}{e^{N_{aEd}} - 1} (f_{cEdD} C_{cEd} - f_{pD} C_p e^{N_{aEd}})]
\end{aligned}$$

## 2. The estimation of geometric parameters for airway epithelium and smooth muscle

**Table. I.** The estimation of geometric parameters of epithelium and smooth muscle based on Yeh Model

Generation	Number of Airways	Diameter (mm)	Length (mm)	Thickness of endothelium ( $\mu\text{m}$ )	Thickness of smooth muscle ( $\mu\text{m}$ )	Basement membrane surface area ( $\text{cm}^2$ )	Epithelium Volume( $\text{cm}^3$ )	Smooth muscle volume( $\text{cm}^3$ )
1	1	3.4	26.8	24	19.3	2.86	0.0069	0.0055
2	2	2.9	7.15	23	18.3	1.30	0.0030	0.0024
3	3	2.63	4	22	17.3	0.99	0.0022	0.0017
4	5	2.03	1.76	21	16.3	0.56	0.0012	0.00091
5	8	1.63	2.08	20	15.3	0.85	0.0017	0.0013
6	14	1.34	1.17	19	14.3	0.69	0.0013	0.00099
7	23	1.23	1.14	18	13.3	1.01	0.0018	0.0013
8	38	1.12	1.3	17	12.3	1.74	0.0029	0.0022
9	65	0.95	0.99	16	11.3	1.92	0.0031	0.0022
10	109	0.87	0.91	15	10.3	2.71	0.0041	0.0028
11	184	0.78	0.96	14	9.3	4.33	0.0061	0.0041
12	309	0.7	0.73	13	8.3	4.96	0.0064	0.0041
13	521	0.58	0.75	12	7.3	7.12	0.0085	0.0052
14	877	0.49	0.6	11	6.3	8.10	0.0089	0.0051
15	1477	0.36	0.55	10	5.3	9.18	0.0092	0.0049
16	2487	0.2	0.35	9	4.3	5.47	0.0049	0.0024
						<b>Total</b>	<b>0.072</b>	<b>0.047</b>

### 3. Parameters used and sensitivity analysis of all parameters

**Table. II.** Constant Parameters in the Model

Symbol	Value	Unit	description
T	310.15	K	Rat body temperature
R	8.314	J / mol / K	Universal gas constant
F	96485.3415	sA / mol	Faraday constant

#### 3.1 Parameters used and parameter sensitivity analysis of the model

Methods: Each parameter in the model (airway and alveolar region) was randomly sampled 1000 times from a uniform distributed variable within certain range of value used. The range is between 1/100 and 100 times of the default value or a realistic span based on prior knowledge. So for each parameter, the absorption half life in whole lung was calculated for each of 1000 simulations given a corresponding range. Then the statistic summary of abs  $T_{50}$  values predicted was generated for each parameter tested and listed in table III and IV. If the predicted abs  $T_{50}$  values for a parameter with certain variation have standard deviation less than 0.0001 minutes, then this parameter was regarded as having no effect, indicated as '----' in the last column of table III and table IV. To check the consistency of the model, the effect of increased values of each parameter on the abs  $T_{50}$  was examined and listed in the table III and IV.

Notation of the name of parameters:  $L$  indicates the volumetric fraction of lipids,  $\gamma$  indicates the activity coefficient,  $A$  indicates the surface area of the membrane,  $V$  indicates the volume of the corresponding compartment.  $E$  indicates the

membrane potential,  $pH$  indicates the pH values in corresponding compartment. The subscripts  $aEp$  indicates the apical side of epithelial cells,  $cEp$  indicates the cytosol of epithelial,  $imEp$  indicates the macrophage/immune cells on the surface of epithelium,  $int$  indicates the interstitium,  $imInt$  indicates the immune cells in the interstitium,  $sm$  indicates the smooth muscle,  $cEd$  indicates the cytosol of endothelium,  $p$  indicates the plasma.

**Table. III Parameter values and sensitivity analysis for airway**

Airway	Values used	unit	range in sensitivity test	Statistics of absT50 values predicted (min)				Effect of increasing value on absT50
				mean	SD	minimal	maximal	
$L_{aEp}$	0.2	-	0.02 ~ 0.5	1.35	0.2513	0.85	1.74	↑
$L_{cEp}$	0.05	-	0.005 ~ 0.5	1.45	0.1367	1.19	1.68	↑
$L_{int}$	0.05	-	0.005 ~ 0.5	1.27	0.0187	1.24	1.31	↑
$L_{imInt}$	0.05	-	0.005 ~ 0.5	1.25	0.0000	1.25	1.25	----
$L_{sm}$	0.05	-	0.005 ~ 0.5	1.63	0.3097	0.89	2.10	↑
$L_{cEd}$	0.05	-	0.005 ~ 0.5	1.26	0.0105	1.24	1.27	↑
$L_p$	0	-	0 ~ 0.2	1.25	0.0000	1.25	1.25	----
Activity coefficient	Values used	unit	range in sensitivity test	mean	SD	minimal	maximal	
$Y_{aEpN}$	1	-	0.5 ~ 1.5	1.25	0.0203	1.22	1.29	↓
$Y_{aEpD}$	1	-	0.5 ~ 1.5	1.28	0.1227	1.12	1.58	↓
$Y_{cEpN}$	1.23	-	0.5 ~ 1.5	1.25	0.0000	1.25	1.25	----
$Y_{cEpD}$	0.74	-	0.5 ~ 1.5	1.23	0.0207	1.21	1.27	↓
$Y_{intN}$	1	-	0.5 ~ 1.5	1.25	0.0000	1.25	1.25	----
$Y_{intD}$	1	-	0.5 ~ 1.5	1.24	0.0057	1.24	1.26	↓
$Y_{imIntN}$	1.23	-	0.5 ~ 1.5	1.25	0.0000	1.25	1.25	----
$Y_{imIntD}$	0.74	-	0.5 ~ 1.5	1.25	0.0000	1.25	1.25	----
$Y_{smN}$	1.23	-	0.5 ~ 1.5	1.25	0.0078	1.24	1.26	↓
$Y_{smD}$	0.74	-	0.5 ~ 1.5	1.16	0.1072	1.02	1.42	↓
$Y_{cEdN}$	1.23	-	0.5 ~ 1.5	1.25	0.0000	1.25	1.25	----



Y <sub>cEd</sub>	0.74	-	0.5 ~ 1.5	1.25	0.0000	1.25	1.25	----
Y <sub>pN</sub>	1	-	0.5 ~ 1.5	1.25	0.0000	1.25	1.25	----
Y <sub>pD</sub>	1	-	0.5 ~ 1.5	1.25	0.0000	1.25	1.25	----
<b>Surface area</b>	<b>Values used</b>	<b>unit</b>	<b>range in sensitivity test</b>	<b>mean</b>	<b>SD</b>	<b>minimal</b>	<b>maximal</b>	
A <sub>aEp</sub>	1.08E-02	m <sup>2</sup>	0.36E-2 ~ 3.24E-2	1.12	0.2497	0.89	2.04	↓
A <sub>bEp</sub>	1.08E-02	m <sup>2</sup>	0.36E-2 ~ 3.24E-2	1.12	0.2497	0.89	2.04	↓
A <sub>imInt</sub>	1.08E-04	m <sup>2</sup>	1.08E-5 ~ 1.08E-3	1.25	0.0000	1.25	1.25	----
A <sub>sm</sub>	2.16E-02	m <sup>2</sup>	2.16E-3 ~ 2.16E-1	1.25	0.0117	1.12	1.26	↑
A <sub>bEd</sub>	2.16E-03	m <sup>2</sup>	0.5E-3 ~ 1E-2	0.99	0.3798	0.67	2.97	↓
A <sub>aEd</sub>	2.16E-03	m <sup>2</sup>	0.5E-3 ~ 1E-2	0.99	0.3798	0.67	2.97	↓
TSL (Thickness of lining liquid)	1.50E-05	m	0.5E-5 ~ 2E-5	1.17	0.1258	0.94	1.37	↑
<b>Volume</b>	<b>Values used</b>	<b>unit</b>	<b>range in sensitivity test</b>	<b>mean</b>	<b>SD</b>	<b>minimal</b>	<b>maximal</b>	
V <sub>aEp</sub>	1.62E-07	m <sup>3</sup>	0.4E-7 ~ 6.4E-7	1.65	0.3863	0.89	2.26	↑
V <sub>cEp</sub>	7.20E-08	m <sup>4</sup>	1.8E-8 ~ 28.8E-8	1.33	0.0788	1.19	1.46	↑
V <sub>int</sub>	1.08E-08	m <sup>5</sup>	1.08E-9 ~ 1.08E-7	1.28	0.0288	1.24	1.32	↑
V <sub>imInt</sub>	1.08E-10	m <sup>6</sup>	1.08E-11 ~ 1.08E-9	1.24	0.0073	1.24	1.26	↑
V <sub>sm</sub>	4.70E-08	m <sup>7</sup>	1.2E-8 ~ 18.8E-8	1.62	0.3598	0.91	2.20	↑
V <sub>cEd</sub>	8.64E-10	m <sup>8</sup>	8.64E-11 ~ 8.64E-9	1.26	0.0127	1.24	1.27	↑
V <sub>p</sub>	5	m <sup>9</sup>	3 ~ 6	1.25	0.0000	1.25	1.25	----
<b>Membrane potential</b>	<b>Values used</b>	<b>unit</b>	<b>range in sensitivity test</b>	<b>mean</b>	<b>SD</b>	<b>minimal</b>	<b>maximal</b>	
E <sub>aEp</sub>	-0.0093	v	-0.03 ~ 0.001	1.19	0.0807	1.06	1.34	↑
E <sub>bEp</sub>	0.0119	v	0.001 ~ 0.03	1.22	0.0690	1.12	1.36	↓
E <sub>sm</sub>	-0.06	v	-0.08 ~ -0.03	1.21	0.1752	0.96	1.56	↓
E <sub>imInt</sub>	-0.06	v	-0.08 ~ -0.03	1.25	0.0000	1.25	1.25	----
E <sub>bEd</sub>	-0.06	v	-0.08 ~ -0.03	1.35	0.2035	1.06	1.76	↑
E <sub>aEd</sub>	-0.03	v	-0.08 ~ -0.03	1.40	0.1065	1.24	1.59	↓
<b>pH values</b>	<b>Values used</b>	<b>unit</b>	<b>range in sensitivity test</b>	<b>mean</b>	<b>SD</b>	<b>minimal</b>	<b>maximal</b>	
pH <sub>aEp</sub>	7.4	-	6 ~ 8	1.24	0.0042	1.24	1.26	↑
pH <sub>cEp</sub>	7.0	-	6 ~ 8	1.25	0.0083	1.24	1.26	↑
pH <sub>int</sub>	7.0	-	6 ~ 8	1.25	0.0202	1.24	1.31	↑
pH <sub>imInt</sub>	7.0	-	6 ~ 8	1.25	0.0000	1.25	1.25	----
pH <sub>sm</sub>	7.0	-	6 ~ 8	1.21	0.0942	1.01	1.31	↓
pH <sub>cEd</sub>	7.0	-	6 ~ 8	1.26	0.0315	1.22	1.32	↑

pH <sub>p</sub>	7.4	-	6 ~ 8	1.25	0.0000	1.25	1.25	----
-----------------	-----	---	-------	------	--------	------	------	------

**Table. IV** Parameter sensitivity analysis for alveolar region

<i>Alveolar Region</i>	Values used	unit	range in sensitivity test	Statistics of absT50 values predicted (min)				
				mean	SD	minimal	maximal	
L <sub>aEp</sub>	0.95	-	0.5 ~ 0.95	1.16	0.0505	1.07	1.24	↑
L <sub>cEp</sub>	0.05	-	0.005 ~ 0.5	1.25	0.0082	1.24	1.26	↑
L <sub>imEp</sub>	0.05	-	0.005 ~ 0.6	1.25	0.0082	1.24	1.26	↑
L <sub>int</sub>	0.05	-	0.005 ~ 0.5	1.25	0.0000	1.25	1.25	----
L <sub>imint</sub>	0.05	-	0.005 ~ 0.5	1.25	0.0000	1.25	1.25	----
L <sub>cEd</sub>	0.05	-	0.005 ~ 0.5	1.25	0.0083	1.24	1.26	↑
L <sub>p</sub>	0	-	0 ~ 0.05	1.25	0.0000	1.25	1.25	----
<b>Activity coefficient</b>	<b>Values used</b>	<b>unit</b>	<b>range in sensitivity test</b>	<b>mean</b>	<b>SD</b>	<b>minimal</b>	<b>maximal</b>	
Y <sub>aEpN</sub>	1	-	0.5 ~ 1.5	1.25	0.0170	1.23	1.29	↓
Y <sub>aEpD</sub>	1	-	0.5 ~ 1.5	1.26	0.0920	1.14	1.48	↓
Y <sub>imEpN</sub>	1.23	-	0.5 ~ 1.5	1.25	0.0000	1.25	1.25	----
Y <sub>imEpD</sub>	0.74	-	0.5 ~ 1.5	1.25	0.0000	1.25	1.25	----
Y <sub>cEpN</sub>	1.23	-	0.5 ~ 1.5	1.25	0.0000	1.25	1.25	----
Y <sub>cEpD</sub>	0.74	-	0.5 ~ 1.5	1.25	0.0000	1.25	1.25	----
Y <sub>intN</sub>	1	-	0.5 ~ 1.5	1.25	0.0000	1.25	1.25	----
Y <sub>intD</sub>	1	-	0.5 ~ 1.5	1.25	0.0000	1.25	1.25	----
Y <sub>imintN</sub>	1.23	-	0.5 ~ 1.5	1.25	0.0000	1.25	1.25	----
Y <sub>imintD</sub>	0.74	-	0.5 ~ 1.5	1.25	0.0000	1.25	1.25	----
Y <sub>cEdN</sub>	1.23	-	0.5 ~ 1.5	1.25	0.0000	1.25	1.25	----
Y <sub>cEdD</sub>	0.74	-	0.5 ~ 1.5	1.25	0.0000	1.25	1.25	----
Y <sub>pN</sub>	1	-	0.5 ~ 1.5	1.25	0.0000	1.25	1.25	----
Y <sub>pD</sub>	1	-	0.5 ~ 1.5	1.25	0.0000	1.25	1.25	----
<b>Surface area</b>	<b>Values used</b>	<b>unit</b>	<b>range in sensitivity test</b>	<b>mean</b>	<b>SD</b>	<b>minimal</b>	<b>maximal</b>	
A <sub>aEp</sub>	0.387	m <sup>2</sup>	0.2 ~ 0.6	1.25	0.0258	1.21	1.29	↓
A <sub>bEp</sub>	0.387	m <sup>2</sup>	0.2 ~ 0.6	1.25	0.0258	1.21	1.29	↓

$A_{imEp}$	0.0041919	$m^2$	0.00042 ~ 0.042	1.25	0.0000	1.25	1.25	----
$A_{imInt}$	0.00041919	$m^2$	0.000042 ~ 0.0042	1.25	0.0000	1.25	1.25	----
$A_{bEd}$	0.452	$m^2$	0.2 ~ 0.7	1.25	0.0225	1.23	1.31	↓
$A_{aEd}$	0.452	$m^2$	0.2 ~ 0.7	1.25	0.0225	1.23	1.31	↓
TSL (Thickness of lining liquid)	5.00E-06	m	1E-6 ~ 8E-6	1.20	0.1408	0.96	1.41	↑
<b>Volume</b>	<b>Values used</b>	<b>unit</b>	<b>range in sensitivity test</b>	<b>mean</b>	<b>SD</b>	<b>minimal</b>	<b>maximal</b>	
$V_{aEp}$	1.94E-06	$m^3$	1.94E-7 ~ 1.94E-5	1.77	0.2968	0.94	2.00	↑
$V_{cEp}$	1.48E-07	$m^3$	1.48E-8 ~ 1.48E-6	1.25	0.0075	1.24	1.26	↑
$V_{imEp}$	2.82E-08	$m^3$	2.82E-9 ~ 2.82E-7	1.25	0.0083	1.24	1.26	↑
$V_{int}$	2.61E-07	$m^3$	2.68E-8 ~ 2.68E-6	1.25	0.0000	1.25	1.25	----
$V_{imInt}$	2.82E-09	$m^3$	2.82E-10 ~ 2.82E-8	1.25	0.0000	1.25	1.25	----
$V_{cEd}$	1.62E-07	$m^3$	1.62E-8 ~ 1.62E-6	1.25	0.0083	1.24	1.26	↑
$V_p$	5	$m^3$	3 ~ 6	1.25	0.0000	1.25	1.25	----
<b>Membrane potential</b>	<b>Values used</b>	<b>unit</b>	<b>range in sensitivity test</b>	<b>mean</b>	<b>SD</b>	<b>minimal</b>	<b>maximal</b>	
$E_{aEp}$	-0.0093	v	-0.03 ~ -0.001	1.20	0.0638	1.09	1.31	↑
$E_{bEp}$	0.0119	v	0.001 ~ 0.03	1.11	0.0523	1.06	1.29	↓
$E_{imEp}$	-0.06	v	- 0.08 ~ -0.03	1.25	0.0000	1.25	1.25	----
$E_{imInt}$	-0.06	v	- 0.08 ~ -0.03	1.25	0.0000	1.25	1.25	----
$E_{bEd}$	-0.06	v	- 0.08 ~ -0.03	1.25	0.0188	1.23	1.29	↑
$E_{aEd}$	-0.03	v	- 0.08 ~ -0.03	1.26	0.0122	1.24	1.28	↓
<b>pH values</b>	<b>Values used</b>	<b>unit</b>	<b>range in sensitivity test</b>	<b>mean</b>	<b>SD</b>	<b>minimal</b>	<b>maximal</b>	
$pH_{aEp}$	7.4	-	6 ~ 8	1.24	0.0042	1.24	1.26	↓
$pH_{imEp}$	7	-	6 ~ 8	1.25	0.0000	1.25	1.25	----
$pH_{cEp}$	7	-	6 ~ 8	1.25	0.0068	1.24	1.26	↑
$pH_{int}$	7	-	6 ~ 8	1.25	0.0065	1.24	1.26	↑
$pH_{imInt}$	7	-	6 ~ 8	1.25	0.0000	1.25	1.25	----
$pH_{cEd}$	7	-	6 ~ 8	1.25	0.0000	1.25	1.25	----
$pH_p$	7.4	-	6 ~ 8	1.25	0.0000	1.25	1.25	----

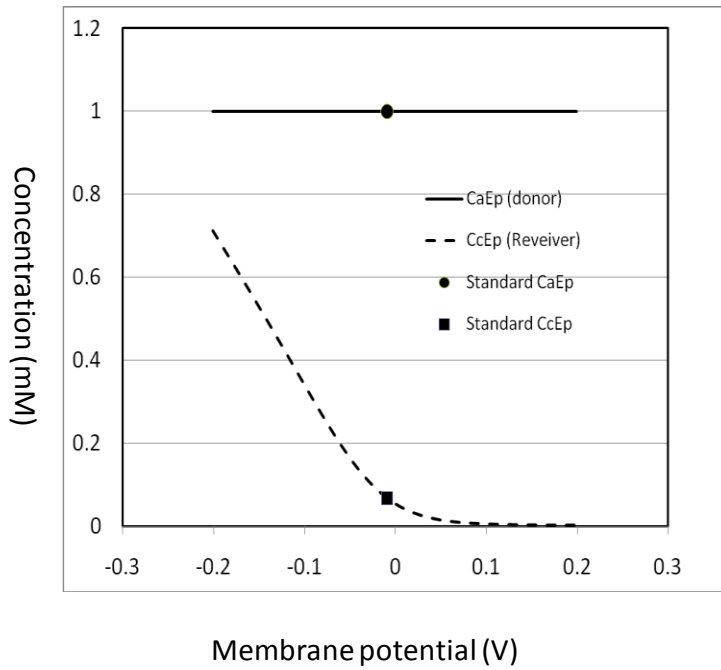
#### 4. Effect of transcellular electrical potential on steady state concentrations

The effect of membrane potential on the concentration under the steady state was examined by running simulation at constant concentration 1mM at the apical side of epithelium (surface lining liquid). For each membrane in the alveolar and airway region, the membrane potential was varied from -0.2 v to +0.2 V to investigate the concentration change at the either side of the membrane caused by the change in the membrane potential. The influence of transmembrane electrical potential on concentrations can be explained by the effect of voltage on the translocation of cations across the membrane. The cations favor entering into the compartment with negative potential. Whenever the membrane potential increase, the negativity of intracellular compartments decreases, hence the corresponding intracellular compartment decreases as shown in the Figure.1 and Figure.2.

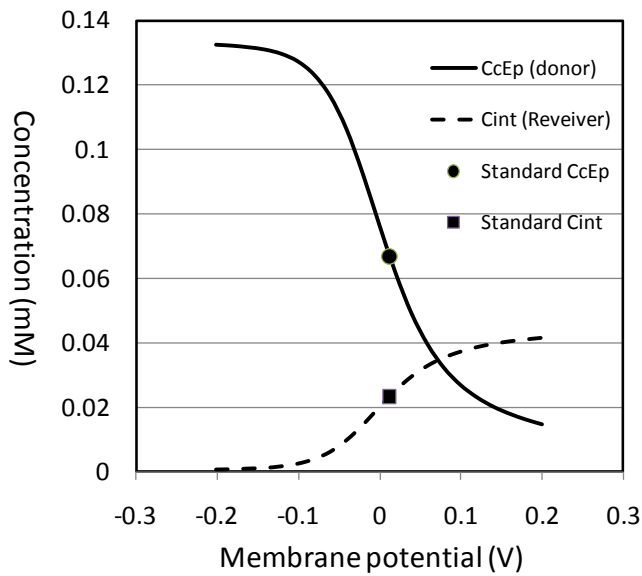
#### **4.1. Effect of membrane potential on concentration at steady state in alveolar region**

**Figure.1.** Alveolar Region: Effect of membrane potential on concentration at steady state

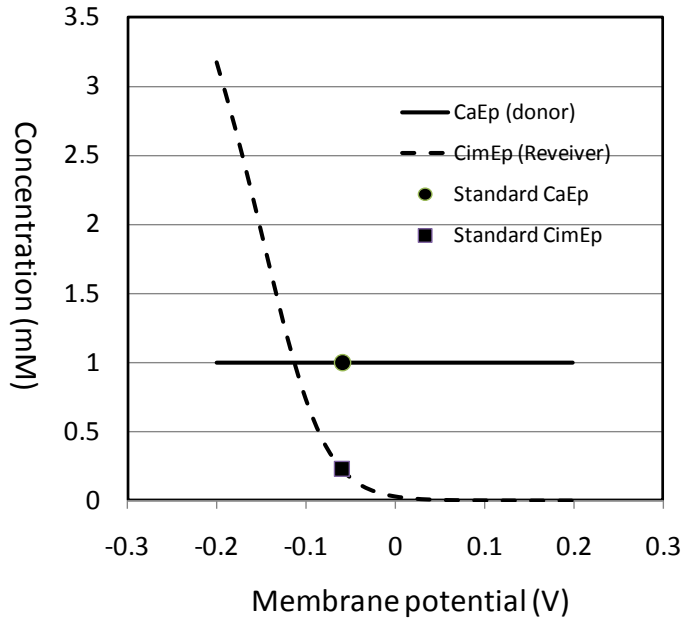
1. Effects of membrane potential of apical membrane of epithelial cells (EaEp) on calculated concentration at steady state.



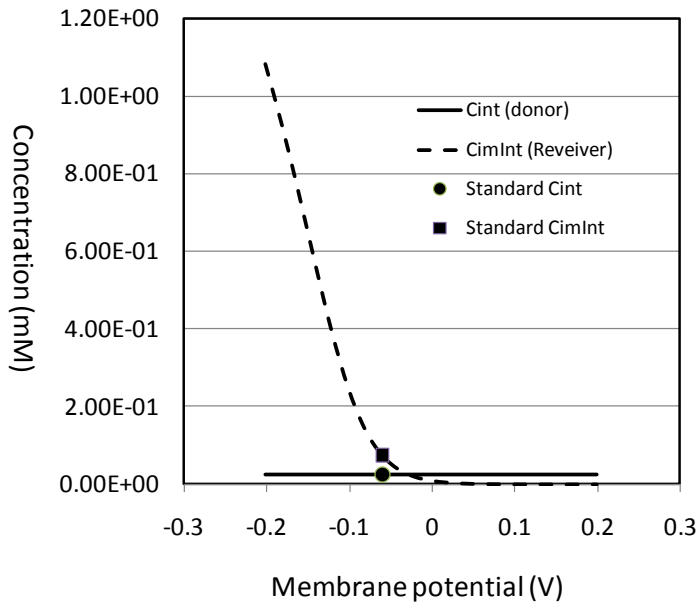
2. Effects of membrane potential of basolateral membrane of epithelial cells ( $E_{bEp}$ ) on calculated concentration at steady state.



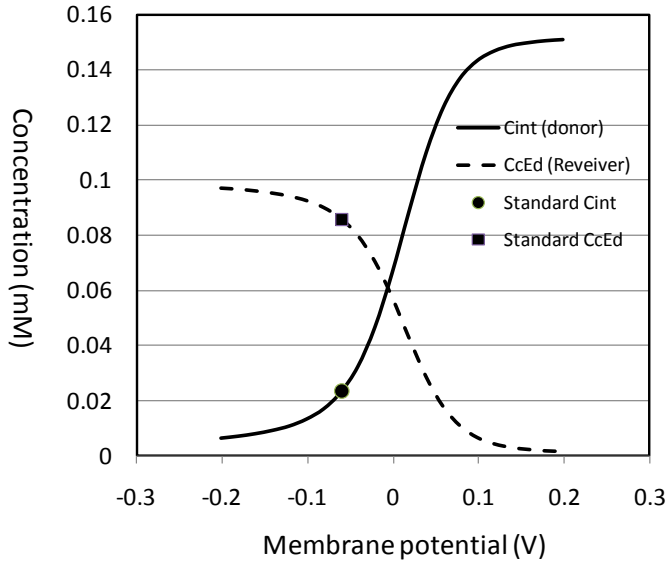
3. Effects of membrane potential of macrophage membrane ( $E_{imEp}$ ) on calculated concentration at steady state.



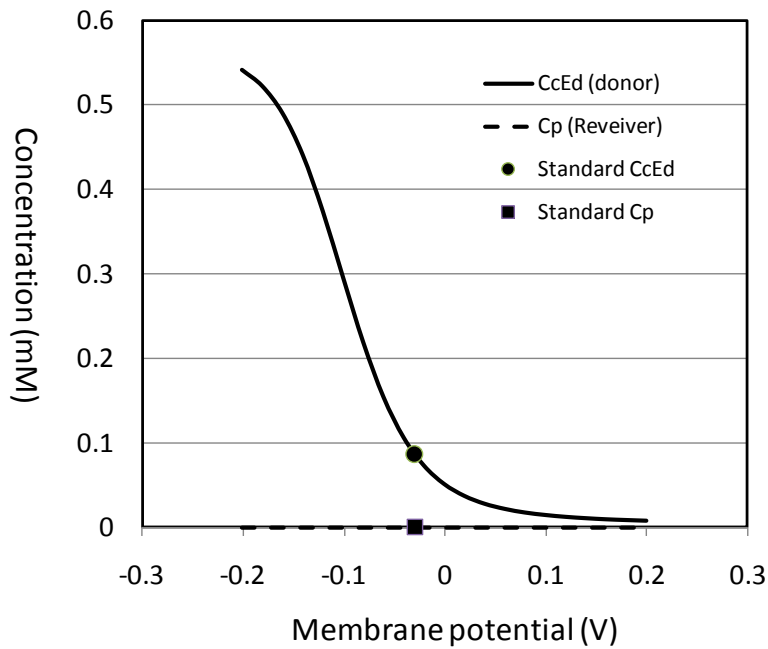
4. Effects of membrane potential of immune cells in interstitium ( $E_{imInt}$ ) on calculated concentration at steady state.



5. Effects of membrane potential of basolateral membrane of endothelium ( $E_{bEd}$ ) on calculated concentration at steady state.



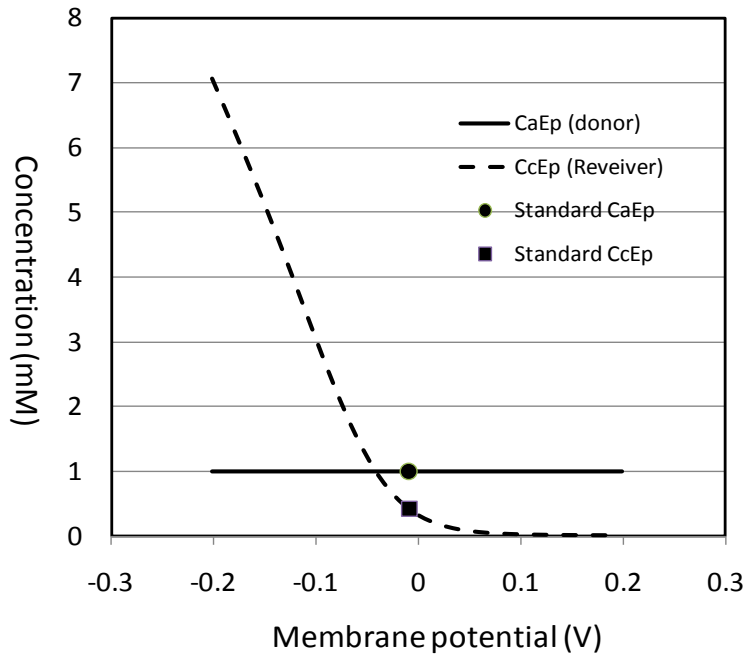
6. Effects of membrane potential of apical membrane of endothelium ( $E_{aEd}$ ) on calculated concentration at steady state.



## 4.2. Effect of membrane potential on concentration at steady state in airway region

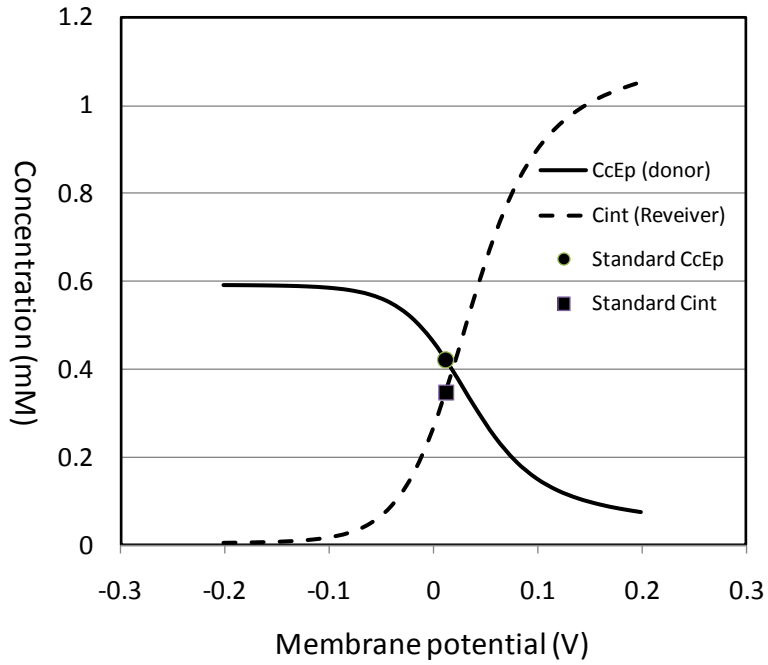
**Figure.2.** Airways: Effect of membrane potential on concentration at steady state

1. Effects of membrane potential of apical membrane of epithelial cells ( $E_{aEp}$ ) on calculated concentration at steady state.

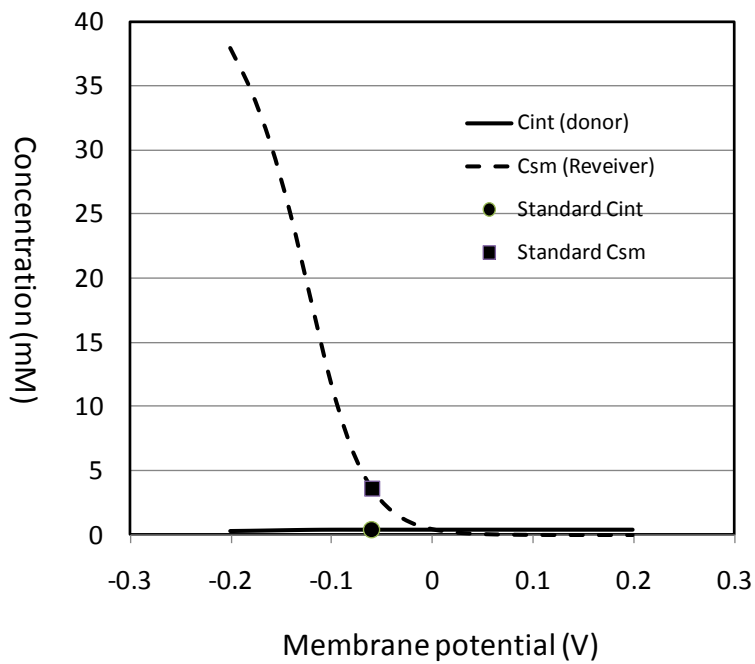


2. Effects of membrane potential of basolateral membrane of epithelial cells ( $E_{bEp}$ ) on calculated concentration at steady state.

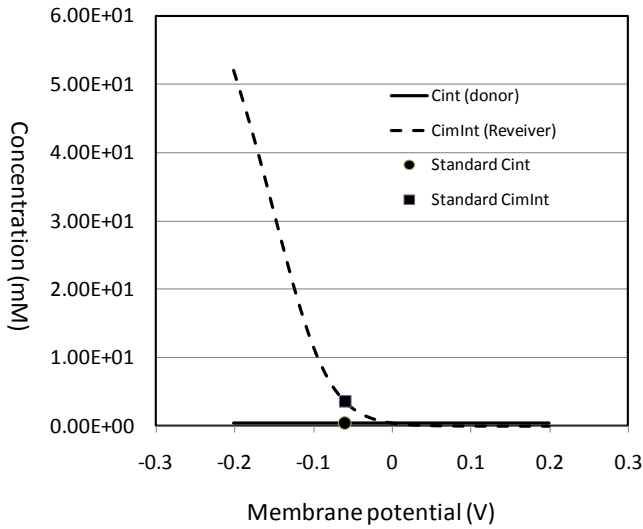




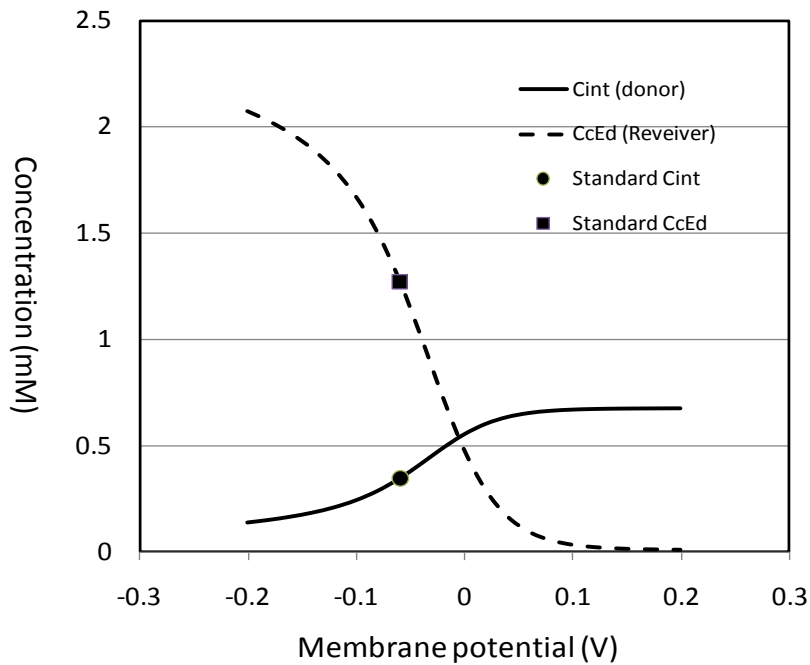
3. Effects of membrane potential of smooth muscle ( $E_{imEp}$ ) on calculated concentration at steady state.



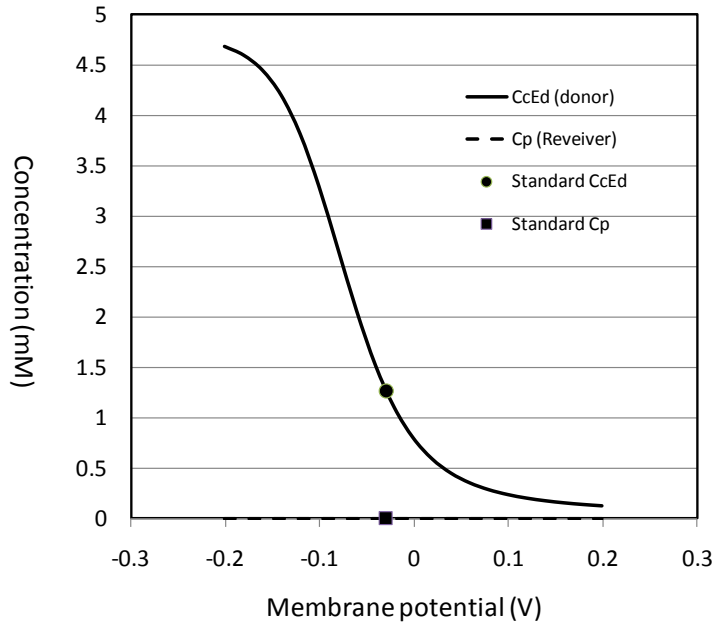
4. Effects of membrane potential of immune cells in interstitium ( $E_{imInt}$ ) on calculated concentration at steady state.



5. Effects of membrane potential of basolateral membrane of endothelium ( $E_{bEd}$ ) on calculated concentration at steady state.



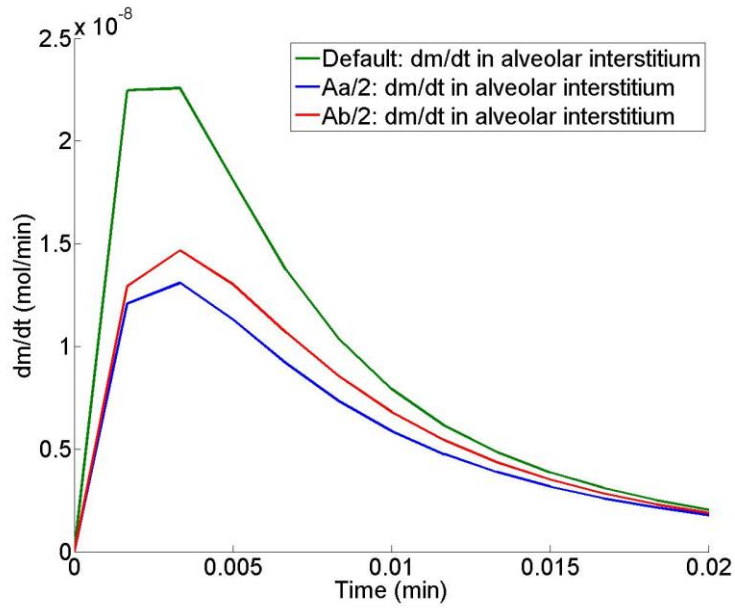
6. Effects of membrane potential of apical membrane of endothelium ( $E_{aEd}$ ) on calculated concentration at steady state.



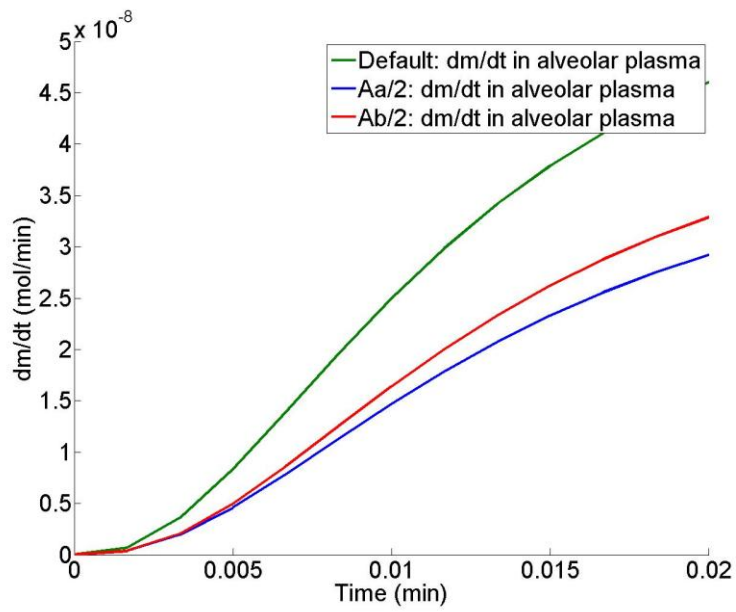
### 5. Rate limiting step across the lung epithelium

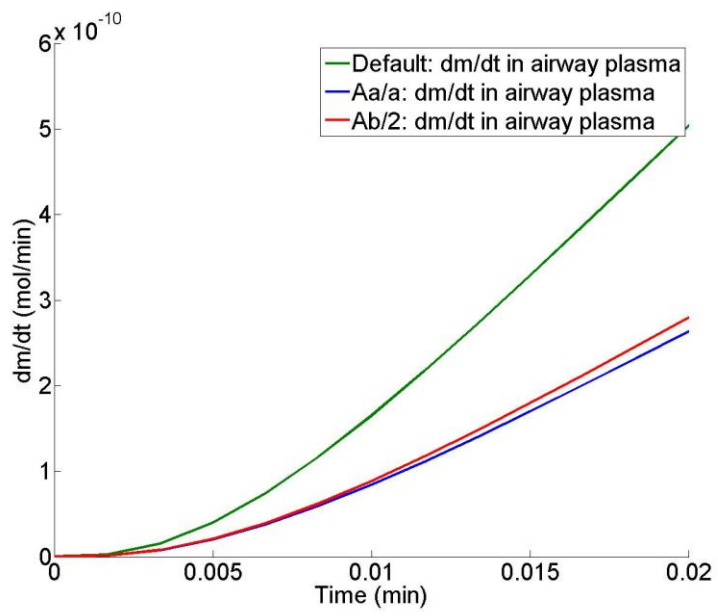
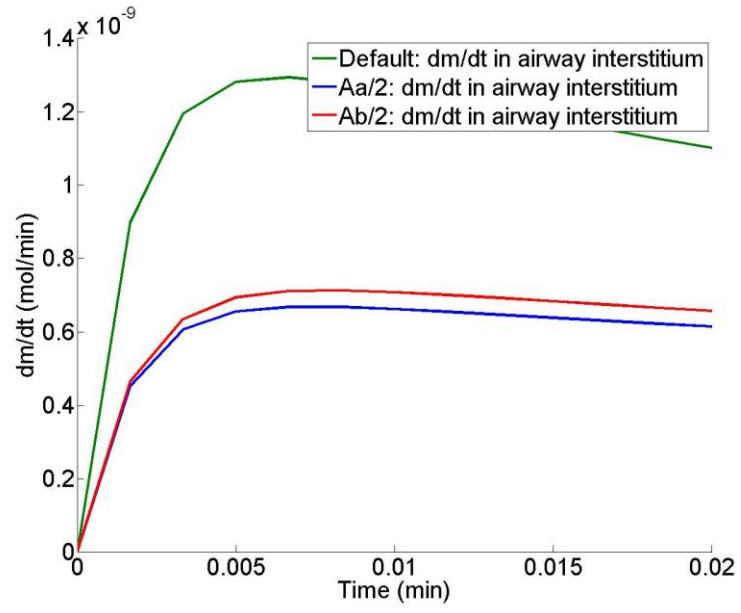
Simulation was performed with initial dose 50 nmol at airway and alveolar region, respectively. To see the rate limiting step across the lung epithelium in airway and alveolar region, we compare the effect of reducing the area of apical and basolateral membrane ( $A_a$  and  $A_b$ ) on the  $dm/dt$  in the corresponding interstitium and plasma compartments. As shown in Figure.3, reduction of the area of apical and basolateral membrane by half decreases the  $dm/dt$  in interstitium and plasma in both airway and alveolar region. More importantly, the effect of reducing the apical membrane area is more pronounced than reducing basolateral membrane area, which means the rate limiting step is the transport across the apical membrane in both regions.

**Figure.3. Effect of reduction of apical and basolateral membrane area on dm/dt in interstitium and plasma in airways and alveolar region**



1.





## Appendix B

### Parameters and Sensitivity Analysis in Chapter 3

**Table. I.** Constant Parameters in the Model

Symbol	Value	Unit	description
T	310.15	K	Rat body temperature
R	8.314	J / mol / K	Universal gas constant
F	96485.3415	sA / mol	Faraday constant

Notation of the name of parameters: L indicates the volumetric fraction of lipids (dimensionless), G indicates the activity coefficient  $\gamma$  (dimensionless), A indicates the surface area of the membrane (unit:  $m^2$ ), V indicates the volume of the corresponding compartment (unit:  $m^3$ ). E indicates the membrane potential (unit: V), pH indicates the pH values in corresponding compartment (dimensionless). Ro indicates the volumetric percentage of organelles in cellular compartments (dimensionless). The subscripts *aEp* indicates the apical side of epithelial cells, *cEp* indicates the cytosol of epithelial, *imEp* indicates the macrophage/immune cells on the surface of epithelium, *int* indicates the interstitium, *imInt* indicates the

immune cells in the interstitium, *sm* indicates the smooth muscle, *cEd* indicates the cytosol of endothelium, *p* indicates the plasma.

**Table. II** Parameter values and sensitivity analysis of AUC (mg/ml\*min) for alveoli

Parameter	Default	Low	High	Mean	SD	CV	Trend
LaEp	0.95	0.05	0.95	0.06148	0.01861	0.3027	+
LimEp	0.05	0.005	0.5	0.09819	0.001462	0.01489	+
LcEp	0.05	0.005	0.5	0.09709	0.000794	0.008183	+
Lint	0	0.005	0.5	0.09702	0.00055	0.005668	+
LimInt	0.05	0.005	0.5	0.09621	5.61E-05	0.000583	+
LcEd	0.05	0.005	0.5	0.09863	0.001656	0.0168	+
Lp	0	0.005	0.5	0.09612	6.08E-12	6.33E-11	-
GaEpN	1	0.5	1.5	0.09677	0.005074	0.05243	-
GaEpD	1	0.5	1.5	0.1017	0.02376	0.2336	-
GimEpN	1.23	0.5	1.5	0.09614	1.45E-05	0.000151	-
GimEpD	0.74	0.5	1.5	0.09569	0.000605	0.006326	-
GcEpN	1.23	0.5	1.5	0.09613	7.49E-06	7.79E-05	-
GcEpD	0.74	0.5	1.5	0.09589	0.000346	0.003612	-
GintN	1	0.5	1.5	0.09612	6.30E-07	6.55E-06	-
GintD	1	0.5	1.5	0.09615	0.000236	0.002452	-
GimIntN	1.23	0.5	1.5	0.09612	6.24E-07	6.50E-06	-
GimIntD	0.74	0.5	1.5	0.0961	2.73E-05	0.000284	-
GcEdN	1.23	0.5	1.5	0.09613	1.86E-05	0.000194	-
GcEdD	0.74	0.5	1.5	0.09553	0.000717	0.007507	-
GpN	1	0.5	1.5	0.09612	6.88E-13	7.16E-12	+
GpD	1	0.5	1.5	0.09612	1.12E-11	1.17E-10	+

AaEp	0.387	0.0387	3.87	0.06819	0.04024	0.5901	-
Aabp	0.387	0.0387	3.87	0.09149	0.01539	0.1682	-
AimEp	0.0042	0.00042	0.042	0.101	0.003111	0.0308	+
AimInt	0.00042	0.000042	0.0042	0.09612	1.32E-09	1.37E-08	+
AbEd	0.452	0.0452	4.52	0.09261	0.008726	0.09422	-
AaEd	0.452	0.0452	4.52	0.09281	0.01073	0.1156	-
ASL	5	0.5	50	0.1065	0.01065	0.1001	+
Vint	2.68E-07	2.68E-08	2.68E-06	0.07264	0.01426	0.1963	-
Ro	0.1	0.01	0.5	0.09777	0.001412	0.01444	+
pHaEp	7.4	4	9	0.09607	0.003608	0.03756	+
pHimEp	7	4	9	0.09593	0.001094	0.01141	-
pHcEp	7	4	9	0.09889	0.005637	0.057	+
pHint	7	4	9	0.1004	0.008185	0.08152	+
pHimInt	7	4	9	0.09612	4.42E-05	0.00046	-
pHcEd	7	4	9	0.09596	0.002246	0.02341	-
pHp	7.4	4	9	0.09612	1.28E-11	1.33E-10	-
EbEd	-0.06	-0.12	0	0.09933	0.01645	0.1656	+
EaEd	-0.06	-0.12	0	0.09759	0.009574	0.0981	-
EimInt	-0.06	-0.12	0	0.09616	0.000112	0.001164	-
EimEp	-0.06	-0.12	0	0.09388	8.63E-05	0.000919	+
EbEp	0.0119	0	0.12	0.07161	0.01334	0.1863	-
EaEp	-0.0093	-0.12	0	0.04605	0.02446	0.1311	+



**Table. III** Parameter values and sensitivity analysis of AUC (mg/ml\*min) for airways

Parameter	Default	Low	High	Mean	SD	CV	Trend
LaEp	0.2	0.05	0.95	8.555	0.8889	0.1039	+
LcEp	0.05	0.005	0.5	7.83	0.3157	0.04032	+
Lint	0	0.005	0.5	7.509	0.03813	0.005078	+
LimInt	0.05	0.005	0.5	7.452	0.003692	0.000495	+
Lsm	0.05	0.005	0.5	9.912	1.706	0.1721	+
LcEd	0.05	0.005	0.5	7.47	0.01523	0.002039	+
Lp	0	0.005	0.5	7.447	1.18E-08	1.58E-09	-
GaEpN	1	0.5	1.5	7.453	0.05194	0.006969	-
GaEpD	1	0.5	1.5	7.54	0.3954	0.05243	-
GcEpN	1.23	0.5	1.5	7.449	0.002974	0.000399	-
GcEpD	0.74	0.5	1.5	7.357	0.1376	0.01871	-
GintN	1	0.5	1.5	7.447	4.36E-05	5.85E-06	-
GintD	1	0.5	1.5	7.449	0.01635	0.002195	-
GimIntN	1.23	0.5	1.5	7.447	4.11E-05	5.52E-06	-
GimIntD	0.74	0.5	1.5	7.446	0.001797	0.000241	-
GsmN	1.23	0.5	1.5	7.461	0.01669	0.002237	-
GsmD	0.74	0.5	1.5	6.921	0.7033	0.1016	-
GcEdN	1.23	0.5	1.5	7.447	0.000171	2.30E-05	-
GcEdD	0.74	0.5	1.5	7.441	0.006594	0.000886	-
GpN	1	0.5	1.5	7.447	8.91E-09	1.20E-09	-
GpD	1	0.5	1.5	7.447	1.99E-08	2.67E-09	-
AaEp	1.08E-02	2.70E-03	4.32E-02	7.291	3.757	0.5153	-
AimInt	1.08E+04	1.08E-05	1.08E-03	7.447	8.62E-08	1.16E-08	+
Asm	2.16E-02	2.16E-03	2.16E-01	15.18	4.173	0.2749	+

AbEd	2.16E-03	5.40E-04	8.64E-03	7.152	1.164	0.1627	-
AaEd	2.16E-03	5.40E-04	8.64E-03	7.116	1.149	0.1614	-
ASL	15	1.5	150	4.889	1.849	0.3781	-
VcEp	7.20E-08	7.20E-09	7.20E-07	5.656	1.082	0.1912	-
Vint	1.08E-08	1.08E-09	1.08E-07	6.774	0.4348	0.06419	-
Vsm	4.70E-08	4.70E-09	4.70E-07	15.56	4.529	0.2911	+
pHaEp	7.4	4	9	7.448	0.1056	0.01418	-
pHcEp	7.0	4	9	7.409	0.07615	0.01028	-
pHint	7.0	4	9	7.805	0.6839	0.08762	+
pHsm	7.0	4	9	7.309	2.272	0.3109	-
pHimInt	7.0	4	9	7.446	0.002912	0.000391	-
pHcEd	7.0	4	9	7.445	0.02066	0.002775	-
pHp	7.4	4	9	7.447	3.19E-08	4.28E-09	-
EbEd	-0.06	-0.12	0	8.59	0.5854	0.06815	+
EaEd	-0.06	-0.12	0	7.79	0.2234	0.02868	-
Esm	-0.06	-0.12	0	10.46	6.49	0.6205	-
EimInt	-0.06	-0.12	0	7.449	0.007372	0.00099	-
EbEp	0.0119	0	0.12	6.296	0.6186	0.09824	-
EaEp	-0.0093	-0.12	0	6.958	0.3514	0.05051	+
Ro	0.1	0.01	0.5	10.44	2.555	0.2448	+

**Table. IV** Parameter values and sensitivity analysis of  $T_{ss}$  (min) for alveoli

Parameter	Default	low	high	Mean	SD	CV	Trend
LaEp	0.95	0.05	0.95	1.795	0.6543	0.3645	+
LimEp	0.05	0.05	0.5	3.297	0.1911	0.05796	+
LcEp	0.05	0.005	0.5	3.021	0.01608	0.005323	+
Lint	0	0.005	0.5	2.992	0.006055	0.002024	-
LimInt	0.05	0.005	0.5	3.016	0.01673	0.005546	+
LcEd	0.05	0.005	0.5	2.912	0.05801	0.01992	-
Lp	0	0.005	0.5	2.998	0.004398	0.001467	-
GaEpN	1	0.5	1.5	3.038	0.1957	0.06441	-
GaEpD	1	0.5	1.5	3.335	0.8703	0.261	-
GimEpN	1.23	0.5	1.5	3.002	0.002848	0.000949	-
GimEpD	0.74	0.5	1.5	2.97	0.05358	0.01804	-
GcEpN	1.23	0.5	1.5	3.001	0.001427	0.000476	+
GcEpD	0.74	0.5	1.5	2.994	0.007105	0.002373	-
GintN	1	0.5	1.5	3.001	0.001191	0.000397	+
GintD	1	0.5	1.5	2.997	0.004986	0.001664	+
GimIntN	1.23	0.5	1.5	2.999	0.002187	0.000729	+
GimIntD	0.74	0.5	1.5	2.998	0.004614	0.001539	-
GcEdN	1.23	0.5	1.5	2.998	0.004602	0.001535	+
GcEdD	0.74	0.5	1.5	3.024	0.03149	0.01041	+
GpN	1	0.5	1.5	3.001	0.00178	0.000593	-
GpD	1	0.5	1.5	2.998	0.004921	0.001641	-
AaEp	0.387	0.0387	3.87	3.259	0.725	0.2225	+
AbEp	0.387	0.0387	3.87	2.924	0.3595	0.1229	-
AimEp	0.0042	0.00042	0.042	2.956	0.03784	0.0128	-

AimInt	0.00042	4.19E-05	0.004192	2.997	0.009786	0.003266	-
AbEd	0.452	0.0452	4.52	2.7	0.2743	0.1016	-
AaEd	0.452	0.0452	4.52	2.774	0.3023	0.109	-
ASL	5	0.5	50	15.3	9.311	0.6087	+
Vint	2.68E-07	2.68E-08	2.68E-06	2.983	0.009908	0.003322	-
EaEp	-0.0093	-0.12	0	1.162	0.08901	0.07661	+
EbEp	0.0119	0	0.12	1.651	0.0762	0.04614	-
EimEp	-0.06	-0.12	0	3.147	0.293	0.09308	-
EimInt	-0.06	-0.12	0	3.007	0.01809	0.006017	-
EbEd	-0.06	-0.12	0	3.338	1.073	0.3214	+
EaEd	-0.06	-0.12	0	3.119	0.3052	0.09785	-
pHaEp	7.4	4	9	2.998	0.09591	0.03199	+
pHimEp	7	4	9	2.977	0.08239	0.02767	-
pHcEp	7	4	9	3.138	0.2374	0.07565	+
pHint	7	4	9	3.226	0.3662	0.1135	+
pHimInt	7	4	9	2.998	0.004545	0.001516	-
pHcEd	7	4	9	3.063	0.1185	0.03868	+
pHp	7.4	4	9	2.997	0.005152	0.001719	-
Ro	0.1	0.01	0.5	2.921	0.06519	0.02232	-

**Table. V** Parameter values and sensitivity analysis of  $T_{ss}$  (min) for airways

Parameter	default	low	high	Mean	SD	CV	Trend
LaEp	0.2	0.05	0.95	34.37	3.208	0.09334	+
LcEp	0.05	0.005	0.5	32.61	1.097	0.03365	+
Lint	0	0.005	0.5	31.26	0.1733	0.005542	+
LimInt	0.05	0.005	0.5	30.99	0.05303	0.001711	-
Lsm	0.05	0.005	0.5	41.89	7.162	0.171	+
LcEd	0.05	0.005	0.5	31	0.05826	0.001879	-
Lp	0	0.005	0.5	30.96	0.0523	0.001689	+
GaEpN	1	0.5	1.5	31	0.1873	0.006043	-
GaEpD	1	0.5	1.5	31.48	1.314	0.04172	-
GcEpN	1.23	0.5	1.5	30.93	0.03826	0.001237	+
GcEpD	0.74	0.5	1.5	30.65	0.4926	0.01607	-
GintN	1	0.5	1.5	30.93	0.02438	0.000788	-
GintD	1	0.5	1.5	30.99	0.09294	0.002999	-
GimIntN	1.23	0.5	1.5	30.92	0.03475	0.001124	+
GimIntD	0.74	0.5	1.5	30.97	0.04729	0.001527	-
GsmN	1.23	0.5	1.5	31.03	0.1006	0.003242	-
GsmD	0.74	0.5	1.5	28.41	3.055	0.1075	-
GcEdN	1.23	0.5	1.5	30.95	0.04532	0.001465	-
GcEdD	0.74	0.5	1.5	30.95	0.04737	0.00153	+
GpN	1	0.5	1.5	30.93	0.02644	0.000855	+
GpD	1	0.5	1.5	30.97	0.05493	0.001774	-
AaEp	1.08E-02	2.70E-03	4.32E-02	31.08	10.23	0.3292	-
AimInt	1.08E+04	1.08E-05	1.08E-03	30.96	0.04623	0.001493	-
Asm	2.16E-02	2.16E-03	2.16E-01	124.4	66.76	0.5367	-

AbEd	2.16E-03	5.40E-04	8.64E-03	22.11	9.556	0.4322	-
AaEd	2.16E-03	5.40E-04	8.64E-03	22.8	10.32	0.4529	-
ASL	15	1.5	150	50.52	15.21	0.301	+
VcEp	7.20E-08	7.20E-09	7.20E-07	45.77	10.24	0.2237	+
Vint	1.08E-08	1.08E-09	1.08E-07	32.05	0.7181	0.02241	+
Vsm	4.70E-08	4.70E-09	4.70E-07	124.4	66.76	0.5367	+
EaEp	-0.0093	-0.12	0	28.33	1.249	0.04409	+
EbEp	0.0119	0	0.12	26.38	2.277	0.08634	-
Esm	-0.06	-0.12	0	40.18	26.64	0.6632	-
EimInt	-0.06	-0.12	0	30.99	0.06302	0.002034	-
EbEd	-0.06	-0.12	0	47.79	3.545	0.07418	+
EaEd	-0.06	-0.12	0	34.99	1.05	0.03001	-
pHaEp	7.4	4	9	30.98	0.2709	0.008745	-
pHcEp	7	4	9	30.79	0.2611	0.008477	-
pHint	7	4	9	32.87	3.068	0.09333	+
pHimInt	7	4	9	30.95	0.05372	0.001736	+
pHcEd	7	4	9	30.94	0.05553	0.001795	-
pHp	7.4	4	9	30.97	0.06052	0.001954	+
Ro	0.1	0.01	0.5	51.29	17.51	0.3415	+

**Table. VI** Parameter values and sensitivity analysis of mass deposition for alveoli (mass fraction in lungs)

Parameter	Default	low	high	Mean	SD	CV	Trend
LaEp	0.95	0.05	0.95	0.8867	0.02451	0.02764	+
LimEp	0.05	0.005	0.5	0.9215	0.000416	0.000452	+
LcEp	0.05	0.005	0.5	0.9215	0.000432	0.000469	+
Lint	0	0.005	0.5	0.9222	0.001027	0.001114	+
LimInt	0.05	0.005	0.5	0.921	9.63E-05	0.000105	+
LcEd	0.05	0.005	0.5	0.9276	0.004776	0.005148	+
Lp	0	0.005	0.5	0.8295	0.05402	0.06512	-
GaEpN	1	0.5	1.5	0.9153	0.003549	0.003877	-
GaEpD	1	0.5	1.5	0.9181	0.01396	0.01521	-
GimEpN	1.23	0.5	1.5	0.9147	4.31E-06	4.71E-06	-
GimEpD	0.74	0.5	1.5	0.9146	0.000202	0.00022	-
GcEpN	1.23	0.5	1.5	0.9147	4.96E-06	5.43E-06	-
GcEpD	0.74	0.5	1.5	0.9146	0.000211	0.000231	-
GintN	1	0.5	1.5	0.9147	1.22E-05	1.34E-05	-
GintD	1	0.5	1.5	0.9149	0.000565	0.000618	-

GimIntN	1.23	0.5	1.5	0.9147	9.48E-07	1.04E-06	-
GimIntD	0.74	0.5	1.5	0.9147	3.95E-05	4.32E-05	-
GcEdN	1.23	0.5	1.5	0.9148	6.31E-05	6.89E-05	-
GcEdD	0.74	0.5	1.5	0.9133	0.002762	0.003024	-
GpN	1	0.5	1.5	0.9147	1.79E-09	1.95E-09	+
GpD	1	0.5	1.5	0.9097	0.02491	0.02738	+
AaEp	0.387	0.0387	3.87	0.9279	0.02019	0.02176	+
AbEp	0.387	0.0387	3.87	0.9208	2.48E-15	2.70E-15	-
AimEp	0.0042	0.00042	0.042	0.9242	0.002247	0.002431	+
AimInt	0.00042	4.19E-05	0.004192	0.9208	2.61E-15	2.83E-15	-
AbEd	0.452	0.0452	4.52	0.9511	0.01806	0.01899	+
AaEd	0.452	0.0452	4.52	0.9208	2.30E-15	2.50E-15	+
ASL	5	0.5	50	0.9693	0.02505	0.02584	+
Vint	2.68E-07	2.68E-08	2.68E-06	0.9266	0.004073	0.004395	+
EaEp	-0.0093	-0.12	0	0.7143	0.1568	0.2196	+
EbEp	0.0119	0	0.12	0.8432	0.05729	0.06795	-
EimEp	-0.06	-0.12	0	0.921	0.00079	0.000858	-
EimInt	-0.06	-0.12	0	0.9209	0.000192	0.000209	-



EbEd	-0.06	-0.12	0	0.9152	0.05026	0.05491	+
EaEd	-0.06	-0.12	0	0.8826	0.09135	0.1035	-
pHaEp	7.4	4	9	0.9213	0.002439	0.002647	+
pHimEp	7	4	9	0.9207	0.000335	0.000364	-
pHcEp	7	4	9	0.9246	0.006427	0.006951	+
pHint	7	4	9	0.9279	0.01363	0.01469	+
pHimInt	7	4	9	0.9208	6.61E-05	7.18E-05	-
pHcEd	7	4	9	0.9169	0.008666	0.009452	-
pHp	7.4	4	9	0.9284	0.01869	0.02013	+
Ro	0.1	0.01	0.5	0.9302	0.008617	0.009263	+

**Table. VII** Parameter and sensitivity analysis of mass deposition for airways (mass fraction in lungs)

Parameter	Default	low	high	Mean	SD	CV	Trend
LaEp	0.2	0.05	0.95	0.08661	0.006106	0.0705	+
LcEp	0.05	0.005	0.5	0.08279	0.002397	0.02896	+
Lint	0	0.005	0.5	0.07976	0.000444	0.00556	+
Lsm	0.05	0.005	0.5	0.1035	0.01537	0.1485	+
LimInt	0.05	0.005	0.5	0.07923	3.87E-05	0.000489	+
LcEd	0.05	0.005	0.5	0.07966	0.000349	0.004382	+
Lp	0	0.005	0.5	0.03946	0.001595	0.04042	-
GaEpN	1	0.5	1.5	0.07924	0.000363	0.004582	-
GaEpD	1	0.5	1.5	0.08016	0.002608	0.03254	-
GcEpN	1.23	0.5	1.5	0.07919	2.40E-05	0.000303	-
GcEpD	0.74	0.5	1.5	0.07833	0.001	0.01277	-
GintN	1	0.5	1.5	0.07917	6.29E-06	7.94E-05	-
GintD	1	0.5	1.5	0.07929	0.00027	0.003408	-
GsmN	1.23	0.5	1.5	0.07936	0.000182	0.002295	-
GsmD	0.74	0.5	1.5	0.07293	0.007359	0.1009	-
GimIntN	1.23	0.5	1.5	0.07917	4.28E-07	5.40E-06	-
GimIntD	0.74	0.5	1.5	0.07916	1.75E-05	0.000221	-
GcEdN	1.23	0.5	1.5	0.07917	3.46E-06	4.36E-05	-
GcEdD	0.74	0.5	1.5	0.07904	0.00013	0.00165	-
GpN	1	0.5	1.5	0.07913	0.000155	0.001964	+
GpD	1	0.5	1.5	0.07391	0.002036	0.02755	+
AaEp	1.08E-02	2.70E-03	4.32E-02	0.08063	0.00408	0.0506	+

AimInt	1.08E+04	1.08E-05	1.08E-03	0.07945	0.000201	0.002525	+
Asm	2.16E-02	2.16E-03	2.16E-01	0.2206	0.1051	0.4766	+
AbEd	2.16E-03	5.40E-04	8.64E-03	0.07947	0.000445	0.005597	+
AaEd	2.16E-03	5.40E-04	8.64E-03	0.0833	0.002652	0.03184	+
Vint	1.08E-08	1.08E-09	1.08E-07	0.08255	0.00229	0.02774	+
EaEp	-0.0093	-0.12	0	0.07357	0.002812	0.03823	+
EbEp	0.0119	0	0.12	0.0688	0.005865	0.08524	-
Esm	-0.06	-0.12	0	0.09275	0.06086	0.6562	-
EimInt	-0.06	-0.12	0	0.0792	8.91E-05	0.001125	-
EbEd	-0.06	-0.12	0	0.1321	0.01128	0.08541	+
EaEd	-0.06	-0.12	0	0.0943	0.007571	0.08028	-
pHaEp	7.4	4	9	0.07907	0.00068	0.008595	-
pHcEp	7	4	9	0.07879	0.000626	0.007948	-
pHint	7	4	9	0.08395	0.007481	0.08911	+
pHsm	7	4	9	0.07023	0.02485	0.3538	-
pHimInt	7	4	9	0.07916	3.29E-05	0.000416	-
pHcEd	7	4	9	0.07901	0.000458	0.005797	-
pHp	7.4	4	9	0.09632	0.003901	0.0405	+
Ro	0.1	0.01	0.5	0.119	0.03917	0.3292	+

## Appendix C

### Matlab Code

```
% 1CellPK based lung model starts here (Rats)
% compartments: HOE
% aEp (surface lining liquied), imEp (Macrophage),
% cEp(epithelial cells),cEpMito(mito of cEp), cEpLyso (lyso of cEp)
% int(Interstitium),imInt(immune cells), sm(smooth muscle),
% cEd(endothelial cells), cEdMito(mito of cEd),cEdLyso (lyso of cEd), p(plasma)

function [M, G, M_v, Vp] = H_al_RL()
%molecular physiochemical property
pKa = 7.8;
logPN = 4.49 ;
logPD = logPN-3.7 ;
z = 1;
% Constant
T = 273.15+37;body temperature
R = 8.314;
F = 96484.56;
%lipid fraction
LaEp = 0.95;
LimEp = 0.05;
LcEp = 0.05 ;
Lint = 0;
LimInt = 0.05;
Lsm = 0;
LcEd = 0.05;
Lp = 0;
%volumetric water fraction=1-lipid fraction
WaEp = 1 - LaEp;
WimEp = 1 - LimEp;
WcEp = 1 - LcEp;
Wint = 1 - Lint;
WimInt = 1 - LimInt;
Wsm = 1 - Lsm;
WcEd = 1 - LcEd;
Wp = 1 - Lp;
```

```

%activity coefficient of species(N:neutral,D:desociated)
GaEpN = 1;
GaEpD = 1;
GimEpN = 1.23;
GimEpD = 0.74;
GcEpN = 1.23;
GcEpD = 0.74;
GintN = 1;
GintD = 1;
GimIntN = 1.23;
GimIntD = 0.74;
GsmN = 1.23;
GsmD = 0.74;
GcEdN = 1.23;
GcEdD = 0.74;
GpN = 1;
GpD = 1;
% By Jingyu Yu (used in publication) Areas and volumes (m^2, m^3) for 7 membranes and
corresponding compartments
AaEp = 0.387;%literature
AbEp = AaEp;%Assuming same with epical side
AimEp = 3.14*10^(-10)*0.89*10^(9)*3/100/2; % 10 um diameter, only half of surface gets
contact with liquid, since ASL = 5 um
AimInt = AimEp/10; % assuming number of immune cells is 1/10 of macrophage
Asm = 0;%No SM
AbEd = 0.452;%literature
AaEd = 0.452;%literature
%volumes for 8 compartments(m3)
ASL = 5; %literature um
VaEp = AaEp*ASL*10^(-6); %5 um thickness
VcEp = AaEp*0.384*10^(-6); % 0.384, literature
VimEp = 0.89*10^(9)*3/100*1058*10^(-18);%number of macrophage(literature)*volume of
macrophage
Vint = AaEp*0.693*10^(-6); % literature
VimInt = VimEp/10;% assuming number of immune cells is 1/10 of macrophage
Vsm = 10^(-30); % VcEp*10^(-12); % can be any number, surface is 0
VcEd = AbEd*0.358*10^(-6); %0.358 um thickness --literature
% Vp = 5; %total huge volume for lung absorption model
#####
% Subcellular compartments in cEp (epithelial cells) and cEd(endothelial cells)
% calculate constant
R_org = 0.1;
VcEpMito = R_org*VcEp ; % 10^(-30); %
VcEpLyso = R_org*VcEp ; % 10^(-30); %
VcEdMito = R_org*VcEd ; % 10^(-30); %
VcEdLyso = R_org*VcEd ; % 10^(-30); %
AcEpMito = 5.9924e+006*VcEpMito; % 0 ;

```

```

AcEpLyso = 5.9924e+006*VcEpLyso; % 0 ;
AcEdMito = 5.9924e+006*VcEdMito; % 0 ;
AcEdLyso = 5.9924e+006*VcEdLyso; % 0 ;
#####
M_v = diag([VaEp,VimEp,VcEp,VcEpMito,VcEpLyso,Vint,Vsm,VimInt,VcEd,VcEdMito,VcEdLyso]);
V_LUN = trace(M_v)*10^6;
Vp = 340*10^(-9)*V_LUN;
% Membrane potential (V)
EaEp = -0.0093;
EbEp = 0.0119;%;
EimEp = -0.06;
EimInt = -0.06;
Esm = -0.06;
EbEd = -0.06;
EaEd = -0.06;
% pH values
pHaEp = 7.4;
pHimEp = 7.0;
pHcEp = 7.0;
pHint = 7.0;
pHimInt = 7.0;
pHsm = 7.0;
pHcEd = 7.0;
pHp = 7.4;
%adjustment for logP
if ( abs(z-1) <= 10^(-6) )
    logP_nlipT = 0.33*logPN+2.2 ;
    logP_dlipT = 0.37*logPD+2 ;
end
if ( abs(z+1) <= 10^(-6) )
    logP_nlipT = 0.37*logPN+2.2 ;
    logP_dlipT = 0.33*logPD+2.6 ;
end
if ( abs(z-0) <= 10^(-5) )
    logP_nlipT = 0.33*logPN+2.2 ;
    logP_dlipT = 0.33*logPD+2.2 ;
end

% Get the first two decimals
logP_n = round(logP_nlipT*100)/100 ;
logP_d = round(logP_dlipT*100)/100 ;
%calculate the membrane permeability
Pn = 10^(logP_n-6.7)*60; % in 1/min
Pd = 10^(logP_d-6.7)*60; % in 1/min
i = -sign(z) ;
%calculate N for flux of ion happening at 7 membranes
C = z*F/(R*T);

```

```

NaEp = C*(-EaEp) ;
NbEp = C*EbEp ;
NimEp = C*EimEp ;
NimInt = C*EimInt ;
Nsm = C*Esm ;
NbEd = C*(-EbEd) ;
NaEd = C*(EaEd) ;
%calculate Kn and Kd for 8 compartments (Optional)
N = 1.22*10^(logP_n);
D = 1.22*10^(logP_d);
% using Rodgers method to get Kd general
Kd = 229.9334;

KaEpN = N*LaEp ;
KaEpD = D*LaEp ;
KimEpN = N*LimEp ;
KimEpD = Kd*LimEp;
KcEpN = N*LcEp ;
KcEpD = Kd*LcEp ;
KintN = N*Lint ;
KintD = D*Lint ;
KimIntN = N*LimInt ;
KimIntD = Kd*LimInt ;
KsmN = N*Lsm ;
KsmD = Kd*Lsm ;
KcEdN = N*LcEd ;
KcEdD = Kd*LcEd ;
KpN = N*Lp ;
KpD = D*Lp ;

%#####
LcEpMito = 0.05 ;
LcEpLyso = 0.05 ;
LcEdMito = 0.05 ;
LcEdLyso = 0.05 ;

WcEpMito = 1-LcEpMito ;
WcEpLyso = 1-LcEpLyso ;
WcEdMito = 1-LcEdMito ;
WcEdLyso = 1-LcEdLyso ;

GcEpMitoN = 1.23 ;
GcEpMitoD = 0.74 ;
GcEpLysoN = 1.23 ;
GcEpLysoD = 0.74 ;
GcEdMitoN = 1.23 ;
GcEdMitoD = 0.74 ;

```

GcEdLysoN = 1.23 ;  
GcEdLysoD = 0.74 ;

EcEpMito = -0.16 ;  
EcEpLyso = +0.01 ;  
EcEdMito = -0.16 ;  
EcEdLyso = +0.01 ;

pHcEpMito = 8 ;  
pHcEpLyso = 5 ;  
pHcEdMito = 8 ;  
pHcEdLyso = 5 ;

NcEpMito = C\*EcEpMito ;  
NcEpLyso = C\*EcEpLyso ;  
NcEdMito = C\*EcEdMito ;  
NcEdLyso = C\*EcEdLyso ;

KcEpMitoN = N\*LcEpMito ;  
KcEpMitoD = Kd\*LcEpMito ;  
KcEpLysoN = N\*LcEpLyso ;  
KcEpLysoD = Kd\*LcEpLyso ;

KcEdMitoN = N\*LcEdMito ;  
KcEdMitoD = Kd\*LcEdMito ;  
KcEdLysoN = N\*LcEdLyso ;  
KcEdLysoD = Kd\*LcEdLyso ;

fcEpMitoN = 1/(WcEpMito/GcEpMitoN+KcEpMitoN/GcEpMitoN+WcEpMito\*10<sup>(i\*(pHcEpMito-pKa))</sup>/GcEpMitoD...  
+KcEpMitoD\*10<sup>(i\*(pHcEpMito-pKa))</sup>/GcEpMitoD);  
fcEpMitoD = fcEpMitoN\*10<sup>(i\*(pHcEpMito-pKa))</sup>;

fcEpLysoN = 1/(WcEpLyso/GcEpLysoN+KcEpLysoN/GcEpLysoN+WcEpLyso\*10<sup>(i\*(pHcEpLyso-pKa))</sup>/GcEpLysoD...  
+KcEpLysoD\*10<sup>(i\*(pHcEpLyso-pKa))</sup>/GcEpLysoD);  
fcEpLysoD = fcEpLysoN\*10<sup>(i\*(pHcEpLyso-pKa))</sup>;

fcEdMitoN = 1/(WcEdMito/GcEdMitoN+KcEdMitoN/GcEdMitoN+WcEdMito\*10<sup>(i\*(pHcEdMito-pKa))</sup>/GcEdMitoD...  
+KcEdMitoD\*10<sup>(i\*(pHcEdMito-pKa))</sup>/GcEdMitoD);  
fcEdMitoD = fcEdMitoN\*10<sup>(i\*(pHcEdMito-pKa))</sup>;

fcEdLysoN = 1/(WcEdLyso/GcEdLysoN+KcEdLysoN/GcEdLysoN+WcEdLyso\*10<sup>(i\*(pHcEdLyso-pKa))</sup>/GcEdLysoD...  
+KcEdLysoD\*10<sup>(i\*(pHcEdLyso-pKa))</sup>/GcEdLysoD);



```

fcEdLysoD = fcEdLysoN*10^(i*(pHcEdLyso-pKa));

%#####

%compute the fn and fd for 8 compartments
faEpN = 1/(WaEp/GaEpN+KaEpN/GaEpN+WaEp*10^(i*(pHaEp-pKa))/GaEpD...
    +KaEpD*10^(i*(pHaEp-pKa))/GaEpD);
faEpD = faEpN*10^(i*(pHaEp-pKa));
fimEpN = 1/(WimEp/GimEpN+KimEpN/GimEpN+WimEp*10^(i*(pHimEp-pKa))/GimEpD...
    +KimEpD*10^(i*(pHimEp-pKa))/GimEpD);
fimEpD = fimEpN*10^(i*(pHimEp-pKa));
fcEpN = 1/(WcEp/GcEpN+KcEpN/GcEpN+WcEp*10^(i*(pHcEp-pKa))/GcEpD...
    +KcEpD*10^(i*(pHcEp-pKa))/GcEpD);
fcEpD = fcEpN*10^(i*(pHcEp-pKa));
fintN = 1/(Wint/GintN+KintN/GintN+Wint*10^(i*(pHint-pKa))/GintD...
    +KintD*10^(i*(pHint-pKa))/GintD);
fintD = fintN*10^(i*(pHint-pKa));
fimIntN = 1/(WimInt/GimIntN+KimIntN/GimIntN+WimInt*10^(i*(pHimInt-pKa))/GimIntD...
    +KimIntD*10^(i*(pHimInt-pKa))/GimIntD);
fimIntD = fimIntN*10^(i*(pHimInt-pKa));
fsmN = 1/(Wsm/GsmN+KsmN/GsmN+Wsm*10^(i*(pHsm-pKa))/GsmD...
    +KsmD*10^(i*(pHsm-pKa))/GsmD);
fsmD = fsmN*10^(i*(pHsm-pKa));
fcEdN = 1/(WcEd/GcEdN+KcEdN/GcEdN+WcEd*10^(i*(pHcEd-pKa))/GcEdD...
    +KcEdD*10^(i*(pHcEd-pKa))/GcEdD);
fcEdD = fcEdN*10^(i*(pHcEd-pKa));
fpN = 1/(Wp/GpN+KpN/GpN+Wp*10^(i*(pHp-pKa))/GpD...
    +KpD*10^(i*(pHp-pKa))/GpD);
fpD = fpN*10^(i*(pHp-pKa));

%mucus clearance
%Ke = 0.02;
Ke = 0;

%compute the coefficient matrix for ODEs
% #1: Surface Lining Liquid (aEp)
KaEp_aEp = AaEp/VaEp*(Pn*(-faEpN)+Pd*NaEp/(exp(NaEp)-1)*(-faEpD)*exp(NaEp))...
    -AimEp/VaEp*(Pn*faEpN+Pd*NimEp/(exp(NimEp)-1)*faEpD)...
    -Ke;
KaEp_imEp = -AimEp/VaEp*(Pn*(-fimEpN)+Pd*NimEp/(exp(NimEp)-1)*(-fimEpD)*exp(NimEp));
KaEp_cEp = AaEp/VaEp*(Pn*(fcEpN)+Pd*NaEp/(exp(NaEp)-1)*(fcEpD));
KaEp_cEpMito = 0;
KaEp_cEpLyso = 0;
KaEp_int = 0;
KaEp_sm = 0;
KaEp_imInt = 0;
KaEp_cEd = 0;

```

```

KaEp_cEdMito = 0;
KaEp_cEdLyso = 0;
KaEp_p = 0;
SaEp = 0;

```

```
% #2: Macrophage (imEp)
```

```

KimEp_aEp = AimEp/VimEp*(Pn*faEpN+Pd*NimEp/(exp(NimEp)-1)*faEpD);
KimEp_imEp = AimEp/VimEp*(Pn*(-fimEpN)+Pd*NimEp/(exp(NimEp)-1)*(-
fimEpD)*exp(NimEp));
KimEp_cEp = 0;
KimEp_cEpMito = 0 ;
KimEp_cEpLyso = 0 ;
KimEp_int = 0;
KimEp_sm = 0;
KimEp_imInt = 0;
KimEp_cEd = 0;
KimEp_cEdMito = 0 ;
KimEp_cEdLyso = 0 ;
KimEp_p = 0;
SimEp = 0;

```

```
% #3: Epithelial Cells (cEp)
```

```

KcEp_aEp = -AaEp/VcEp*(Pn*(-faEpN)+Pd*NaEp/(exp(NaEp)-1)*(-faEpD)*exp(NaEp));
KcEp_imEp = 0;
KcEp_cEp = -AaEp/VcEp*(Pn*(fcEpN)+Pd*NaEp/(exp(NaEp)-1)*(fcEpD))...
-AcEpMito/VcEp*(Pn*fcEpN+Pd*NcEpMito/(exp(NcEpMito)-1)*fcEpD)...
-AcEpLyso/VcEp*(Pn*fcEpN+Pd*NcEpLyso/(exp(NcEpLyso)-1)*fcEpD)...
+ AbEp/VcEp*(Pn*(-fcEpN)+Pd*NbEp/(exp(NbEp)-1)*(-fcEpD)*exp(NbEp));
KcEp_cEpMito = -AcEpMito/VcEp*(Pn*(-fcEpMitoN)+Pd*NcEpMito/(exp(NcEpMito)-1)*(-
fcEpMitoD)*exp(NcEpMito)) ;
KcEp_cEpLyso = -AcEpLyso/VcEp*(Pn*(-fcEpLysoN)+Pd*NcEpLyso/(exp(NcEpLyso)-1)*(-
fcEpLysoD)*exp(NcEpLyso)) ;
KcEp_int = AbEp/VcEp*(Pn*(fintN)+Pd*NbEp/(exp(NbEp)-1)*(fintD));
KcEp_sm = 0;
KcEp_imInt = 0;
KcEp_cEd = 0;
KcEp_cEdMito = 0 ;
KcEp_cEdLyso = 0 ;
KcEp_p = 0;
ScEp = 0;

```

```
% #4: : Epithelial Cells (cEpMito)
```

```

KcEpMito_aEp = 0;
KcEpMito_imEp = 0;
KcEpMito_cEp = AcEpMito/VcEpMito*(Pn*(fcEpN)+Pd*NcEpMito/(exp(NcEpMito)-1)*(fcEpD));
KcEpMito_cEpMito = AcEpMito/VcEpMito*(Pn*(-fcEpMitoN)+Pd*NcEpMito/(exp(NcEpMito)-
1)*(-fcEpMitoD)*exp(NcEpMito));

```

```

KcEpMito_cEpLyso = 0 ;
KcEpMito_int = 0 ;
KcEpMito_sm = 0;
KcEpMito_imInt = 0;
KcEpMito_cEd = 0;
KcEpMito_cEdMito = 0 ;
KcEpMito_cEdLyso = 0 ;
KcEpMito_p = 0;
ScEpMito = 0;

```

% #5: : Epithelial Cells (cEpLyso)

```

KcEpLyso_aEp = 0;
KcEpLyso_imEp = 0;
KcEpLyso_cEp = AcEpLyso/VcEpLyso*(Pn*(fcEpN)+Pd*NcEpLyso/(exp(NcEpLyso)-1)*(fcEpD));
KcEpLyso_cEpMito = 0 ;
KcEpLyso_cEpLyso = AcEpLyso/VcEpLyso*(Pn*(-fcEpLysoN)+Pd*NcEpLyso/(exp(NcEpLyso)-1)*(-fcEpLysoD)*exp(NcEpLyso));
KcEpLyso_int = 0 ;
KcEpLyso_sm = 0;
KcEpLyso_imInt = 0;
KcEpLyso_cEd = 0;
KcEpLyso_cEdMito = 0 ;
KcEpLyso_cEdLyso = 0 ;
KcEpLyso_p = 0;
ScEpLyso = 0;

```

% #6: : Interstitium (int)

```

Kint_aEp = 0;
Kint_imEp = 0;
Kint_cEp = -AbEp/Vint*(Pn*(-fcEpN)+Pd*NbEp/(exp(NbEp)-1)*(-fcEpD)*exp(NbEp));
Kint_cEpMito = 0 ;
Kint_cEpLyso = 0 ;
Kint_int = -AbEp/Vint*(Pn*(fintN)+Pd*NbEp/(exp(NbEp)-1)*(fintD))...
          -Asm/Vint*(Pn*fintN+Pd*Nsm/(exp(Nsm)-1)*fintD)...
          -AimInt/Vint*(Pn*fintN+Pd*NimInt/(exp(NimInt)-1)*fintD)...
          +AbEd/Vint*(Pn*(-fintN)+Pd*NbEd/(exp(NbEd)-1)*(-fintD)*exp(NbEd));
Kint_sm = -Asm/Vint*(Pn*(-fsmN)+Pd*Nsm/(exp(Nsm)-1)*(-fsmD)*exp(Nsm));
Kint_imInt = -AimInt/Vint*(Pn*(-fimIntN)+Pd*NimInt/(exp(NimInt)-1)*(-fimIntD)*exp(NimInt));
Kint_cEd = AbEd/Vint*(Pn*(fcEdN)+Pd*NbEd/(exp(NbEd)-1)*(fcEdD));
Kint_cEdMito = 0 ;
Kint_cEdLyso = 0 ;
Kint_p = 0;
Sint = 0;

```

% #7: Smooth Muscle (sm)

```

Ksm_aEp = 0;
Ksm_imEp = 0;

```

```

Ksm_cEp = 0;
Ksm_cEpMito = 0 ;
Ksm_cEpLyso = 0 ;
Ksm_int = Asm/Vsm*(Pn*fintN+Pd*Nsm/(exp(Nsm)-1)*fintD);
Ksm_sm = Asm/Vsm*(Pn*(-fsmN)+Pd*Nsm/(exp(Nsm)-1)*(-fsmD)*exp(Nsm));
Ksm_imInt = 0;
Ksm_cEd = 0;
Ksm_cEdMito = 0 ;
Ksm_cEdLyso = 0 ;
Ksm_p = 0;
Ssm = 0;

```

```

% #8: Immune Cells (imInt)

```

```

KimInt_aEp = 0;
KimInt_imEp = 0;
KimInt_cEp = 0;
KimInt_cEpMito = 0;
KimInt_cEpLyso = 0;
KimInt_int = AimInt/VimInt*(Pn*fintN+Pd*NimInt/(exp(NimInt)-1)*fintD);
KimInt_sm = 0;
KimInt_imInt = AimInt/VimInt*(Pn*(-fimIntN)+Pd*NimInt/(exp(NimInt)-1)*(-fimIntD)*exp(NimInt));
KimInt_cEd = 0;
KimInt_cEdMito = 0;
KimInt_cEdLyso = 0;
KimInt_p = 0;
SimInt = 0;

```

```

% #9: Endothelial celss (cEd)

```

```

KcEd_aEp = 0;
KcEd_imEp = 0;
KcEd_cEp = 0;
KcEd_cEpMito = 0;
KcEd_cEpLyso = 0;
KcEd_int = -AbEd/VcEd*(Pn*(-fintN)+Pd*NbEd/(exp(NbEd)-1)*(-fintD)*exp(NbEd));
KcEd_sm = 0;
KcEd_imInt = 0;
KcEd_cEd = -AbEd/VcEd*(Pn*(fcEdN)+Pd*NbEd/(exp(NbEd)-1)*(fcEdD))...
    -AcEdMito/VcEd*(Pn*fcEdN+Pd*NcEdMito/(exp(NcEdMito)-1)*fcEdD)...
    -AcEdLyso/VcEd*(Pn*fcEdN+Pd*NcEdLyso/(exp(NcEdLyso)-1)*fcEdD)...
    +AaEd/VcEd*(Pn*(-fcEdN)+Pd*NaEd/(exp(NaEd)-1)*(-fcEdD)*exp(NaEd));
KcEd_cEdMito = -AcEdMito/VcEd*(Pn*(-fcEdMitoN)+Pd*NcEdMito/(exp(NcEdMito)-1)*(-fcEdMitoD)*exp(NcEdMito));
KcEd_cEdLyso = -AcEdLyso/VcEd*(Pn*(-fcEdLysoN)+Pd*NcEdLyso/(exp(NcEdLyso)-1)*(-fcEdLysoD)*exp(NcEdLyso));
KcEd_p = AaEd/VcEd*(Pn*(fpN)+Pd*NaEd/(exp(NaEd)-1)*(fpD));
ScEd = 0;

```

% #10: Endothelial celss (cEd) Mito

```
KcEdMito_aEp = 0;
KcEdMito_imEp = 0;
KcEdMito_cEp = 0;
KcEdMito_cEpMito = 0;
KcEdMito_cEpLyso = 0;
KcEdMito_int = 0;
KcEdMito_sm = 0;
KcEdMito_imInt = 0;
KcEdMito_cEd = AcEdMito/VcEdMito*(Pn*(fcEdN)+Pd*NcEdMito/(exp(NcEdMito)-1)*(fcEdD)) ;
KcEdMito_cEdMito = AcEdMito/VcEdMito*(Pn*(-fcEdMitoN)+Pd*NcEdMito/(exp(NcEdMito)-1)*(-fcEdMitoD)*exp(NcEdMito));
KcEdMito_cEdLyso = 0;
KcEdMito_p = 0 ;
ScEdMito = 0;
```

% #11: Endothelial celss (cEd) Lyso

```
KcEdLyso_aEp = 0;
KcEdLyso_imEp = 0;
KcEdLyso_cEp = 0;
KcEdLyso_cEpMito = 0;
KcEdLyso_cEpLyso = 0;
KcEdLyso_int = 0 ;
KcEdLyso_sm = 0;
KcEdLyso_imInt = 0;
KcEdLyso_cEd = AcEdLyso/VcEdLyso*(Pn*(fcEdN)+Pd*NcEdLyso/(exp(NcEdLyso)-1)*(fcEdD)) ;
KcEdLyso_cEdMito = 0;
KcEdLyso_cEdLyso = AcEdLyso/VcEdLyso*(Pn*(-fcEdLysoN)+Pd*NcEdLyso/(exp(NcEdLyso)-1)*(-fcEdLysoD)*exp(NcEdLyso));
KcEdLyso_p = 0;
ScEdLyso = 0;
```

% #12: plasma(p)

```
Kp_aEp = 0;
Kp_imEp = 0;
Kp_cEp = 0;
Kp_cEpMito = 0;
Kp_cEpLyso = 0;
Kp_int = 0;
Kp_sm = 0;
Kp_imInt = 0;
Kp_cEd = -AaEd/Vp*(Pn*(-fcEdN)+Pd*NaEd/(exp(NaEd)-1)*(-fcEdD)*exp(NaEd));
Kp_cEdMito = 0;
Kp_cEdLyso = 0;
Kp_p = -AaEd/Vp*(Pn*(fpN)+Pd*NaEd/(exp(NaEd)-1)*(fpD));
```

```

Sp = 0;

M =
[KaEp_aEp,KaEp_imEp,KaEp_cEp,KaEp_cEpMito,KaEp_cEpLyso,KaEp_int,KaEp_sm,KaEp_imInt,K
aEp_cEd,KaEp_cEdMito,KaEp_cEdLyso,KaEp_p;...

KimEp_aEp,KimEp_imEp,KimEp_cEp,KimEp_cEpMito,KimEp_cEpLyso,KimEp_int,KimEp_sm,KimE
p_imInt,KimEp_cEd,KimEp_cEdMito,KimEp_cEdLyso,KimEp_p;...

KcEp_aEp,KcEp_imEp,KcEp_cEp,KcEp_cEpMito,KcEp_cEpLyso,KcEp_int,KcEp_sm,KcEp_imInt,KcE
p_cEd,KcEp_cEdMito,KcEp_cEdLyso,KcEp_p;...

KcEpMito_aEp,KcEpMito_imEp,KcEpMito_cEp,KcEpMito_cEpMito,KcEpMito_cEpLyso,KcEpMito_
int,KcEpMito_sm,KcEpMito_imInt,KcEpMito_cEd,KcEpMito_cEdMito,KcEpMito_cEdLyso,KcEpMi
to_p;...

KcEpLyso_aEp,KcEpLyso_imEp,KcEpLyso_cEp,KcEpLyso_cEpMito,KcEpLyso_cEpLyso,KcEpLyso_in
t,KcEpLyso_sm,KcEpLyso_imInt,KcEpLyso_cEd,KcEpLyso_cEdMito,KcEpLyso_cEdLyso,KcEpLyso_p
;...

Kint_aEp,Kint_imEp,Kint_cEp,Kint_cEpMito,Kint_cEpLyso,Kint_int,Kint_sm,Kint_imInt,Kint_cEd,K
int_cEdMito,Kint_cEdLyso,Kint_p;...

Ksm_aEp,Ksm_imEp,Ksm_cEp,Ksm_cEpMito,Ksm_cEpLyso,Ksm_int,Ksm_sm,Ksm_imInt,Ksm_cE
d,Ksm_cEdMito,Ksm_cEdLyso,Ksm_p;...

KimInt_aEp,KimInt_imEp,KimInt_cEp,KimInt_cEpMito,KimInt_cEpLyso,KimInt_int,KimInt_sm,Kim
Int_imInt,KimInt_cEd,KimInt_cEdMito,KimInt_cEdLyso,KimInt_p;...

KcEd_aEp,KcEd_imEp,KcEd_cEp,KcEd_cEpMito,KcEd_cEpLyso,KcEd_int,KcEd_sm,KcEd_imInt,KcE
d_cEd,KcEd_cEdMito,KcEd_cEdLyso,KcEd_p;...

KcEdMito_aEp,KcEdMito_imEp,KcEdMito_cEp,KcEdMito_cEpMito,KcEdMito_cEpLyso,KcEdMito_
int,KcEdMito_sm,KcEdMito_imInt,KcEdMito_cEd,KcEdMito_cEdMito,KcEdMito_cEdLyso,KcEdMi
to_p;...

KcEdLyso_aEp,KcEdLyso_imEp,KcEdLyso_cEp,KcEdLyso_cEpMito,KcEdLyso_cEpLyso,KcEdLyso_in
t,KcEdLyso_sm,KcEdLyso_imInt,KcEdLyso_cEd,KcEdLyso_cEdMito,KcEdLyso_cEdLyso,KcEdLyso_p
;...

Kp_aEp,Kp_imEp,Kp_cEp,Kp_cEpMito,Kp_cEpLyso,Kp_int,Kp_sm,Kp_imInt,Kp_cEd,Kp_cEdMito,K
p_cEdLyso,Kp_p];

G = [SaEp,SimEp,ScEp,ScEpMito,ScEpLyso,Sint,Ssm,SimInt,ScEd,ScEdMito,ScEdLyso,Sp]';

%% 1CellPK based lung model starts here (Rats)
%% Compartments,Airways, :

```

```

% aEp (surface lining liquied), imEp (Macrophage),
% cEp(epithelial cells),cEpMito(mito of cEp), cEpLyso (lyso of cEp)
% int(Interstitial),imInt(immune cells), sm(smooth muscle),
% cEd(endothelial cells), cEdMito(mito of cEd),cEdLyso (lyso of cEd), p(plasma)

```

```

function [M, G, M_v, Vp] = H_aw_RL()
%molecular physiochemical property
pKa = 7.8;
logPN = 4.49 ;
logPD = logPN-3.7 ;
z = 1;
% %weighted
% Constant
T = 273.15+37;
R = 8.314;
F = 96484.56;
%lipid fraction
LaEp = 0.2;
LimEp = 0.05;
LcEp = 0.05 ;
Lint = 0;
Lsm = 0.05;
LimInt = 0.05;
LcEd = 0.05;
Lp = 0;
%volumetric water fraction=1-lipid fraction
WaEp = 1 - LaEp;
WimEp = 1 - LimEp;
WcEp = 1 - LcEp;
Wint = 1 - Lint;
Wsm = 1 - Lsm;
WimInt = 1 - LimInt;
WcEd = 1 - LcEd;
Wp = 1 - Lp;
%activity coefficient of species(N:neutral,D:desociated)
GaEpN = 1;
GaEpD = 1;
GimEpN = 1.23;
GimEpD = 0.74;
GcEpN = 1.23;
GcEpD = 0.74;
GintN = 1;
GintD = 1;
GsmN = 1.23;
GsmD = 0.74;
GimIntN = 1.23;
GimIntD = 0.74;

```

```

GcEdN = 1.23;
GcEdD = 0.74;
GpN = 1;
GpD = 1;

% By Jingyu Yu (used in publication) parameters in airways
% Areas and volumes (m^2, m^3) for 7 membranes and corresponding compartments
AaEp = 108*10^(-4);%literature
AbEp = AaEp;%assuming same with apical
AimEp = 0;%No macrophage
AimInt = 0.01*AaEp;%estimate
Asm = AaEp*2; % two side, double the surface area of airway,T model
AbEd = AaEp/5;%estimated 1/5 surface of epithelium
AaEd = AbEd;% same as basical side
%volumes for 8 compartments(m3)
ASL = 15; %um literature
VaEp = AaEp*ASL*10^(-6); %15 um thickness
VimEp = 10^(-30); %10^(-12)*VaEp; % Anynumber,No macrophage at surface
VcEp = 0.072*10^(-6); % estimated from yori model,basement membrane->surface area-
>thickness of each generation
Vint = AaEp*1*10^(-6);%estimated
Vsm = 0.047*10^(-6);%% estimated from yori model,basement membrane->surface area-
>thickness of each generation
VimInt = 0.01*Vint;%setimated
VcEd = AbEd*0.4*10^(-6); %estimated from literature,thickness of endothelium in AW
% Vp = 5; %total blood

R_org = 0.1;
% calculate constant
VcEpMito = R_org*VcEp;
VcEpLyso = R_org*VcEp;
VcEdMito = R_org*VcEd ;
VcEdLyso = R_org*VcEd ;
VsmMito = R_org*Vsm;
VsmLyso = R_org*Vsm;

AcEpMito = 5.9924e+006*VcEpMito ;
AcEpLyso = 5.9924e+006*VcEpLyso ;
AcEdMito = 5.9924e+006*VcEdMito ;
AcEdLyso = 5.9924e+006*VcEdLyso ;
AsmMito = 5.9924e+006*VsmMito ;
AsmLyso = 5.9924e+006*VsmMito ;
%#####

M_v = diag([VaEp,VimEp,VcEp,VcEpMito,VcEpLyso,Vint,Vsm, VsmMito, VsmLyso, VimInt, VcEd,
VcEdMito, VcEdLyso]);
V_LUN = trace(M_v)*10^6;

```



```

Vp = 340*10^(-9)*V_LUN;

% Membrane potential (V)
EaEp = -0.0093;
EbEp = 0.0119;%0.0119;
EimEp = -0.06;
Esm = -0.06;
EimInt = -0.06;
EbEd = -0.06;
EaEd = -0.06;
% pH values
pHaEp = 7.4;
pHimEp = 7.0;
pHcEp = 7.0;
pHint = 7.0;
pHsm = 7.0;
pHimInt = 7.0;
pHcEd = 7.0;
pHp = 7.4;

%adjustment for logP
if ( abs(z-1) <= 10^(-6) )
    logP_nlipT = 0.33*logPN+2.2 ;
    logP_dlipT = 0.37*logPD+2 ;
end
if ( abs(z+1) <= 10^(-6) )
    logP_nlipT = 0.37*logPN+2.2 ;
    logP_dlipT = 0.33*logPD+2.6 ;
end
if ( abs(z-0) <= 10^(-5) )
    logP_nlipT = 0.33*logPN+2.2 ;
    logP_dlipT = 0.33*logPD+2.2 ;
end

% logP_nlipT = logPN;
% logP_dlipT = logPD;

% Get the first two decimals
logP_n = round(logP_nlipT*100)/100 ;
logP_d = round(logP_dlipT*100)/100 ;
%calculate the membrane permeability
% logP_n = logPN;
% logP_d = logPD;
Pn = 10^(logP_n-6.7)*60; % in 1/min
Pd = 10^(logP_d-6.7)*60; % in 1/min

i = -sign(z) ;

```

```

%calculate N for flux of ion happening at 7 membranes
C = z*F/(R*T);
NaEp = C*(-EaEp) ;
NbEp = C*EbEp ;
NimEp = C*EimEp ;
Nsm = C*Esm ;
NimInt = C*EimInt ;
NbEd = C*(-EbEd) ;
NaEd = C*EaEd ;
%calculate Kn and Kd for 8 compartments
N = 1.22*10^(logP_n);
D = 1.22*10^(logP_d);

Kd = 229.9334;

KaEpN = N*LaEp ;
KaEpD = D*LaEp ;
KimEpN = N*LimEp ;
KimEpD = Kd*LimEp ;
KcEpN = N*LcEp ;
KcEpD = Kd*LcEp ;
KintN = N*Lint ;
KintD = D*Lint ;
KsmN = N*Lsm ;
KsmD = Kd*Lsm ;
KimIntN = N*LimInt ;
KimIntD = Kd*LimInt ;
KcEdN = N*LcEd ;
KcEdD = Kd*LcEd ;
KpN = N*Lp ;
KpD = D*Lp ;

%#####for mito and lyso compartments in cEp, sm and
cEd#####
LcEpMito = 0.05 ;
LcEpLyso = 0.05 ;
LsmMito = 0.05 ;
LsmLyso = 0.05 ;
LcEdMito = 0.05 ;
LcEdLyso = 0.05 ;

WcEpMito = 1-LcEpMito ;
WcEpLyso = 1-LcEpLyso ;
WsmMito = 1-LsmMito ;
WsmLyso = 1-LsmLyso ;
WcEdMito = 1-LcEdMito ;

```

WcEdLyso = 1-LcEdLyso ;

GcEpMitoN = 1.23 ;

GcEpMitoD = 0.74 ;

GcEpLysoN = 1.23 ;

GcEpLysoD = 0.74 ;

GsmMitoN = 1.23 ;

GsmMitoD = 0.74 ;

GsmLysoN = 1.23 ;

GsmLysoD = 0.74 ;

GcEdMitoN = 1.23 ;

GcEdMitoD = 0.74 ;

GcEdLysoN = 1.23 ;

GcEdLysoD = 0.74 ;

EcEpMito = -0.16 ;

EcEpLyso = +0.01 ;

EsmMito = -0.16 ;

EsmLyso = +0.01 ;

EcEdMito = -0.16 ;

EcEdLyso = +0.01 ;

pHcEpMito = 8 ;

pHcEpLyso = 5 ;

pHsmMito = 8 ;

pHsmLyso = 5 ;

pHcEdMito = 8 ;

pHcEdLyso = 5 ;

NcEpMito = C\*EcEpMito ;

NcEpLyso = C\*EcEpLyso ;

NsmMito = C\*EsmMito ;

NsmLyso = C\*EsmLyso ;

NcEdMito = C\*EcEdMito ;

NcEdLyso = C\*EcEdLyso ;

KcEpMitoN = N\*LcEpMito ;

KcEpMitoD = Kd\*LcEpMito ;

KcEpLysoN = N\*LcEpLyso ;

KcEpLysoD = Kd\*LcEpLyso ;

KsmMitoN = N\*LsmMito ;

KsmMitoD = Kd\*LsmMito ;

KsmLysoN = N\*LsmLyso ;  
KsmLysoD = Kd\*LsmLyso ;

KcEdMitoN = N\*LcEdMito ;  
KcEdMitoD = Kd\*LcEdMito ;  
KcEdLysoN = N\*LcEdLyso ;  
KcEdLysoD = Kd\*LcEdLyso ;

fcEpMitoN = 1/(WcEpMito/GcEpMitoN+KcEpMitoN/GcEpMitoN+WcEpMito\*10^(i\*(pHcEpMito-pKa))/GcEpMitoD...  
+KcEpMitoD\*10^(i\*(pHcEpMito-pKa))/GcEpMitoD);  
fcEpMitoD = fcEpMitoN\*10^(i\*(pHcEpMito-pKa));

fcEpLysoN = 1/(WcEpLyso/GcEpLysoN+KcEpLysoN/GcEpLysoN+WcEpLyso\*10^(i\*(pHcEpLyso-pKa))/GcEpLysoD...  
+KcEpLysoD\*10^(i\*(pHcEpLyso-pKa))/GcEpLysoD);  
fcEpLysoD = fcEpLysoN\*10^(i\*(pHcEpLyso-pKa));

fsmMitoN = 1/(WsmMito/GsmMitoN+KsmMitoN/GsmMitoN+WsmMito\*10^(i\*(pHsmMito-pKa))/GsmMitoD...  
+KsmMitoD\*10^(i\*(pHsmMito-pKa))/GsmMitoD);  
fsmMitoD = fsmMitoN\*10^(i\*(pHsmMito-pKa));

fsmLysoN = 1/(WsmLyso/GsmLysoN+KsmLysoN/GsmLysoN+WsmLyso\*10^(i\*(pHsmLyso-pKa))/GsmLysoD...  
+KsmLysoD\*10^(i\*(pHsmLyso-pKa))/GsmLysoD);  
fsmLysoD = fsmLysoN\*10^(i\*(pHsmLyso-pKa));

fcEdMitoN = 1/(WcEdMito/GcEdMitoN+KcEdMitoN/GcEdMitoN+WcEdMito\*10^(i\*(pHcEdMito-pKa))/GcEdMitoD...  
+KcEdMitoD\*10^(i\*(pHcEdMito-pKa))/GcEdMitoD);  
fcEdMitoD = fcEdMitoN\*10^(i\*(pHcEdMito-pKa));

fcEdLysoN = 1/(WcEdLyso/GcEdLysoN+KcEdLysoN/GcEdLysoN+WcEdLyso\*10^(i\*(pHcEdLyso-pKa))/GcEdLysoD...  
+KcEdLysoD\*10^(i\*(pHcEdLyso-pKa))/GcEdLysoD);  
fcEdLysoD = fcEdLysoN\*10^(i\*(pHcEdLyso-pKa));

%#####

%compute the fn and fd for 8 compartments

faEpN = 1/(WaEp/GaEpN+KaEpN/GaEpN+WaEp\*10^(i\*(pHaEp-pKa))/GaEpD...  
+KaEpD\*10^(i\*(pHaEp-pKa))/GaEpD);

```

faEpD = faEpN*10^(i*(pHaEp-pKa));
fimEpN = 1/(WimEp/GimEpN+KimEpN/GimEpN+WimEp*10^(i*(pHimEp-pKa))/GimEpD...
+KimEpD*10^(i*(pHimEp-pKa))/GimEpD);
fimEpD = fimEpN*10^(i*(pHimEp-pKa));
fcEpN = 1/(WcEp/GcEpN+KcEpN/GcEpN+WcEp*10^(i*(pHcEp-pKa))/GcEpD...
+KcEpD*10^(i*(pHcEp-pKa))/GcEpD);
fcEpD = fcEpN*10^(i*(pHcEp-pKa));
fintN = 1/(Wint/GintN+KintN/GintN+Wint*10^(i*(pHint-pKa))/GintD...
+KintD*10^(i*(pHint-pKa))/GintD);
fintD = fintN*10^(i*(pHint-pKa));
fimIntN = 1/(WimInt/GimIntN+KimIntN/GimIntN+WimInt*10^(i*(pHimInt-pKa))/GimIntD...
+KimIntD*10^(i*(pHimInt-pKa))/GimIntD);
fimIntD = fimIntN*10^(i*(pHimInt-pKa));
fsmN = 1/(Wsm/GsmN+KsmN/GsmN+Wsm*10^(i*(pHsm-pKa))/GsmD...
+KsmD*10^(i*(pHsm-pKa))/GsmD);
fsmD = fsmN*10^(i*(pHsm-pKa));
fcEdN = 1/(WcEd/GcEdN+KcEdN/GcEdN+WcEd*10^(i*(pHcEd-pKa))/GcEdD...
+KcEdD*10^(i*(pHcEd-pKa))/GcEdD);
fcEdD = fcEdN*10^(i*(pHcEd-pKa));
fpN = 1/(Wp/GpN+KpN/GpN+Wp*10^(i*(pHp-pKa))/GpD...
+KpD*10^(i*(pHp-pKa))/GpD);
fpD = fpN*10^(i*(pHp-pKa));

%mucus clearance
%Ke = 0.02;
Ke = 0;

%compute the coefficient matrix for ODEs
% #1: Surface Lining Liquid (aEp)
KaEp_aEp = AaEp/VaEp*(Pn*(-faEpN)+Pd*NaEp/(exp(NaEp)-1)*(-faEpD)*exp(NaEp))...
-AimEp/VaEp*(Pn*faEpN+Pd*NimEp/(exp(NimEp)-1)*faEpD)...
-Ke;
KaEp_imEp = -AimEp/VaEp*(Pn*(-fimEpN)+Pd*NimEp/(exp(NimEp)-1)*(-fimEpD)*exp(NimEp));
KaEp_cEp = AaEp/VaEp*(Pn*(fcEpN)+Pd*NaEp/(exp(NaEp)-1)*(fcEpD));
KaEp_cEpMito = 0;
KaEp_cEpLyso = 0;
KaEp_int = 0;
KaEp_sm = 0;
KaEp_smMito = 0;
KaEp_smLyso = 0;
KaEp_imInt = 0;
KaEp_cEd = 0;
KaEp_cEdMito = 0;
KaEp_cEdLyso = 0;
KaEp_p = 0;
SaEp = 0;

```

% #2: Macrophage (imEp)

KimEp\_aEp = AimEp/VimEp\*(Pn\*faEpN+Pd\*NimEp/(exp(NimEp)-1)\*faEpD);

KimEp\_imEp = AimEp/VimEp\*(Pn\*(-fimEpN)+Pd\*NimEp/(exp(NimEp)-1)\*(-fimEpD)\*exp(NimEp));

KimEp\_cEp = 0;

KimEp\_cEpMito = 0 ;

KimEp\_cEpLyso = 0 ;

KimEp\_int = 0;

KimEp\_sm = 0;

KimEp\_smMito = 0;

KimEp\_smLyso = 0;

KimEp\_imInt = 0;

KimEp\_cEd = 0;

KimEp\_cEdMito = 0 ;

KimEp\_cEdLyso = 0 ;

KimEp\_p = 0;

SimEp = 0;

% #3: Epithelial Cells (cEp)

KcEp\_aEp = -AaEp/VcEp\*(Pn\*(-faEpN)+Pd\*NaEp/(exp(NaEp)-1)\*(-faEpD)\*exp(NaEp));

KcEp\_imEp = 0;

KcEp\_cEp = -AaEp/VcEp\*(Pn\*(fcEpN)+Pd\*NaEp/(exp(NaEp)-1)\*(fcEpD))...

-AcEpMito/VcEp\*(Pn\*fcEpN+Pd\*NcEpMito/(exp(NcEpMito)-1)\*fcEpD)...

-AcEpLyso/VcEp\*(Pn\*fcEpN+Pd\*NcEpLyso/(exp(NcEpLyso)-1)\*fcEpD)...

+AbEp/VcEp\*(Pn\*(-fcEpN)+Pd\*NbEp/(exp(NbEp)-1)\*(-fcEpD)\*exp(NbEp));

KcEp\_cEpMito = -AcEpMito/VcEp\*(Pn\*(-fcEpMitoN)+Pd\*NcEpMito/(exp(NcEpMito)-1)\*(-fcEpMitoD)\*exp(NcEpMito)) ;

KcEp\_cEpLyso = -AcEpLyso/VcEp\*(Pn\*(-fcEpLysoN)+Pd\*NcEpLyso/(exp(NcEpLyso)-1)\*(-fcEpLysoD)\*exp(NcEpLyso)) ;

KcEp\_int = AbEp/VcEp\*(Pn\*(fintN)+Pd\*NbEp/(exp(NbEp)-1)\*(fintD));

KcEp\_sm = 0;

KcEp\_smMito = 0;

KcEp\_smLyso = 0;

KcEp\_imInt = 0;

KcEp\_cEd = 0;

KcEp\_cEdMito = 0 ;

KcEp\_cEdLyso = 0 ;

KcEp\_p = 0;

ScEp = 0;

% #4: : Epithelial Cells (cEpMito)

KcEpMito\_aEp = 0;

KcEpMito\_imEp = 0;

KcEpMito\_cEp = AcEpMito/VcEpMito\*(Pn\*(fcEpN)+Pd\*NcEpMito/(exp(NcEpMito)-1)\*(fcEpD));

KcEpMito\_cEpMito = AcEpMito/VcEpMito\*(Pn\*(-fcEpMitoN)+Pd\*NcEpMito/(exp(NcEpMito)-1)\*(-fcEpMitoD)\*exp(NcEpMito));

KcEpMito\_cEpLyso = 0 ;

```

KcEpMito_int = 0 ;
KcEpMito_sm = 0;
KcEpMito_smMito = 0;
KcEpMito_smLyso = 0;
KcEpMito_imInt = 0;
KcEpMito_cEd = 0;
KcEpMito_cEdMito = 0 ;
KcEpMito_cEdLyso = 0 ;
KcEpMito_p = 0;
ScEpMito = 0;

```

% #5: : Epithelial Cells (cEpLyso)

```

KcEpLyso_aEp = 0;
KcEpLyso_imEp = 0;
KcEpLyso_cEp = AcEpLyso/VcEpLyso*(Pn*(fcEpN)+Pd*NcEpLyso/(exp(NcEpLyso)-1)*(fcEpD));
KcEpLyso_cEpMito = 0 ;
KcEpLyso_cEpLyso = AcEpLyso/VcEpLyso*(Pn*(-fcEpLysoN)+Pd*NcEpLyso/(exp(NcEpLyso)-1)*(-fcEpLysoD)*exp(NcEpLyso));
KcEpLyso_int = 0 ;
KcEpLyso_sm = 0;
KcEpLyso_smMito = 0;
KcEpLyso_smLyso = 0;
KcEpLyso_imInt = 0;
KcEpLyso_cEd = 0;
KcEpLyso_cEdMito = 0 ;
KcEpLyso_cEdLyso = 0 ;
KcEpLyso_p = 0;
ScEpLyso = 0;

```

% #6: : Interstitium (int)

```

Kint_aEp = 0;
Kint_imEp = 0;
Kint_cEp = -AbEp/Vint*(Pn*(-fcEpN)+Pd*NbEp/(exp(NbEp)-1)*(-fcEpD)*exp(NbEp));
Kint_cEpMito = 0 ;
Kint_cEpLyso = 0 ;
Kint_int = -AbEp/Vint*(Pn*(fintN)+Pd*NbEp/(exp(NbEp)-1)*(fintD))...
          -Asm/Vint*(Pn*fintN+Pd*Nsm/(exp(Nsm)-1)*fintD)...
          -AimInt/Vint*(Pn*fintN+Pd*NimInt/(exp(NimInt)-1)*fintD)...
          +AbEd/Vint*(Pn*(-fintN)+Pd*NbEd/(exp(NbEd)-1)*(-fintD)*exp(NbEd));
Kint_sm = -Asm/Vint*(Pn*(-fsmN)+Pd*Nsm/(exp(Nsm)-1)*(-fsmD)*exp(Nsm));
Kint_smMito = 0;
Kint_smLyso = 0;
Kint_imInt = -AimInt/Vint*(Pn*(-fimIntN)+Pd*NimInt/(exp(NimInt)-1)*(-fimIntD)*exp(NimInt));
Kint_cEd = AbEd/Vint*(Pn*(fcEdN)+Pd*NbEd/(exp(NbEd)-1)*(fcEdD));
Kint_cEdMito = 0 ;
Kint_cEdLyso = 0 ;
Kint_p = 0;

```

Sint = 0;

% #7: Smooth Muscle (sm)

Ksm\_aEp = 0;

Ksm\_imEp = 0;

Ksm\_cEp = 0;

Ksm\_cEpMito = 0 ;

Ksm\_cEpLyso = 0 ;

Ksm\_int = Asm/Vsm\*(Pn\*fintN+Pd\*Nsm/(exp(Nsm)-1)\*fintD);

Ksm\_sm = Asm/Vsm\*(Pn\*(-fsmN)+Pd\*Nsm/(exp(Nsm)-1)\*(-fsmD)\*exp(Nsm))...

-AsmMito/Vsm\*(Pn\*fsmN+Pd\*NsmMito/(exp(NsmMito)-1)\*fsmD)...

-AsmLyso/Vsm\*(Pn\*fsmN+Pd\*NsmLyso/(exp(NsmLyso)-1)\*fsmD);

Ksm\_smMito = -AsmMito/Vsm\*(Pn\*(-fsmMitoN)+Pd\*NsmMito/(exp(NsmMito)-1)\*(-fsmMitoD)\*exp(NsmMito)) ;

Ksm\_smLyso = -AsmLyso/Vsm\*(Pn\*(-fsmLysoN)+Pd\*NsmLyso/(exp(NsmLyso)-1)\*(-fsmLysoD)\*exp(NsmLyso)) ;

Ksm\_imInt = 0;

Ksm\_cEd = 0;

Ksm\_cEdMito = 0 ;

Ksm\_cEdLyso = 0 ;

Ksm\_p = 0;

Ssm = 0;

% #8: Smooth Muscle (smMito)

KsmMito\_aEp = 0;

KsmMito\_imEp = 0;

KsmMito\_cEp = 0;

KsmMito\_cEpMito = 0;

KsmMito\_cEpLyso = 0 ;

KsmMito\_int = 0 ;

KsmMito\_sm = AsmMito/VsmMito\*(Pn\*(fsmN)+Pd\*NsmMito/(exp(NsmMito)-1)\*(fsmD));

KsmMito\_smMito = AsmMito/VsmMito\*(Pn\*(-fsmMitoN)+Pd\*NsmMito/(exp(NsmMito)-1)\*(-fsmMitoD)\*exp(NsmMito));

KsmMito\_smLyso = 0;

KsmMito\_imInt = 0;

KsmMito\_cEd = 0;

KsmMito\_cEdMito = 0 ;

KsmMito\_cEdLyso = 0 ;

KsmMito\_p = 0;

SsmMito = 0;

% #9: Smooth Muscle (smLyso)

KsmLyso\_aEp = 0;

KsmLyso\_imEp = 0;

KsmLyso\_cEp = 0;

KsmLyso\_cEpMito = 0 ;



```

KsmLyso_cEpLyso = 0;
KsmLyso_int = 0 ;
KsmLyso_sm = AsmLyso/VsmLyso*(Pn*(fsmN)+Pd*NsmLyso/(exp(NsmLyso)-1)*(fsmD));
KsmLyso_smMito = 0;
KsmLyso_smLyso = AsmLyso/VsmLyso*(Pn*(-fsmLysoN)+Pd*NsmLyso/(exp(NsmLyso)-1)*(-fsmLysoD)*exp(NsmLyso));
KsmLyso_imInt = 0;
KsmLyso_cEd = 0;
KsmLyso_cEdMito = 0 ;
KsmLyso_cEdLyso = 0 ;
KsmLyso_p = 0;
SsmLyso = 0;

```

```

% #10: Immune Cells (imInt)

```

```

KimInt_aEp = 0;
KimInt_imEp = 0;
KimInt_cEp = 0;
KimInt_cEpMito = 0;
KimInt_cEpLyso = 0;
KimInt_int = AimInt/VimInt*(Pn*fintN+Pd*NimInt/(exp(NimInt)-1)*fintD);
KimInt_sm = 0;
KimInt_smMito = 0;
KimInt_smLyso = 0;
KimInt_imInt = AimInt/VimInt*(Pn*(-fimIntN)+Pd*NimInt/(exp(NimInt)-1)*(-fimIntD)*exp(NimInt));
KimInt_cEd = 0;
KimInt_cEdMito = 0;
KimInt_cEdLyso = 0;
KimInt_p = 0;
SimInt = 0;

```

```

% #11: Endothelial celss (cEd)

```

```

KcEd_aEp = 0;
KcEd_imEp = 0;
KcEd_cEp = 0;
KcEd_cEpMito = 0;
KcEd_cEpLyso = 0;
KcEd_int = -AbEd/VcEd*(Pn*(-fintN)+Pd*NbEd/(exp(NbEd)-1)*(-fintD)*exp(NbEd));
KcEd_sm = 0;
KcEd_smMito = 0;
KcEd_smLyso = 0;
KcEd_imInt = 0;
KcEd_cEd = -AbEd/VcEd*(Pn*(fcEdN)+Pd*NbEd/(exp(NbEd)-1)*(fcEdD))...
    -AcEdMito/VcEd*(Pn*fcEdN+Pd*NcEdMito/(exp(NcEdMito)-1)*fcEdD)...
    -AcEdLyso/VcEd*(Pn*fcEdN+Pd*NcEdLyso/(exp(NcEdLyso)-1)*fcEdD)...
    +AaEd/VcEd*(Pn*(-fcEdN)+Pd*NaEd/(exp(NaEd)-1)*(-fcEdD)*exp(NaEd));

```

```

KcEd_cEdMito = -AcEdMito/VcEd*(Pn*(-fcEdMitoN)+Pd*NcEdMito/(exp(NcEdMito)-1)*(-
fcEdMitoD)*exp(NcEdMito));
KcEd_cEdLyso = -AcEdLyso/VcEd*(Pn*(-fcEdLysoN)+Pd*NcEdLyso/(exp(NcEdLyso)-1)*(-
fcEdLysoD)*exp(NcEdLyso));
KcEd_p = AaEd/VcEd*(Pn*(fpN)+Pd*NaEd/(exp(NaEd)-1)*(fpD));
ScEd = 0;

% #12: Endothelial celss (cEd) Mito
KcEdMito_aEp = 0;
KcEdMito_imEp = 0;
KcEdMito_cEp = 0;
KcEdMito_cEpMito = 0;
KcEdMito_cEpLyso = 0;
KcEdMito_int = 0;
KcEdMito_sm = 0;
KcEdMito_smMito = 0;
KcEdMito_smLyso = 0;
KcEdMito_imInt = 0;
KcEdMito_cEd = AcEdMito/VcEdMito*(Pn*(fcEdN)+Pd*NcEdMito/(exp(NcEdMito)-1)*(fcEdD)) ;
KcEdMito_cEdMito = AcEdMito/VcEdMito*(Pn*(-fcEdMitoN)+Pd*NcEdMito/(exp(NcEdMito)-
1)*(-fcEdMitoD)*exp(NcEdMito));
KcEdMito_cEdLyso = 0;
KcEdMito_p = 0 ;
ScEdMito = 0;

% #13: Endothelial celss (cEd) Lyso
KcEdLyso_aEp = 0;
KcEdLyso_imEp = 0;
KcEdLyso_cEp = 0;
KcEdLyso_cEpMito = 0;
KcEdLyso_cEpLyso = 0;
KcEdLyso_int = 0 ;
KcEdLyso_sm = 0;
KcEdLyso_smMito = 0;
KcEdLyso_smLyso = 0;
KcEdLyso_imInt = 0;
KcEdLyso_cEd = AcEdLyso/VcEdLyso*(Pn*(fcEdN)+Pd*NcEdLyso/(exp(NcEdLyso)-1)*(fcEdD)) ;
KcEdLyso_cEdMito = 0;
KcEdLyso_cEdLyso = AcEdLyso/VcEdLyso*(Pn*(-fcEdLysoN)+Pd*NcEdLyso/(exp(NcEdLyso)-1)*(-
fcEdLysoD)*exp(NcEdLyso));
KcEdLyso_p = 0;
ScEdLyso = 0;

% #14: plasma(p)
Kp_aEp = 0;
Kp_imEp = 0;
Kp_cEp = 0;

```

$Kp\_cEpMito = 0;$   
 $Kp\_cEpLyso = 0;$   
 $Kp\_int = 0;$   
 $Kp\_sm = 0;$   
 $Kp\_smMito = 0;$   
 $Kp\_smLyso = 0;$   
 $Kp\_imInt = 0;$   
 $Kp\_cEd = -AaEd/Vp*(Pn*(-fcEdN)+Pd*NaEd/(exp(NaEd)-1)*(-fcEdD)*exp(NaEd));$   
 $Kp\_cEdMito = 0;$   
 $Kp\_cEdLyso = 0;$   
 $Kp\_p = -AaEd/Vp*(Pn*(fpN)+Pd*NaEd/(exp(NaEd)-1)*(fpD));$   
 $Sp = 0;$

M =

[KaEp\_aEp,KaEp\_imEp,KaEp\_cEp,KaEp\_cEpMito,KaEp\_cEpLyso,KaEp\_int,KaEp\_sm,KaEp\_smMito,KaEp\_smLyso,KaEp\_imInt,KaEp\_cEd,KaEp\_cEdMito,KaEp\_cEdLyso,KaEp\_p;...

KimEp\_aEp,KimEp\_imEp,KimEp\_cEp,KimEp\_cEpMito,KimEp\_cEpLyso,KimEp\_int,KimEp\_sm,KimEp\_smMito,KimEp\_smLyso,KimEp\_imInt,KimEp\_cEd,KimEp\_cEdMito,KimEp\_cEdLyso,KimEp\_p;...

KcEp\_aEp,KcEp\_imEp,KcEp\_cEp,KcEp\_cEpMito,KcEp\_cEpLyso,KcEp\_int,KcEp\_sm,KcEp\_smMito,KcEp\_smLyso,KcEp\_imInt,KcEp\_cEd,KcEp\_cEdMito,KcEp\_cEdLyso,KcEp\_p;...

KcEpMito\_aEp,KcEpMito\_imEp,KcEpMito\_cEp,KcEpMito\_cEpMito,KcEpMito\_cEpLyso,KcEpMito\_int,KcEpMito\_sm,KcEpMito\_smMito,KcEpMito\_smLyso,KcEpMito\_imInt,KcEpMito\_cEd,KcEpMito\_cEdMito,KcEpMito\_cEdLyso,KcEpMito\_p;...

KcEpLyso\_aEp,KcEpLyso\_imEp,KcEpLyso\_cEp,KcEpLyso\_cEpMito,KcEpLyso\_cEpLyso,KcEpLyso\_int,KcEpLyso\_sm,KcEpLyso\_smMito,KcEpLyso\_smLyso,KcEpLyso\_imInt,KcEpLyso\_cEd,KcEpLyso\_cEdMito,KcEpLyso\_cEdLyso,KcEpLyso\_p;...

Kint\_aEp,Kint\_imEp,Kint\_cEp,Kint\_cEpMito,Kint\_cEpLyso,Kint\_int,Kint\_sm,Kint\_smMito,Kint\_smLyso,Kint\_imInt,Kint\_cEd,Kint\_cEdMito,Kint\_cEdLyso,Kint\_p;...

Ksm\_aEp,Ksm\_imEp,Ksm\_cEp,Ksm\_cEpMito,Ksm\_cEpLyso,Ksm\_int,Ksm\_sm,Ksm\_smMito,Ksm\_smLyso,Ksm\_imInt,Ksm\_cEd,Ksm\_cEdMito,Ksm\_cEdLyso,Ksm\_p;...

KsmMito\_aEp,KsmMito\_imEp,KsmMito\_cEp,KsmMito\_cEpMito,KsmMito\_cEpLyso,KsmMito\_int,KsmMito\_sm,KsmMito\_smMito,KsmMito\_smLyso,KsmMito\_imInt,KsmMito\_cEd,KsmMito\_cEdMito,KsmMito\_cEdLyso,KsmMito\_p;...

KsmLyso\_aEp,KsmLyso\_imEp,KsmLyso\_cEp,KsmLyso\_cEpMito,KsmLyso\_cEpLyso,KsmLyso\_int,KsmLyso\_sm,KsmLyso\_smMito,KsmLyso\_smLyso,KsmLyso\_imInt,KsmLyso\_cEd,KsmLyso\_cEdMito,KsmLyso\_cEdLyso,KsmLyso\_p;...

KimInt\_aEp,KimInt\_imEp,KimInt\_cEp,KimInt\_cEpMito,KimInt\_cEpLyso,KimInt\_int,KimInt\_sm,Kim

Int\_smMito, KimInt\_smLyso, KimInt\_imInt, KimInt\_cEd, KimInt\_cEdMito, KimInt\_cEdLyso, KimInt\_p;  
...

KcEd\_aEp, KcEd\_imEp, KcEd\_cEp, KcEd\_cEpMito, KcEd\_cEpLyso, KcEd\_int, KcEd\_sm, KcEd\_smMito, KcEd\_smLyso, KcEd\_imInt, KcEd\_cEd, KcEd\_cEdMito, KcEd\_cEdLyso, KcEd\_p;...

KcEdMito\_aEp, KcEdMito\_imEp, KcEdMito\_cEp, KcEdMito\_cEpMito, KcEdMito\_cEpLyso, KcEdMito\_int, KcEdMito\_sm, KcEdMito\_smMito, KcEdMito\_smLyso, KcEdMito\_imInt, KcEdMito\_cEd, KcEdMito\_cEdMito, KcEdMito\_cEdLyso, KcEdMito\_p;...

KcEdLyso\_aEp, KcEdLyso\_imEp, KcEdLyso\_cEp, KcEdLyso\_cEpMito, KcEdLyso\_cEpLyso, KcEdLyso\_int, KcEdLyso\_sm, KcEdLyso\_smMito, KcEdLyso\_smLyso, KcEdLyso\_imInt, KcEdLyso\_cEd, KcEdLyso\_cEdMito, KcEdLyso\_cEdLyso, KcEdLyso\_p;...

Kp\_aEp, Kp\_imEp, Kp\_cEp, Kp\_cEpMito, Kp\_cEpLyso, Kp\_int, Kp\_sm, Kp\_smMito, Kp\_smLyso, Kp\_imInt, Kp\_cEd, Kp\_cEdMito, Kp\_cEdLyso, Kp\_p];

G =  
[SaEp, SimEp, ScEp, ScEpMito, ScEpLyso, Sint, Ssm, SsmMito, SsmLyso, SimInt, ScEd, ScEdMito, ScEdLyso, Sp]';

% This is the generic PBPK model of atenolol in rat  
% Data were extracted from: Street JA, Hemsworth BA, Roach AG, Day MD  
% Tissue levels of several radiolabelled beta-adrenoceptor antagonists after intravenous administration in rats.  
% Arch Int Pharmacodyn Ther. 1979 Feb;237(2):180-90.  
% tissue pharmacokinetic data  
%#####

% Virtual Lung (with Mito and Lyso in cEp and cEd) - PBPK  
% Six big compartment model: arterial blood, lung, venous blood, liver, brain, and rest

```
function [dConc] = H_Lung_RL(t, Conc)
global V_VEN Vp fup B2P Vtot; % V_ART V_LUN V_LUNp V_LUNb V_HRT V_BRA V_LIV V_GUT
V_KID V_MUS V_SKN V_ADI V_SPL V_BON ;
%call lung model
[LungM, LungG, M_v, Vp] = H_al_RL(); % get the coefficients for the Alveolar Region
[LungM_Airways, LungG_Airways, M_v_Airways, Vp_Airways] = H_aw_RL(); % get the
coefficients for the airways
```

% Body weight (kg)  
BW = 0.25 ;

% From PATRICK POULIN, FRANK-PETER. THEIL Prediction of Pharmacokinetics prior to In Vivo Studies.

```

% II. Generic Physiologically Based Pharmacokinetic Models of Drug Disposition
% Blood flow rate (mL/min)
% Note that 'Q_HRT+Q_BRA+Q_LIV+Q_KID+Q_MUS+Q_SKN+Q_ADI+Q_BON ' should be equal to
or less than 'Q_tot'
% Less than: if other tissues are not considered, such as testes, thymus
% Also note that Q_GUT and Q_SPL are not input for Q_tot
% Q (liver hepatic artery) = Q_LIV - Q_GUT - Q_SPL
Q_tot = 0.235*BW^0.75*1000 ; % Total cardiac output = 0.235 * body weight (kg)^0.75 (L/min)
% Q_tot = 80 ;
Q_LUN = Q_tot ;
Q_HRT = 0.049*Q_tot ;
Q_BRA = 0.02*Q_tot ;
Q_LIV = 0.175*Q_tot ; % Q(hepatic arterial) = Q_LIV-Q_GUT-Q_SPL
Q_GUT = 0.131*Q_tot ;
Q_KID = 0.141*Q_tot ;
Q_MUS = 0.278*Q_tot ;
Q_SKN = 0.058*Q_tot ;
Q_ADI = 0.07*Q_tot ;
Q_SPL = 0.02*Q_tot ;
Q_BON = 0.122*Q_tot ;
Q_Airways = 0.01*Q_tot;
Q_RES = Q_tot - Q_HRT - Q_BRA - Q_LIV - Q_KID - Q_MUS - Q_SKN - Q_ADI - Q_BON -
Q_Airways ;

```

```

% From PATRICK POULIN, FRANK-PETER. THEILPrediction of Pharmacokinetics prior to In Vivo
Studies.

```

```

% II. Generic Physiologically Based Pharmacokinetic Models of Drug Disposition
% test = V_ART + V_LUN + V_VEN + V_HRT + V_BRA + V_LIV + V_GUT + V_KID + V_MUS + V_SKN
+ V_ADI + V_SPL + V_BON
% test
=0.0272+0.005+0.0544+0.0033+0.0057+0.0366+0.027+0.0073+0.404+0.19+0.076+0.002+0.0415
= 0.88

```

```

% Volume of each organ (mL)= fraction of total body volume (L/kg)*BW*1000
V_ART = 0.0272*BW*1000 ;
V_LUN = trace(M_v)*10^6; % total lung volume, in mL
V_LUNp = Vp*10^(6) ; % plasma volume in the lung, obtained from 'LungRatReverse' (in m^3),
converted to mL
V_LUNb = 519*10^(-3)*V_LUN ; % total blood volume in the lung = 519uL/g
V_VEN = 0.0544*BW*1000 ;
V_HRT = 0.0033*BW*1000 ;
V_BRA = 0.0057*BW*1000 ;
V_LIV = 0.0366*BW*1000 ;
V_GUT = 0.027*BW*1000 ;
V_KID = 0.0073*BW*1000 ;
V_MUS = 0.404*BW*1000 ;

```

```

V_SKN = 0.19*BW*1000 ;
V_ADI = 0.076*BW*1000 ;
V_SPL = 0.002*BW*1000 ;
V_BON = 0.04148*BW*1000 ;
V_LUN_Airways = trace(M_v_Airways)*10^6 ;
V_LUNp_Airways = Vp_Airways*10^(6) ;
V_LUNb_Airways = 519*10^(-3)*V_LUN_Airways ;

V_RES = BW*1000-V_ART-V_LUN-V_LUNp-V_LUNb-V_LUN_Airways-V_LUNp_Airways-
V_LUNb_Airways-V_VEN - V_HRT...
-V_BRA-V_LIV-V_GUT-V_KID-V_MUS-V_SKN-V_ADI-V_SPL-V_BON ;

```

```

% Tissue : Blood partition coefficient = K(Tissue:Plasma)/B2P
% from PATRICK POULIN, FRANK-PETER THEIL. Prediction of Pharmacokinetics prior to In Vivo
Studies.

```

```

% II. Generic Physiologically Based Pharmacokinetic Models of Drug Disposition
% predicted values; experimental values are used if available

```

```

B2P = 0.80 ;
fup = 0.13 ;
% B2P = 1.03;%0.80 ;
% fup = 0.0735;%0.13 ;

% Kp_LUN = 6.46/B2P ;
Kp_LUN = 54.90/B2P ; % exp data
% Kp_HRT = 4.38/B2P ;
Kp_HRT = 4.97/B2P ; % exp data
%Kp_BRA = 13.54/B2P ;
Kp_BRA = 9.20/B2P ; % exp data
Kp_LIV = 5.67/B2P ;
Kp_GUT = 8.22/B2P ;
% Kp_KID = 5.18/B2P ;
Kp_KID = 3.80/B2P ; % exp data
% Kp_MUS = 3.20/B2P ;
Kp_MUS = 2.20/B2P ; % exp data
Kp_SKN = 7.22/B2P ;
Kp_ADI = 0.18/B2P ;
Kp_SPL = 2.98/B2P ;
Kp_BON = 6.90/B2P ;
Kp_RES = 1/B2P ; % arbitrary, could be optimized

```

```

% Dosing information mg/kg, rats weight = 0.25kg
Kiv = 0 ;

```

```

% Mass balance
% 1 - Arterial, ART

```

% 2 - Lung alveoli plasma free concentration, LUN,  
 % Cellular compartments of the lung alveoli:  
 % 15 - Surface lining liquid (aEp)  
 % 16 - Macrophage (imEp)  
 % 17 - Epithelial cells (cEp)  
 % 18 - Epithelial cells Mito (cEpMito)  
 % 19 - Epithelial cells Lyso (cEpLyso)  
 % 20 - Interstitium (int)  
 % 21 - Smooth muscle (sm)  
 % 22 - Immune cells (imInt)  
 % 23 - Endothelial cells (cEd)  
 % 24 - Endothelial cells Mito (cEdMito)  
 % 25 - Endothelial cells Lyso (cEdLyso)  
 % 3 - Venous, VEN  
 % 4 - Heart, HRT  
 % 5 - Brain, BRA  
 % 6 - Liver, LIV, may be eliminatin organ  
 % 7 - Gut, GUT  
 % 8 - Spleen, SPL  
 % 9 - Kidney, KID, may be elimination organ  
 % 10 - Muscle, MUS  
 % 11 - Skin, SKN  
 % 12 - Adipose, ADI  
 % 13 - Bone, BON  
 % 14 - Rest of body, RES  
 % 26 - Lung airway plasma free concentration, LUN\_airways  
 % Cellular compartments of the lung airways:  
 % 27 - Surface lining liquid (aEp\_airway)  
 % 28 - Macrophage (imEp\_airway)  
 % 29 - Epithelial cells (cEp\_airway)  
 % 30 - Epithelial cells Mito (cEpMito\_airway)  
 % 31 - Epithelial cells Lyso (cEpLyso\_airway)  
 % 32 - Interstitium (int\_airway)  
 % 33 - Smooth muscle (sm\_airway)  
 % 34 - Smooth muscle Mito (smMito\_airway)  
 % 35 - Smooth muscle Lyso (smLyso\_airway)  
 % 36 - Immune cells (imInt\_airway)  
 % 37 - Endothelial cells (cEd\_airway)  
 % 38 - Endothelial cells Mito (cEdMito\_airway)  
 % 39 - Endothelial cells Lyso (cEdLyso\_airway)

% fup: fraction of unbound in the plamsa

% Kp: Tissue:Blood partition coefficients =  $C_{\text{tissue, tot}} : C_{\text{blood, tot}}$

$d\text{Conc}(1) = \text{Conc}(2) * Q_{\text{tot}} / V_{\text{ART}} - \text{Conc}(1) * Q_{\text{tot}} / V_{\text{ART}} ; \% \text{ ART, arterial blood}$

$dConc(2) = Conc(3)*Q\_tot/V\_LUNb + (LungM(12,1)*Conc(15) + LungM(12,2)*Conc(16) + LungM(12,3)*Conc(17) + LungM(12,4)*Conc(18)...$   
 $+ LungM(12,5)*Conc(19) + LungM(12,6)*Conc(21) + LungM(12,7)*Conc(21) + LungM(12,8)*Conc(22) + LungM(12,9)*Conc(23) ...$   
 $+ LungM(12,10)*Conc(24) + LungM(12,11)*Conc(25) + LungM(12,12)*Conc(2)*fup/B2P + LungG(12))*V\_LUNp/V\_LUNb - Conc(2)*Q\_tot/V\_LUNb ;$   
 % 2 -Lung total blood concentration,  $C(2)*fup/B2P =$  free plasma conc in the lung alveoli

$dConc(15) = LungM(1,1)*Conc(15) + LungM(1,2)*Conc(16) + LungM(1,3)*Conc(17) + LungM(1,4)*Conc(18) + LungM(1,5)*Conc(19)...$   
 $+ LungM(1,6)*Conc(20) + LungM(1,7)*Conc(21) + LungM(1,8)*Conc(22) + LungM(1,9)*Conc(23) + LungM(1,10)*Conc(24)...$   
 $+ LungM(1,11)*Conc(25) + LungM(1,12)*Conc(2)*fup/B2P + LungG(1);$   
 % 15 - SurfaConce lining liquid (aEp)

$dConc(16) = LungM(2,1)*Conc(15) + LungM(2,2)*Conc(16) + LungM(2,3)*Conc(17) + LungM(2,4)*Conc(18) + LungM(2,5)*Conc(19)...$   
 $+ LungM(2,6)*Conc(20) + LungM(2,7)*Conc(21) + LungM(2,8)*Conc(22) + LungM(2,9)*Conc(23) + LungM(2,10)*Conc(24)...$   
 $+ LungM(2,11)*Conc(25) + LungM(2,12)*Conc(2)*fup/B2P + LungG(2);$   
 % 16 - Macrophage (imEp)

$dConc(17) = LungM(3,1)*Conc(15) + LungM(3,2)*Conc(16) + LungM(3,3)*Conc(17) + LungM(3,4)*Conc(18) + LungM(3,5)*Conc(19)...$   
 $+ LungM(3,6)*Conc(20) + LungM(3,7)*Conc(21) + LungM(3,8)*Conc(22) + LungM(3,9)*Conc(23) + LungM(3,10)*Conc(24)...$   
 $+ LungM(3,11)*Conc(25) + LungM(3,12)*Conc(2)*fup/B2P + LungG(3);$   
 % 17 - Epithelial cells (cEp)

$dConc(18) = LungM(4,1)*Conc(15) + LungM(4,2)*Conc(16) + LungM(4,3)*Conc(17) + LungM(4,4)*Conc(18) + LungM(4,5)*Conc(19)...$   
 $+ LungM(4,6)*Conc(20) + LungM(4,7)*Conc(21) + LungM(4,8)*Conc(22) + LungM(4,9)*Conc(23) + LungM(4,10)*Conc(24)...$   
 $+ LungM(4,11)*Conc(25) + LungM(4,12)*Conc(2)*fup/B2P + LungG(4);$   
 % 18 - Epithelial cells (cEpMito)

$dConc(19) = LungM(5,1)*Conc(15) + LungM(5,2)*Conc(16) + LungM(5,3)*Conc(17) + LungM(5,4)*Conc(18) + LungM(5,5)*Conc(19)...$   
 $+ LungM(5,6)*Conc(20) + LungM(5,7)*Conc(21) + LungM(5,8)*Conc(22) + LungM(5,9)*Conc(23) + LungM(5,10)*Conc(24)...$   
 $+ LungM(5,11)*Conc(25) + LungM(5,12)*Conc(2)*fup/B2P + LungG(5);$   
 % 19 - Epithelial cells (cEpLyso)

$dConc(20) = LungM(6,1)*Conc(15) + LungM(6,2)*Conc(16) + LungM(6,3)*Conc(17) + LungM(6,4)*Conc(18) + LungM(6,5)*Conc(19)...$



+ LungM(6,6)\*Conc(20) + LungM(6,7)\*Conc(21) + LungM(6,8)\*Conc(22) +  
LungM(6,9)\*Conc(23) + LungM(6,10)\*Conc(24)...  
+ LungM(6,11)\*Conc(25) + LungM(6,12)\*Conc(2)\*fup/B2P + LungG(6);  
% 20 - Interstitium (int)

dConc(21) = LungM(7,1)\*Conc(15) + LungM(7,2)\*Conc(16) + LungM(7,3)\*Conc(17) +  
LungM(7,4)\*Conc(18) + LungM(7,5)\*Conc(19)...  
+ LungM(7,6)\*Conc(20) + LungM(7,7)\*Conc(21) + LungM(7,8)\*Conc(22) +  
LungM(7,9)\*Conc(23) + LungM(7,10)\*Conc(24)...  
+ LungM(7,11)\*Conc(25) + LungM(7,12)\*Conc(2)\*fup/B2P + LungG(7);  
% 21 - Smooth muscle (sm)

dConc(22) = LungM(8,1)\*Conc(15) + LungM(8,2)\*Conc(16) + LungM(8,3)\*Conc(17) +  
LungM(8,4)\*Conc(18) + LungM(8,5)\*Conc(19)...  
+ LungM(8,6)\*Conc(20) + LungM(8,7)\*Conc(21) + LungM(8,8)\*Conc(22) +  
LungM(8,9)\*Conc(23) + LungM(8,10)\*Conc(24)...  
+ LungM(8,11)\*Conc(25) + LungM(8,12)\*Conc(2)\*fup/B2P + LungG(8);  
% 22 - Immune cells (imInt)

dConc(23) = LungM(9,1)\*Conc(15) + LungM(9,2)\*Conc(16) + LungM(9,3)\*Conc(17) +  
LungM(9,4)\*Conc(18) + LungM(9,5)\*Conc(19)...  
+ LungM(9,6)\*Conc(20) + LungM(9,7)\*Conc(21) + LungM(9,8)\*Conc(22) +  
LungM(9,9)\*Conc(23) + LungM(9,10)\*Conc(24)...  
+ LungM(9,11)\*Conc(25) + LungM(9,12)\*Conc(2)\*fup/B2P + LungG(9);  
% 23 - Endothelial cells (cEd)

dConc(24) = LungM(10,1)\*Conc(15) + LungM(10,2)\*Conc(16) + LungM(10,3)\*Conc(17) +  
LungM(10,4)\*Conc(18) + LungM(10,5)\*Conc(19)...  
+ LungM(10,6)\*Conc(20) + LungM(10,7)\*Conc(21) + LungM(10,8)\*Conc(22) +  
LungM(10,9)\*Conc(23) + LungM(10,10)\*Conc(24)...  
+ LungM(10,11)\*Conc(25) + LungM(10,12)\*Conc(2)\*fup/B2P + LungG(10);  
% 24 - Endothelial cells (cEdMito)

dConc(25) = LungM(11,1)\*Conc(15) + LungM(11,2)\*Conc(16) + LungM(11,3)\*Conc(17) +  
LungM(11,4)\*Conc(18) + LungM(11,5)\*Conc(19)...  
+ LungM(11,6)\*Conc(20) + LungM(11,7)\*Conc(21) + LungM(11,8)\*Conc(22) +  
LungM(11,9)\*Conc(23) + LungM(11,10)\*Conc(24)...  
+ LungM(11,11)\*Conc(25) + LungM(11,12)\*Conc(2)\*fup/B2P + LungG(11);  
% 25 - Endothelial cells (cEdLyso)

dConc(3) = Conc(4)\*Q\_HRT/Kp\_HRT/V\_VEN + Conc(5)\*Q\_BRA/Kp\_BRA/V\_VEN +  
Conc(6)\*Q\_LIV/Kp\_LIV/V\_VEN...  
+ Conc(9)\*Q\_KID/Kp\_KID/V\_VEN + Conc(10)\*Q\_MUS/Kp\_MUS/V\_VEN +  
Conc(11)\*Q\_SKN/Kp\_SKN/V\_VEN...

+ Conc(12)\*Q\_ADI/Kp\_ADI/V\_VEN + Conc(13)\*Q\_BON/Kp\_BON/V\_VEN +  
 Conc(14)\*Q\_RES/Kp\_RES/V\_VEN...  
 + Conc(26)\*Q\_Airways/V\_VEN - Conc(3)\*Q\_tot/V\_VEN + Kiv/V\_VEN ; % Venous blood

dConc(4) = Conc(1)\*Q\_HRT/V\_HRT - Conc(4)\*Q\_HRT/Kp\_HRT/V\_HRT ;

% Heart

dConc(5) = Conc(1)\*Q\_BRA/V\_BRA - Conc(5)\*Q\_BRA/Kp\_BRA/V\_BRA ;

% Brain

% Metabolism information

% from PATRICK POULIN, FRANK-PETER THEIL. Prediction of Pharmacokinetics prior to In Vivo Studies.

% II. Generic Physiologically Based Pharmacokinetic Models of Drug Disposition

% Microsomal recovery (rat 60.1 mg/g; human 33–52.5 mg/g)

% Hepatocellularity (rat 109 million cells/g; human 107–120 million cells/g)

% determined in vitro from a suspension of rat hepatocytes: uL/min/10<sup>6</sup> cells

% CLint = 1000;

% CL\_LIV = CLint \* 109 \* V\_LIV \* 10<sup>(-3)</sup> ; % mL/min

% If consider the extraction ratio, per definition  $E = (C_a - C_v)/C_a$

% equation comes from: PATRICK POULIN, FRANK-PETER. THEIL Prediction of Pharmacokinetics prior to In Vivo Studies.

% II. Generic Physiologically Based Pharmacokinetic Models of Drug Disposition

% E\_LIV = 0.985 ; % E\_LIV = 0.930 % by exp

E\_LIV = 0; % 0.985 ;

dConc(6) = (((Q\_LIV-Q\_GUT-Q\_SPL)\*Conc(1)+(Q\_GUT\*Conc(7)/Kp\_GUT +  
 Q\_SPL\*Conc(8)/Kp\_SPL - Q\_LIV\*Conc(6)/Kp\_LIV))/V\_LIV)...

- (((Q\_LIV-Q\_GUT-Q\_SPL)\*Conc(1)+(Q\_GUT\*Conc(7)/Kp\_GUT +  
 Q\_SPL\*Conc(8)/Kp\_SPL))\*E\_LIV))/V\_LIV ;

dConc(7) = Conc(1)\*Q\_GUT/V\_GUT - Conc(7)\*Q\_GUT/Kp\_GUT/V\_GUT ;

% Gut

dConc(8) = Conc(1)\*Q\_SPL/V\_SPL - Conc(8)\*Q\_SPL/Kp\_SPL/V\_SPL ;

%

Spleen

dConc(9) = Conc(1)\*Q\_KID/V\_KID - Conc(9)\*Q\_KID/Kp\_KID/V\_KID ;

%

Kidney

dConc(10) = Conc(1)\*Q\_MUS/V\_MUS - Conc(10)\*Q\_MUS/Kp\_MUS/V\_MUS ;

% Muscle

dConc(11) = Conc(1)\*Q\_SKN/V\_SKN - Conc(11)\*Q\_SKN/Kp\_SKN/V\_SKN ;

% Skin

dConc(12) = Conc(1)\*Q\_ADI/V\_ADI - Conc(12)\*Q\_ADI/Kp\_ADI/V\_ADI ;

% Adipose

dConc(13) = Conc(1)\*Q\_BON/V\_BON - Conc(13)\*Q\_BON/Kp\_BON/V\_BON ;

% Bone

dConc(14) = Conc(1)\*Q\_RES/V\_RES - Conc(14)\*Q\_RES/Kp\_RES/V\_RES ;

% Rest of body

$dConc(26) = Conc(1)*Q\_Airways/V\_LUNb\_Airways - Conc(26)*Q\_Airways/V\_LUNb\_Airways... \%$   
 26 -Lung airways blood concentration,  $C(2)*fup/B2P =$  free plasma conc  
 $+ (LungM\_Airways(14,1)*Conc(27) + LungM\_Airways(14,2)*Conc(28) +$   
 $LungM\_Airways(14,3)*Conc(29) + LungM\_Airways(14,4)*Conc(30)...$   
 $+ LungM\_Airways(14,5)*Conc(31) + LungM\_Airways(14,6)*Conc(24) +$   
 $LungM\_Airways(14,7)*Conc(33) + LungM\_Airways(14,8)*Conc(34)...$   
 $+ LungM\_Airways(14,9)*Conc(35) + LungM\_Airways(14,10)*Conc(36) +$   
 $LungM\_Airways(14,11)*Conc(37) + LungM\_Airways(14,12)*Conc(38)...$   
 $+ LungM\_Airways(14,13)*Conc(39) + LungM\_Airways(14,14)*Conc(26)*fup/B2P +$   
 $LungG\_Airways(14))*V\_LUNp\_Airways/V\_LUNb\_Airways; \%$  26 -Lung airways blood  
 concentration,  $C(2)*fup/B2P =$  free plasma conc

$dConc(27) = LungM\_Airways(1,1)*Conc(27) + LungM\_Airways(1,2)*Conc(28) +$   
 $LungM\_Airways(1,3)*Conc(29) + LungM\_Airways(1,4)*Conc(30) +$   
 $LungM\_Airways(1,5)*Conc(31)...$   
 $+ LungM\_Airways(1,6)*Conc(32) + LungM\_Airways(1,7)*Conc(33) +$   
 $LungM\_Airways(1,8)*Conc(34) + LungM\_Airways(1,9)*Conc(35) +$   
 $LungM\_Airways(1,10)*Conc(36)...$   
 $+ LungM\_Airways(1,11)*Conc(37) + LungM\_Airways(1,12)*Conc(38) +$   
 $LungM\_Airways(1,13)*Conc(39) ...$   
 $+ LungM\_Airways(1,14)*Conc(26)*fup/B2P + LungG\_Airways(1); \%$  27  
 - Airways SurfaConce lining liquid (aEp)

$dConc(28) = LungM\_Airways(2,1)*Conc(27) + LungM\_Airways(2,2)*Conc(28) +$   
 $LungM\_Airways(2,3)*Conc(29) + LungM\_Airways(2,4)*Conc(30) +$   
 $LungM\_Airways(2,5)*Conc(31)...$   
 $+ LungM\_Airways(2,6)*Conc(32) + LungM\_Airways(2,7)*Conc(33) +$   
 $LungM\_Airways(2,8)*Conc(34) + LungM\_Airways(2,9)*Conc(35) +$   
 $LungM\_Airways(2,10)*Conc(36)...$   
 $+ LungM\_Airways(2,11)*Conc(37) + LungM\_Airways(2,12)*Conc(38) +$   
 $LungM\_Airways(2,13)*Conc(39) ...$   
 $+ LungM\_Airways(2,14)*Conc(26)*fup/B2P + LungG\_Airways(2); \%$  28  
 - Airways Macrophage (imEp)

$dConc(29) = LungM\_Airways(3,1)*Conc(27) + LungM\_Airways(3,2)*Conc(28) +$   
 $LungM\_Airways(3,3)*Conc(29) + LungM\_Airways(3,4)*Conc(30) +$   
 $LungM\_Airways(3,5)*Conc(31)...$   
 $+ LungM\_Airways(3,6)*Conc(32) + LungM\_Airways(3,7)*Conc(33) +$   
 $LungM\_Airways(3,8)*Conc(34) + LungM\_Airways(3,9)*Conc(35) +$   
 $LungM\_Airways(3,10)*Conc(36)...$   
 $+ LungM\_Airways(3,11)*Conc(37) + LungM\_Airways(3,12)*Conc(38) +$   
 $LungM\_Airways(3,13)*Conc(39) ...$   
 $+ LungM\_Airways(3,14)*Conc(26)*fup/B2P + LungG\_Airways(3); \%$  29 -  
 Airways Epithelial cells (cEp)

$dConc(30) = LungM\_Airways(4,1)*Conc(27) + LungM\_Airways(4,2)*Conc(28) +$   
 $LungM\_Airways(4,3)*Conc(29) + LungM\_Airways(4,4)*Conc(30) +$   
 $LungM\_Airways(4,5)*Conc(31)...$   
 $+ LungM\_Airways(4,6)*Conc(32) + LungM\_Airways(4,7)*Conc(33) +$   
 $LungM\_Airways(4,8)*Conc(34) + LungM\_Airways(4,9)*Conc(35) +$   
 $LungM\_Airways(4,10)*Conc(36)...$   
 $+ LungM\_Airways(4,11)*Conc(37)+ LungM\_Airways(4,12)*Conc(38)+$   
 $LungM\_Airways(4,13)*Conc(39) ...$   
 $+ LungM\_Airways(4,14)*Conc(26)*fup/B2P + LungG\_Airways(4);$  % 30 -  
 Airways Epithelial cells (cEpMito)

$dConc(31) = LungM\_Airways(5,1)*Conc(27) + LungM\_Airways(5,2)*Conc(28) +$   
 $LungM\_Airways(5,3)*Conc(29) + LungM\_Airways(5,4)*Conc(30) +$   
 $LungM\_Airways(5,5)*Conc(31)...$   
 $+ LungM\_Airways(5,6)*Conc(32) + LungM\_Airways(5,7)*Conc(33) +$   
 $LungM\_Airways(5,8)*Conc(34) + LungM\_Airways(5,9)*Conc(35) +$   
 $LungM\_Airways(5,10)*Conc(36)...$   
 $+ LungM\_Airways(5,11)*Conc(37)+ LungM\_Airways(5,12)*Conc(38)+$   
 $LungM\_Airways(5,13)*Conc(39) ...$   
 $+ LungM\_Airways(5,14)*Conc(26)*fup/B2P + LungG\_Airways(5);$  % 31  
 - Airways Epithelial cells (cEpLyso)

$dConc(32) = LungM\_Airways(6,1)*Conc(27) + LungM\_Airways(6,2)*Conc(28) +$   
 $LungM\_Airways(6,3)*Conc(29) + LungM\_Airways(6,4)*Conc(30) +$   
 $LungM\_Airways(6,5)*Conc(31)...$   
 $+ LungM\_Airways(6,6)*Conc(32) + LungM\_Airways(6,7)*Conc(33) +$   
 $LungM\_Airways(6,8)*Conc(34) + LungM\_Airways(6,9)*Conc(35) +$   
 $LungM\_Airways(6,10)*Conc(36)...$   
 $+ LungM\_Airways(6,11)*Conc(37)+ LungM\_Airways(6,12)*Conc(38)+$   
 $LungM\_Airways(6,13)*Conc(39) ...$   
 $+ LungM\_Airways(6,14)*Conc(26)*fup/B2P + LungG\_Airways(6);$  % 32  
 - Airways Interstitium (int)

$dConc(33) = LungM\_Airways(7,1)*Conc(27) + LungM\_Airways(7,2)*Conc(28) +$   
 $LungM\_Airways(7,3)*Conc(29) + LungM\_Airways(7,4)*Conc(30) +$   
 $LungM\_Airways(7,5)*Conc(31)...$   
 $+ LungM\_Airways(7,6)*Conc(32) + LungM\_Airways(7,7)*Conc(33) +$   
 $LungM\_Airways(7,8)*Conc(34) + LungM\_Airways(7,9)*Conc(35) +$   
 $LungM\_Airways(7,10)*Conc(36)...$   
 $+ LungM\_Airways(7,14)*Conc(37)+ LungM\_Airways(7,12)*Conc(38)+$   
 $LungM\_Airways(7,13)*Conc(39) ...$   
 $+ LungM\_Airways(7,12)*Conc(26)*fup/B2P + LungG\_Airways(7);$  % 33  
 - Airways Smooth muscle (sm)

$dConc(34) = LungM\_Airways(8,1)*Conc(27) + LungM\_Airways(8,2)*Conc(28) +$   
 $LungM\_Airways(8,3)*Conc(29) + LungM\_Airways(8,4)*Conc(30) +$   
 $LungM\_Airways(8,5)*Conc(31)...$   
 $+ LungM\_Airways(8,6)*Conc(32) + LungM\_Airways(8,7)*Conc(33) +$   
 $LungM\_Airways(8,8)*Conc(34) + LungM\_Airways(8,9)*Conc(35) +$   
 $LungM\_Airways(8,10)*Conc(36)...$   
 $+ LungM\_Airways(8,11)*Conc(37) + LungM\_Airways(8,12)*Conc(38) +$   
 $LungM\_Airways(8,13)*Conc(39) ...$   
 $+ LungM\_Airways(8,14)*Conc(26)*fup/B2P + LungG\_Airways(8);$  % 34  
 - Airways Smooth muscle (smMito)

$dConc(35) = LungM\_Airways(9,1)*Conc(27) + LungM\_Airways(9,2)*Conc(28) +$   
 $LungM\_Airways(9,3)*Conc(29) + LungM\_Airways(9,4)*Conc(30) +$   
 $LungM\_Airways(9,5)*Conc(31)...$   
 $+ LungM\_Airways(9,6)*Conc(32) + LungM\_Airways(9,7)*Conc(33) +$   
 $LungM\_Airways(9,8)*Conc(34) + LungM\_Airways(9,9)*Conc(35) +$   
 $LungM\_Airways(9,10)*Conc(36)...$   
 $+ LungM\_Airways(9,11)*Conc(37) + LungM\_Airways(9,12)*Conc(38) +$   
 $LungM\_Airways(9,13)*Conc(39) ...$   
 $+ LungM\_Airways(9,14)*Conc(26)*fup/B2P + LungG\_Airways(9);$  % 35  
 - Airways Smooth muscle (smLyso)

$dConc(36) = LungM\_Airways(10,1)*Conc(27) + LungM\_Airways(10,2)*Conc(28) +$   
 $LungM\_Airways(10,3)*Conc(29) + LungM\_Airways(10,4)*Conc(30) +$   
 $LungM\_Airways(10,5)*Conc(31)...$   
 $+ LungM\_Airways(10,6)*Conc(32) + LungM\_Airways(10,7)*Conc(33) +$   
 $LungM\_Airways(10,8)*Conc(34) + LungM\_Airways(10,9)*Conc(35) +$   
 $LungM\_Airways(10,10)*Conc(36)...$   
 $+ LungM\_Airways(10,11)*Conc(37) + LungM\_Airways(10,12)*Conc(38) +$   
 $LungM\_Airways(10,13)*Conc(39) ...$   
 $+ LungM\_Airways(10,14)*Conc(26)*fup/B2P + LungG\_Airways(10);$  % 36  
 - Airways Immune cells (imInt)

$dConc(37) = LungM\_Airways(11,1)*Conc(27) + LungM\_Airways(11,2)*Conc(28) +$   
 $LungM\_Airways(11,3)*Conc(29) + LungM\_Airways(11,4)*Conc(30) +$   
 $LungM\_Airways(11,5)*Conc(31)...$   
 $+ LungM\_Airways(11,6)*Conc(32) + LungM\_Airways(11,7)*Conc(33) +$   
 $LungM\_Airways(11,8)*Conc(34) + LungM\_Airways(11,9)*Conc(35) +$   
 $LungM\_Airways(11,10)*Conc(36)...$   
 $+ LungM\_Airways(11,11)*Conc(37) + LungM\_Airways(11,12)*Conc(38) +$   
 $LungM\_Airways(11,13)*Conc(39) ...$   
 $+ LungM\_Airways(11,14)*Conc(26)*fup/B2P + LungG\_Airways(11);$  %  
 37 - Airways Endothelial cells

$dConc(38) = LungM\_Airways(12,1)*Conc(27) + LungM\_Airways(12,2)*Conc(28) +$   
 $LungM\_Airways(12,3)*Conc(29) + LungM\_Airways(12,4)*Conc(30) +$   
 $LungM\_Airways(12,5)*Conc(31)...$

```

+ LungM_Airways(12,6)*Conc(32) + LungM_Airways(12,7)*Conc(33) +
LungM_Airways(12,8)*Conc(34) + LungM_Airways(12,9)*Conc(35) +
LungM_Airways(12,10)*Conc(36)...
+ LungM_Airways(12,11)*Conc(37)+ LungM_Airways(12,12)*Conc(38)+
LungM_Airways(12,13)*Conc(39) ...
+ LungM_Airways(12,14)*Conc(26)*fup/B2P + LungG_Airways(12); % 38
- Endothelial cells (cEdMito)

```

```

dConc(39) = LungM_Airways(13,1)*Conc(27) + LungM_Airways(13,2)*Conc(28) +
LungM_Airways(13,3)*Conc(29) + LungM_Airways(13,4)*Conc(30) +
LungM_Airways(13,5)*Conc(31)...
+ LungM_Airways(13,6)*Conc(32) + LungM_Airways(13,7)*Conc(33) +
LungM_Airways(13,8)*Conc(34) + LungM_Airways(13,9)*Conc(35) +
LungM_Airways(13,10)*Conc(36)...
+ LungM_Airways(13,11)*Conc(37)+ LungM_Airways(13,12)*Conc(38)+
LungM_Airways(13,13)*Conc(39) ...
+ LungM_Airways(13,14)*Conc(26)*fup/B2P + LungG_Airways(13); %
39 - Endothelial cells (cEdLyso)

```

```

Vtot = diag([V_ART V_LUNb V_VEN V_HRT V_BRA V_LIV V_GUT V_SPL V_KID....
V_MUS V_SKN V_ADI V_BON V_RES diag(M_v)'*10^6 V_LUNb_Airways
diag(M_v_Airways)'*10^6]);

```

```

dConc = [dConc(1), dConc(2), dConc(3), dConc(4), dConc(5), dConc(6), dConc(7), dConc(8),
dConc(9), dConc(10),...
dConc(11), dConc(12), dConc(13), dConc(14), dConc(15), dConc(16), dConc(17), dConc(18),
dConc(19), dConc(20),...
dConc(21), dConc(22), dConc(23), dConc(24), dConc(25), dConc(26), dConc(27), dConc(28),
dConc(29), dConc(30),...
dConc(31), dConc(32), dConc(33), dConc(34), dConc(35), dConc(36), dConc(37), dConc(38),
dConc(39)]';

```

```

function [T,Y,Conc_LUNSim,Con_al,Con_aw,Mass_LUNtemp,Mass_Airwaystemp]=
H_RL_IH_fun()
global BW V_VEN fup B2P Vtot;

```

```

% calculate the concentration accumulated in the lung by Jerry's model
[M, G, M_v, Vp] = H_al_RL();
[M_Airways, G_Airways, M_v_Airways, Vp_Airways] = H_aw_RL();

```

```

%observed tissue concentration
Conc_Lung = [13.05,6.30,1.71,0.96]*10^3;%ng/ml;Schneck 1977 paper
t_obs = [20,60,120,240];

```

```

BW = 0.25 ;
V_VEN = 0.0544*BW*1000 ;
Y0 = zeros(39,1) ;
%IV dose
%Y0(3) = 1.5*10^6*BW/V_VEN ;%ng/ml

%inhale dose
Y0(15) = 1*10^6;%0.5*2*10^6*BW/(M_v(1,1)*10^6) ; % 1*10^6;%% AL,ng/mL
Y0(27) = 1*10^6;%0.5*2*10^6*BW/(M_v_Airways(1,1)*10^6) ; %1*10^6;% % AW,ng/mL

Yopt = 1e-13 * ones(1,39) ;
options = odeset('RelTol',1e-13,'AbsTol',Yopt);
[T,Y] = ode15s(@H_Lung_RL,[0 10*60],Y0,options);
len = length(T) ;
Conc_LUNtemp = Y(:,15:25) ;
Mass_LUNtemp = Conc_LUNtemp*(M_v*10^6) ; %ng,alveo

Conc_Airwaystemp = Y(:,27:39) ;
Mass_Airwaystemp = Conc_Airwaystemp*(M_v_Airways*10^6) ; %ng

Mass_LUNSim = sum(Mass_LUNtemp, 2) + sum(Mass_Airwaystemp, 2) ;%ng
Conc_LUNSim = Mass_LUNSim / ((trace(M_v)*10^6)+(trace(M_v_Airways)*10^6)); %ng/mL

Con_al = sum(Mass_LUNtemp, 2)/(trace(M_v)*10^6);%ng/ml
Con_aw = sum(Mass_Airwaystemp, 2)/(trace(M_v_Airways)*10^6);%ng/ml

% lung:venous blood concentration ratio (Kp_LUN)
Kpulung = Conc_LUNSim(len)/(Y(len,3)*fup/B2P) ;
Kplung = Conc_LUNSim(len)/Y(len,3) ;
Conc_LUN_1hr = Conc_LUNSim(len);%ng/ml
Conc_ven_1hr = Y(len,3);%ng/ml

% organelle mass/concentration
Mass = Y*Vtot;%ng
%mito
Mass_mito = Mass(:,18) + Mass(:,24) + Mass(:,30) + Mass(:,34) + Mass(:,38);
V_mito = Vtot(18,18) + Vtot(24,24) + Vtot(30,30) + Vtot(34,34) + Vtot(38,38);
C_mito = Mass_mito/V_mito;
%lyso
Mass_lyso = Mass(:,19) + Mass(:,25) + Mass(:,31) + Mass(:,35) + Mass(:,39);
V_lyso = Vtot(19,19) + Vtot(25,25) + Vtot(31,31) + Vtot(35,35) + Vtot(39,39);
C_lyso = Mass_lyso/V_lyso;
%cyto
Mass_cyto = Mass(:,16) + Mass(:,17) + Mass(:,21) + Mass(:,22) + Mass(:,23)...
+ Mass(:,28) + Mass(:,29) + Mass(:,33) + Mass(:,36) + Mass(:,37);
V_cyto = Vtot(16,16) + Vtot(17,17) + Vtot(21,21) + Vtot(22,22) + Vtot(23,23)...

```

```

+ Vtot(28,28) + Vtot(29,29) + Vtot(33,33) + Vtot(36,36) + Vtot(37,37);
C_cyto = Mass_cyto/V_cyto;
end

```

```

% 1CellPK based lung model starts here (Rats)
% 12 compartments:
% aEp (surface lining liquied), imEp (Macrophage),
% cEp(epithelial cells),cEpMito(mito of cEp), cEpLyso (lyso of cEp)
% int(Interstitial),imInt(immune cells), sm(smooth muscle),
% cEd(endothelial cells), cEdMito(mito of cEd),cEdLyso (lyso of cEd), p(plasma)

```

```

function [M, G, M_v, Vp] = AT_al_RL()

```

```

%molecular physiochemical property

```

```

pKa = 100;
logPN = 0.16 ;
logPD = -1.57;%logPN-3.7 ;
z = 1;
% %weighted

```

```

% Constant
T = 273.15+37;
R = 8.314;
F = 96484.56;
%lipid fraction
LaEp = 0.95;
LimEp = 0.05;
LcEp = 0.05 ;
Lint = 0;
LimInt = 0.05;
Lsm = 0;
LcEd = 0.05;
Lp = 0;
%volumetric water fraction=1-lipid fraction
WaEp = 1 - LaEp;
WimEp = 1 - LimEp;
WcEp = 1 - LcEp;
Wint = 1 - Lint;
WimInt = 1 - LimInt;

```



```

Wsm = 1 - Lsm;
WcEd = 1 - LcEd;
Wp = 1 - Lp;
%activity coefficient of species(N:neutral,D:desociated)
GaEpN = 1;
GaEpD = 1;
GimEpN = 1.23;
GimEpD = 0.74;
GcEpN = 1.23;
GcEpD = 0.74;
GintN = 1;
GintD = 1;
GimIntN = 1.23;
GimIntD = 0.74;
GsmN = 1.23;
GsmD = 0.74;
GcEdN = 1.23;
GcEdD = 0.74;
GpN = 1;
GpD = 1;

% By Jingyu Yu (used in publication) Areas and volumes (m^2, m^3) for 7 membranes and
corresponding compartments
AaEp = 0.387;%literature
AbEp = AaEp;%Assuming same with epical side
AimEp = 3.14*10^(-10)*0.89*10^(9)*3/100/2; % 10 um diameter, only half of surface gets
contact with liquid, since ASL = 5 um
AimInt = AimEp/10; % assuming number of immune cells is 1/10 of macrophage
Asm = 0;%No SM
AbEd = 0.452;%literature
AaEd = 0.452;%literature
%volumes for 8 compartments(m3)
ASL = 5; %literature um
VaEp = AaEp*ASL*10^(-6); %5 um thickness
VcEp = AaEp*0.384*10^(-6); % 0.384, literature
VimEp = 0.89*10^(9)*3/100*1058*10^(-18);%number of macrophage(literature)*volume of
macrophage
Vint = AaEp*0.693*10^(-6); % literature
VimInt = VimEp/10;% assuming number of immune cells is 1/10 of macrophage
Vsm = 10^(-30); % VcEp*10^(-12); % can be any number, surface is 0
VcEd = AbEd*0.358*10^(-6); %0.358 um thickness --literature
% Vp = 5; %total huge volume for lung absorption model

#####
% Subcellular compartments in cEp (epithelial cells) and cEd(endothelial cells)
% calculate constant
R_org = 0.1;

```

```

VcEpMito = R_org*VcEp ; % 10^(-30); %
VcEpLyso = R_org*VcEp ; % 10^(-30); %
VcEdMito = R_org*VcEd ; % 10^(-30); %
VcEdLyso = R_org*VcEd ; % 10^(-30); %

AcEpMito = 5.9924e+006*VcEpMito; % 0 ;
AcEpLyso = 5.9924e+006*VcEpLyso; % 0 ;
AcEdMito = 5.9924e+006*VcEdMito; % 0 ;
AcEdLyso = 5.9924e+006*VcEdLyso; % 0 ;
#####

M_v = diag([VaEp,VimEp,VcEp,VcEpMito,VcEpLyso,Vint,Vsm,VimInt,VcEd,VcEdMito,VcEdLyso]);
V_LUN = trace(M_v)*10^6;
Vp = 340*10^(-9)*V_LUN;

% Membrane potential (V)
EaEp = -0.0093;
EbEp = 0.0119;%0.0119;
EimEp = -0.06;
EimInt = -0.06;
Esm = -0.06;
EbEd = -0.06;
EaEd = -0.06;
% pH values
pHaEp = 7.4;
pHimEp = 7.0;
pHcEp = 7.0;
pHint = 7.0;
pHimInt = 7.0;
pHsm = 7.0;
pHcEd = 7.0;
pHp = 7.4;

%adjustment for logP
if ( abs(z-1) <= 10^(-6) )
    logP_nlipT = 0.33*logPN+2.2 ;
    logP_dlipT = 0.37*logPD+2 ;
end
if ( abs(z+1) <= 10^(-6) )
    logP_nlipT = 0.37*logPN+2.2 ;
    logP_dlipT = 0.33*logPD+2.6 ;
end
if ( abs(z-0) <= 10^(-5) )
    logP_nlipT = 0.33*logPN+2.2 ;
    logP_dlipT = 0.33*logPD+2.2 ;
end

```

```

% Get the first two decimals
logP_n = round(logP_nlipT*100)/100 ;
logP_d = round(logP_dlipT*100)/100 ;
%calculate the membrane permeability

Pn = 10^(logP_n-6.7)*60; % in 1/min
Pd = 10^(logP_d-6.7)*60; % in 1/min

i = -sign(z) ;
%calculate N for flux of ion happening at 7 membranes
C = z*F/(R*T);
NaEp = C*(-EaEp) ;
NbEp = C*EbEp ;
NimEp = C*EimEp ;
NimInt = C*EimInt ;
Nsm = C*Esm ;
NbEd = C*(-EbEd) ;
NaEd = C*(EaEd) ;

%calculate Kn and Kd for 8 compartments
N = 1.22*10^(logP_n);
D = 1.22*10^(logP_d);

%calculate Kn and Kd for 8 compartments
% using Rodgers method to get Kd general
KpuBC = 1.15/0.96;
pHBc = 7.22;
fiw_bc = 0.603;
fnl_bc = 0.0017;
fnp_bc = 0.0029;
AP_BC = 0.5;
AP_lung = 3.91;
P = 10^(logP_n);
Ka = (KpuBC - (1+10^(pKa - pHBc))/(1+10^(pKa - pHp))*fiw_bc -
(P*fnl_bc+(0.3*P+0.7)*fnp_bc)/(1+10^(pKa-pHp)))*(1+10^(pKa-pHp))/(AP_BC*10^(pKa-pHBc));
Kd = Ka*AP_lung;
%Kd_p = n*Ka*AP_BC;
if (Kd < 0)
    Kd = 0;
end

KaEpN = N*LaEp ;
KaEpD = D*LaEp ;
KimEpN = N*LimEp ;
KimEpD = D*LimEp;
KcEpN = N*LcEp ;
KcEpD = D*LcEp ;

```

KintN = N\*Lint ;  
KintD = D\*Lint ;  
KimIntN = N\*LimInt ;  
KimIntD = D\*LimInt ;  
KsmN = N\*Lsm ;  
KsmD = D\*Lsm ;  
KcEdN = N\*LcEd ;  
KcEdD = D\*LcEd ;  
KpN = N\*Lp ;  
KpD = D\*Lp ;

%#####

LcEpMito = 0.05 ;  
LcEpLyso = 0.05 ;  
LcEdMito = 0.05 ;  
LcEdLyso = 0.05 ;

WcEpMito = 1-LcEpMito ;  
WcEpLyso = 1-LcEpLyso ;  
WcEdMito = 1-LcEdMito ;  
WcEdLyso = 1-LcEdLyso ;

GcEpMitoN = 1.23 ;  
GcEpMitoD = 0.74 ;  
GcEpLysoN = 1.23 ;  
GcEpLysoD = 0.74 ;  
GcEdMitoN = 1.23 ;  
GcEdMitoD = 0.74 ;  
GcEdLysoN = 1.23 ;  
GcEdLysoD = 0.74 ;

EcEpMito = -0.16 ;  
EcEpLyso = +0.01 ;  
EcEdMito = -0.16 ;  
EcEdLyso = +0.01 ;

pHcEpMito = 8 ;  
pHcEpLyso = 5 ;  
pHcEdMito = 8 ;  
pHcEdLyso = 5 ;

NcEpMito = C\*EcEpMito ;  
NcEpLyso = C\*EcEpLyso ;  
NcEdMito = C\*EcEdMito ;  
NcEdLyso = C\*EcEdLyso ;

KcEpMitoN = N\*LcEpMito ;  
 KcEpMitoD = D\*LcEpMito ;  
 KcEpLysoN = N\*LcEpLyso ;  
 KcEpLysoD = D\*LcEpLyso ;

KcEdMitoN = N\*LcEdMito ;  
 KcEdMitoD = D\*LcEdMito ;  
 KcEdLysoN = N\*LcEdLyso ;  
 KcEdLysoD = D\*LcEdLyso ;

fcEpMitoN = 1/(WcEpMito/GcEpMitoN+KcEpMitoN/GcEpMitoN+WcEpMito\*10^(i\*(pHcEpMito-pKa)))/GcEpMitoD...  
 +KcEpMitoD\*10^(i\*(pHcEpMito-pKa))/GcEpMitoD);  
 fcEpMitoD = fcEpMitoN\*10^(i\*(pHcEpMito-pKa));

fcEpLysoN = 1/(WcEpLyso/GcEpLysoN+KcEpLysoN/GcEpLysoN+WcEpLyso\*10^(i\*(pHcEpLyso-pKa)))/GcEpLysoD...  
 +KcEpLysoD\*10^(i\*(pHcEpLyso-pKa))/GcEpLysoD);  
 fcEpLysoD = fcEpLysoN\*10^(i\*(pHcEpLyso-pKa));

fcEdMitoN = 1/(WcEdMito/GcEdMitoN+KcEdMitoN/GcEdMitoN+WcEdMito\*10^(i\*(pHcEdMito-pKa)))/GcEdMitoD...  
 +KcEdMitoD\*10^(i\*(pHcEdMito-pKa))/GcEdMitoD);  
 fcEdMitoD = fcEdMitoN\*10^(i\*(pHcEdMito-pKa));

fcEdLysoN = 1/(WcEdLyso/GcEdLysoN+KcEdLysoN/GcEdLysoN+WcEdLyso\*10^(i\*(pHcEdLyso-pKa)))/GcEdLysoD...  
 +KcEdLysoD\*10^(i\*(pHcEdLyso-pKa))/GcEdLysoD);  
 fcEdLysoD = fcEdLysoN\*10^(i\*(pHcEdLyso-pKa));

%#####

%compute the fn and fd for 8 compartments

faEpN = 1/(WaEp/GaEpN+KaEpN/GaEpN+WaEp\*10^(i\*(pHaEp-pKa)))/GaEpD...  
 +KaEpD\*10^(i\*(pHaEp-pKa))/GaEpD);

faEpD = faEpN\*10^(i\*(pHaEp-pKa));

fimEpN = 1/(WimEp/GimEpN+KimEpN/GimEpN+WimEp\*10^(i\*(pHimEp-pKa)))/GimEpD...  
 +KimEpD\*10^(i\*(pHimEp-pKa))/GimEpD);

fimEpD = fimEpN\*10^(i\*(pHimEp-pKa));

fcEpN = 1/(WcEp/GcEpN+KcEpN/GcEpN+WcEp\*10^(i\*(pHcEp-pKa)))/GcEpD...  
 +KcEpD\*10^(i\*(pHcEp-pKa))/GcEpD);

fcEpD = fcEpN\*10^(i\*(pHcEp-pKa));

fintN = 1/(Wint/GintN+KintN/GintN+Wint\*10^(i\*(pHint-pKa)))/GintD...  
 +KintD\*10^(i\*(pHint-pKa))/GintD);

fintD = fintN\*10^(i\*(pHint-pKa));

fimIntN = 1/(WimInt/GimIntN+KimIntN/GimIntN+WimInt\*10^(i\*(pHimInt-pKa)))/GimIntD...  
 +KimIntD\*10^(i\*(pHimInt-pKa))/GimIntD);

```

fimIntD = fimIntN*10^(i*(pHimInt-pKa));
fsmN = 1/(Wsm/GsmN+KsmN/GsmN+Wsm*10^(i*(pHsm-pKa)))/GsmD...
      +KsmD*10^(i*(pHsm-pKa))/GsmD);
fsmD = fsmN*10^(i*(pHsm-pKa));
fcEdN = 1/(WcEd/GcEdN+KcEdN/GcEdN+WcEd*10^(i*(pHcEd-pKa)))/GcEdD...
      +KcEdD*10^(i*(pHcEd-pKa))/GcEdD);
fcEdD = fcEdN*10^(i*(pHcEd-pKa));
fpN = 1/(Wp/GpN+KpN/GpN+Wp*10^(i*(pHp-pKa)))/GpD...
      +KpD*10^(i*(pHp-pKa))/GpD);
fpD = fpN*10^(i*(pHp-pKa));

%mucus clearance
%Ke = 0.02;
Ke = 0;

%compute the coefficient matrix for ODEs
% #1: Surface Lining Liquid (aEp)
KaEp_aEp = AaEp/VaEp*(Pn*(-faEpN)+Pd*NaEp/(exp(NaEp)-1)*(-faEpD)*exp(NaEp))...
      -AimEp/VaEp*(Pn*faEpN+Pd*NimEp/(exp(NimEp)-1)*faEpD)...
      -Ke;
KaEp_imEp = -AimEp/VaEp*(Pn*(-fimEpN)+Pd*NimEp/(exp(NimEp)-1)*(-fimEpD)*exp(NimEp));
KaEp_cEp = AaEp/VaEp*(Pn*(fcEpN)+Pd*NaEp/(exp(NaEp)-1)*(fcEpD));
KaEp_cEpMito = 0;
KaEp_cEpLyso = 0;
KaEp_int = 0;
KaEp_sm = 0;
KaEp_imInt = 0;
KaEp_cEd = 0;
KaEp_cEdMito = 0;
KaEp_cEdLyso = 0;
KaEp_p = 0;
SaEp = 0;

% #2: Macrophage (imEp)
KimEp_aEp = AimEp/VimEp*(Pn*faEpN+Pd*NimEp/(exp(NimEp)-1)*faEpD);
KimEp_imEp = AimEp/VimEp*(Pn*(-fimEpN)+Pd*NimEp/(exp(NimEp)-1)*(-
fimEpD)*exp(NimEp));
KimEp_cEp = 0;
KimEp_cEpMito = 0 ;
KimEp_cEpLyso = 0 ;
KimEp_int = 0;
KimEp_sm = 0;
KimEp_imInt = 0;
KimEp_cEd = 0;
KimEp_cEdMito = 0 ;
KimEp_cEdLyso = 0 ;
KimEp_p = 0;

```

SimEp = 0;

% #3: Epithelial Cells (cEp)

KcEp\_aEp = -AaEp/VcEp\*(Pn\*(-faEpN)+Pd\*NaEp/(exp(NaEp)-1)\*(-faEpD)\*exp(NaEp));

KcEp\_imEp = 0;

KcEp\_cEp = -AaEp/VcEp\*(Pn\*(fcEpN)+Pd\*NaEp/(exp(NaEp)-1)\*(fcEpD))...

-AcEpMito/VcEp\*(Pn\*fcEpN+Pd\*NcEpMito/(exp(NcEpMito)-1)\*fcEpD)...

-AcEpLyso/VcEp\*(Pn\*fcEpN+Pd\*NcEpLyso/(exp(NcEpLyso)-1)\*fcEpD)...

+ AbEp/VcEp\*(Pn\*(-fcEpN)+Pd\*NbEp/(exp(NbEp)-1)\*(-fcEpD)\*exp(NbEp));

KcEp\_cEpMito = -AcEpMito/VcEp\*(Pn\*(-fcEpMitoN)+Pd\*NcEpMito/(exp(NcEpMito)-1)\*(-fcEpMitoD)\*exp(NcEpMito)) ;

KcEp\_cEpLyso = -AcEpLyso/VcEp\*(Pn\*(-fcEpLysoN)+Pd\*NcEpLyso/(exp(NcEpLyso)-1)\*(-fcEpLysoD)\*exp(NcEpLyso)) ;

KcEp\_int = AbEp/VcEp\*(Pn\*(fintN)+Pd\*NbEp/(exp(NbEp)-1)\*(fintD));

KcEp\_sm = 0;

KcEp\_imInt = 0;

KcEp\_cEd = 0;

KcEp\_cEdMito = 0 ;

KcEp\_cEdLyso = 0 ;

KcEp\_p = 0;

ScEp = 0;

% #4: : Epithelial Cells (cEpMito)

KcEpMito\_aEp = 0;

KcEpMito\_imEp = 0;

KcEpMito\_cEp = AcEpMito/VcEpMito\*(Pn\*(fcEpN)+Pd\*NcEpMito/(exp(NcEpMito)-1)\*(fcEpD));

KcEpMito\_cEpMito = AcEpMito/VcEpMito\*(Pn\*(-fcEpMitoN)+Pd\*NcEpMito/(exp(NcEpMito)-1)\*(-fcEpMitoD)\*exp(NcEpMito));

KcEpMito\_cEpLyso = 0 ;

KcEpMito\_int = 0 ;

KcEpMito\_sm = 0;

KcEpMito\_imInt = 0;

KcEpMito\_cEd = 0;

KcEpMito\_cEdMito = 0 ;

KcEpMito\_cEdLyso = 0 ;

KcEpMito\_p = 0;

ScEpMito = 0;

% #5: : Epithelial Cells (cEpLyso)

KcEpLyso\_aEp = 0;

KcEpLyso\_imEp = 0;

KcEpLyso\_cEp = AcEpLyso/VcEpLyso\*(Pn\*(fcEpN)+Pd\*NcEpLyso/(exp(NcEpLyso)-1)\*(fcEpD));

KcEpLyso\_cEpMito = 0 ;

KcEpLyso\_cEpLyso = AcEpLyso/VcEpLyso\*(Pn\*(-fcEpLysoN)+Pd\*NcEpLyso/(exp(NcEpLyso)-1)\*(-fcEpLysoD)\*exp(NcEpLyso));

KcEpLyso\_int = 0 ;

KcEpLyso\_sm = 0;

```

KcEpLyso_imInt = 0;
KcEpLyso_cEd = 0;
KcEpLyso_cEdMito = 0 ;
KcEpLyso_cEdLyso = 0 ;
KcEpLyso_p = 0;
ScEpLyso = 0;

```

```

% #6: : Interstitium (int)

```

```

Kint_aEp = 0;
Kint_imEp = 0;
Kint_cEp = -AbEp/Vint*(Pn*(-fcEpN)+Pd*NbEp/(exp(NbEp)-1)*(-fcEpD)*exp(NbEp));
Kint_cEpMito = 0 ;
Kint_cEpLyso = 0 ;
Kint_int = -AbEp/Vint*(Pn*(fintN)+Pd*NbEp/(exp(NbEp)-1)*(fintD))...
          -Asm/Vint*(Pn*fintN+Pd*Nsm/(exp(Nsm)-1)*fintD)...
          -AimInt/Vint*(Pn*fintN+Pd*NimInt/(exp(NimInt)-1)*fintD)...
          +AbEd/Vint*(Pn*(-fintN)+Pd*NbEd/(exp(NbEd)-1)*(-fintD)*exp(NbEd));
Kint_sm = -Asm/Vint*(Pn*(-fsmN)+Pd*Nsm/(exp(Nsm)-1)*(-fsmD)*exp(Nsm));
Kint_imInt = -AimInt/Vint*(Pn*(-fimIntN)+Pd*NimInt/(exp(NimInt)-1)*(-fimIntD)*exp(NimInt));
Kint_cEd = AbEd/Vint*(Pn*(fcEdN)+Pd*NbEd/(exp(NbEd)-1)*(fcEdD));
Kint_cEdMito = 0 ;
Kint_cEdLyso = 0 ;
Kint_p = 0;
Sint = 0;

```

```

% #7: Smooth Muscle (sm)

```

```

Ksm_aEp = 0;
Ksm_imEp = 0;
Ksm_cEp = 0;
Ksm_cEpMito = 0 ;
Ksm_cEpLyso = 0 ;
Ksm_int = Asm/Vsm*(Pn*fintN+Pd*Nsm/(exp(Nsm)-1)*fintD);
Ksm_sm = Asm/Vsm*(Pn*(-fsmN)+Pd*Nsm/(exp(Nsm)-1)*(-fsmD)*exp(Nsm));
Ksm_imInt = 0;
Ksm_cEd = 0;
Ksm_cEdMito = 0 ;
Ksm_cEdLyso = 0 ;
Ksm_p = 0;
Ssm = 0;

```

```

% #8: Immune Cells (imInt)

```

```

KimInt_aEp = 0;
KimInt_imEp = 0;
KimInt_cEp = 0;
KimInt_cEpMito = 0;

```



```

KimInt_cEpLyso = 0;
KimInt_int = AimInt/VimInt*(Pn*fintN+Pd*NimInt/(exp(NimInt)-1)*fintD);
KimInt_sm = 0;
KimInt_imInt = AimInt/VimInt*(Pn*(-fimIntN)+Pd*NimInt/(exp(NimInt)-1)*(-
fimIntD)*exp(NimInt));
KimInt_cEd = 0;
KimInt_cEdMito = 0;
KimInt_cEdLyso = 0;
KimInt_p = 0;
SimInt = 0;

```

% #9: Endothelial celss (cEd)

```

KcEd_aEp = 0;
KcEd_imEp = 0;
KcEd_cEp = 0;
KcEd_cEpMito = 0;
KcEd_cEpLyso = 0;
KcEd_int = -AbEd/VcEd*(Pn*(-fintN)+Pd*NbEd/(exp(NbEd)-1)*(-fintD)*exp(NbEd));
KcEd_sm = 0;
KcEd_imInt = 0;
KcEd_cEd = -AbEd/VcEd*(Pn*(fcEdN)+Pd*NbEd/(exp(NbEd)-1)*(fcEdD))...
    -AcEdMito/VcEd*(Pn*fcEdN+Pd*NcEdMito/(exp(NcEdMito)-1)*fcEdD)...
    -AcEdLyso/VcEd*(Pn*fcEdN+Pd*NcEdLyso/(exp(NcEdLyso)-1)*fcEdD)...
    +AaEd/VcEd*(Pn*(-fcEdN)+Pd*NaEd/(exp(NaEd)-1)*(-fcEdD)*exp(NaEd));
KcEd_cEdMito = -AcEdMito/VcEd*(Pn*(-fcEdMitoN)+Pd*NcEdMito/(exp(NcEdMito)-1)*(-
fcEdMitoD)*exp(NcEdMito));
KcEd_cEdLyso = -AcEdLyso/VcEd*(Pn*(-fcEdLysoN)+Pd*NcEdLyso/(exp(NcEdLyso)-1)*(-
fcEdLysoD)*exp(NcEdLyso));
KcEd_p = AaEd/VcEd*(Pn*(fpN)+Pd*NaEd/(exp(NaEd)-1)*(fpD));
ScEd = 0;

```

% #10: Endothelial celss (cEd) Mito

```

KcEdMito_aEp = 0;
KcEdMito_imEp = 0;
KcEdMito_cEp = 0;
KcEdMito_cEpMito = 0;
KcEdMito_cEpLyso = 0;
KcEdMito_int = 0;
KcEdMito_sm = 0;
KcEdMito_imInt = 0;
KcEdMito_cEd = AcEdMito/VcEdMito*(Pn*(fcEdN)+Pd*NcEdMito/(exp(NcEdMito)-1)*(fcEdD));
KcEdMito_cEdMito = AcEdMito/VcEdMito*(Pn*(-fcEdMitoN)+Pd*NcEdMito/(exp(NcEdMito)-
1)*(-fcEdMitoD)*exp(NcEdMito));
KcEdMito_cEdLyso = 0;
KcEdMito_p = 0;
ScEdMito = 0;

```

% #11: Endothelial celss (cEd) Lyso

```
KcEdLyso_aEp = 0;
KcEdLyso_imEp = 0;
KcEdLyso_cEp = 0;
KcEdLyso_cEpMito = 0;
KcEdLyso_cEpLyso = 0;
KcEdLyso_int = 0 ;
KcEdLyso_sm = 0;
KcEdLyso_imInt = 0;
KcEdLyso_cEd = AcEdLyso/VcEdLyso*(Pn*(fcEdN)+Pd*NcEdLyso/(exp(NcEdLyso)-1)*(fcEdD)) ;
KcEdLyso_cEdMito = 0;
KcEdLyso_cEdLyso = AcEdLyso/VcEdLyso*(Pn*(-fcEdLysoN)+Pd*NcEdLyso/(exp(NcEdLyso)-1)*(-fcEdLysoD)*exp(NcEdLyso));
KcEdLyso_p = 0;
ScEdLyso = 0;
```

% #12: plasma(p)

```
Kp_aEp = 0;
Kp_imEp = 0;
Kp_cEp = 0;
Kp_cEpMito = 0;
Kp_cEpLyso = 0;
Kp_int = 0;
Kp_sm = 0;
Kp_imInt = 0;
Kp_cEd = -AaEd/Vp*(Pn*(-fcEdN)+Pd*NaEd/(exp(NaEd)-1)*(-fcEdD)*exp(NaEd));
Kp_cEdMito = 0;
Kp_cEdLyso = 0;
Kp_p = -AaEd/Vp*(Pn*(fpN)+Pd*NaEd/(exp(NaEd)-1)*(fpD));
Sp = 0;
```

M =

[KaEp\_aEp,KaEp\_imEp,KaEp\_cEp,KaEp\_cEpMito,KaEp\_cEpLyso,KaEp\_int,KaEp\_sm,KaEp\_imInt,KaEp\_cEd,KaEp\_cEdMito,KaEp\_cEdLyso,KaEp\_p;...

KimEp\_aEp,KimEp\_imEp,KimEp\_cEp,KimEp\_cEpMito,KimEp\_cEpLyso,KimEp\_int,KimEp\_sm,KimEp\_p\_imInt,KimEp\_cEd,KimEp\_cEdMito,KimEp\_cEdLyso,KimEp\_p;...

KcEp\_aEp,KcEp\_imEp,KcEp\_cEp,KcEp\_cEpMito,KcEp\_cEpLyso,KcEp\_int,KcEp\_sm,KcEp\_imInt,KcEp\_p\_cEd,KcEp\_cEdMito,KcEp\_cEdLyso,KcEp\_p;...

KcEpMito\_aEp,KcEpMito\_imEp,KcEpMito\_cEp,KcEpMito\_cEpMito,KcEpMito\_cEpLyso,KcEpMito\_int,KcEpMito\_sm,KcEpMito\_imInt,KcEpMito\_cEd,KcEpMito\_cEdMito,KcEpMito\_cEdLyso,KcEpMito\_p;...

KcEpLyso\_aEp,KcEpLyso\_imEp,KcEpLyso\_cEp,KcEpLyso\_cEpMito,KcEpLyso\_cEpLyso,KcEpLyso\_in

t,KcEpLyso\_sm,KcEpLyso\_imInt,KcEpLyso\_cEd,KcEpLyso\_cEdMito,KcEpLyso\_cEdLyso,KcEpLyso\_p  
;...

Kint\_aEp,Kint\_imEp,Kint\_cEp,Kint\_cEpMito,Kint\_cEpLyso,Kint\_int,Kint\_sm,Kint\_imInt,Kint\_cEd,K  
int\_cEdMito,Kint\_cEdLyso,Kint\_p;...

Ksm\_aEp,Ksm\_imEp,Ksm\_cEp,Ksm\_cEpMito,Ksm\_cEpLyso,Ksm\_int,Ksm\_sm,Ksm\_imInt,Ksm\_cE  
d,Ksm\_cEdMito,Ksm\_cEdLyso,Ksm\_p;...

KimInt\_aEp,KimInt\_imEp,KimInt\_cEp,KimInt\_cEpMito,KimInt\_cEpLyso,KimInt\_int,KimInt\_sm,Kim  
Int\_imInt,KimInt\_cEd,KimInt\_cEdMito,KimInt\_cEdLyso,KimInt\_p;...

KcEd\_aEp,KcEd\_imEp,KcEd\_cEp,KcEd\_cEpMito,KcEd\_cEpLyso,KcEd\_int,KcEd\_sm,KcEd\_imInt,KcE  
d\_cEd,KcEd\_cEdMito,KcEd\_cEdLyso,KcEd\_p;...

KcEdMito\_aEp,KcEdMito\_imEp,KcEdMito\_cEp,KcEdMito\_cEpMito,KcEdMito\_cEpLyso,KcEdMito\_  
int,KcEdMito\_sm,KcEdMito\_imInt,KcEdMito\_cEd,KcEdMito\_cEdMito,KcEdMito\_cEdLyso,KcEdMi  
to\_p;...

KcEdLyso\_aEp,KcEdLyso\_imEp,KcEdLyso\_cEp,KcEdLyso\_cEpMito,KcEdLyso\_cEpLyso,KcEdLyso\_in  
t,KcEdLyso\_sm,KcEdLyso\_imInt,KcEdLyso\_cEd,KcEdLyso\_cEdMito,KcEdLyso\_cEdLyso,KcEdLyso\_p  
;...

Kp\_aEp,Kp\_imEp,Kp\_cEp,Kp\_cEpMito,Kp\_cEpLyso,Kp\_int,Kp\_sm,Kp\_imInt,Kp\_cEd,Kp\_cEdMito,K  
p\_cEdLyso,Kp\_p];

G = [SaEp,SimEp,ScEp,ScEpMito,ScEpLyso,Sint,Ssm,SimInt,ScEd,ScEdMito,ScEdLyso,Sp]';

```

% 1CellPK based lung model starts here (Rats)
% 12 compartments:
% aEp (surface lining liquied), imEp (Macrophage),
% cEp(epithelial cells),cEpMito(mito of cEp), cEpLyso (lyso of cEp)
% int(Interstitium),imInt(immune cells), sm(smooth muscle),
% cEd(endothelial cells), cEdMito(mito of cEd),cEdLyso (lyso of cEd), p(plasma)

function [M, G, M_v, Vp] = AT_aw_RL()

%molecular physiochemical property

pKa = 100;
logPN = 0.16 ;
logPD = -1.57;%logPN-3.7 ;

%atenolol, chemAxon calculation
% pKa = 9.32;
z = 1;
% %weighted

% Constant
T = 273.15+37;
R = 8.314;
F = 96484.56;
%lipid fraction
LaEp = 0.2;
LimEp = 0.05;
LcEp = 0.05 ;
Lint = 0;
Lsm = 0.05;
LimInt = 0.05;
LcEd = 0.05;
Lp = 0;
%volumetric water fraction=1-lipid fraction
WaEp = 1 - LaEp;
WimEp = 1 - LimEp;
WcEp = 1 - LcEp;
Wint = 1 - Lint;
Wsm = 1 - Lsm;
WimInt = 1 - LimInt;
WcEd = 1 - LcEd;
Wp = 1 - Lp;
%activity coefficient of species(N:neutral,D:desociated)
GaEpN = 1;
GaEpD = 1;
GimEpN = 1.23;

```

```

GimEpD = 0.74;
GcEpN = 1.23;
GcEpD = 0.74;
GintN = 1;
GintD = 1;
GsmN = 1.23;
GsmD = 0.74;
GimIntN = 1.23;
GimIntD = 0.74;
GcEdN = 1.23;
GcEdD = 0.74;
GpN = 1;
GpD = 1;

```

```

% By Jingyu Yu (used in publication) parameters in airways
% Areas and volumes (m^2, m^3) for 7 membranes and corresponding compartments
AaEp = 108*10^(-4);%literature
AbEp = AaEp;%assuming same with apical
AimEp = 0;%No macrophage
AimInt = 0.01*AaEp;%estimate
Asm = AaEp*2; % two side, double the surface area of airway,T model
AbEd = AaEp/5;%estimated 1/5 surface of epithelium
AaEd = AbEd;% same as basical side
%volumes for 8 compartments(m3)
ASL = 15; %um literature
VaEp = AaEp*ASL*10^(-6); %15 um thickness
VimEp = 10^(-30); %10^(-12)*VaEp; % Anynumber,No macrophage at surface
VcEp = 0.072*10^(-6); % estimated from yori model,basement membrane->surface area-
>thickness of each generation
Vint = AaEp*1*10^(-6);%estimated
Vsm = 0.047*10^(-6);%% estimated from yori model,basement membrane->surface area-
>thickness of each generation
VimInt = 0.01*Vint;%setimated
VcEd = AbEd*0.4*10^(-6); %estimated from literature,thickness of endothelium in AW
% Vp = 5; %total blood

```

```

R_org = 0.1;
% calculate constant
VcEpMito = R_org*VcEp;
VcEpLyso = R_org*VcEp;
VcEdMito = R_org*VcEd ;
VcEdLyso = R_org*VcEd ;
VsmMito = R_org*Vsm;
VsmLyso = R_org*Vsm;

AcEpMito = 5.9924e+006*VcEpMito ;
AcEpLyso = 5.9924e+006*VcEpLyso ;

```

```

AcEdMito = 5.9924e+006*VcEdMito ;
AcEdLyso = 5.9924e+006*VcEdLyso ;
AsmMito = 5.9924e+006*VsmMito ;
AsmLyso = 5.9924e+006*VsmMito ;
#####

M_v = diag([VaEp,VimEp,VcEp,VcEpMito,VcEpLyso,Vint,Vsm, VsmMito, VsmLyso, VimInt, VcEd,
VcEdMito, VcEdLyso]);
V_LUN = trace(M_v)*10^6;
Vp = 340*10^(-9)*V_LUN;

% Membrane potential (V)
EaEp = -0.0093;
EbEp = 0.0119;%0.0119;
EimEp = -0.06;
Esm = -0.06;
EimInt = -0.06;
EbEd = -0.06;
EaEd = -0.06;
% pH values
pHaEp = 7.4;
pHimEp = 7.0;
pHcEp = 7.0;
pHint = 7.0;
pHsm = 7.0;
pHimInt = 7.0;
pHcEd = 7.0;
pHp = 7.4;

%adjustment for logP
if ( abs(z-1) <= 10^(-6) )
    logP_nlipT = 0.33*logPN+2.2 ;
    logP_dlipT = 0.37*logPD+2 ;
end
if ( abs(z+1) <= 10^(-6) )
    logP_nlipT = 0.37*logPN+2.2 ;
    logP_dlipT = 0.33*logPD+2.6 ;
end
if ( abs(z-0) <= 10^(-5) )
    logP_nlipT = 0.33*logPN+2.2 ;
    logP_dlipT = 0.33*logPD+2.2 ;
end

% logP_nlipT = logPN;
% logP_dlipT = logPD;

```

```

% Get the first two decimals
logP_n = round(logP_nlipT*100)/100 ;
logP_d = round(logP_dlipT*100)/100 ;
%calculate the membrane permeability
% logP_n = logPN;
% logP_d = logPD;
Pn = 10^(logP_n-6.7)*60; % in 1/min
Pd = 10^(logP_d-6.7)*60; % in 1/min

i = -sign(z) ;
%calculate N for flux of ion happening at 7 membranes
C = z*F/(R*T);
NaEp = C*(-EaEp) ;
NbEp = C*EbEp ;
NimEp = C*EimEp ;
Nsm = C*Esm ;
NimInt = C*EimInt ;
NbEd = C*(-EbEd) ;
NaEd = C*EaEd ;
%calculate Kn and Kd for 8 compartments
N = 1.22*10^(logP_n);
D = 1.22*10^(logP_d);

%calculate Kn and Kd for 8 compartments
% using Rodgers method to get Kd general
KpuBC = 1.15/0.96;
pHBc = 7.22;
fiw_bc = 0.603;
fnl_bc = 0.0017;
fnp_bc = 0.0029;
AP_BC = 0.5;
AP_lung = 3.91;
P = 10^(logP_n);
Ka = (KpuBC - (1+10^(pKa - pHBc))/(1+10^(pKa - pHp))*fiw_bc -
(P*fnl_bc+(0.3*P+0.7)*fnp_bc)/(1+10^(pKa-pHp)))*(1+10^(pKa-pHp))/(AP_BC*10^(pKa-pHBc));
Kd = Ka*AP_lung;
%Kd_p = n*Ka*AP_BC;
if (Kd < 0)
    Kd = 0;
end

KaEpN = N*LaEp ;
KaEpD = D*LaEp ;
KimEpN = N*LimEp ;
KimEpD = D*LimEp ;
KcEpN = N*LcEp ;
KcEpD = D*LcEp ;

```

KintN = N\*Lint ;  
KintD = D\*Lint ;  
KsmN = N\*Lsm ;  
KsmD = D\*Lsm ;  
KimIntN = N\*LimInt ;  
KimIntD = D\*LimInt ;  
KcEdN = N\*LcEd ;  
KcEdD = D\*LcEd ;  
KpN = N\*Lp ;  
KpD = D\*Lp ;

%#####for mito and lyso compartments in cEp, sm and  
cEd#####

LcEpMito = 0.05 ;  
LcEpLyso = 0.05 ;  
LsmMito = 0.05 ;  
LsmLyso = 0.05 ;  
LcEdMito = 0.05 ;  
LcEdLyso = 0.05 ;

WcEpMito = 1-LcEpMito ;  
WcEpLyso = 1-LcEpLyso ;  
WsmMito = 1-LsmMito ;  
WsmLyso = 1-LsmLyso ;  
WcEdMito = 1-LcEdMito ;  
WcEdLyso = 1-LcEdLyso ;

GcEpMitoN = 1.23 ;  
GcEpMitoD = 0.74 ;  
GcEpLysoN = 1.23 ;  
GcEpLysoD = 0.74 ;

GsmMitoN = 1.23 ;  
GsmMitoD = 0.74 ;  
GsmLysoN = 1.23 ;  
GsmLysoD = 0.74 ;

GcEdMitoN = 1.23 ;  
GcEdMitoD = 0.74 ;  
GcEdLysoN = 1.23 ;  
GcEdLysoD = 0.74 ;

EcEpMito = -0.16 ;  
EcEpLyso = +0.01 ;  
EsmMito = -0.16 ;  
EsmLyso = +0.01 ;



EcEdMito = -0.16 ;  
EcEdLyso = +0.01 ;

pHcEpMito = 8 ;  
pHcEpLyso = 5 ;  
pHsmMito = 8 ;  
pHsmLyso = 5 ;  
pHcEdMito = 8 ;  
pHcEdLyso = 5 ;

NcEpMito = C\*EcEpMito ;  
NcEpLyso = C\*EcEpLyso ;  
NsmMito = C\*EsmMito ;  
NsmLyso = C\*EsmLyso ;  
NcEdMito = C\*EcEdMito ;  
NcEdLyso = C\*EcEdLyso ;

KcEpMitoN = N\*LcEpMito ;  
KcEpMitoD = D\*LcEpMito ;  
KcEpLysoN = N\*LcEpLyso ;  
KcEpLysoD = D\*LcEpLyso ;

KsmMitoN = N\*LsmMito ;  
KsmMitoD = D\*LsmMito ;  
KsmLysoN = N\*LsmLyso ;  
KsmLysoD = D\*LsmLyso ;

KcEdMitoN = N\*LcEdMito ;  
KcEdMitoD = D\*LcEdMito ;  
KcEdLysoN = N\*LcEdLyso ;  
KcEdLysoD = D\*LcEdLyso ;

fcEpMitoN = 1/(WcEpMito/GcEpMitoN+KcEpMitoN/GcEpMitoN+WcEpMito\*10<sup>(i\*(pHcEpMito-pKa))</sup>/GcEpMitoD...  
+KcEpMitoD\*10<sup>(i\*(pHcEpMito-pKa))</sup>/GcEpMitoD);  
fcEpMitoD = fcEpMitoN\*10<sup>(i\*(pHcEpMito-pKa))</sup>;

fcEpLysoN = 1/(WcEpLyso/GcEpLysoN+KcEpLysoN/GcEpLysoN+WcEpLyso\*10<sup>(i\*(pHcEpLyso-pKa))</sup>/GcEpLysoD...  
+KcEpLysoD\*10<sup>(i\*(pHcEpLyso-pKa))</sup>/GcEpLysoD);  
fcEpLysoD = fcEpLysoN\*10<sup>(i\*(pHcEpLyso-pKa))</sup>;

```
fsmMitoN = 1/(WsmMito/GsmMitoN+KsmMitoN/GsmMitoN+WsmMito*10^(i*(pHsmMito-
pKa))/GsmMitoD...
+KsmMitoD*10^(i*(pHsmMito-pKa))/GsmMitoD);
fsmMitoD = fsmMitoN*10^(i*(pHsmMito-pKa));
```

```
fsmLysoN = 1/(WsmLyso/GsmLysoN+KsmLysoN/GsmLysoN+WsmLyso*10^(i*(pHsmLyso-
pKa))/GsmLysoD...
+KsmLysoD*10^(i*(pHsmLyso-pKa))/GsmLysoD);
fsmLysoD = fsmLysoN*10^(i*(pHsmLyso-pKa));
```

```
fcEdMitoN = 1/(WcEdMito/GcEdMitoN+KcEdMitoN/GcEdMitoN+WcEdMito*10^(i*(pHcEdMito-
pKa))/GcEdMitoD...
+KcEdMitoD*10^(i*(pHcEdMito-pKa))/GcEdMitoD);
fcEdMitoD = fcEdMitoN*10^(i*(pHcEdMito-pKa));
```

```
fcEdLysoN = 1/(WcEdLyso/GcEdLysoN+KcEdLysoN/GcEdLysoN+WcEdLyso*10^(i*(pHcEdLyso-
pKa))/GcEdLysoD...
+KcEdLysoD*10^(i*(pHcEdLyso-pKa))/GcEdLysoD);
fcEdLysoD = fcEdLysoN*10^(i*(pHcEdLyso-pKa));
```

```
%#####
```

```
%compute the fn and fd for 8 compartments
faEpN = 1/(WaEp/GaEpN+KaEpN/GaEpN+WaEp*10^(i*(pHaEp-pKa))/GaEpD...
+KaEpD*10^(i*(pHaEp-pKa))/GaEpD);
faEpD = faEpN*10^(i*(pHaEp-pKa));
fimEpN = 1/(WimEp/GimEpN+KimEpN/GimEpN+WimEp*10^(i*(pHimEp-pKa))/GimEpD...
+KimEpD*10^(i*(pHimEp-pKa))/GimEpD);
fimEpD = fimEpN*10^(i*(pHimEp-pKa));
fcEpN = 1/(WcEp/GcEpN+KcEpN/GcEpN+WcEp*10^(i*(pHcEp-pKa))/GcEpD...
+KcEpD*10^(i*(pHcEp-pKa))/GcEpD);
fcEpD = fcEpN*10^(i*(pHcEp-pKa));
fintN = 1/(Wint/GintN+KintN/GintN+Wint*10^(i*(pHint-pKa))/GintD...
+KintD*10^(i*(pHint-pKa))/GintD);
fintD = fintN*10^(i*(pHint-pKa));
fimIntN = 1/(WimInt/GimIntN+KimIntN/GimIntN+WimInt*10^(i*(pHimInt-pKa))/GimIntD...
+KimIntD*10^(i*(pHimInt-pKa))/GimIntD);
fimIntD = fimIntN*10^(i*(pHimInt-pKa));
fsmN = 1/(Wsm/GsmN+KsmN/GsmN+Wsm*10^(i*(pHsm-pKa))/GsmD...
+KsmD*10^(i*(pHsm-pKa))/GsmD);
fsmD = fsmN*10^(i*(pHsm-pKa));
fcEdN = 1/(WcEd/GcEdN+KcEdN/GcEdN+WcEd*10^(i*(pHcEd-pKa))/GcEdD...
+KcEdD*10^(i*(pHcEd-pKa))/GcEdD);
fcEdD = fcEdN*10^(i*(pHcEd-pKa));
fpN = 1/(Wp/GpN+KpN/GpN+Wp*10^(i*(pHp-pKa))/GpD...
+KpD*10^(i*(pHp-pKa))/GpD);
```

```

fpD = fpN*10^(i*(pHp-pKa));

%mucus clearance
%Ke = 0.02;
Ke = 0;

%compute the coefficient matrix for ODEs
% #1: Surface Lining Liquid (aEp)
KaEp_aEp = AaEp/VaEp*(Pn*(-faEpN)+Pd*NaEp/(exp(NaEp)-1)*(-faEpD)*exp(NaEp))...
    -AimEp/VaEp*(Pn*faEpN+Pd*NimEp/(exp(NimEp)-1)*faEpD)...
    -Ke;
KaEp_imEp = -AimEp/VaEp*(Pn*(-fimEpN)+Pd*NimEp/(exp(NimEp)-1)*(-fimEpD)*exp(NimEp));
KaEp_cEp = AaEp/VaEp*(Pn*(fcEpN)+Pd*NaEp/(exp(NaEp)-1)*(fcEpD));
KaEp_cEpMito = 0;
KaEp_cEpLyso = 0;
KaEp_int = 0;
KaEp_sm = 0;
KaEp_smMito = 0;
KaEp_smLyso = 0;
KaEp_imInt = 0;
KaEp_cEd = 0;
KaEp_cEdMito = 0;
KaEp_cEdLyso = 0;
KaEp_p = 0;
SaEp = 0;

% #2: Macrophage (imEp)
KimEp_aEp = AimEp/VimEp*(Pn*faEpN+Pd*NimEp/(exp(NimEp)-1)*faEpD);
KimEp_imEp = AimEp/VimEp*(Pn*(-fimEpN)+Pd*NimEp/(exp(NimEp)-1)*(-
fimEpD)*exp(NimEp));
KimEp_cEp = 0;
KimEp_cEpMito = 0 ;
KimEp_cEpLyso = 0 ;
KimEp_int = 0;
KimEp_sm = 0;
KimEp_smMito = 0;
KimEp_smLyso = 0;
KimEp_imInt = 0;
KimEp_cEd = 0;
KimEp_cEdMito = 0 ;
KimEp_cEdLyso = 0 ;
KimEp_p = 0;
SimEp = 0;

% #3: Epithelial Cells (cEp)
KcEp_aEp = -AaEp/VcEp*(Pn*(-faEpN)+Pd*NaEp/(exp(NaEp)-1)*(-faEpD)*exp(NaEp));
KcEp_imEp = 0;

```

```

KcEp_cEp = -AaEp/VcEp*(Pn*(fcEpN)+Pd*NaEp/(exp(NaEp)-1)*(fcEpD))...
-AcEpMito/VcEp*(Pn*fcEpN+Pd*NcEpMito/(exp(NcEpMito)-1)*fcEpD)...
-AcEpLyso/VcEp*(Pn*fcEpN+Pd*NcEpLyso/(exp(NcEpLyso)-1)*fcEpD)...
+AbEp/VcEp*(Pn*(-fcEpN)+Pd*NbEp/(exp(NbEp)-1)*(-fcEpD)*exp(NbEp));
KcEp_cEpMito = -AcEpMito/VcEp*(Pn*(-fcEpMitoN)+Pd*NcEpMito/(exp(NcEpMito)-1)*(-
fcEpMitoD)*exp(NcEpMito)) ;
KcEp_cEpLyso = -AcEpLyso/VcEp*(Pn*(-fcEpLysoN)+Pd*NcEpLyso/(exp(NcEpLyso)-1)*(-
fcEpLysoD)*exp(NcEpLyso)) ;
KcEp_int = AbEp/VcEp*(Pn*(fintN)+Pd*NbEp/(exp(NbEp)-1)*(fintD));
KcEp_sm = 0;
KcEp_smMito = 0;
KcEp_smLyso = 0;
KcEp_imInt = 0;
KcEp_cEd = 0;
KcEp_cEdMito = 0 ;
KcEp_cEdLyso = 0 ;
KcEp_p = 0;
ScEp = 0;

% #4: : Epithelial Cells (cEpMito)
KcEpMito_aEp = 0;
KcEpMito_imEp = 0;
KcEpMito_cEp = AcEpMito/VcEpMito*(Pn*(fcEpN)+Pd*NcEpMito/(exp(NcEpMito)-1)*(fcEpD));
KcEpMito_cEpMito = AcEpMito/VcEpMito*(Pn*(-fcEpMitoN)+Pd*NcEpMito/(exp(NcEpMito)-
1)*(-fcEpMitoD)*exp(NcEpMito));
KcEpMito_cEpLyso = 0 ;
KcEpMito_int = 0 ;
KcEpMito_sm = 0;
KcEpMito_smMito = 0;
KcEpMito_smLyso = 0;
KcEpMito_imInt = 0;
KcEpMito_cEd = 0;
KcEpMito_cEdMito = 0 ;
KcEpMito_cEdLyso = 0 ;
KcEpMito_p = 0;
ScEpMito = 0;

% #5: : Epithelial Cells (cEpLyso)
KcEpLyso_aEp = 0;
KcEpLyso_imEp = 0;
KcEpLyso_cEp = AcEpLyso/VcEpLyso*(Pn*(fcEpN)+Pd*NcEpLyso/(exp(NcEpLyso)-1)*(fcEpD));
KcEpLyso_cEpMito = 0 ;
KcEpLyso_cEpLyso = AcEpLyso/VcEpLyso*(Pn*(-fcEpLysoN)+Pd*NcEpLyso/(exp(NcEpLyso)-1)*(-
fcEpLysoD)*exp(NcEpLyso));
KcEpLyso_int = 0 ;
KcEpLyso_sm = 0;
KcEpLyso_smMito = 0;

```

```

KcEpLyso_smLyso = 0;
KcEpLyso_imInt = 0;
KcEpLyso_cEd = 0;
KcEpLyso_cEdMito = 0 ;
KcEpLyso_cEdLyso = 0 ;
KcEpLyso_p = 0;
ScEpLyso = 0;

% #6: : Interstitium (int)
Kint_aEp = 0;
Kint_imEp = 0;
Kint_cEp = -AbEp/Vint*(Pn*(-fcEpN)+Pd*NbEp/(exp(NbEp)-1)*(-fcEpD)*exp(NbEp));
Kint_cEpMito = 0 ;
Kint_cEpLyso = 0 ;
Kint_int = -AbEp/Vint*(Pn*(fintN)+Pd*NbEp/(exp(NbEp)-1)*(fintD))...
    -Asm/Vint*(Pn*fintN+Pd*Nsm/(exp(Nsm)-1)*fintD)...
    -AimInt/Vint*(Pn*fintN+Pd*NimInt/(exp(NimInt)-1)*fintD)...
    +AbEd/Vint*(Pn*(-fintN)+Pd*NbEd/(exp(NbEd)-1)*(-fintD)*exp(NbEd));
Kint_sm = -Asm/Vint*(Pn*(-fsmN)+Pd*Nsm/(exp(Nsm)-1)*(-fsmD)*exp(Nsm));
Kint_smMito = 0;
Kint_smLyso = 0;
Kint_imInt = -AimInt/Vint*(Pn*(-fimIntN)+Pd*NimInt/(exp(NimInt)-1)*(-fimIntD)*exp(NimInt));
Kint_cEd = AbEd/Vint*(Pn*(fcEdN)+Pd*NbEd/(exp(NbEd)-1)*(fcEdD));
Kint_cEdMito = 0 ;
Kint_cEdLyso = 0 ;
Kint_p = 0;
Sint = 0;

% #7: Smooth Muscle (sm)
Ksm_aEp = 0;
Ksm_imEp = 0;
Ksm_cEp = 0;
Ksm_cEpMito = 0 ;
Ksm_cEpLyso = 0 ;
Ksm_int = Asm/Vsm*(Pn*fintN+Pd*Nsm/(exp(Nsm)-1)*fintD);
Ksm_sm = Asm/Vsm*(Pn*(-fsmN)+Pd*Nsm/(exp(Nsm)-1)*(-fsmD)*exp(Nsm))...
    -AsmMito/Vsm*(Pn*fsmN+Pd*NsmMito/(exp(NsmMito)-1)*fsmD)...
    -AsmLyso/Vsm*(Pn*fsmN+Pd*NsmLyso/(exp(NsmLyso)-1)*fsmD);
Ksm_smMito = -AsmMito/Vsm*(Pn*(-fsmMitoN)+Pd*NsmMito/(exp(NsmMito)-1)*(-fsmMitoD)*exp(NsmMito)) ;
Ksm_smLyso = -AsmLyso/Vsm*(Pn*(-fsmLysoN)+Pd*NsmLyso/(exp(NsmLyso)-1)*(-fsmLysoD)*exp(NsmLyso)) ;
Ksm_imInt = 0;
Ksm_cEd = 0;
Ksm_cEdMito = 0 ;
Ksm_cEdLyso = 0 ;

```

```
Ksm_p = 0;  
Ssm = 0;
```

```
% #8: Smooth Muscle (smMito)
```

```
KsmMito_aEp = 0;  
KsmMito_imEp = 0;  
KsmMito_cEp = 0;  
KsmMito_cEpMito = 0;  
KsmMito_cEpLyso = 0 ;  
KsmMito_int = 0 ;  
KsmMito_sm = AsmMito/VsmMito*(Pn*(fsmN)+Pd*NsmMito/(exp(NsmMito)-1)*(fsmD));  
KsmMito_smMito = AsmMito/VsmMito*(Pn*(-fsmMitoN)+Pd*NsmMito/(exp(NsmMito)-1)*(-  
fsmMitoD)*exp(NsmMito));  
KsmMito_smLyso = 0;  
KsmMito_imInt = 0;  
KsmMito_cEd = 0;  
KsmMito_cEdMito = 0 ;  
KsmMito_cEdLyso = 0 ;  
KsmMito_p = 0;  
SsmMito = 0;
```

```
% #9: Smooth Muscle (smLyso)
```

```
KsmLyso_aEp = 0;  
KsmLyso_imEp = 0;  
KsmLyso_cEp = 0;  
KsmLyso_cEpMito = 0 ;  
KsmLyso_cEpLyso = 0;  
KsmLyso_int = 0 ;  
KsmLyso_sm = AsmLyso/VsmLyso*(Pn*(fsmN)+Pd*NsmLyso/(exp(NsmLyso)-1)*(fsmD));  
KsmLyso_smMito = 0;  
KsmLyso_smLyso = AsmLyso/VsmLyso*(Pn*(-fsmLysoN)+Pd*NsmLyso/(exp(NsmLyso)-1)*(-  
fsmLysoD)*exp(NsmLyso));  
KsmLyso_imInt = 0;  
KsmLyso_cEd = 0;  
KsmLyso_cEdMito = 0 ;  
KsmLyso_cEdLyso = 0 ;  
KsmLyso_p = 0;  
SsmLyso = 0;
```

```
% #10: Immune Cells (imInt)
```

```
KimInt_aEp = 0;  
KimInt_imEp = 0;  
KimInt_cEp = 0;  
KimInt_cEpMito = 0;  
KimInt_cEpLyso = 0;  
KimInt_int = AimInt/VimInt*(Pn*fintN+Pd*NimInt/(exp(NimInt)-1)*fintD);  
KimInt_sm = 0;
```

```

KimInt_smMito = 0;
KimInt_smLyso = 0;
KimInt_imInt = AimInt/VimInt*(Pn*(-fimIntN)+Pd*NimInt/(exp(NimInt)-1)*(-
fimIntD)*exp(NimInt));
KimInt_cEd = 0;
KimInt_cEdMito = 0;
KimInt_cEdLyso = 0;
KimInt_p = 0;
SimInt = 0;

% #11: Endothelial celss (cEd)
KcEd_aEp = 0;
KcEd_imEp = 0;
KcEd_cEp = 0;
KcEd_cEpMito = 0;
KcEd_cEpLyso = 0;
KcEd_int = -AbEd/VcEd*(Pn*(-fintN)+Pd*NbEd/(exp(NbEd)-1)*(-fintD)*exp(NbEd));
KcEd_sm = 0;
KcEd_smMito = 0;
KcEd_smLyso = 0;
KcEd_imInt = 0;
KcEd_cEd = -AbEd/VcEd*(Pn*(fcEdN)+Pd*NbEd/(exp(NbEd)-1)*(fcEdD))...
    -AcEdMito/VcEd*(Pn*fcEdN+Pd*NcEdMito/(exp(NcEdMito)-1)*fcEdD)...
    -AcEdLyso/VcEd*(Pn*fcEdN+Pd*NcEdLyso/(exp(NcEdLyso)-1)*fcEdD)...
    +AaEd/VcEd*(Pn*(-fcEdN)+Pd*NaEd/(exp(NaEd)-1)*(-fcEdD)*exp(NaEd));
KcEd_cEdMito = -AcEdMito/VcEd*(Pn*(-fcEdMitoN)+Pd*NcEdMito/(exp(NcEdMito)-1)*(-
fcEdMitoD)*exp(NcEdMito));
KcEd_cEdLyso = -AcEdLyso/VcEd*(Pn*(-fcEdLysoN)+Pd*NcEdLyso/(exp(NcEdLyso)-1)*(-
fcEdLysoD)*exp(NcEdLyso));
KcEd_p = AaEd/VcEd*(Pn*(fpN)+Pd*NaEd/(exp(NaEd)-1)*(fpD));
ScEd = 0;

% #12: Endothelial celss (cEd) Mito
KcEdMito_aEp = 0;
KcEdMito_imEp = 0;
KcEdMito_cEp = 0;
KcEdMito_cEpMito = 0;
KcEdMito_cEpLyso = 0;
KcEdMito_int = 0;
KcEdMito_sm = 0;
KcEdMito_smMito = 0;
KcEdMito_smLyso = 0;
KcEdMito_imInt = 0;
KcEdMito_cEd = AcEdMito/VcEdMito*(Pn*(fcEdN)+Pd*NcEdMito/(exp(NcEdMito)-1)*(fcEdD)) ;
KcEdMito_cEdMito = AcEdMito/VcEdMito*(Pn*(-fcEdMitoN)+Pd*NcEdMito/(exp(NcEdMito)-
1)*(-fcEdMitoD)*exp(NcEdMito));
KcEdMito_cEdLyso = 0;

```

```
KcEdMito_p = 0 ;
ScEdMito = 0;
```

```
% #13: Endothelial celss (cEd) Lyso
```

```
KcEdLyso_aEp = 0;
KcEdLyso_imEp = 0;
KcEdLyso_cEp = 0;
KcEdLyso_cEpMito = 0;
KcEdLyso_cEpLyso = 0;
KcEdLyso_int = 0 ;
KcEdLyso_sm = 0;
KcEdLyso_smMito = 0;
KcEdLyso_smLyso = 0;
KcEdLyso_imInt = 0;
KcEdLyso_cEd = AcEdLyso/VcEdLyso*(Pn*(fcEdN)+Pd*NcEdLyso/(exp(NcEdLyso)-1)*(fcEdD)) ;
KcEdLyso_cEdMito = 0;
KcEdLyso_cEdLyso = AcEdLyso/VcEdLyso*(Pn*(-fcEdLysoN)+Pd*NcEdLyso/(exp(NcEdLyso)-1)*(-fcEdLysoD)*exp(NcEdLyso));
KcEdLyso_p = 0;
ScEdLyso = 0;
```

```
% #14: plasma(p)
```

```
Kp_aEp = 0;
Kp_imEp = 0;
Kp_cEp = 0;
Kp_cEpMito = 0;
Kp_cEpLyso = 0;
Kp_int = 0;
Kp_sm = 0;
Kp_smMito = 0;
Kp_smLyso = 0;
Kp_imInt = 0;
Kp_cEd = -AaEd/Vp*(Pn*(-fcEdN)+Pd*NaEd/(exp(NaEd)-1)*(-fcEdD)*exp(NaEd));
Kp_cEdMito = 0;
Kp_cEdLyso = 0;
Kp_p = -AaEd/Vp*(Pn*(fpN)+Pd*NaEd/(exp(NaEd)-1)*(fpD));
Sp = 0;
```

```
M =
```

```
[KaEp_aEp,KaEp_imEp,KaEp_cEp,KaEp_cEpMito,KaEp_cEpLyso,KaEp_int,KaEp_sm,KaEp_smMito
,KaEp_smLyso,KaEp_imInt,KaEp_cEd,KaEp_cEdMito,KaEp_cEdLyso,KaEp_p;...
```

```
KimEp_aEp,KimEp_imEp,KimEp_cEp,KimEp_cEpMito,KimEp_cEpLyso,KimEp_int,KimEp_sm,KimE
p_smMito,KimEp_smLyso,KimEp_imInt,KimEp_cEd,KimEp_cEdMito,KimEp_cEdLyso,KimEp_p;...
```

```
KcEp_aEp,KcEp_imEp,KcEp_cEp,KcEp_cEpMito,KcEp_cEpLyso,KcEp_int,KcEp_sm,KcEP_smMito,K
cEp_smLyso,KcEp_imInt,KcEp_cEd,KcEp_cEdMito,KcEp_cEdLyso,KcEp_p;...
```



KcEpMito\_aEp,KcEpMito\_imEp,KcEpMito\_cEp,KcEpMito\_cEpMito,KcEpMito\_cEpLyso,KcEpMito\_int,KcEpMito\_sm,KcEpMito\_smMito,KcEpMito\_smLyso,KcEpMito\_imInt,KcEpMito\_cEd,KcEpMito\_cEdMito,KcEpMito\_cEdLyso,KcEpMito\_p;...

KcEpLyso\_aEp,KcEpLyso\_imEp,KcEpLyso\_cEp,KcEpLyso\_cEpMito,KcEpLyso\_cEpLyso,KcEpLyso\_int,KcEpLyso\_sm,KcEpLyso\_smMito,KcEpLyso\_smLyso,KcEpLyso\_imInt,KcEpLyso\_cEd,KcEpLyso\_cEdMito,KcEpLyso\_cEdLyso,KcEpLyso\_p;...

Kint\_aEp,Kint\_imEp,Kint\_cEp,Kint\_cEpMito,Kint\_cEpLyso,Kint\_int,Kint\_sm,Kint\_smMito,Kint\_smLyso,Kint\_imInt,Kint\_cEd,Kint\_cEdMito,Kint\_cEdLyso,Kint\_p;...

Ksm\_aEp,Ksm\_imEp,Ksm\_cEp,Ksm\_cEpMito,Ksm\_cEpLyso,Ksm\_int,Ksm\_sm,Ksm\_smMito,Ksm\_smLyso,Ksm\_imInt,Ksm\_cEd,Ksm\_cEdMito,Ksm\_cEdLyso,Ksm\_p;...

KsmMito\_aEp,KsmMito\_imEp,KsmMito\_cEp,KsmMito\_cEpMito,KsmMito\_cEpLyso,KsmMito\_int,KsmMito\_sm,KsmMito\_smMito,KsmMito\_smLyso,KsmMito\_imInt,KsmMito\_cEd,KsmMito\_cEdMito,KsmMito\_cEdLyso,KsmMito\_p;...

KsmLyso\_aEp,KsmLyso\_imEp,KsmLyso\_cEp,KsmLyso\_cEpMito,KsmLyso\_cEpLyso,KsmLyso\_int,KsmLyso\_sm,KsmLyso\_smMito,KsmLyso\_smLyso,KsmLyso\_imInt,KsmLyso\_cEd,KsmLyso\_cEdMito,KsmLyso\_cEdLyso,KsmLyso\_p;...

KimInt\_aEp,KimInt\_imEp,KimInt\_cEp,KimInt\_cEpMito,KimInt\_cEpLyso,KimInt\_int,KimInt\_sm,KimInt\_smMito,KimInt\_smLyso,KimInt\_imInt,KimInt\_cEd,KimInt\_cEdMito,KimInt\_cEdLyso,KimInt\_p;...  
...

KcEd\_aEp,KcEd\_imEp,KcEd\_cEp,KcEd\_cEpMito,KcEd\_cEpLyso,KcEd\_int,KcEd\_sm,KcEd\_smMito,KcEd\_smLyso,KcEd\_imInt,KcEd\_cEd,KcEd\_cEdMito,KcEd\_cEdLyso,KcEd\_p;...

KcEdMito\_aEp,KcEdMito\_imEp,KcEdMito\_cEp,KcEdMito\_cEpMito,KcEdMito\_cEpLyso,KcEdMito\_int,KcEdMito\_sm,KcEdMito\_smMito,KcEdMito\_smLyso,KcEdMito\_imInt,KcEdMito\_cEd,KcEdMito\_cEdMito,KcEdMito\_cEdLyso,KcEdMito\_p;...

KcEdLyso\_aEp,KcEdLyso\_imEp,KcEdLyso\_cEp,KcEdLyso\_cEpMito,KcEdLyso\_cEpLyso,KcEdLyso\_int,KcEdLyso\_sm,KcEdLyso\_smMito,KcEdLyso\_smLyso,KcEdLyso\_imInt,KcEdLyso\_cEd,KcEdLyso\_cEdMito,KcEdLyso\_cEdLyso,KcEdLyso\_p;...

Kp\_aEp,Kp\_imEp,Kp\_cEp,Kp\_cEpMito,Kp\_cEpLyso,Kp\_int,Kp\_sm,Kp\_smMito,Kp\_smLyso,Kp\_imInt,Kp\_cEd,Kp\_cEdMito,Kp\_cEdLyso,Kp\_p];

G =

[SaEp,SimEp,ScEp,ScEpMito,ScEpLyso,Sint,Ssm,SsmMito,SsmLyso,SimInt,ScEd,ScEdMito,ScEdLyso,Sp]';